Multylayer Ceramic Composite Formation by Electrophoretic Deposition

L. Gal-Or, S. Liubovich,
M. Folman, D. Sherman

Israel Institute of Metals
Technion Research and Development Foundation

Final: Scientific Report
May 1, 1993 - April 30, 1996
Research Project 524-702
F4 9620-93-1-0233

Prepared for
EOARD - London, England
AFOSR - Washington D.C. 20332, U.S.A.

REPORT DOCUMENTATION PAGE

Form Approved
OMB No. 0704-0188

1. AGENCY USE ONLY (Leave blank)	2. REPORT DATE	3. REPORT TYPE AND DATES COVERED
	June 30, 96	Final report 1 May 93 - 30 April 96

4. TITLE AND SUBTITLE
Multilayer ceramic composite formation by electrophoretic deposition

5. FUNDING NUMBERS
F49620-93-1-0233

6. AUTHOR(S)
L. Gal-Or, S. Liubovich, M. Folman

7. PERFORMING ORGANIZATION NAME(S) AND ADDRESS(ES)
Technion R&D Foundation
Technion - Israel Institute of Technology
Senate House, Technion City, Haifa 32000, Israel

8. PERFORMING ORGANIZATION REPORT NUMBER

9. SPONSORING/MONITORING AGENCY NAME(S) AND ADDRESS(ES)
EOARD 223/231 Old Marylbone Rd., London
NW1 5TH UK
AFOSR/NE Dr. A. Pechenik, Bolling AFB, Washington, D.C. 20332-6448

10. SPONSORING/MONITORING AGENCY REPORT NUMBER

11. SUPPLEMENTARY NOTES

12a. DISTRIBUTION/AVAILABILITY STATEMENT
Unlimited

12b. DISTRIBUTION CODE

13. ABSTRACT (Maximum 200 words)

Multilayer ceramic composites are of great interest due to prospects for enhancement of fracture toughness. A novel approach to multilayer formation based on electrophoretic deposition is adopted in this work. Alternating layers of ZrO_2 and Al_2O_3 are deposited by alternating immersion in two different suspensions. Deposition rates, green and fired densities and suspensions stability were studied as function of deposition parameters. These parameters are: electric field strength, particle concentration, deposition duration. An extensive study was performed on the effect of additives on the above mentioned criteria. The variation of layer thickness in a constant voltage and constant current regime was studied. Layered structures with up to 300 layers were obtained. Initial microhardness and bending tests were performed indicating crack confinement and significant enhancement of bending strength. The process of scale-up of specimen dimensions needed for fracture toughness measurements encountered difficulties expressed mainly in cracking of green and sintered specimens. Further optimization of deposition parameters was performed in the last stage. Based on these results further work is needed for preparation of the scaled-up specimens and performance of fracture toughness measurements.

14. SUBJECT TERMS
Electrophoresis, Ceramics, Multilayer, Microcomposites

15. NUMBER OF PAGES

16. PRICE CODE

17. SECURITY CLASSIFICATION OF REPORT	18. SECURITY CLASSIFICATION OF THIS PAGE	19. SECURITY CLASSIFICATION OF ABSTRACT	20. LIMITATION OF ABSTRACT
Unclassified	Unclassified	Unclasified	Unlimited

List of Personnel

Dr. L. Gal-Or - Principal Investigator

Mrs. S. Liubovich - Research Associate

Dr. O. Korotkina - Research Associate

Mr. R. Goldner - Student

Prof. M. Folman - Consultant

Dr. D. Sherman - Consultant

List of Publications and Presentations

1. L. Gal-Or, S. Liubovich, M. Folman, "Multilayer Ceramic Composite Formation by Electrophoretic Deposition," Interim Sci. Report, F4 9620-93-1-0233, May 1/93 - April 30/94.

2. L. Gal-Or, S. Liubovich, M. Folman,"Multylayer Ceramic Composite Formation by Electrophoretic Deposition", Interim Sci. Report, F4 9620-93-1-0233, May 1/94 - April 30/95.

3. L. Gal-Or, Air Force Ceramic Materials Contractor's Conference, Hueston Woods, Collage Corner, OH May 19-20, 1994.

4. L. Gal-Or, Air Force Ceramic Materials Contractor's Conference, Hueston Woods, Collage Corner, OH May 25-26, 1995.

SUMMARY OF FINAL REPORT

The objective of this project is to develop a method for the formation of ZrO_2/Al_2O_3 multilayer microcomposites based on electrophoretic deposition. The interest in layered ceramic structures stems from the possibility to obtain increased fracture toughness of such composites. Recently the increase in fracture toughness in Al_2O_3/ZrO_2 microcomposites due to modification of size and shape of the transformation zones around cracks was demonstrated.

Several approaches are currently adopted for the formation of multilayered structures among them slip and tape casting as well as sequential centrifuging.

In the present work a novel approach to formation of a multilayered composite is studied. The approach is based on electrophoretic deposition of alternating layers of two kinds of ceramic materials by alternating immersion of a substrate in different suspensions while applying selected deposition parameters.

Electrophoretic deposition has several advantages over the existing methods of multilayer formation, these are:

- Rigid and easy control of layer thickness.
- Wide range of layer thickness variation (from a few microns to millimeters).
- The possibility to form intricate shapes of composites.
- Low cost equipment and possibility of automation.

The first year of this work concentrated on studies of the deposition rates of Al_2O_3 and ZrO_2 particles from suspensions based on isopropanol. The deposition parameters varied were:

the electric field strength, particle concentration and deposition time. In addition to the kinetics of deposition the effect of deposition parameters on the green and fired density of the deposits was studied. It is known that the stability and homogeneity of the suspension have a strong effect on the density of the deposit. Therefore, the influence of additives which enhance these properties was studied. Initial green and sintered multilayer ZrO_2/Al_2O_3 structures were formed with individual layer thicknesses in the range of 10-100 microns.

During the second year the following studies of the characteristics of multilayer structure formation were performed:

- Layer thickness variation and control during deposition.
- Planarity of layers.
- "Throwing power" - variation in deposit thickness on substrate area.
- Variation in layer composition due to contamination of ZrO_2 suspension with Al_2O_3 and vice versa.
- Initial measurements of bending strength and layer hardness.

The initial mechanical tests were performed on beams with 20 mm length, 13 mm span and 1.85 mm height, with a layer thickness of about 15 μ.
In order to perform fracture toughness measurements a scaling-up of specimen size and of layer thickness while maintaining a constant layer thickness through the whole cross-section was performed.

Extensive experiments were performed on preparation of round discs of 40 mm diameter and rectangular specimens of 45X45 mm

with a thickness of >5 mm. Significant difficulties were encountered during the above mentioned specimens preparation. These were related to:

Cracking of "green" specimens during removal from conductive substrate, cracking due to drying shrinkage, macro defects caused by localized accumulation of hydrogen produced at the cathode concurrent with particle deposition, deformation during sintering.

In order to improve specimen quality it was deemed necessary to optimize further conditions.

Since the zeta potential is a crucial parameter in electrophoretic deposition both in rate of deposit formation as well as deposit quality (green and fired density, mechanical strength) the deposition rate which is proportional to the zeta potential was used as a criterion in the majority of the experiments.

The previous stages of work concentrated on isopropanol as solvent, acetylacetone as additive, stainless steel as substrate material and experiments were performed at constant voltage.

In this stage experiments were performed in addition to isopropanol also in ethanol and mixtures of ethanol + MEK. Additives studied were also Fish Oil and Phosphate Ester, Al foil was used as substrate in addition to stainless steel and part of the experiments were performed at a constant current regime.

The results obtained in this project can be summarized as follows:

The kinetics of deposition of Al_2O_3 and ZrO_2 particles from isopropanol suspensions on both anode and cathode was studied. It was found that submicron Al_2O_3 and ZrO_2, particles suspended in isopropanol acquired spontaneously a positive charge and were deposited on the cathode.

- The addition of Acetyl Acetone (AcAc) to isopropanol suspensions of both Al_2O_3 and ZrO_2 improves the suspension stability and increases the deposition rate.

- AcAc increases the zeta potential of both Al_2O_3 and ZrO_2 particles in isopropanol.

- AcAc increases appreciably the green density of the deposits. Alumina and zirconia deposits with a green density of 62% (of the theoretical value) were obtained from respective isopropanol suspensions with 0.05-1.5% (v/v) AcAc at 200 v/cm and 100-300 g/l concentration of solids. Addition of AcAc increased the green density from 42 to 62% for Al_2O_3 and from 33 to 62% for ZrO_2.

- The effect of AcAc is explained by the following mechanism:
  A keto-enolic equilibrium exists for the AcAc molecular structure. The enolic group has a relatively high dissociation constant resulting in the formation of H+ ions. These are adsorbed on the ceramic particles increasing their positive charge, leading to the increase in zeta potential which in turn increases the deposition rate and the stability of the suspension due to enhanced electrostatic repulsion between particles. The increased green density of the deposits is due to hindrance of agglomeration of particles.

- Al_2O_3/ZrO_2 laminar composites of up to 80 layers and total thickness of 1.5 mm were prepared by alternating deposition of the two powders from respective isopropanol suspensions at a constant field intensity of 200 v/cm, 100 and 300 g/l concentration of solids in the presence of 1.5% (v/v) AcAc.

- The composites were characterized by well defined and dense interfaces between layers and a rather dense packing of grains, the Al_2O_3 grains being about twice the size of ZrO_2 grains.

- The separation of the multilayer structure from the steel substrate (electrode) is facilitated by dipping in glycerine immediately and removal from the deposition bath. Nevertheless, the problem of damage of the structure due to occasional bending exists.

- At a later stage of the project $Al_2O_3/Ce\text{-}ZrO_2$ and $Al_2O_3+Ce\text{-}ZrO_2/Ce\text{-}ZrO_2$ laminar composites of up to 300 layers and a total thickness of up to 5.5 mm were obtained by electrophoretic deposition from appropriate suspensions. The deposition was performed at a constant field intensity of 200 v/cm and particle concentration of 100 g/l.

- Individual layer thickness was varied in the range of 5-100 μ.

- The composition of the deposited layers differs from that of the suspensions due to a lower deposition rate of the $Ce\text{-}ZrO_2$ as compared to that of the Al_2O_3.
Improval in thickness uniformity of the composite was obtained by adjusting the anode/cathode ratio.

- Planarity of Al_2O_3 layers is achieved when $Ce\text{-}ZrO_2$ is added to the Al_2O_3 suspension. Planarity of $Ce\text{-}ZrO_2$ has been obtained at all experimental conditions.

- The electric resistance of the deposit increases with increase of deposit thickness. However, up to about 2 mm thickness this increase is negligible. This behaviour is explained by a preferential deposition of large particles resulting in an initial porous less resistant layer.

- As a result of suspension depletion and increase of deposit resistance the individual thickness of the layers decreases during deposition at constant field intensity and uncorrected suspension concentration.

- A $Ce\text{-}ZrO_2/Al_2O_3+Ce\text{-}ZrO_2$ laminar composite with small variation in layer thickness was obtained under conditions of increasing field strength and deposition time for each layer.

- Particle size affects the deposition rate when no additives are present with larger particles depositing at a lower rate. However, upon addition of an effective additive, the deposition rate was found similar for different particle sizes in the range of submicron up to 5 μ average particle size.

- The study was extended to additional solvents to include ethanol and mixtures of ethanol+methyl ethyl ketone (MEK). Also additional additives were studied - fish oil and phosphate ester. It was found that the highest deposition rate is achieved in a mixture of 60 ml ethanol + 40 ml MEK.

- Experiments performed with a constant current regime as opposed to a constant voltage regime indicate on the possibility to obtain a constant layer thickness without variation of other deposition parameters.

- Preliminary tests of microhardness of individual layers showed confinement of cracks to the Al_2O_3 layer. Bending tests performed on beam specimens with dimensions described earlier indicate an enhancement of the bending strength. Thus a MOR of 895 MPa was obtained in a 3 point bend test and 587 MPa in a 4 point bend test.

  Further work has to be performed in order to obtain specimens which will allow fracture toughness measurements. Based on the additional optimization of deposition parameters performed in the third year of this work further work on preparation of multilayer microcomposites should be done with a constant current regime, in a solvent of ethanol+MEK with a phosphate ester additive.

Report for Period May 1/95 - April 30/96

L.Gal-Or
S. Liubovich

Israel Inst. of Metals

Technion Research and Development Foundation

Table of Contents

Chapter 1 - Introduction

This report covers the last research period of this project which concentrated on the preparation of specimens for mechanical testing. Preparation of round specimens with a diameter of 40 mm in the green state and square specimens of 45 X 45 mm with a thickness of at least 5 mm was the objective at this stage. Difficulties arose during scale-up of specimen dimensions such as: cracking of specimens during detachment from substrate, cracking due to drying shrinkage macroporosity caused by gas formation during deposition.

In view of the difficulties which arose during specimen preparation it was necessary to further optimize deposition conditions and therefore extensive work was carried out on optimization of the following parameters:

- Preliminary treatment of powders.
- Suspension fluid ("solvent").
- Suspension additives.
- Particle size.
- Ratio between Al_2O_3 and ZrO_2 conc. in suspension.

A determing factor both of the kinetics of deposition as well as of the properties of the "green" and sintered body is the Zeta potential of the particles. Therefore the deposition rate which is proportional to the Zeta potential, when the other parameter are constant, was chosen as the main criterion for the experiments. In addition, suspension stability and "green" density were also studied.

Chapter 2 - Materials and Methods

a. Substrates

Two kinds of substrates were used:
Stainless steel (AiSi 316) discs 40 mm and Al foil which enveloped the same stainless disc. For rectangular specimens 45X45 mm the same materials were used as substrates.

b. Ceramic Powders

- Al_2O_3 powder D-50 produced by "Ceralox" U.S.A, average particle size 0.45μ and surface area of 7.5 m^2/g.
- ZrO_2 powder Y2N5 produced by "Tioceram" , England with a surface area of 13.6 m^2/g.

c. Solvents

Three kinds of solvents were used, sometimes as mixtures:

- Isopropanol - "Bio-Lab Ltd"
  dielectric constant - ϵ - 18
  viscosity - - 2.4 cp
  ϵ/η - 7.5
- Ethanol absolute - "Bio - Lab Ltd"
  dielectric constant - 24
  viscosity - 1.2 cp
  ϵ/η - 20
- MEK - methyl ethyl ketone - "Riedel de Haen"
  dielectric constant - 18
  viscosity - 0.4 cp
  ϵ/η - 45

d. Additives

- Acetyl Acetone (AcAc) - AR Grade
- Fish Oil - Menhaden - Sigma Corp.
- Emphos PS - 21 A, Witco Corp. (Phosphate Ester).

e. Deposition Parameters

Deposition voltage - 50-200v
Electrode distance - 2.5 cm
Particle conc. - 100 g/l
Deposition time - 60 sec.
Temp. - room.

f. Preparation of specimens

Specimens were cleaned ultrasonically in ethanol for 5 min and dried in an oven at 200C° for 10 min.

g. Experimental set-up

The experimental set-up is described in the previous reports.

h. Drying and Sintering

Drying was performed in a desiccator with an ethanol container and sintering was performed as described in the previous reports.

i. Testing of Deposits

Deposit weight was determined by weighing the substrate before deposition and after drying of deposit.

j. Preliminary Treatment of Powder

Powders were subjected to the following preliminary alternative or subsequent treatments:

- Ball milling - in a polyethylene container using a mixture of 3/8" and 1/4" ZrO_2 balls, at 100 rev/min.
- Sonication - using a Sonic Dismembeator, Fisher Scientific, Model 550.

Chapter 3 - Results and Discussion

3.1 Effect of Powder Pretreatment

This was tested by determining deposit weight obtained from a suspension of Al_2O_3 and ZrO_2 in isopropanol at 100 v, 100 g/l during 60 sec. Table 1 summarizes the results.

Table 1: Deposit weight as function of powder pretreatment (100 g/l, 100v, 60 sec.), mg/cm².

Treatment	Al_2O_3	ZrO_2
Ball millig - 2 hrs	26.5	1.0
Sonication - 12 min	3.8	9.0
No Pretreatment	10.4	0.5

The effect of pretreatment on deposition rate is significant also in the presence of additives such as AcAc (see Fig. 1).

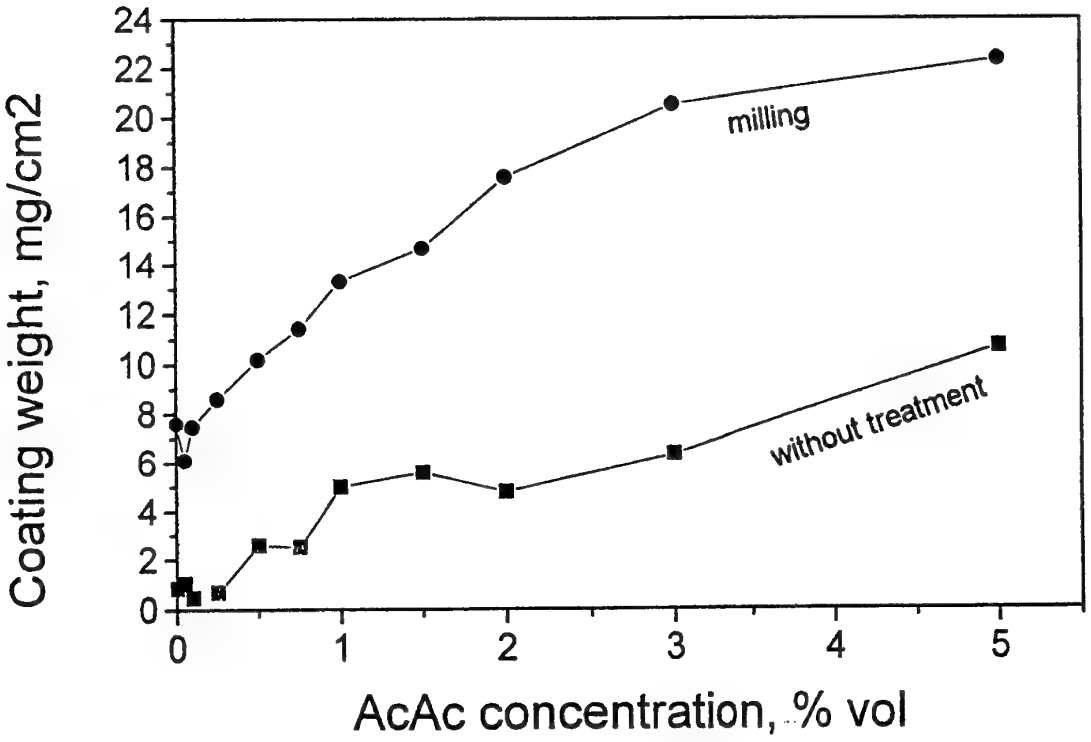

Fig 1 - Deposition rate as function of AcAc conc. for ZrO_2 without treatment and after milling for 2 hrs (100 g/l, 100v, 60 sec).

The results show that the effect of pretreatment depends on the powder, thus Al_2O_3 deposition is significantly enhanced by ball milling, while ZrO_2 deposition is enhanced strongly by sonication. For both powders pretreatment is important particularly for ZrO_2 deposition which is very slow without pretreatment. The effect of pretreatment is expressed also in the presence of additives.

3.2 Effect of Solvent and Additives

The effect of type of solvent, type of additive and their combined effect on deposition rate are seen in the following tables and figures. Experiments were carried out in mixed suspensions where the weight ratio of Al_2O_3/ZrO_2 was 90/10 and 20/80.

Table 2: Coating weight (mg/cm²) as function of solvent and additive conc. (Emphos) for a 90/10 Al_2O_3/ZrO_2 suspension (100v, 100 g /l, 60 sec, 2hr milling).

	Coating weight in		
% Emphos 21	Iso-propanol	Ethanol	MEK+Ethanol
0	1.41	47.64	57.57
0.05	2.38	25.12	52.01
0.1	2.49	26.83	44.87
0.25	3.04	34.02	63.53
0.5	28.32	37.26	64.18
0.75	25.13	38.42	58.51
1	24.27	45	55.82
1.25	22.07	37.98	57.23
1.5	19.88	35.37	54.39
2	19.21	32.92	51.96

Table 3: Coating weight (mg/cm²) as function of solvent type and additive conc. (AcAc) for a 90/10 Al_2O_3/ZrO_2 suspension. Deposition conditions as in Table 1.

	Coating weight in		
% AcAc	Iso-propanol	Ethanol	MEK+Ethanol
0	12	20.8	61.4
0.05		53.1	69.4
0.1		54.6	63.1
0.25	21.9	54.7	53.2
0.5	17.9	48.8	53.9
0.75	16.3	47.6	
1	16.7	45.7	
1.25		41.9	
1.5	19.9	42.1	
2	17	40	

Table 4: Coating weight (mg/cm²) as function of solvent type and additive conc. (Fish Oil) for a 90/10 Al_2O_3/ZrO_2 suspension. Deposition parameters as in Table 1.

	Coating weight in		
% Fish Oil	Iso-propanol	Ethanol	MEK+Ethanol
0	17.96		32.92
0.01	17.22		
0.025	17.29		
0.05	17.64		29.2
0.075	17.4		
0.1	17.12		28.02
0.25	16.99		28.94
0.5	17.02		33.91
0.75	16.43		29.26
1	16.32		25.51
1.25			24.97
1.5	15.91		27.07
2	15.89		28.38

Following are figures presenting the above results.

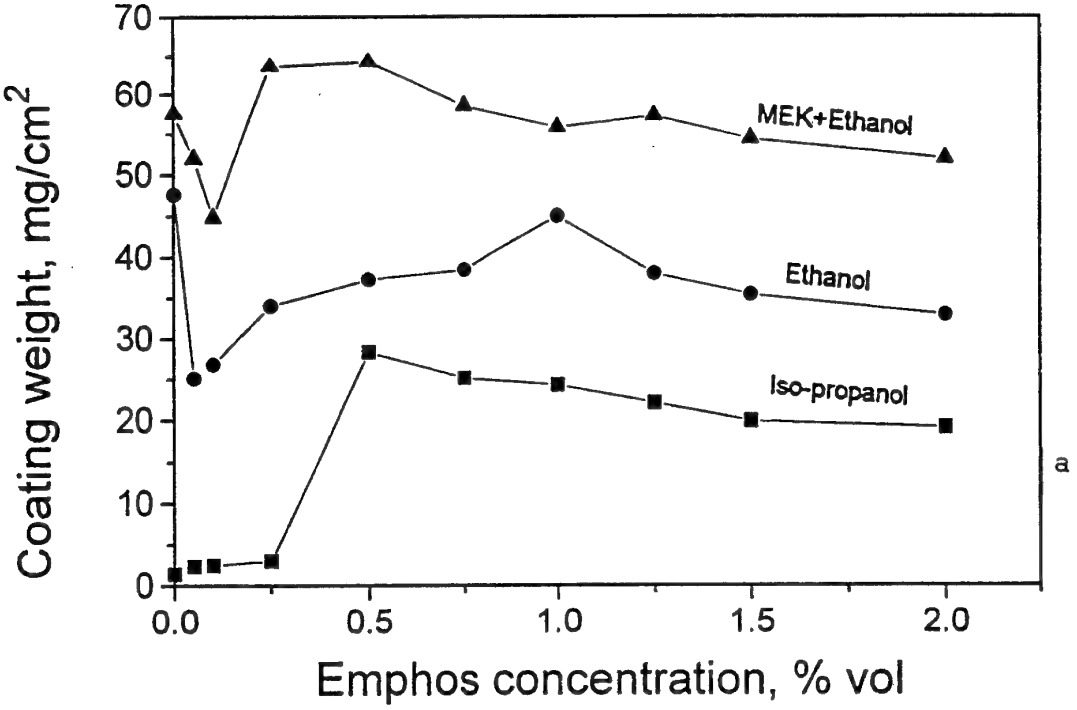

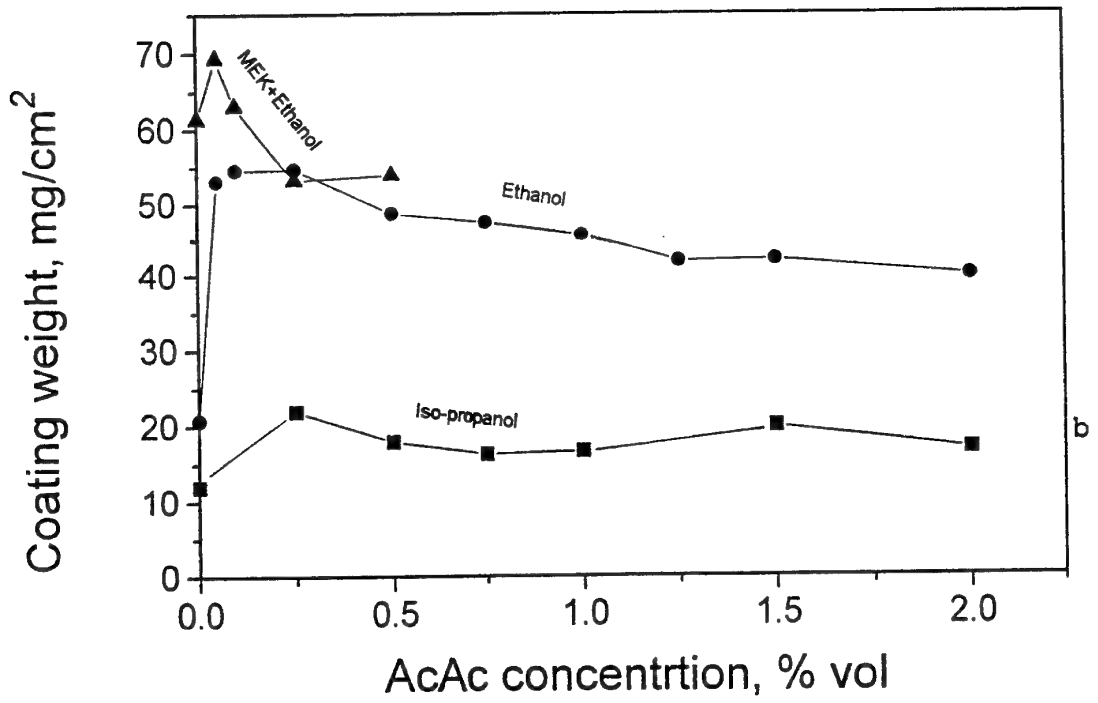

a(Emphos 21) b(AcAc) c(Fish Oil)

Fig. 2: Coating weight as function of solvent type and conc. of additive for a 90/10 Al_2O_3/ZrO_2 suspension.

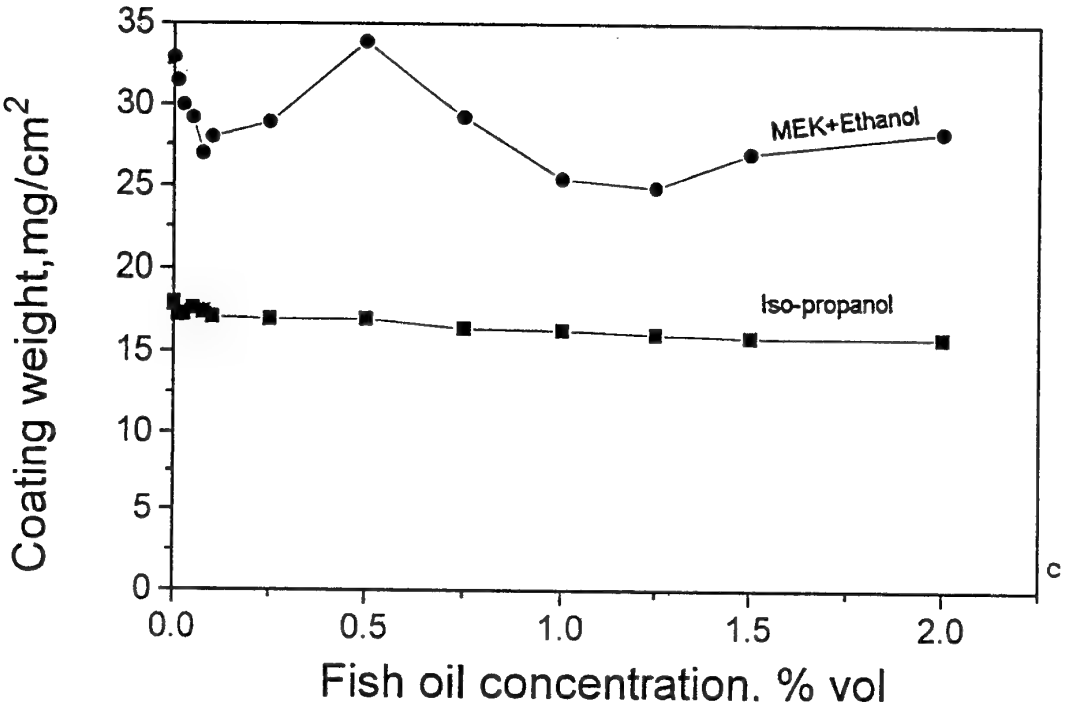

Continuation of Fig. 2.

The tables and figures show that in all deposition experiments the deposition increased in the following order of solvent type isopropanol<ethanol<MEK + ethanol. This order coincides, as expected, with the ratio ϵ/η of these solvents: 7.5(iPA)< 20(ethanol)<45(MEK). (ϵ/η for MEK + ethanol 1:1 is certainly higher than that for ethanol alone).

The effect of the additive is selective as to the type of solvent. Thus Emphos affects deposition rate in ipropanol and not in ethanol and MEK + ethanol, while AcAc has an effect in all solvents and fish oil was not found to affect the deposition in isopropanol nor in MEK + ethanol.

Specific effect of additive on Al_2O_3, ZrO_2 and their mixtures

The effect of one additive (AcAc) on deposition of pure Al_2O_3, pure ZrO_2 and mixtures of them was studied.
The study was extended also to different pretreatments.
The experiments were carried out in isopropanol solutions.
Tables 5-7 and figs. 3-5 contain the the results.

Table 5 - Coating weight vs AcAc conc. (100 g/l, 100 v, 60 sec., isopropanol, no pretreatment of powder), mg/cm².

% AcAc	100% Al2O3	50% Al2O3	100% ZrO2
0	16.62	6.24	0.86
0.05		5.08	1.06
0.1	16.68	6.57	0.5
0.25	17.78	7.41	0.7
0.5	18.94	7.83	2.59
0.75	18.38	8.2	1.52
1	19.26	8.4	5.01
1.5	19.27	10.56	5.59
2	19.36	11.74	4.8
3	18.16	13.42	6.34
5	18.86	15.67	10.69

Table 6 - Coating weight vs. AcAc conc. (100 g/l, 100 v, 60 sec, isopropanol, after 2 hrs milling) mg/cm².

% AcAc	100% Al2O3	50% Al2O3	20% Al2O3	10% Al2O3	100% ZrO2
0	26.53	13.87	9.2	7.99	0.76
0.05	29.36	18.31	12.1	9.94	5.11
0.1	22.5	20	14.32	10.67	7.48
0.25	27.57	23.23	15.94	10.63	8.6
0.5	26.91	24.73	21.74	14.33	10.21
0.75	27.06	26.4	21.77	14.96	11.43
1	25.6	26.32	23.56	15.7	13.33
1.5	26.22	27.24	24.17	16.8	14.7
2	25.17	27.19	26.37	16.63	17.6
3	24.89	29.04	28.2	18.17	20.53
5	24.21	30.09	28.96	19.56	22.36

Table 7 - Coating weight as function of AcAc conc. after 2 hrs ball milling + 12 min sonication, other parameters as in Table 6.

%AcAc	80% Al2O3 + 20% ZrO2	20% Al2O3 + 80% ZrO2	10% Al2O3 + 90% ZrO2
0	1.93	2.87	3.3
0.05	30.36	18.44	15.04
0.1	31.33	21.59	19.07
0.25	29.38	22.61	21.02
0.5	26.69	23.46	20.68
0.75	25.42	23.27	20.98
1	25.07	21.6	20.23
1.5	24.44	26.72	21.9
2	25.12	27.09	23.4
3	22.96	27.06	24.38
5	24.63	31.11	27.3

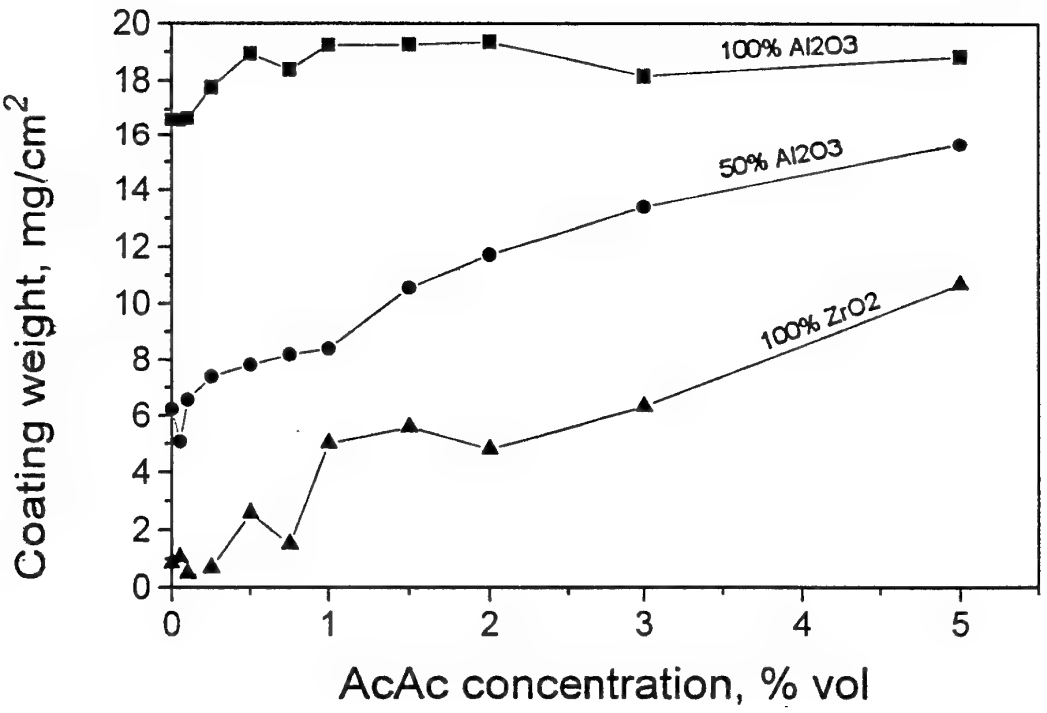

Fig. 3 - Coating weight vs AcAc conc. (100 g/l, 100 v, 60 sec., isopropanol, no pretreatment of powder)

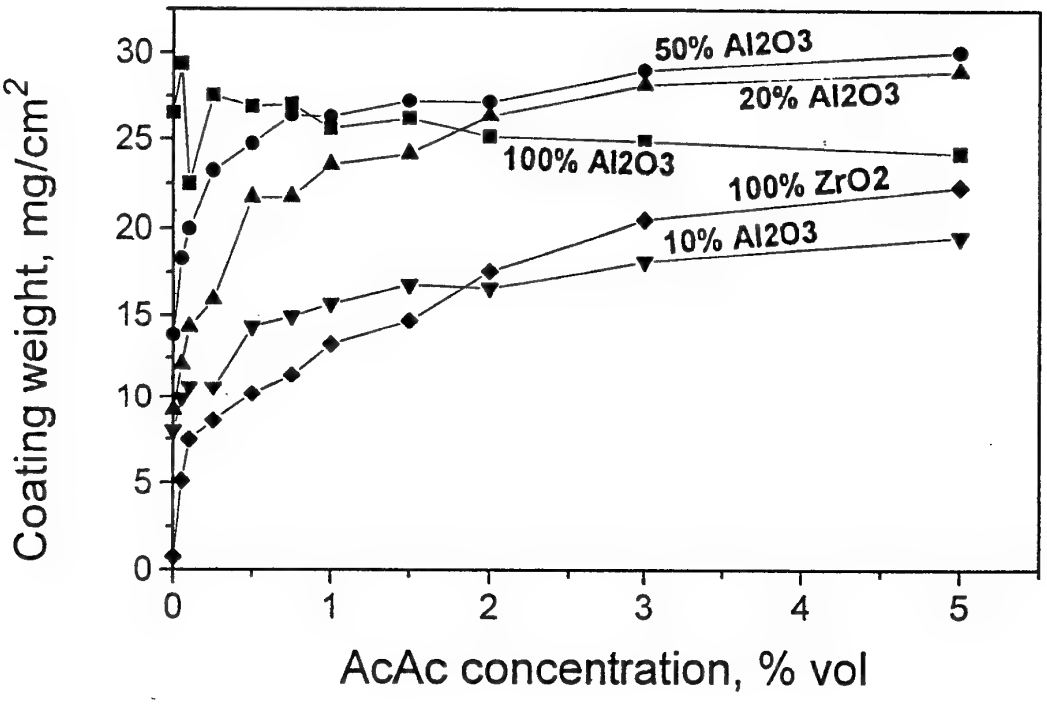

Fig. 4 - Coating weight vs. AcAc conc. (100 g/l, 100 v, 60 sec, isopropanol, after 2 hrs milling)

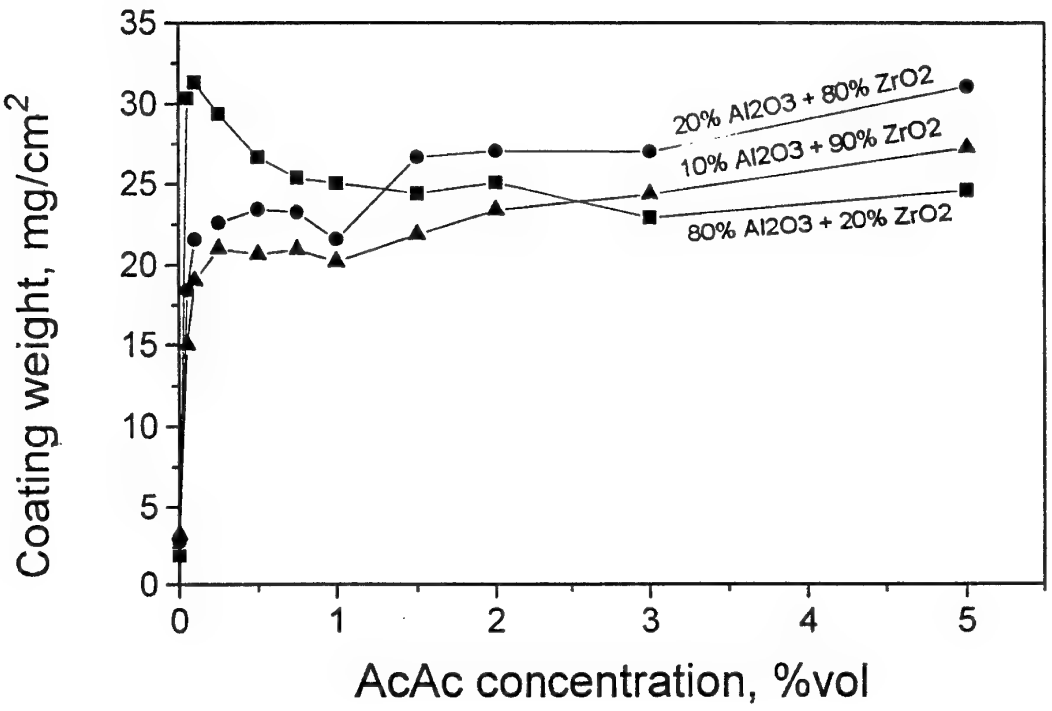

Fig. 5 - Coating weight as function of AcAc conc. after 2 hrs ball milling + 12 min sonication, other parameters as in Table 6 .

It is seen in these results that the AcAc additive affects pure ZrO_2 and mixtures with appreciable conc. of ZrO_2 for all pretreatments. while pure Al_2O_3 is not affected when untreated or when ball milled. However, when sonication is also preformed a strong effect of AcAc on deposition rate is seen for all powders when conc. is raised from 0 to 0.1%.

Another additive, Triethanolamine (TEA), has also shown a strong effect on ZrO_2 deposition (Fig. 6), while Tributylphosphate (TBPh) known for its role as additive did not affect Al_2O_3 deposition (Fig. 7).

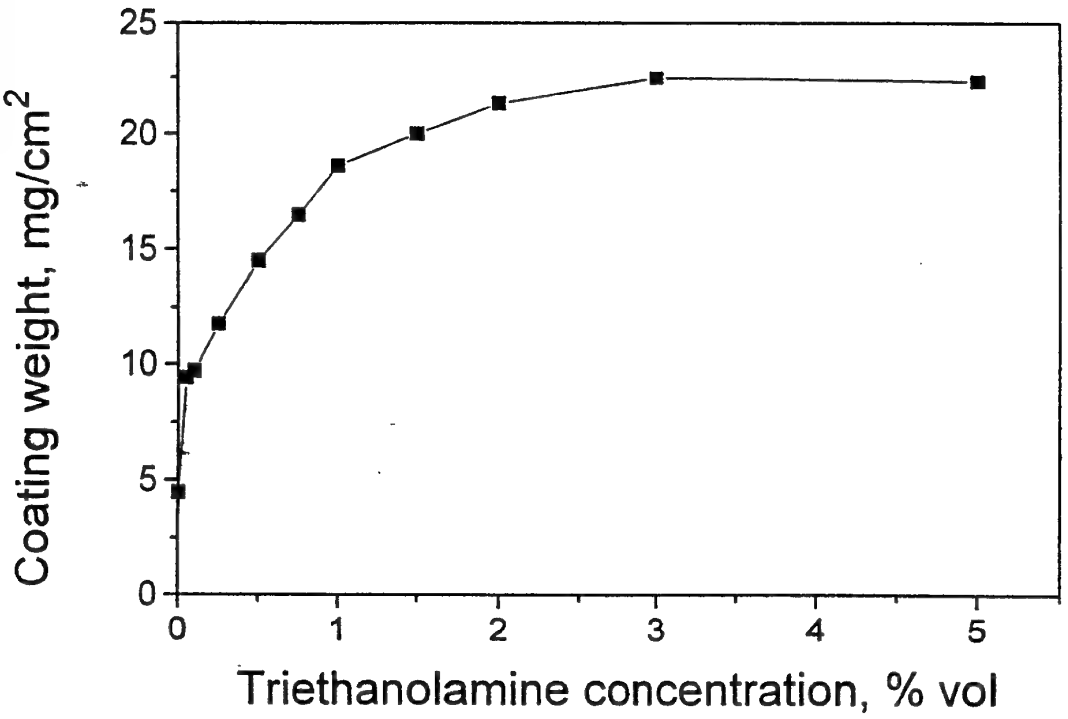

Fig. 6 - Effect of TEA on deposition rate from a suspension of 90% ZrO_2 + 10% Al_2O_3.

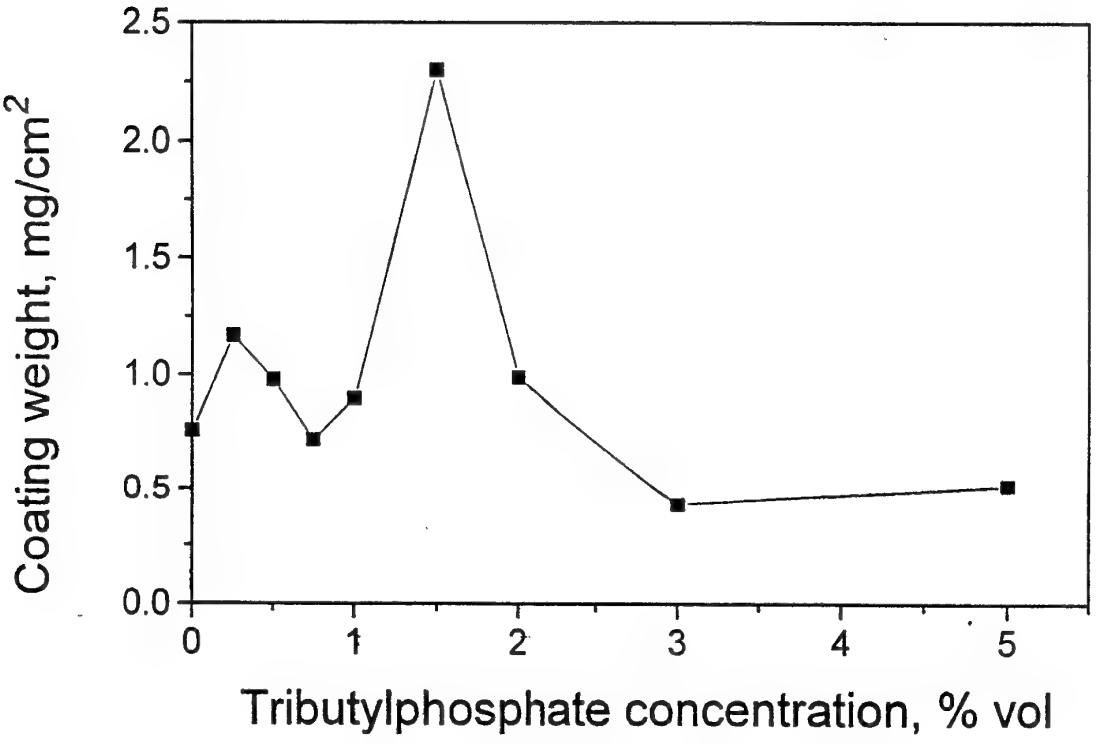

Fig 7 - Effect of TBPh on deposition rate from a suspension of 90% Al_2O_3 + 10% ZrO_2.

3.3 Stability of Suspension

The stability of suspension was studied by following the deposition rate of the powder from the same suspension as function of suspension age. Figs. 8 and 9 show the deposition rate from Al_2O_3 and 90% Al_2O_3 + 10% ZrO_2 suspensions in isopropanol with AcAc additive on consecutive five days.

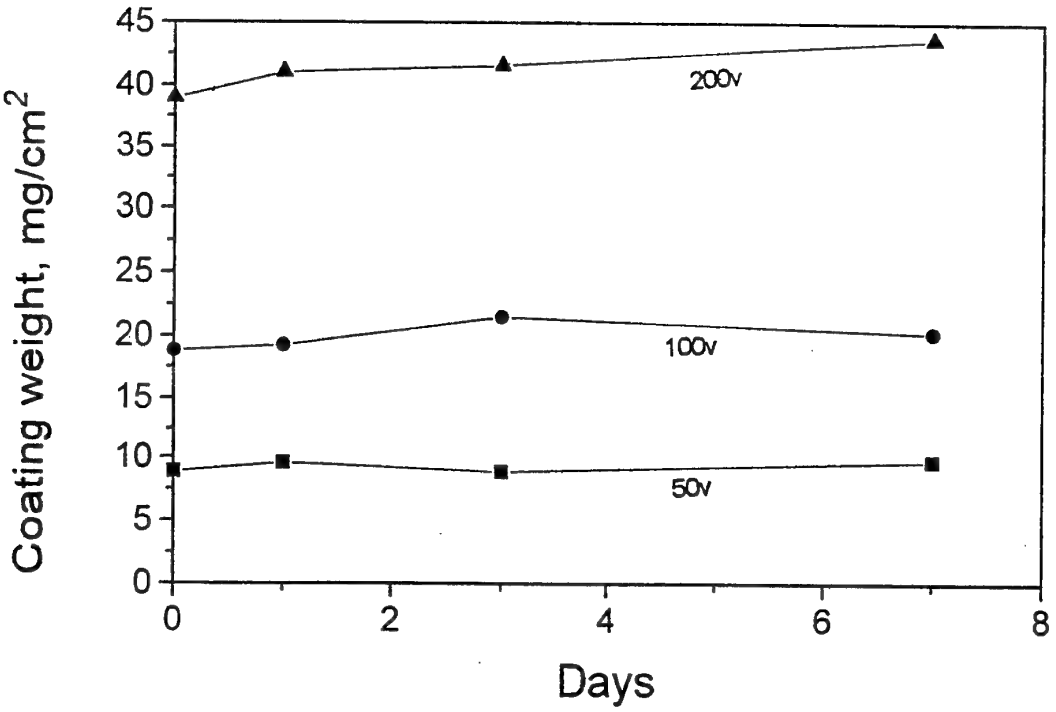

Fig. 8 - Coating weight as function of suspension age for 100% Al_2O_3 in isopropanol , 100 g/l, 60 sec.

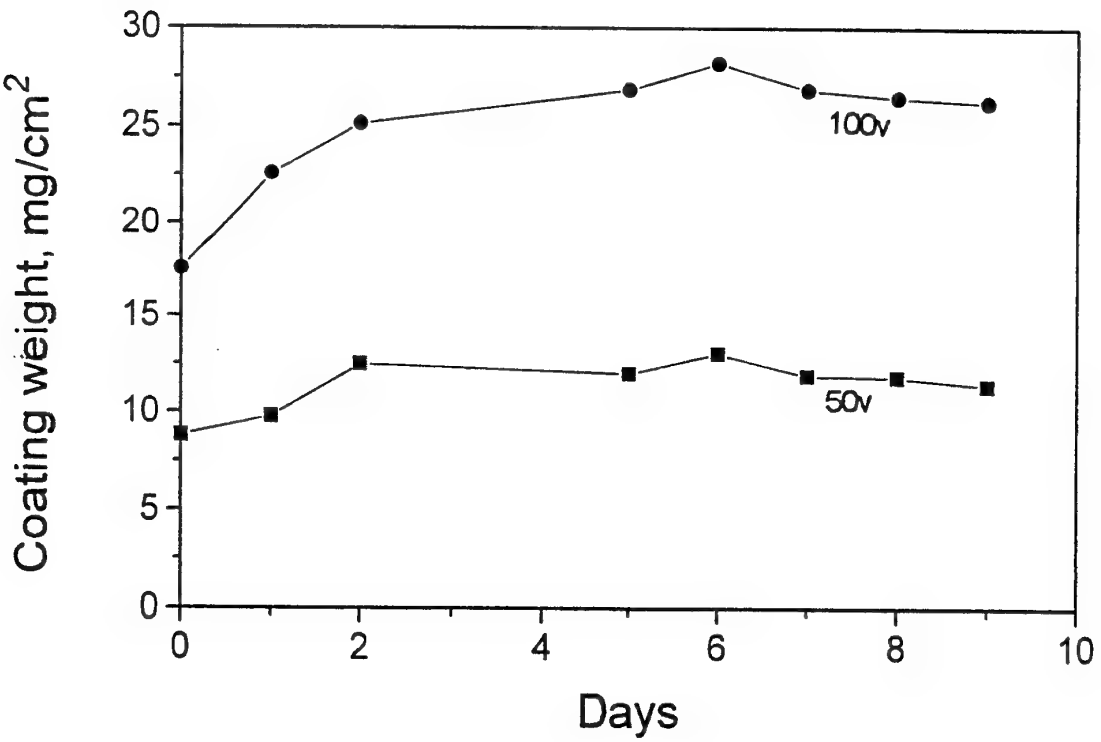

Fig. 9 - Same as in Fig. 8 for a suspension of 90% Al_2O_3 + 10% ZrO_2.

Both suspensions exhibit good stability. No variation in deposition rate was observed up to 9 days of suspension age.

3.4 Effect of particle size

The effect of particle size on deposition rate was studied in suspension of 90% Al_2O_3 + 10% ZrO_2 and 80% Al_2O_3 + 20% ZrO_2 . Figs. 10 and 11 show the variation of coating weight as function of AcAc conc. for suspensions with Al_2O_3 average particles sizes of three dimensions: 5μ, 0.5μ and submicron (0.03 μ). The ZrO_2 addition was of a constant particle size: 0.3 μ.

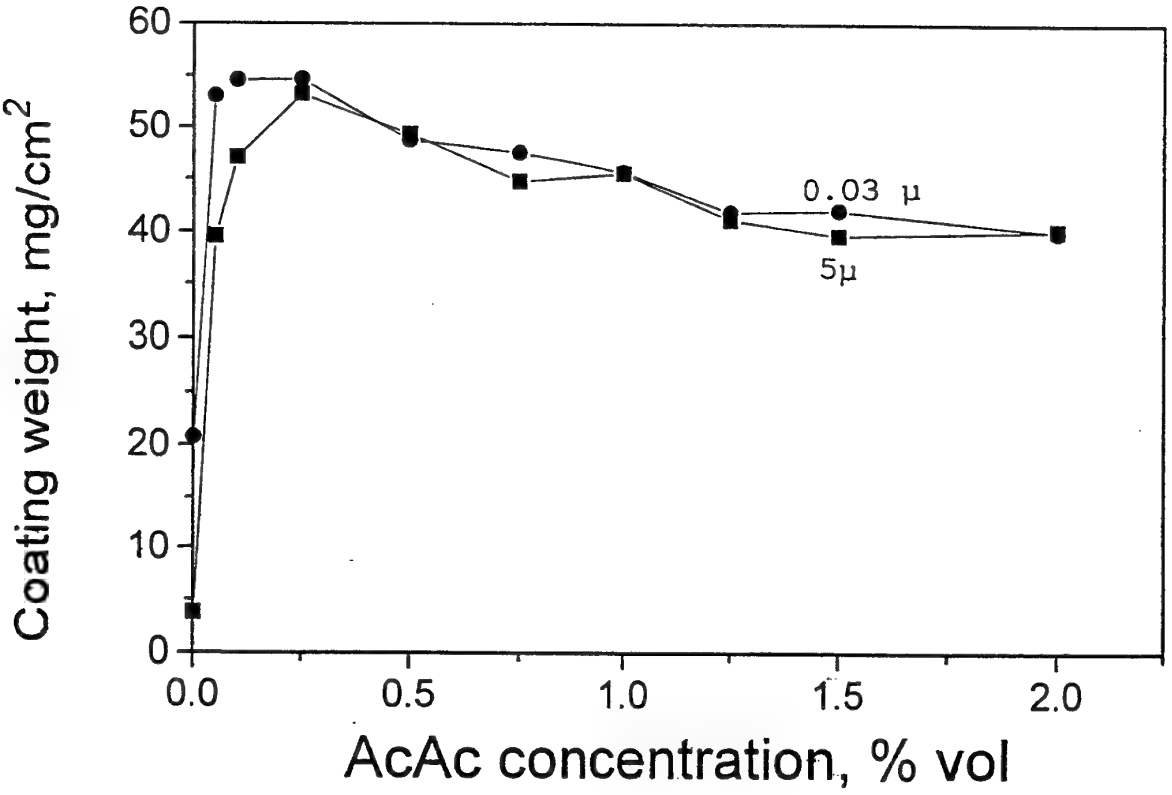

Fig 10: Coating weight as function of AcAc conc. for 5μ and submicron (0.03 μ) suspensions of 90% Al_2O_3 + 10% ZrO_2 in ethanol, 100 g/l, 100 v, 60 sec.

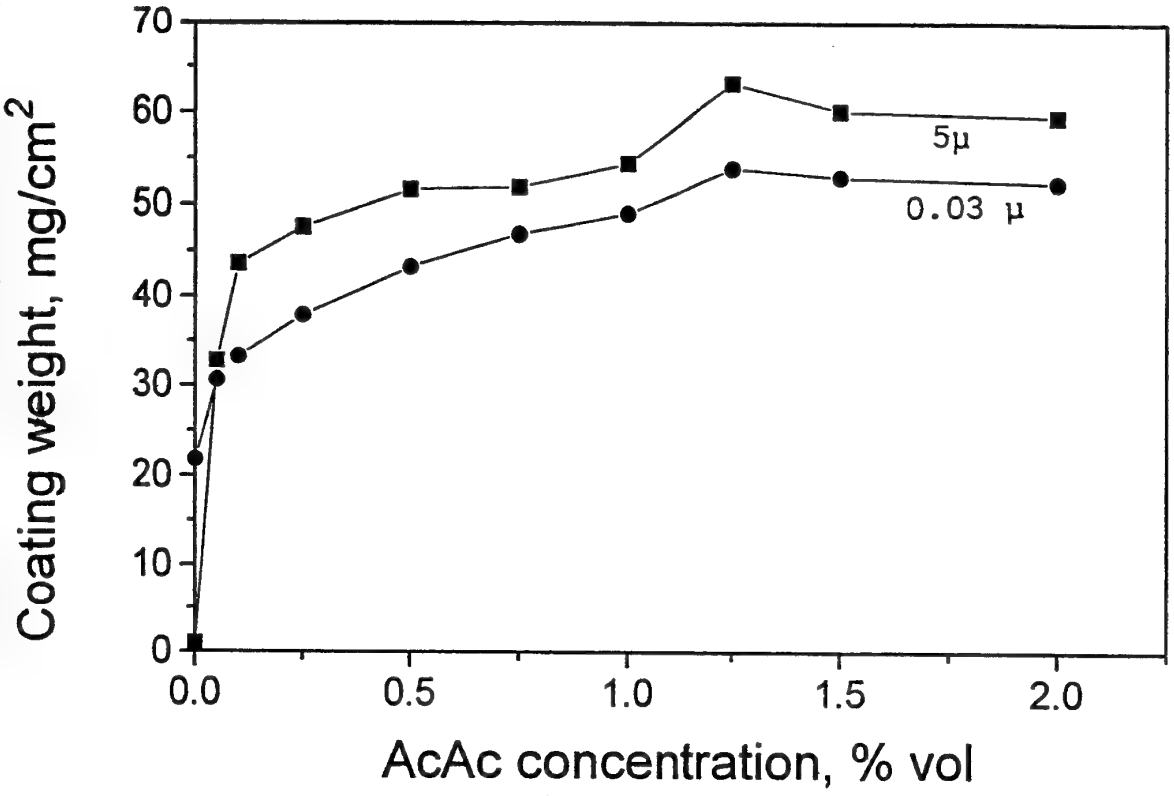

Fig. 11 - As in Fig. 10 but for a 80% Al_2O_3 + 20% ZrO_2 suspension.

As is seen in both suspensions a difference in deposition rate exists when no additives are present in the suspension with larger particles depositing at a lower rate. However upon addition of an effective additive (AcAc) the deposition rate becomes similar for all particle sizes.

3.5 Multilayer Deposition at Constant Current

In the previous stages of work, deposition of multilayer structures was performed at constant voltage. The reduction in layer thickness as result of the building - up of resistivity of the deposit was demonstrated and reported in the previous reports. Currently deposition experiments at constant current were performed and the variation of voltage was followed. Figs. 12-14 present this variation for three c.ds in a suspension of 85% Al_2O_3 and 15% ZrO_2 in a mixture of ethanol and MEK.

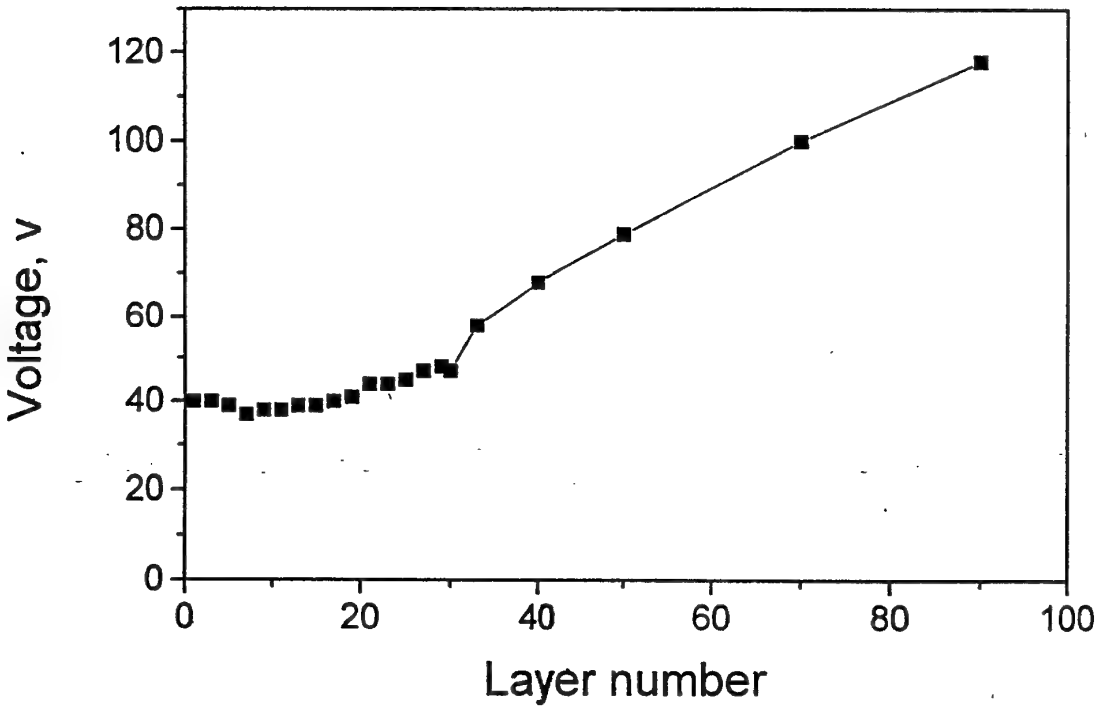

Fig. 12 - Variation of voltage as function of layer number in a suspension of 85% Al_2O_3 + 15% ZrO_2, at 0.2 mA/cm² (100 g/l, 100V, 60 sec.).

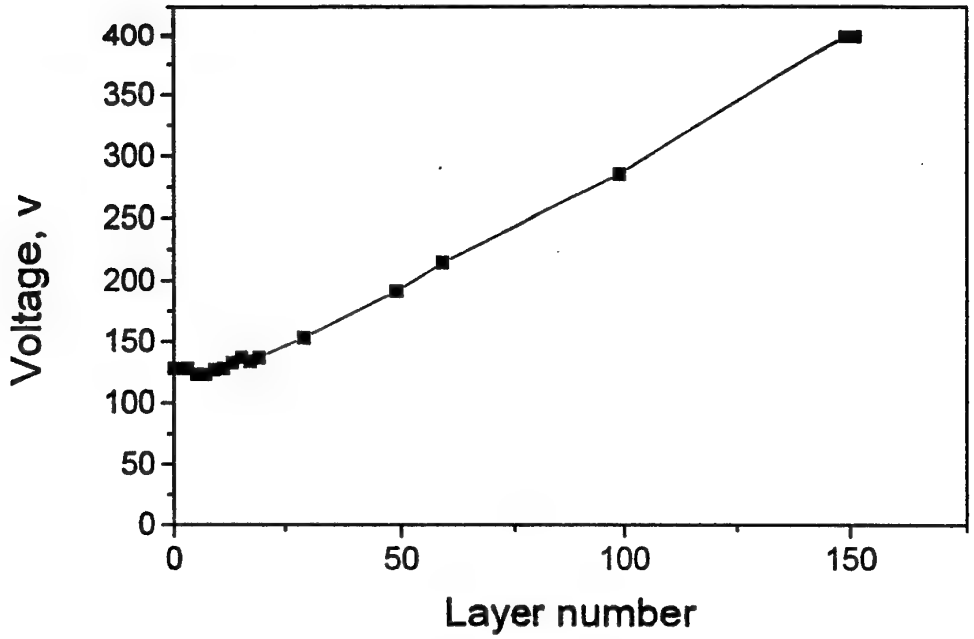

Fig 13 - As in Fig. 12 but c.d. 0.3 mA/cm²

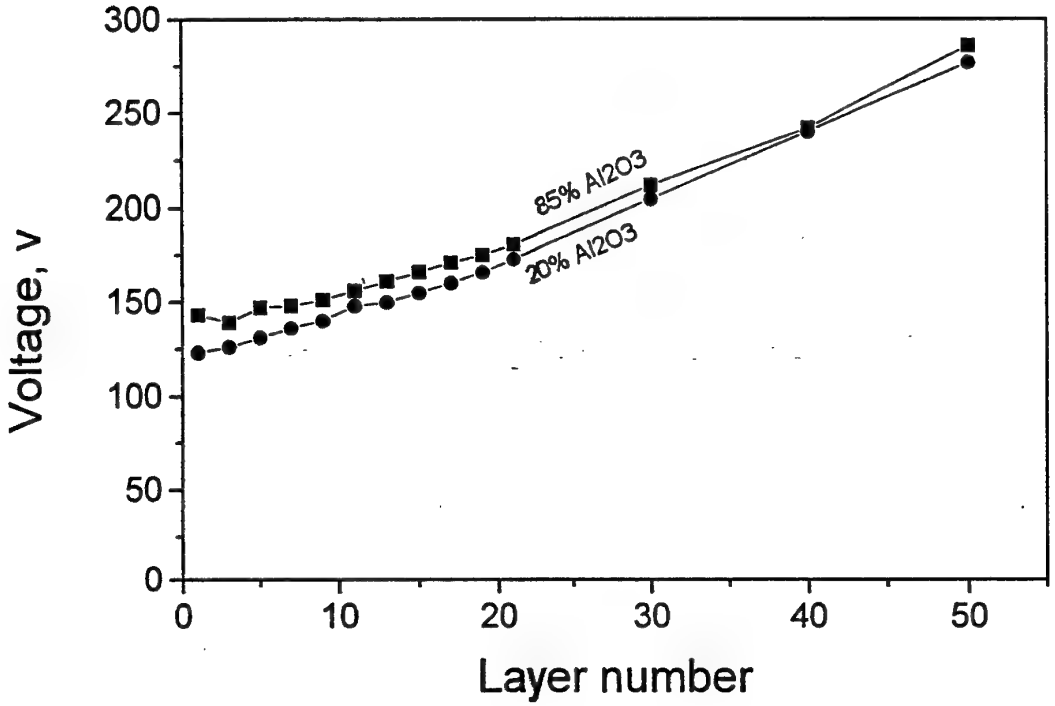

Fig. 14 - As in Fig. 13 but c.d. 0.4 mA/cm²

As was found in the previous experiments performed at constant voltage the resistivity build-up is not a monotonous function of deposit thickness. Up to a build-up of 20-30 layers (green thickness of about 0.6 mm) the voltage is almost unchanged and only after this thickness it starts to increase. This indicates that the porous nature of the deposit is able to sustain increase of current without voltage increase up to this thickness.

Chapter 4 - Summary and Future work

In the previous stage of this work initial mechanical testing was performed. The tests included 3 and 4 point bending tests and microhardness measurements. These tests were performed on beams of 20 mm length, 13 mm span and 1.85 mm in height. The layer thickness was about 15μ.

The MOR was found to be 895 MPa in the 3 point test and 587 MPa in the 4 point test. However, due to the small dimensions of the specimens particularly the overall thickness and due to the small layer thickness no evaluation of fracture toughness could be performed.

It was therefore the intention at this stage of work to scale-up the size of the specimens and of the layer thickness while maintaining a constant layer thickness through the whole crossection.

Extensive experiments were performed on preparation of round discs of 40 mm diameter and rectangular specimens of 45 X 45 mm with a thickness of >5 mm. Significant difficulties were encountered during above mentioned specimens preparation. These were related to:
Cracking of "green" specimen during removal from conductive substrate, cracking due to drying shrinkage, macro defects caused by localized accumulation of hydrogen produced at the cathode concurrent with particle deposition, deformation during sintering.

In order to improve specimen quality it was deemed necessary to optimize further conditions.

Since the Zeta potential is a crucial parameter in electrophoretic deposition both in rate of deposit formation as well as deposit quality (green and fired density, mechanical strength) the deposition rate which is proportional to the Zeta potential was used as a criterion in the majority of the experiments.

The previous stages work concentrated on isopropanol as solvent, Acetylacetone as additive, stainless steel as substrate material and experiments were performed at constant voltage.

In this stage experiments were performed in addition to isopropanol also in ethanol and mixtures of ethanol + MEK. Additives studied were also Fish Oil and Phosphate Ester, Al foil was used as substrate in addition to stainless steel and part of the experiments were performed at constant current regime.

It was found that pretreatment of powders has a strong effect on deposition rate, thus ball milling was found to enhance significantly the deposition of Al_2O_3 and sonication that of ZrO_2.

The type of solvent affects the deposition rate. Deposition rate increased in the following order:
isopropanol<ethanol<MEK + ethanol (40/60 volume ratio).

The type of additive was found to be selective as to the solvent and type of powder.

It was found that particles size affects deposition rate when no additives are present with larger particles depositing at a lower rate. However, upon addition of an effective additive, deposition rate is similar for the different particle sizes in the range studied (submicron - 5μ average particle size).

Stability of suspensions in presence of ACAC additive was found good.

Experiments at constant current regime showed that the resistivity of the deposit does not increase appreciably up to an overall thickness of about 0.8 mm. At this thickness the necessary voltage for further deposition increases sharply.
The regime of constant current enables to obtain a constant layer thickness as opposed to variation of layer thickness obtained in a constant voltage regime.

It is suggested to concentrate future work on preparation of scaled - up specimens based on the optimal conditions as found in this work.

Multilayer Ceramic Composite Formation by Electrophoretic Deposition

L. Gal-Or, S. Liubovich,
M. Folman, D. Sherman

Israel Institute of Metals
Technion Research and Development Foundation

Interim Scientific Report
May 1, 1994 - April 30, 1995
Research Project 524-702
F4 9620-93-1-0233

Prepared for
EOARD - London, England
AFOSR - Washington D.C., 20332, U.S.A.

REPORT DOCUMENTATION PAGE

Form Approved
OMB No. 0704-0188

1. AGENCY USE ONLY *(Leave blank)*	2. REPORT DATE	3. REPORT TYPE AND DATES COVERED
	30 June 1995	Annual 2, May 1994-April 30, 1995.

4. TITLE AND SUBTITLE

Multilayer Ceramic Composite Formation by Electrophoretic Deposition

5. FUNDING NUMBERS

F49620-93-1-0233

6. AUTHOR(S)

L. Gal-Or, S. Liubovich, M. Folman

7. PERFORMING ORGANIZATION NAME(S) AND ADDRESS(ES)

Technion R&D Foundation
Technion - Israel Institute of Technology
Senate House, Technion City, Haifa 32000, Israel

8. PERFORMING ORGANIZATION REPORT NUMBER

9. SPONSORING/MONITORING AGENCY NAME(S) AND ADDRESS(ES)

EORD 223&231 Old Marylebone Rd., London
NW1 5TH UK
AFOSR&NE Dr. A. Pechenik, Bolling AFB,
Washington DC 20332-6448

10. SPONSORING/MONITORING AGENCY REPORT NUMBER

11. SUPPLEMENTARY NOTES

12a. DISTRIBUTION/AVAILABILITY STATEMENT

Unlimited

12b. DISTRIBUTION CODE

13. ABSTRACT *(Maximum 200 words)*

The formation of multilayer ceramic composites by electrophoretic deposition is further studied in a system based on alternating layers of Al_2O_3 and ZrO_2. In a previous stage deposition rates of the ceramic particles were studied as function of deposition parameters such as electric field strength, particle concentration and deposition time. Green and fired densities of the deposits were studied and improved by use of appropriate additives. During this stage of the work the following aspects of the deposition process were studied: the variation of layer thickness during the deposition as a result of depletion of the suspension and increase in electric resistance of the growing deposit, variation in deposit thickness on substrate surface, planarity of the layers. Initial measurements of bending strength and layer hardness were performed.
Layered structures with up to 300 layers and total sintered laminate thickness up to 5.5 mm were prepared.

14. SUBJECT TERMS

Electrophoresis, ceramics, multilayer, microcomposites

15. NUMBER OF PAGES

16. PRICE CODE

17. SECURITY CLASSIFICATION OF REPORT	18. SECURITY CLASSIFICATION OF THIS PAGE	19. SECURITY CLASSIFICATION OF ABSTRACT	20. LIMITATION OF ABSTRAC
Unclassified	Unclassified	Unclassified	Unlimited

List of Personnel

Dr. L. Gal-Or - Principal Investigator

Mrs. S. Liubovich - Research Associate

Dr. O. Korotkina - Research Associate

Mr. R. Goldner - Student

Prof. M. Folman - Consultant

Dr. D. Sherman - Consultant

TABLE OF CONTENTS

CHAPTER 1 - INTRODUCTION

The objective of this project is to develop a method for formation of ZrO_2/Al_2O_3 multilayer composites based on electrophoretic deposition. The experimental foundation for the preparation of the composites has been laid in the first stage of the work (05.93-04.94). The most important results of this stage were the following:

- Submicron Al_2O_3 (Baikalox SM-8) and ZrO_2 (TOSOH TZ-12CE) particles suspended in isopropanol acquire spontaneously a positive charge and are deposited on the cathode.

- Acetylacetone additive (0.05-1.5 vol%) increases appreciably the zeta potential of both Al_2O_3 and ZrO_2 particles in isopropanol leading to a considerable improvement of suspension stability, an increase of the green density of respective deposits (to 60% of the theoretical value) and an increase of the deposition rate.

- Initial green and sintered a ZrO_2/Al_2O_3 laminar composites with a number of layers up to 80 and individual layer thickness in the range of 10-100 microns were formed. The composites are characterized by a well-defined and dense interface between layers and rather dense packing of grains was obtained.

During this year the following studies of the characteristics of multilayer structure formation were performed:

- Layer thickness variation and control during deposition
- Planarity of layers
- "Throwing power" - variation in deposit thickness on substrate area
- Variation in layer composition due to contamination of ZrO_2 suspension with Al_2O_3 and vice versa.
- Initial measurements of bending strength and layer hardness.

CHAPTER 2 - LITERATURE SURVEY

2.1 The Electrophoretic Mobility of Ceramic Particles

The electrophoretic mobility of a particle μ=V/E, V and E being the velocity and electric field strength respectively, is an extremely important characteristic for electrophoresis and electrophoretic deposition. In the previous report (05.93-04.94) the mobility - μ was briefly discussed and the Smoluchowski equation (valid for large particles in relatively concentrated solutions) was presented. In the present study the mobility of the suspended particles has been addressed in more detail.

When an electrically charged colloidal particle surrounded by a diffuse cloud of counterions moves under an applied electric field in a fluid, it is subjected to (1) an electric driving force (equal to the field times the charge of the particle); (2) Stokes' frictional resistance of a fluid and (3) forces (F' and F'') arising from the mutual interactions between the particle and its counterion cloud (see Fig. 1).

These mutual interactions may be simplified to two main effects:

- A moving particle under an applied electric field drags its double layer. In front of the particle fresh ions become attached to it as some are left behind. This reconstruction of the double layer does not take place instantaneously. The process requires time. The particle keeps moving with its ionic atmosphere. The ionic cloud acquires an egg shape [1] (fig. 1). Now the center of charge on the particle does not coincide with the center of charge of its oppositely charged cloud. An electric force F' develops between the particle and its lagging cloud in a direction opposite to the direction of the driving force (the externally applied electric field), retarding the particle.

- An applied electric field acts not only on the particle but also on its counterions. Clearly counterions tend to move in a direction opposite to that of the particle trying to carry the particle along with them. One more retarding force F'' arises, (see Fig. 1).

Taking into account all the forces acting on a particle Henry (1931) obtained the following expression [in 2] for the mobility μ ($= \frac{V}{E}$):

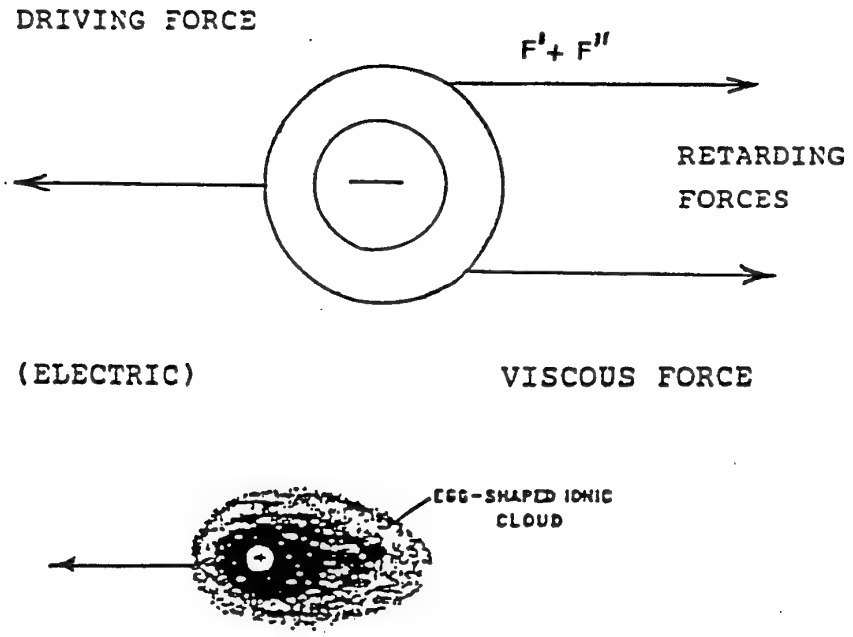

Fig. 1 Egg-shaped ionic cloud and forces acting on a moving particle

$$\mu = \frac{\epsilon \zeta_p}{6 \in \eta} \cdot f(Kr) \qquad (1)$$

where:

V	- electrophoretic velocity
μ	- mobility
E	- electric field strength
ϵ	- dielectric constant of a fluid
ζ_p	- zeta potential of a particle
η	- viscosity of fluid
K	- 1/double layer thickness
r	- radius of a particle
f(Kr)	- the Henry numerical correction factor

The function f(Kr) depends on the particle shape and, for a sphere, its values are given in Table 1 [2] and Fig. 2 [3].

For very small particles in dilute solution where the double layer thickness K^{-1} is large so that $Kr \rightarrow 0$ the correction factor $f(Kr) \rightarrow 1{,}0$. However, for large particles in more concentrated solutions $Kr \rightarrow \infty$ (in practice >100) and $f(Kr) \rightarrow 1.5$. If the particles conduct electricity, a further correction is needed.

Table 1 [2] Values of the Henry correction factor f(Kr) as a function of Kr

Kr	f(Kr)	Kr	f(Kr)
0	1,000	5	1,160
1	1,027	10	1,239
2	1,066	25	1,370
3	1,101	100	1,460
4	1,133	∞	1,500

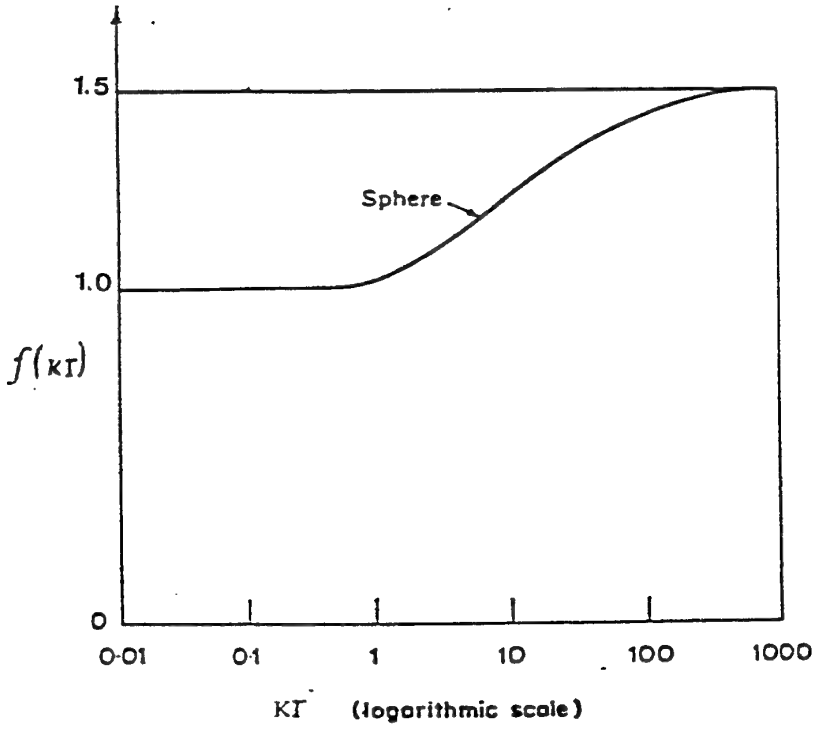

Fig. 2. The variation of the numerical correction factor f(Kr) with the ratio of the radius r of the particle to the effective thickness K^{-1} of the diffuse-charge region.

The important conclusion deduced from equation (1) is that larger particles have higher electrophoretic mobilities than smaller ones.

If only the driving electric force and the retarding viscous force are taken into account then the Stokes' law approach gives the Hückel equation for μ and the electroosmotic approach gives the Smoluchowski equation.

The Hückel equation

$$\mu = \frac{\epsilon \zeta_p}{6\pi\eta} \qquad (2)$$

with f(Kr) = 1 is a particular case of eq. (1) for rK $\ll$ 1 (the particle is small compared with the thickness of the double layer).

The Smoluchowski equation

$$\mu = \frac{\epsilon \zeta_p}{4\pi\eta} \qquad (3)$$

with f(Kr) = 1,5 is another special case of eq. (1) for rK $\gg$ 1 (the particle is large in comparison with the double layer thickness).

2.2 Kinetic aspects of electrophoretic deposition

When applying electrophoretic deposition as a technique for consolidation of ceramic particles the control over the thickness of the deposit is of extreme importance. The electrophoretic yield is given by [4]

$$W = A\int \mu ECS \, dt \qquad (4)$$

where
- W – the weight of a deposit
- A – yield constant
- $\int \mu$ – mobility of a particle
- E – field strength
- C – particles concentration
- S – area of an electrode
- t – deposition time

The yield constant A characterizes the deposition efficiency. It is equal to 1 when all the particles having reached an electrode are deposited on it, the efficiency being 100%. Usually the efficiency is much lower partly due to concurrent electrolytic reactions and partly due to the mechanism of the electrodeposition itself. An efficiency of 13–15% was reported in [5].

The dependence $W = f(t)$ is complicated. The kinetic models of Y. Hirata et al. [5] and Z. Zhang et al. [6] represent approximations to equation (4).

2.2.1 The kinetic model of Y. Hirata et al. [5]

Hirata et al. [5] assumed that (1) the solid particles concentration C in a suspension and (2) the electric field strength E across the suspension (determining the velocity of a particle $V = \mu E$) do not change during the electrophoretic deposition process.

From Faraday's law they derived

$$dw = \mu ECS\, dt \qquad (5)$$

And for c = const and E const the linear dependence of the weight of a deposit on deposition time was obtained:

$$W = \mu Ecst \qquad (6)$$

Studying electrophoretic deposition of α - alumina particles from aqueous suspensions at pH = 2,5 they obtained a linear dependence of W on t in agreement with their kinetic model.

Linear dependencies $W = f(t)$ and $W = f(E)$ were also reported in [7] where electrophoretic deposition of Al_2O_3 articles ($<1\ \mu m$) from ethanol-based suspensions stabilized with polyacrylic acid was studied.

The assumption of a constant particle concentration during deposition is not realistic. The assumption of a constant electric field strength across the bulk of a suspension during deposition is not realistic as well. With the growing of the deposit its electrical resistance ΔR increases. Therefore, the potential drop across the deposited layer ΔE increases and the potential drop across the bulk of the suspension decreases from E to $E-\Delta E$.

It is obvious that the linear dependence W = f(t) (eq. (5) and (6)) is only the first approximation to the complicated dependence w = f(t). Only when the initial concentration of solids is high enough in comparison with the weight of the deposit and the externally applied electric field strength E is much higher than the potential drop across the deposit, the linear dependence w = f(t) is valid. Those are the conditions of the initial stage of deposition. And the Hirata approximation is valid only at initial deposition stage.

2.2.2 The kinetic model of Z. Zhang et al. [6]

Z. Zhang et al. [6] suggested another dependence w = f(t). They also relied on Faraday's law eq. (5) $\frac{dW}{dt} = \mu ECS$. But they took into consideration the decrease of concentration of the suspension during electrophoretic deposition

$$C = \frac{W_0 - W}{u}$$

where W_0 – the initial weight of solids in the suspension
W – the weight of the deposit
u – the volume of the suspension

The following W = f(t) dependence has been obtained:

$$W = W_0(1 - e^{-K_1 t}) \qquad (7)$$

$$\frac{dW}{dt} = W_0 K_1 e^{-K_1 t} \qquad (8)$$

where the kinetic constant K_1 is equal to:

$$K_1 = \frac{S}{u}\mu(E - \Delta E) \qquad (9)$$

Equations (7) – (9) describe the Zhang's kinetic model of electrophoretic deposition. Eq. (8) shows that the rate of deposition, dw/dt, is an exponential function of time (according to Hirata's model dw/dt = const) and depends on the kinetic constant K_1. If the kinetic constant is larger the initial rate of ED is higher, but the rate decreases faster.

It must be noted that when the operation time is very short, $t \to 0$, equation (7) becomes Hirata's eq. (6):

$$W = W_0 K_1 t$$

or, substituting eq. (9) for K_1

$$W = \mu E C s t \qquad (6)$$

The Hirata et al. model [5] in which a linear function of W and t is expected is a special case of the more general Z. Zhang et al. model.

The experimental dependence W = f(t) obtained by Z. Zhang et al. [6] for ZrO_2/SiC (whiskers) composite agreed with their predictions based on eq. (7) and (8)) (see Fig. 3).

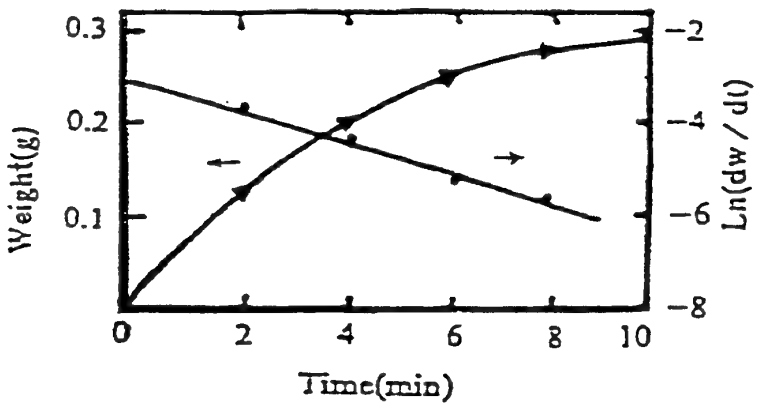

Fig. 3 Deposit weight versus deposition time

Non-linear dependences W = f(t) when the rate of deposition decreases with deposition time are usually reported for electrophoretic deposition of ceramic particles (18, 9, 10, for example), but no information is available to what extent they correspond to the exponential dependence of Zhang et al. (eq. (7) - (9)).

Zhang et al. also measured the electric field drop ΔE, across the growing deposit at different thicknesses $\Delta \ell$. They obtained a linear dependence of ΔE on $\Delta \ell$:

$$\Delta E = f \times \Delta \ell.$$

The coefficient f depends on the conductivity of the ceramic powder and the density (porosity) of the deposit. The experimental results are presented in Fig. 4.

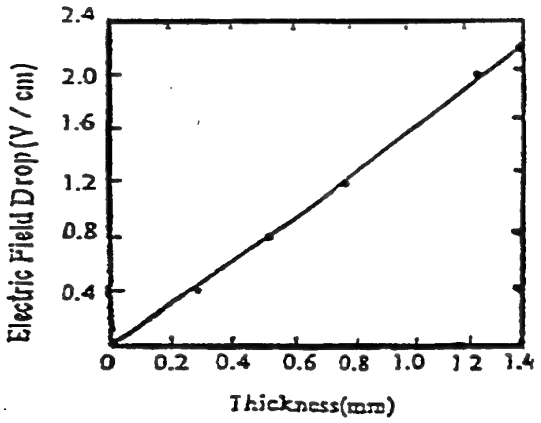

Fig. 4 Electric field drop versus thickness of deposit.

The kinetic model of Z. Zhang et al. described by eqs. (7) - (9) does not account for the variation of the electric field drop across the suspension (from E to E-ΔE) during the deposition, the kinetic constant K_1 being assumed to be invariable. It is, in fact, not consistent with the experimental results.

The Zhang et al. exponential dependence of deposition rate on time is an approximation of a more general and complicated dependence W = f(t) as is the Hirata et al. linear dependence w = f(t). But Zhang's approximation is of a higher order than that of Hirata's.

The Zhang kinetic model is valid for small ΔE/E. In their system [6] they found for $\Delta\ell$<1,0 mm, that ΔE/E < 7.5% and is too small to affect the kinetic constant K_1, so it can be neglected. Only for $\Delta\ell$ substantially higher than 1,0mm the influence of ΔE on K_1 cannot be ignored.

The growing deposit has, in fact, two effects on the deposition rate:

- One of them has just been discussed. The decrease of the electric field drop across the suspension from E to E-ΔE lowers electrophoretic velocity of a particle and hence the deposition rate.

- The increasing electrical resistance of a growing deposit presents a higher resistance path for ions through the deposit hindering charge transfer reactions and slowing the deposition rate.

2.2.3 The thickness and density of a growing deposit

R. Nass et al. [7] measured the density of alumina compacts of different thickness in the range of 0.2mm–1.5mm. The compacts were deposited form ethanol suspension stabilized with polyacrylic acid. Alumina particles less than 1 μm were used. The results shown in Fig. 5 were unexpected.

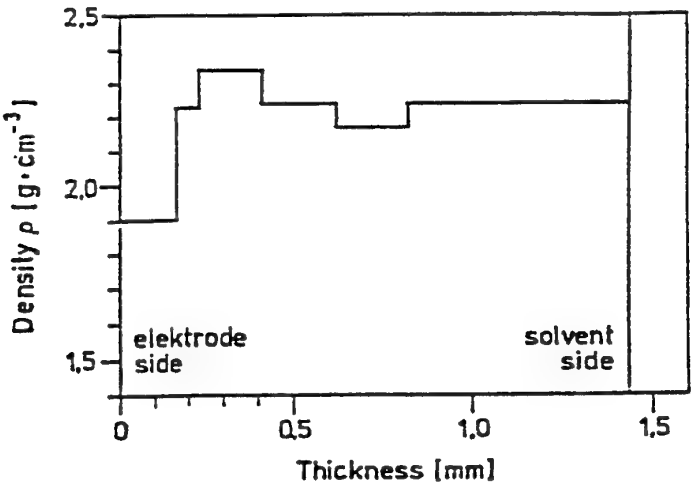

Fig. 5 Density as a function of the deposit thickness

The density of the first layer (200 μm) was found to be significantly lower (1.9 gr/cm^3) than the overage density of the deposit (2.25 gr/cm^3). Moreover, the density does not vary monotonically but rather periodically.

SEM micrographs indicated that the deposit surface which faces the solvent exhibited a homogeneous microstructure with densely packed particles. In contrast, the microstructure of the surface facing the substrate was more heterogeneous containing agglomerates and large pores. Determined by the Hg–penetration method, the pore size distribution of the first layer showed a higher number of pores which are larger than 10 μm.

The authors observed the formation of a porous layer adjacent to the substrate for different suspensions and deposition parameters. They studied the influence of the deposition voltage on the layer density. The results are shown in Fig. 6.

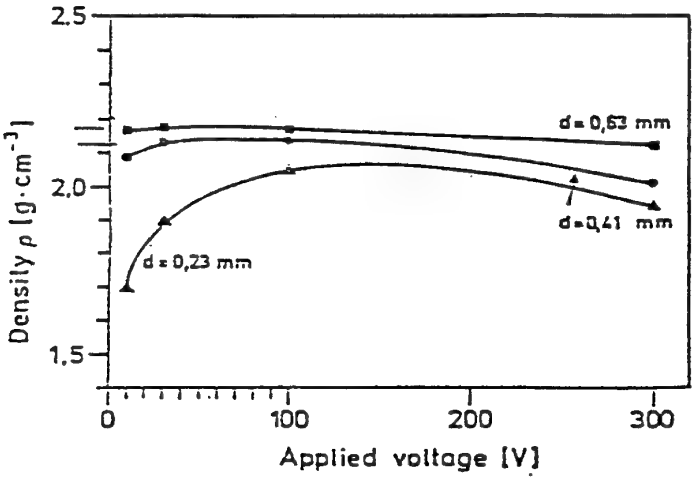

Fig. 6 Density versus applied voltage for green layers of different thickness.

The density of the first deposited layer (0.23 mm thick) varies noticeably with the variation of voltage. The effect of the applied voltage on the density of the thicker layers (with the density approaching the average density) is not so distinct.

Nass et al., suggested that the formation of a porous layer with a distinct thickness is likely to be attributed to the mechanism of the deposition process and discharge of the particles. However, no further explanation was given by the authors.

Similar results were reported also in the article by Y. Hirata et al. [5] (section 2.2.1). The weight W of deposits and their thickness $\Delta\ell_{mes}$ were measured at different deposition times. The thickness was measured $\Delta\ell_{mes}$ by means of a micrometer with an accuracy of $\pm$ 0.01 mm. In addition to the calculated thickness $\Delta\ell_{cal}$ was determined from the weight of the deposit.

$$\Delta\ell_{cal} = \frac{W}{\rho S}$$

where ρ – density of deposit

S – surface area of substrate

Figure 7 presents the comparison of the calculated (dotted lines) and measured thickness

of an alumina layer as function of deposition time.

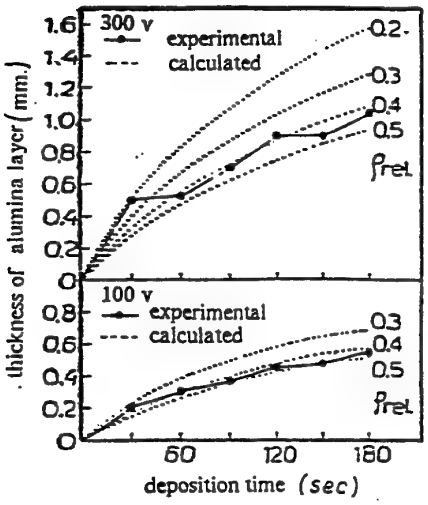

Fig. 7 Comparison of calculated and measured thickness of alumina layers as function of deposition time at 100 and 300 v

The experimental results demonstrate that:

- a porous alumina layer (with a comparatively low density) is formed at early deposition times and grows densely with time;
- the alumina layer grows with alternative increase in density and thickness with deposition time.

The authors do not give an explanation for this phenomenon. The experimental results presented in [5] and [6] are unexpected. Possibly the following rough and approximate model will help to understand the phenomena to some extent.

As it has been indicated above (section 2.1) large particles move electrophoreticcally somewhat faster than smaller ones. Therefore, at an early deposition time the deposit might be enriched with large particles and characterized by loose packing, large voids and a heterogeneous microstructure. The growing heterogeneous structure triggers a well-known self-correcting growth mechanism based on the fact that a region of lower thickness has a lower resistance and therefore the deposition rate on it will be higher. In the "healing" process of the deposit smaller particles are more effective because of steric reasons. Thus a porous layer is followed by a more dense deposit.

It is obvious that further experiments are required in order to elucidate fully the mechanism.

CHAPTER 3 – MATERIALS AND METHODS

a) Ceramic Powders

– A submicrometer alumina powder Al_2O_3 (Baikalox SM–8) acquired from Baikowski Ceramic Aluminas, USA.

Table 2: Properties of Baikalox SM–8 alumina powder

Purity, $\%Al_2O_3$	99.99
Specific surface area B.E.T.m^2/g	10 ± 1
Major phase	alfa
% Major phase	95%
Crystal Density g/cm^3	3.98
Bulk density g/cm^3	0.93
Pressed density 2200 PSI g/cm^3	1.85
Ultimate particle size, microns	0.15
Loss on ignition, %	–

Table 3: The Baikalox SM–8 Al_2O_3 particles size distribution

Size Distribution	% weight
$<0.3\mu m$	65
$<0.4\mu m$	78
$<0.5\mu m$	90
$<0.6\mu m$	95
$<1.0\mu m$	100
$<2\mu m$	--
$<5\mu m$	--

Table 4: Chemical analysis - Baikowski Aluminas (99.99% purity)

Element	Na	K	Si	Fe	Ca
Typical value of impurities ppm	8	35	35	6	3

- Submicrometer zirconia partially stabilized with CeO_2 acquired from TOSOH Zirconia Process Company, grade TZ-12CE with following characteristics:

1. Chemical composition of ZrO_2 powder:

Table 5 Chemical Analysis in wt%

CeO_2	Al_2O_3	SiO_2	Fe_2O_3	Na_2O	Ig. loss
16.69	-	<0.002	0.004	0.021	0.43

2. Crystallite Size 234 Å
3. Specific Surface Area 9.4 m^2/g

b) Solvent

- Isopropanol, its relevant properties according to literature data (room temperature) are:

Density	0.785 g/cm³
Boiling point	82.3°C
Surface tension	22mN/M
Dielectric constant ϵ	18
Viscosity	2.4 cp
ϵ/η	7.5

c) Additive

- Acetylacetone (2.4-Pentadion), $CH_3COCH_2COCH_3$, Ar Grade

d) Substrate

- Stainless steel (AISI 316) discs ϕ 35.4 mm and 6 and 15 mm thick.

e) Electrophoretic deposition

- Deposition was carried out from four kinds of isopropanol suspensions with 1.5% (v/v) AcAc

1. Al_2O_3
2. ZrO_2
3. 96% (w) Al_2O_3 + 4%(w) ZrO_2
4. 50% (w) Al_2O_3 + 50% (w) ZrO_2

Stirring was applied during deposition.

Preparation of specimens

Specimens were cleaned ultrasonically in ethanol for 5 min and dried in an oven with air circulation at 200°C for 10 min.

Experimental set-up

The experimental set-up is shown in Fig. 8. To minimize edge effects the ratio of the anode to cathode areas was 1:12.5.

Deposition parameters

1. Particle concentration - 100 g/l
2. Electric field intensity - 100v/cm - 300v/cm
3. Deposition time - 10-120 sec
4. Temperature - room
5. Distance between electrodes - 17 mm

f) Removal of composites from substrate

- Removal of a green ceramic compact from a substrate without damaging it is a very difficult task. At the first stage of the work a blade was used for removal of a green multilayer compact from the stainless steel cathode. Short dipping of the deposit in glycerol immediately after its removal from the deposition cell was necessary to make it more flexible and to facilitate the removal from the substrate without damage. As it has been pointed out, the technique is far from perfect. Sometimes bending of the deposit layer occurred causing its cracking.

1- Power supply
2- Ammeter
3- Voltmeter
4- Suspension
5- Teflon cover
6- Thermometer
7- Holder
8- Stainless steel anode
9- Cathode (specimen)
10- Stirrer
11- Plate

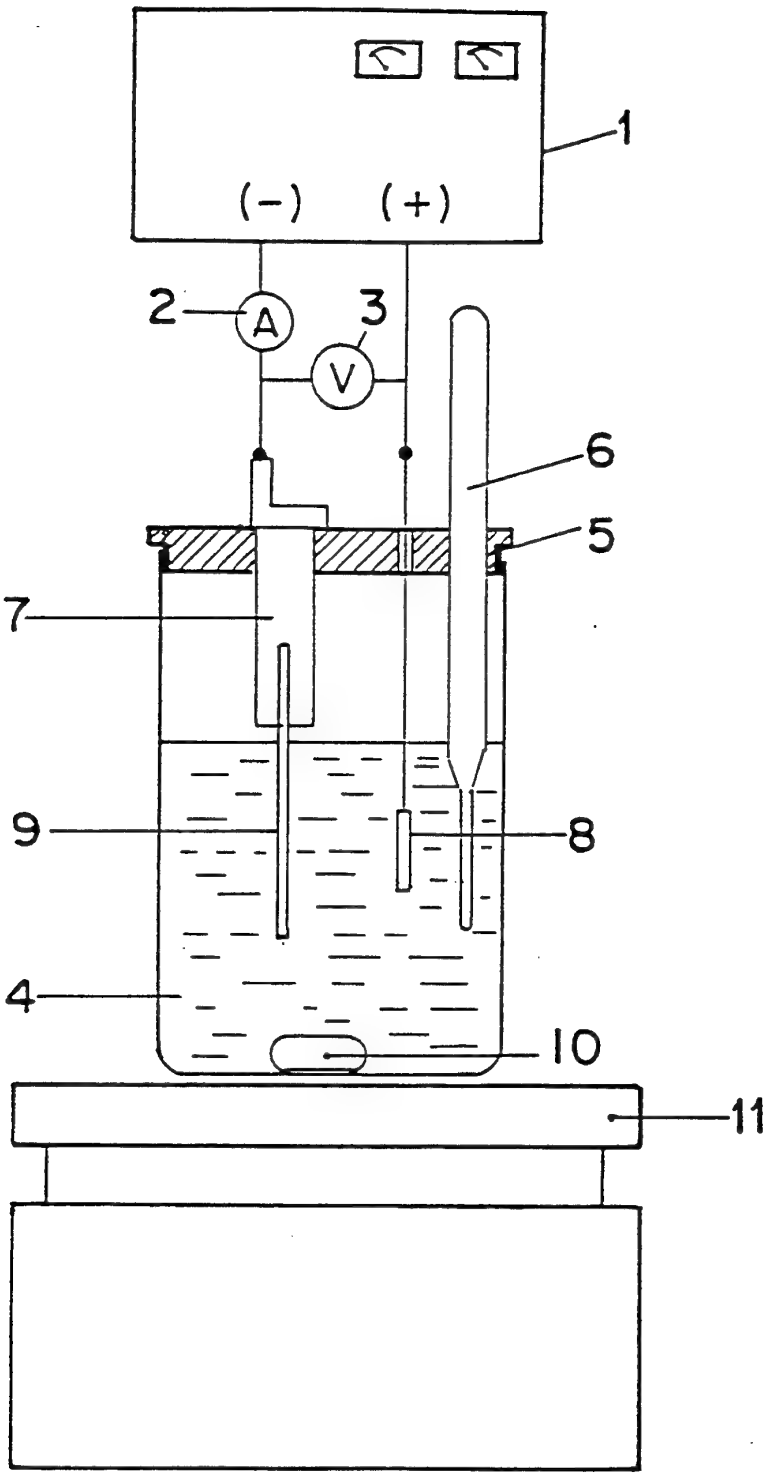

Fig. 8: Experimental set-up for electrophoresis

During this stage we have continued to search for a better technique. Coating of the stainless steel substrate with a thin layer of teflon was tried without improvement (Fig. 9). The next step was the use of a thin 0.015 mm aluminium foil (Fig. 10). The removal of the green deposit form the stainless steel cathode covered with the foil did not require any blade, the hazard of damaging of the composite being minimized.

Nevertheless, this technique has its difficulties. It has proven to be almost impossible to avoid any defect on the surface of a very thin aluminium foil covering the substrate. The defects cause uneven growth of the deposit and may lead to cracking during drying and sintering.

The use of a thin aluminum foil although it facilitated considerably the removal of the green deposit from a substrate it has not fully solved the problem. Further work in this direction is required.

g) **Drying and sintering**

Multilayered composites of 1.5-6mm thickness removed from a substrate were immediately placed in a desiccator over a 10% solution of glycerol in propanol for 168h/one week). After that they were dried in air at room temperature for 24 hours. The composites were transferred into an oven for final slow drying and sintering. The schedule was as follows:

Rate of heating, °C/min	Heating temperature,°C	Time of exposure, hour
0.6	50	10
"	100	10
"	200	3
"	900	-
1.7	1500	2
"	1600	2
Rate of cooling °C/min	Cooling temperature,°C	Time of exposure, hour
3	to 600°C	-
uncontrolled	to room	-

Table 6: The schedule for final slow drying and sintering

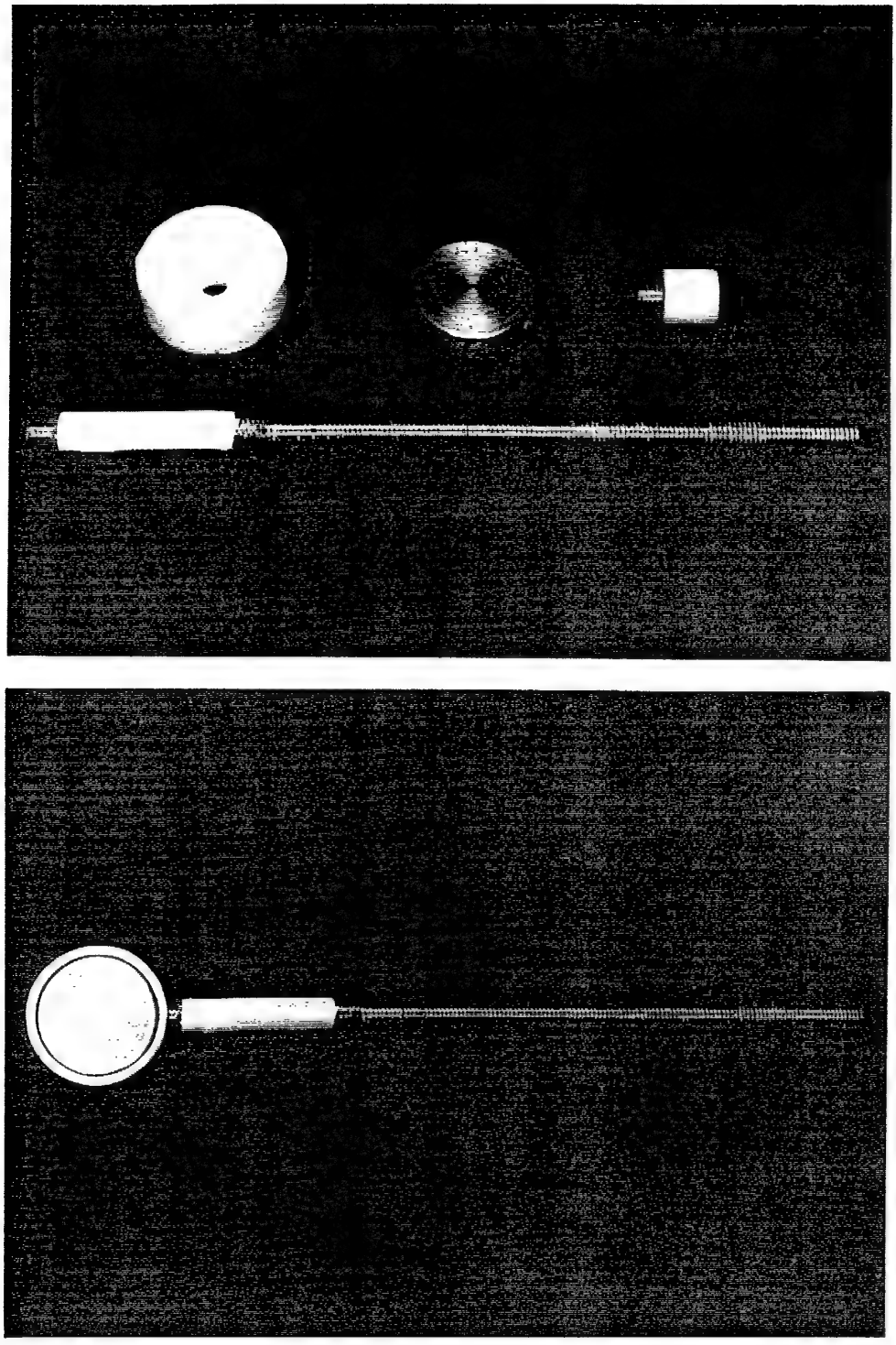

Fig. 9: The teflon frame device for the stainless steel substrate

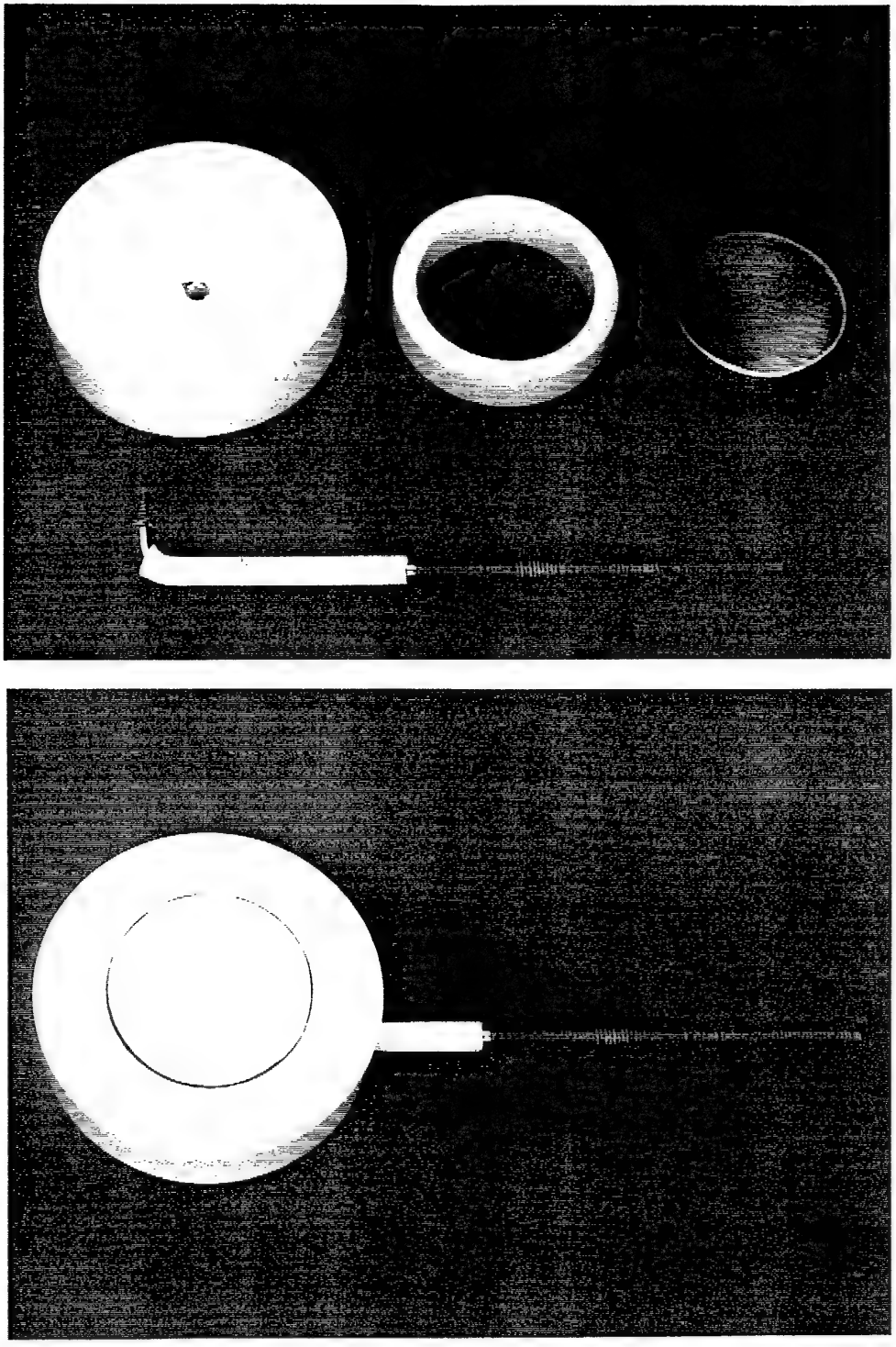

Fig. 10: The teflon sleeve device for a foil covered substrate

h) Testing of deposits

The microstructure and composition of deposits were studied by an electron microscope (JEOL 840 SEM) on polished cross-sections:
The sintered specimens were embedded in an Epofix (Struers) resin and cured for 24 hours at room temperature. The composite blocks with cut specimens were polished with SiC paper (400-2000 grits) and then with a diamond paste of 0.25 μm grain size.

i) Measurement of deposit resistance and thickness

The resistance ΔR of a growing deposit was determined as follows:
- According to Ohm's law the resistance R of a conductor is given by

$$R = \frac{V}{I}$$

where V - external applied voltage across a conductor
I - current flowing through a conductor
Before the deposit was formed ($\Delta\ell$=0), the initial electric current I_0 under the applied voltage V was recorded. The resistance of the suspension R_s was computed:

$$R_s = \frac{V}{I_0}$$

- At the end of the deposition when the deposit thickness reached $\Delta\ell$ the diminished electric current $I_{\Delta\ell}$ was recorded. The resistance R comprising the suspension resistance (R_s) and the deposit resistance (ΔR) was computed:

$$R = \frac{V}{I_{\Delta\ell}}$$

- The resistance of a deposit with a $\Delta\ell$ thickness is equal to:

$$\Delta R = R - R_s = \frac{V}{I_{\Delta\ell}} - \frac{V}{I_0}.$$

Then the deposit was removed form the bath and dried to a constant weight. The thickness of the green deposit was computed form its weight W, green density ρ and surface area S:

$$\Delta\ell = \frac{W}{\rho \cdot S}$$

Note: green density was taken to be ρ=60% of theoretical density.

CHAPTER 4 - RESULTS AND DISCUSSION

In the first year of the research project the experimental foundation for the formation of ZrO_2/Al_2O_3 multilayer composites has been laid and initial green and sintered structures with a number of layers up to 80 and individual layer thickness in the range of 10-100 microns were obtained.

In the second year of the research the formation of laminar structures with a higher number of layers was initiated. Studies of the characteristics of multilayer structure formation were also performed. The studies related to:

- Layer thickness variation and its control during deposition
- Variation of deposit thickness on the substrate area (edge effects)
- Planarity of layers
- Variation in layer composition due to mutual contamination of the ZrO_2 and Al_2O_3 suspensions.

4.1 Laminar structures with a higher number of layers

Laminar composites of three types were fabricated:

- ZrO_2/Al_2O_3 multilayers received from ZrO_2 and Al_2O_3 suspensions
- ZrO_2/Al_2O_3 + ZrO_2 multilayers received from ZrO_2 and 96 weight % Al_2O_3 + 4 weight % ZrO_2 suspensions
- ZrO_2/Al_2O_3 + ZrO_2 received from ZrO_2 and 50 weight % Al_2O_3 + 50 weight of ZrO_2 suspensions.

It must be noted that the composition of a mixed (Al_2O_3 + ZrO_2) layer cannot be expected to be the same as the composition of the respective suspensions because the deposition rates of ZrO_2 and Al_2O_3 differ considerably, see previous report (section 4.5, 1994).

Multilayered composites of the three types with 100-300 layers and 1-5mm total thickness (in sintered state) were fabricated. Individual layer thickness was in the range of 5-100 μm.

Fig. 11 shows an optical micrograph of the cross-section of a sintered 160 layers laminated structure with a total thickness of about 3mm at a magnification of 50. The thickness of Al_2O_3 + ZrO_2 layers (dark layers) is in the range of 5-38 μm. The thickness of the ZrO_2 layers (light layers) is in the range of 20-35μ.

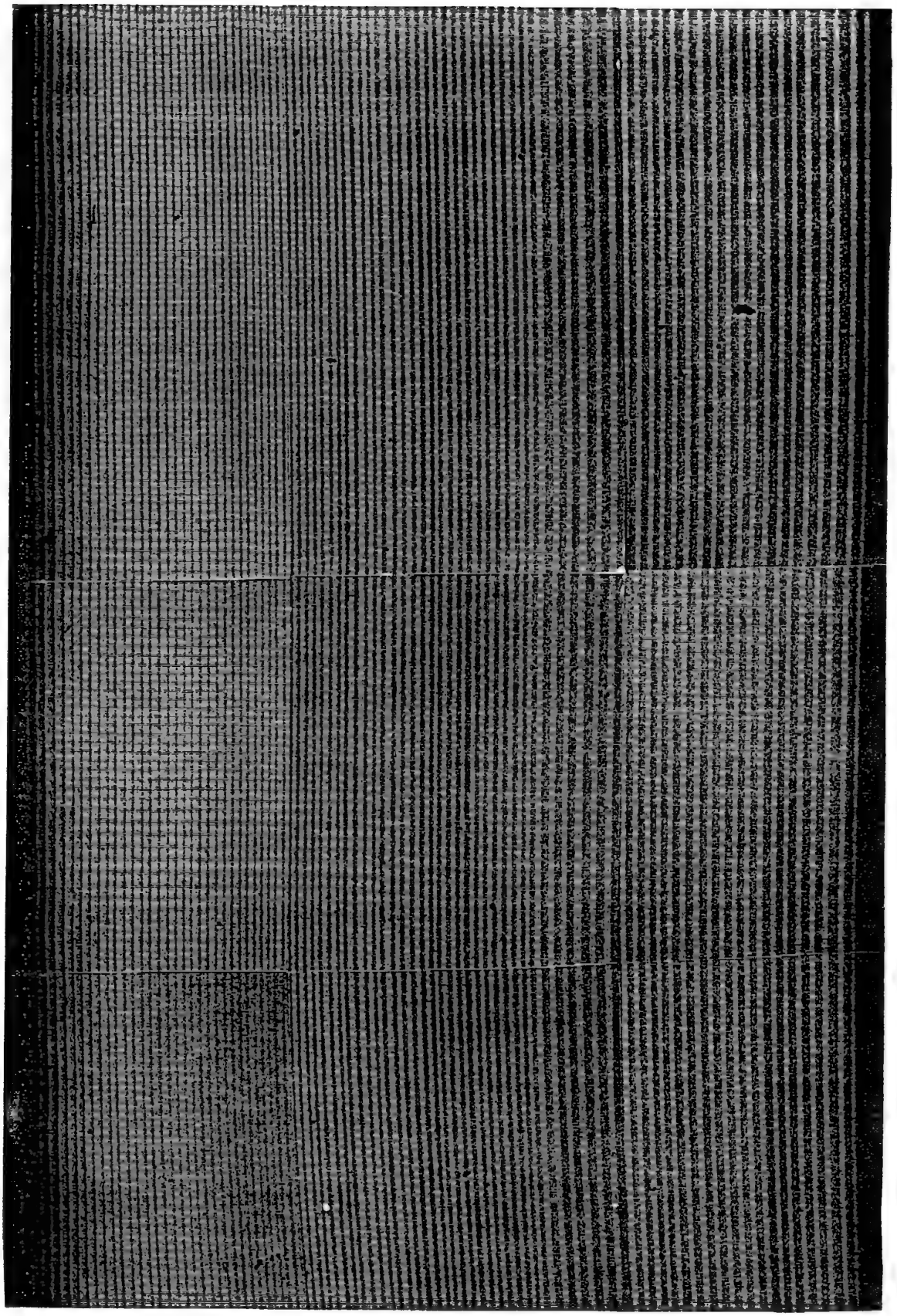

Fig. 11. Optical micgoraphs of sintered $ZrO_2/Al_2O_3 + ZrO_2$

The photo was prepared by matching exactly several pictures. Differences in contrast could not be eliminated.

On the way of obtaining thick laminar structures several problems have arisen. One problem is the decrease in layer thickness during the progress of deposition.

4.2 Layer thickness variation during deposition

The thickness of an individual layer is an important factor for a laminar structure. Therefore laminar composites were formed with all deposition parameters constant except the particle concentration which varies during the process as a result of their deposition from the suspension.

Figs. 12 and 13 demonstrate how the individual layer thickness varies across a multilayer structure obtained at constant applied voltage, constant deposition time and uncorrected particle concentration. A sintered finer structure of 307 layers and about 3,3 mm total thickness is seen in Fig. 12 at the magnification of 75. It is clearly seen that the thickness of an individual layer decreases across the multilayer from 20μ to 5μ – for both types of layers.

A coarser sintered laminar structure of 151 layers and about 5 mm total thickness at a magnification of 40 is seen in Fig. 13. Fig. 14 shows three zones of the same structure (beginning, midst and end) at a larger magnification ($\times$ 200).

The decrease of the individual layer thickness across the multilayer is all the more distinct. The thickness of ZrO_2 layer varies from 75 to 15 microns, the thickness of Al_2O_3 + ZrO_2 layers varies from 90 to 17 microns.

Fig. 15 demonstrates the dependence of the layer thickness (both for ZrO_2 and Al_2O_3+ZrO_2 layers) measured in the multilayer structure (see in Figs. 13 and 14) as a function of the total thickness of the underlayer (for the n_{th} layer the underlayer consists of n−1 layers). The multilayer was deposited from ZrO_2 and 50 weight % Al_2O_3 + 50 weight % ZrO_2 suspensions at 200 v/cm. The starting initial solid concentration was about 85 gr/l for both suspensions. The deposition time was kept at 120 sec for ZrO_2 layers and at 90 sec for mixed layers through the deposition.

It is seen that the decrease in layer thickness during the deposition process does not proceed monotonically. The variation is very slow up to a 2mm total thickness, after that the layer thickness decreases steeply.

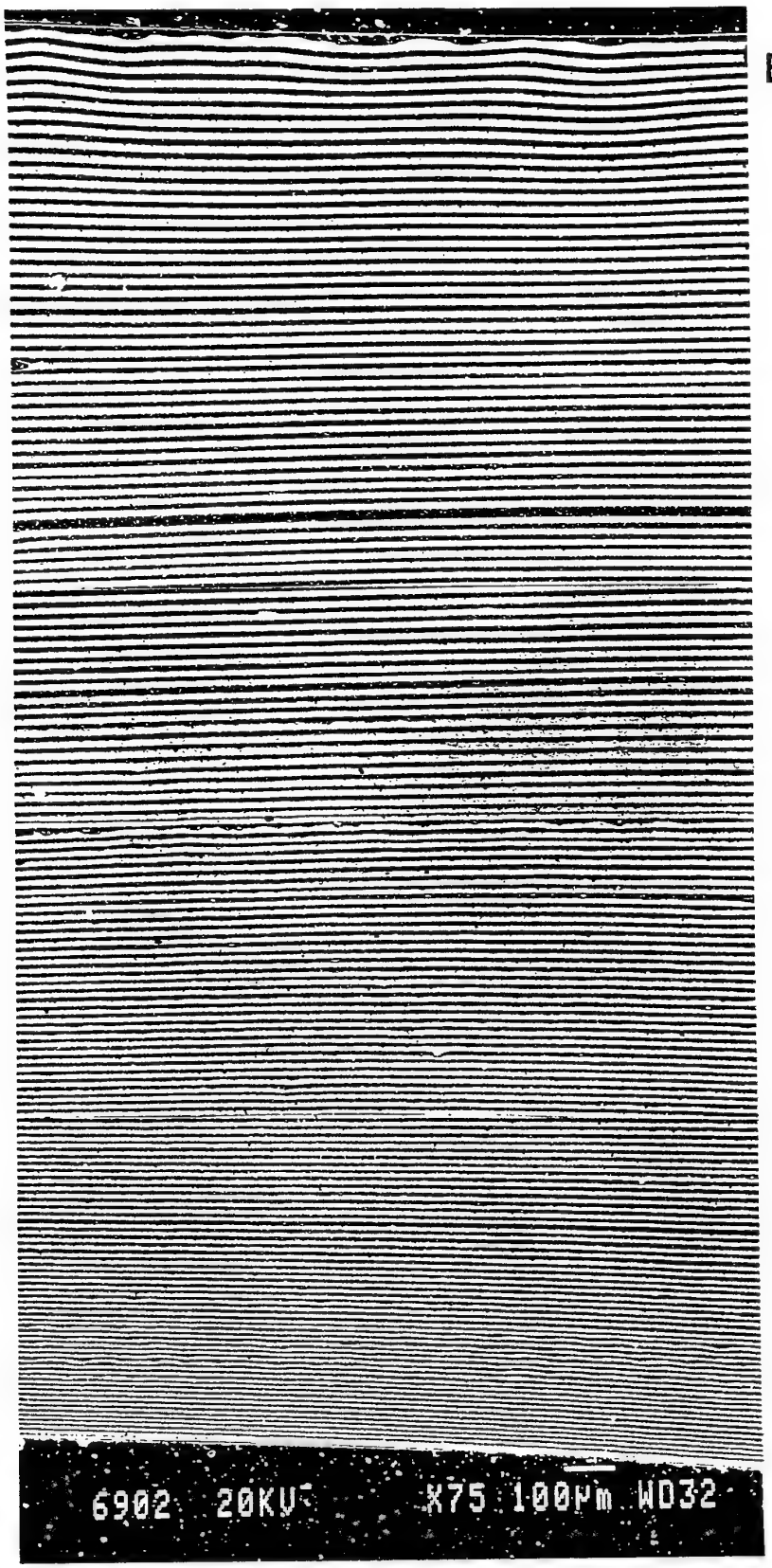

Figure 12: Scanning electron micrograph of the 307 layers $ZrO_2/Al_2O_3+ZrO_2$ laminate structure (in sintered state). Total average thickness of the laminate – 3.3 mm. Individual layers thickness from 20 to 5μ.

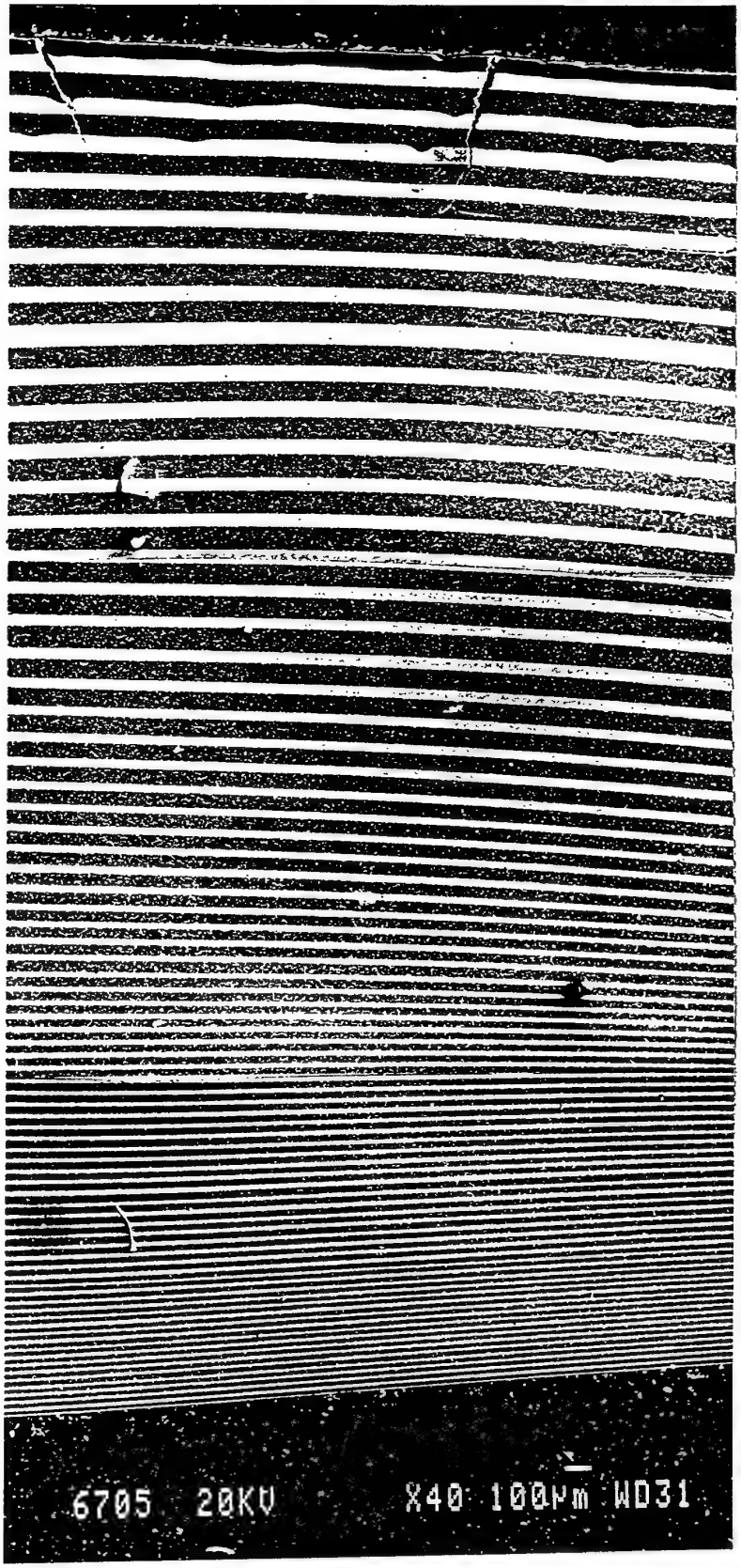

Figure 13: Scanning electron micrograph of a 151 layers $ZrO_2/Al_2O_3+ZrO_2$ laminate structure (in sintered state). Total average thickness of the laminate – 5 mm. Individual layers thickness from 90μ to 15μ.

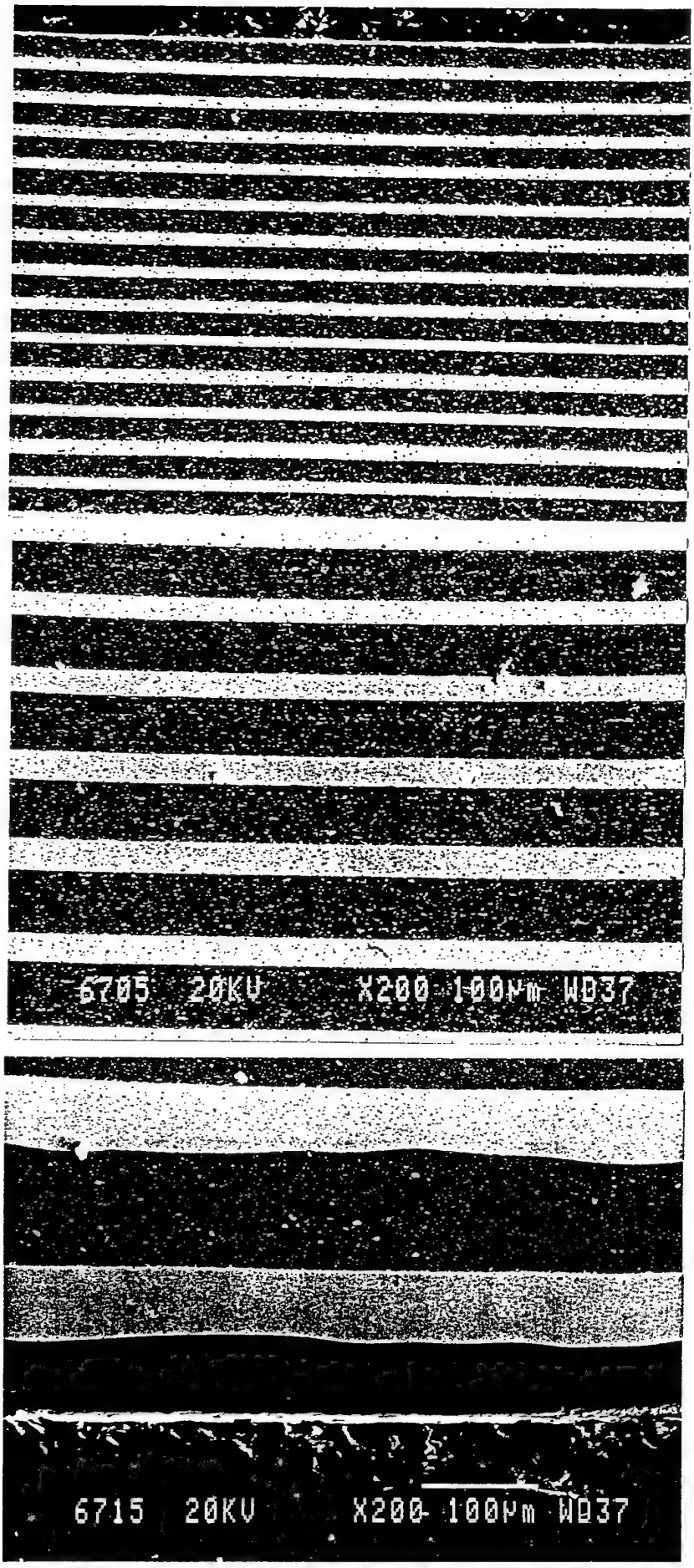

end
layers 126-151

midst
layers 49-38

beginning
layers 1-4

Fig. 14. Different regions of cross-section of sintered $ZrO_2/Al_2O_3+ZrO_2$ laminate structure see in Fig. 13.

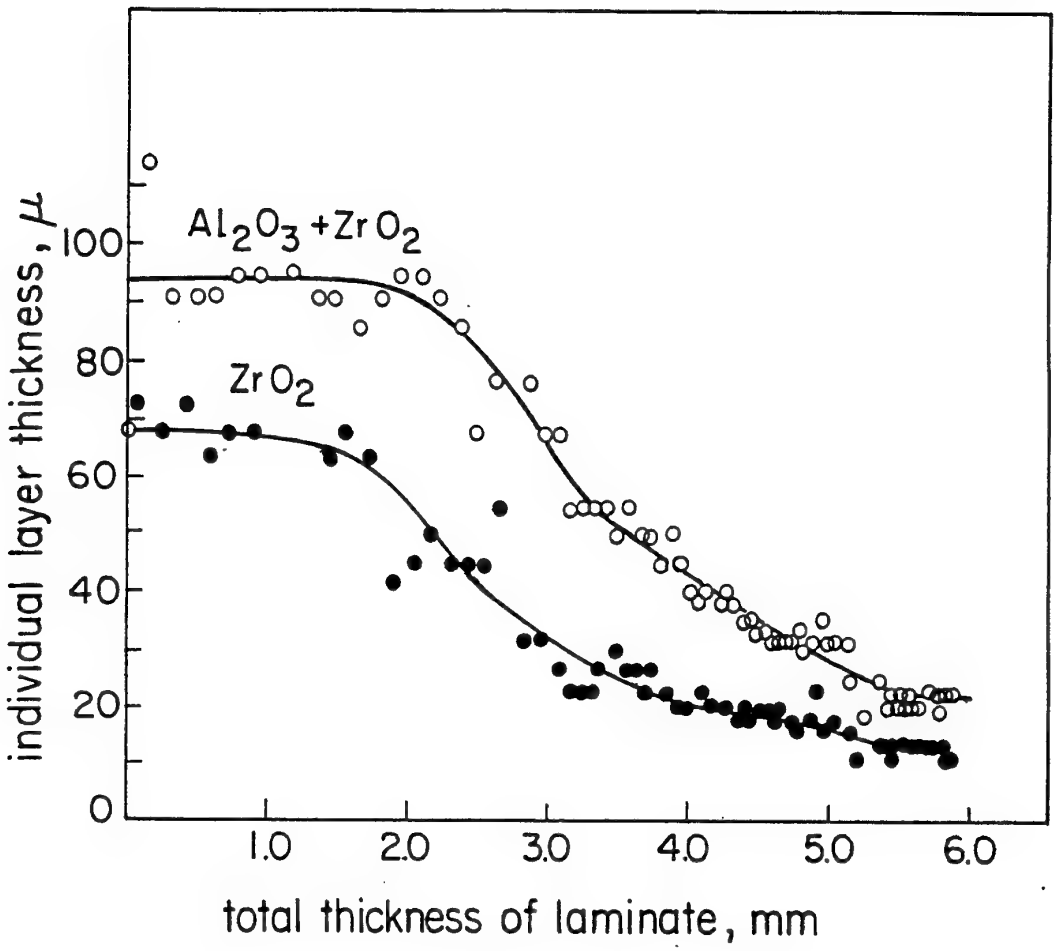

Fig. 15: Variation of layer thickness as a function of total thickness at constant E and t

The decrease in layer thickness during deposition is due to two reasons:

(1) decrease of the particle concentration in the suspension.

(2) increase in an electric resistance of the deposit with increase in its thickness.

4.2.1 The variation in solids concentration

The decrease of solids content in the suspension during deposition of a thick laminated structure is considerable. The initial weight of solid particles in both suspensions from which the multilayer under discussion (Fig. 13-14) was fabricated was equal to 85 grams. The weight removed during the deposition was about 20-22 grams for the ZrO_2 suspension and about 26-28 grams for the mixed suspension. This means 25-30% decrease in concentration. The decrease in the concentration for a slow variation zone (up to 2 mm total thickness, Fig. 15) was in the 10% limit.

Under the conditions of a varying particle concentration the deposition rate is described by the Z. Zhang et al. [6] equations (8) and (9) (Section 2.2):

$$\frac{dw}{dt} = \mu c(E=\Delta E)e^{-K_1 t} \qquad (8)$$

$$K_1 = \frac{s}{u}\mu(E-\Delta E) \qquad (9)$$

where w - weight of deposit
c - initial concentration of solids in suspension
μ - mobility of a particle
$E-\Delta E$ - electric field intensity across the suspension
s - area of electrode
u - volume of suspension

Although having its own limitations the Zhang et al. dependence is much more realistic than Hirata's [5] $dw/dt = \mu ce$. It indicates that the deposition rate falls exponentially with time in a deposition process.

4.2.2 The electric resistance of a deposit

In order to gain a better insight into the problem of layer thickness variation, the variation of the electric resistance of a growing deposit as a function of its thickness was

studied. Fig. 16 shows the total resistance of ZrO_2 compacts as a function of their green thickness. The ZrO_2 compacts were deposited from a 100 gr/l isopropanol suspension with 1.5% (v/v) acetyl-acetone additive. The green thickness of the deposits was calculated from their weight and assuming a green density equal to 60% of the theoretical value.

A slow increase is seen up to about 500 microns and a steeper increase after that. The electrical resistance of the suspension remains approximately constant although the concentration of solids has changed almost twofold from 100 gr/l (starting concentration) to about 50 gr/l after the deposition of eleven zirconia compacts).

According to Ohm's law the relationship between the change of the electric resistance of a conductor ΔR, and the change in its length $\Delta \ell$ is:

$$\Delta R = k\Delta \ell ,$$

k being a constant. A similar dependence should exist for ceramic deposits, $\Delta \ell$ being the deposit thickness. The coefficient k depends on the conductivity of the ceramic powder and the density of the deposit. If properties of the deposit (mainly its density) do not change with growing the relation $\Delta R = k(\Delta \ell)$ is likely to be linear.

Such a linear dependence was reported in [6] for SiC whisker-tetragonal zirconia deposits up to a 1.4 mm total thickness.

The non-linear dependence $\Delta R = k(\Delta \ell)$ presented in Fig. 16 may be the indication of the variation in the density of a growing ZrO_2 deposit. There are indications [5,7] that the density is not constant through the deposit. It should be noted that the dependence depicted in Fig. 16 may not be very accurate because the deposit thickness was calculated from the deposit weight with the assumption of a constant density.

The increasing electrical resistance of a growing deposit has two main effects on the rate of deposition:

1. The potential drop across the deposit ΔE lowers the potential drop across the suspension from $E_s=E$ to $E_s=E-\Delta E$, E being an externally applied electric field intensity. If R_s is the electrical resistance of the suspension and ΔR_d is the resistance of the deposit, then:

$$E_s = E-\Delta E = E\frac{R_s}{R_s+\Delta R_d}$$

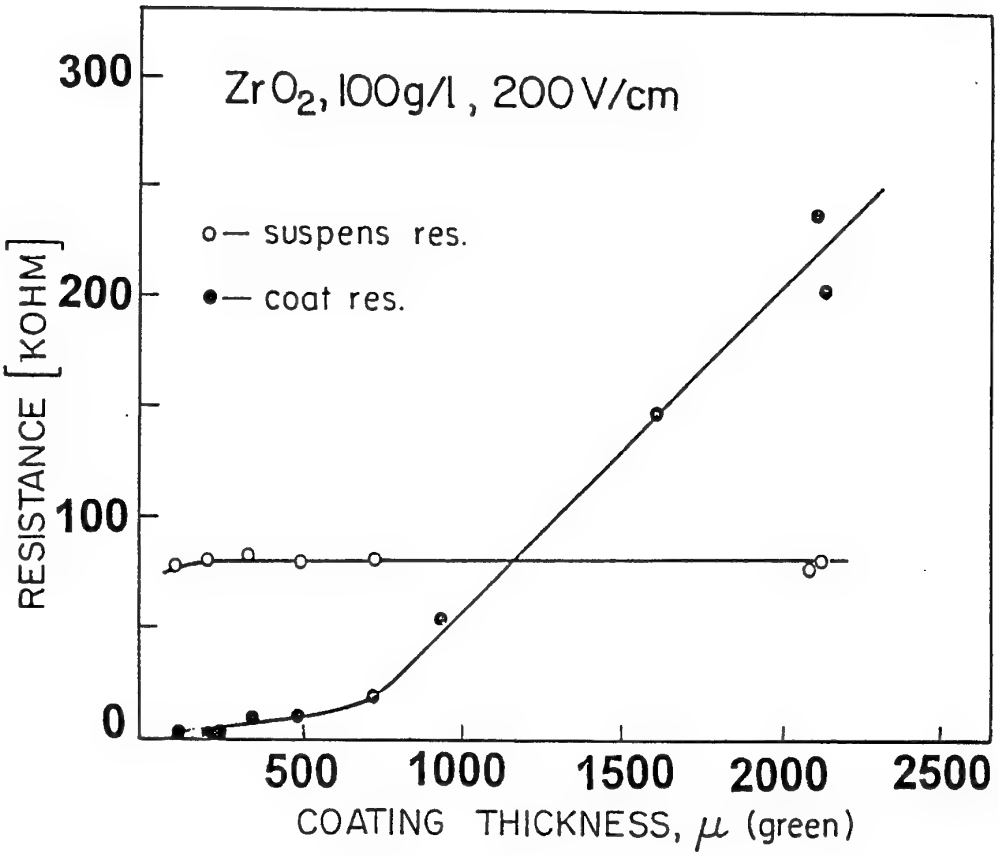

Fig. 16: Resistance vs. coating thickness of ZrO_2 deposit

The field intensity drop across the suspension E_s, determines the electrophoretic velocity of the particles $v = \mu E$ and their deposition rate, see eq. (8) and (9) in 4.2.1.

Fig. 16, depicting $\Delta R_d = k(\Delta \ell)$ and R_s during deposition of ZrO_2 layers, shows that at early deposition time E_s differs from E very slightly but for a 0.5 mm deposit $E_s \approx 0.85E$, for a 1.2mm deposit $E_s \approx 0.5E$ and for a 2 mm deposit E_s is only 0.3E. Such steep decrease in the electric field intensity across the suspension (about threefold for a 4mm deposit) should lead to a steep decrease (threefold or more) in deposition rate.

The growing deposit presents a higher resistant path for ions hindering charge and mass transfer reactions that in principle lower the deposition rate.

Approximate estimations of the variations of solid concentration of the suspension, electrical resistance of the growing deposit, and variation of electric field intensity drop across the suspensions and the influence of these variations on the deposition rate explain in principle (but not in detail) the variation of individual layer thickness during deposition as seen in Fig. 15. The slow decrease in layer thickness at the beginning is explained by a relatively small change of solids concentration (less than 10%) and yet low electric resistance of the deposit (Fig. 16). Steep increase in electric resistance of the deposit in the next stages of deposition combined with marked decrease in concentration ($\approx$ 25–30%) leads to a steep decrease in the layer thickness that follows the initial nearby constant thickness layers.

It is believed that the problem can be solved in the following stages:

- First, the suspension concentration has to be kept constant. This will be done by using large reservoirs for both suspensions which will be circulated through a small deposition bath. The question whether the specimen will be static and the suspension changed in the deposition bath or the specimen will be transferred is still open.
- The problem of resistance increase which in our experiments accounts for the most part of the effect (of uncontrolled variation in thickness) will be overcome by gradual increase of voltage and/or deposition time. In a system of constant concentration we shall try to obtain a quantitative relationship between R (the resistance) and deposition time. From such a relationship a regime for variation of voltage and for time will be worked out.

In a preliminary experiment we have formed a ZrO_2/Al_2O_3+ZrO_2 multilayer (from ZrO_2 and 50 weight %Al_2O_3 + 50 weight % ZrO_2 suspension) under conditions of increasing deposition time and increasing voltage. No correction for the suspension concentration

was made. The deposition time has been raised gradually from 60 to 105 sec for ZrO_2 layers, and from 10 to 52 sec for mixed layers. The field intensity was raised once from 200 to 300 v/cm, after 119 layers. The schedule was selected intuitively. A cross-section of the sintered multilayer with 160 layers and 3mm total thickness, is presented in Fig. 17. The picture is made by matching exactly several photos similarly to that picture in Fig. 11. It is seen that the individual layer thickness variation through the structure is less distinct than for multilayers obtained at the constant voltage and constant deposition time shown in Figs. 12 and 13.

4.3 Edge Effect

The next problem encountered in the process of fabrication of thick multilayers was the variation of total deposit thickness on the substrate surface. The phenomenon was most pronounced on the edges of the specimen where the deposit was much thicker than on the rest of the surface. This problem is referred to as edge effect.

The phenomenon is well known in the practice of electrodeposition [11,12]. The distribution of the deposit thickness on an electrode surface (termed "throwing power") is fully determined by the current density distribution over the surface which an applied potential will produce and that, in general, is not uniform.

The achievement of a uniform distribution of current on an electrode surface is one of the very difficult tasks in the field of electrochemistry. The current distribution depends on many diverse factors, the most important of which may be grouped as follows:

- Geometrical factors: (1) the shape and size of the electrodes; (2) the shape and size of the vessel; (3) the position of the electrodes.

As an example we attach Fig. 18 from [11] which shows the distribution of a metal deposit on a flat cathode for two baths of different width with plane-parallel electrodes.

It is seen that even in this very simple case of 2 plane-parallel electrodes the distribution of the deposit over the substrate surface is uniform - only for a very special case (no. 1 in fig. 18). For a more general case (No. 2), the distribution is not uniform because in this case the current passes not only through the portion of the electrolyte situated between the electrodes but also through the remainder of the solution. The density of electric field lines is larger at the edges of the cathode which leads to a thicker deposit as compared to

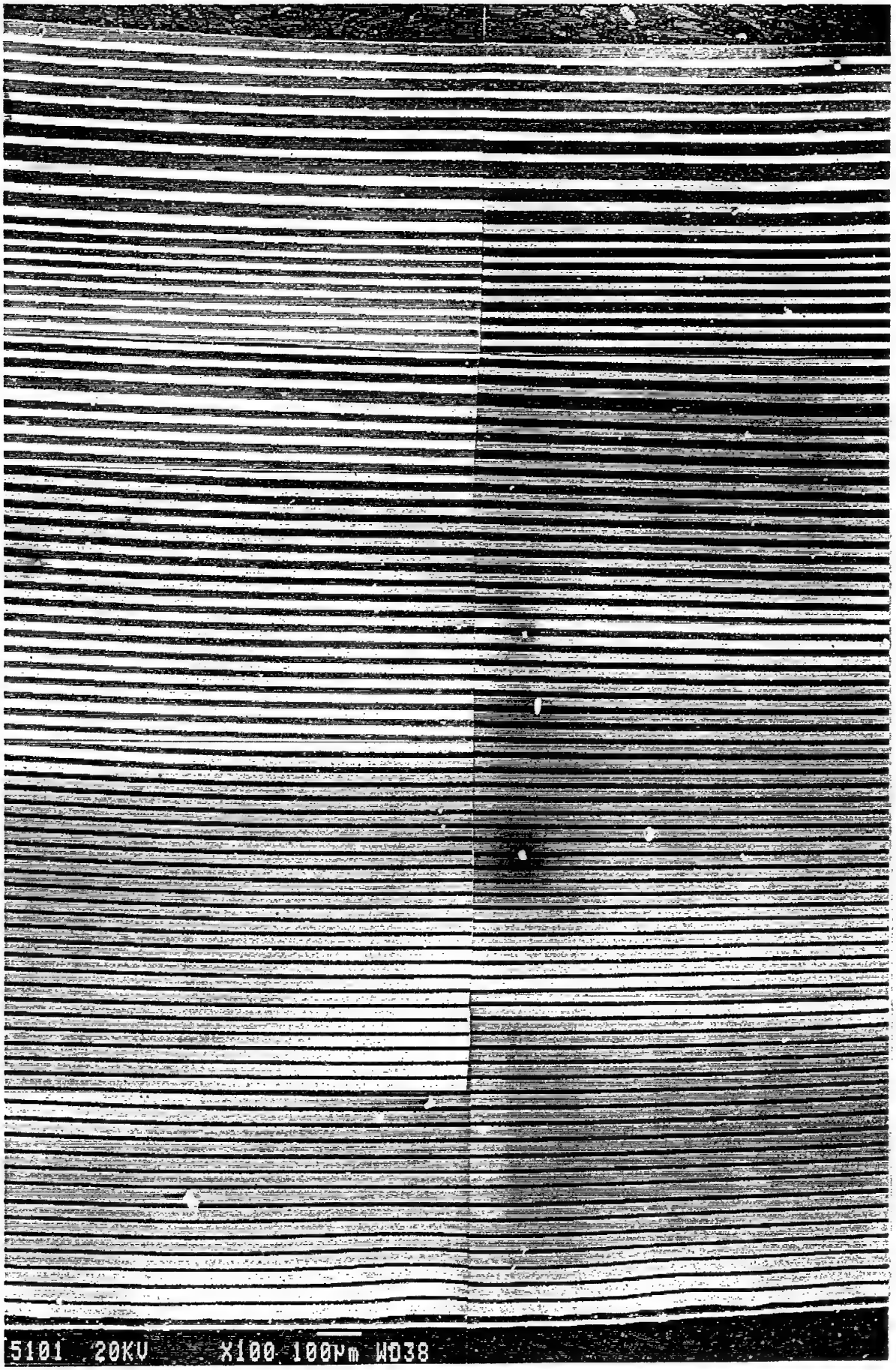

Fig. 17. Scanning electron micrographs of sintered Al_2O_3+ZrO_2/ZrO_2 laminar structure

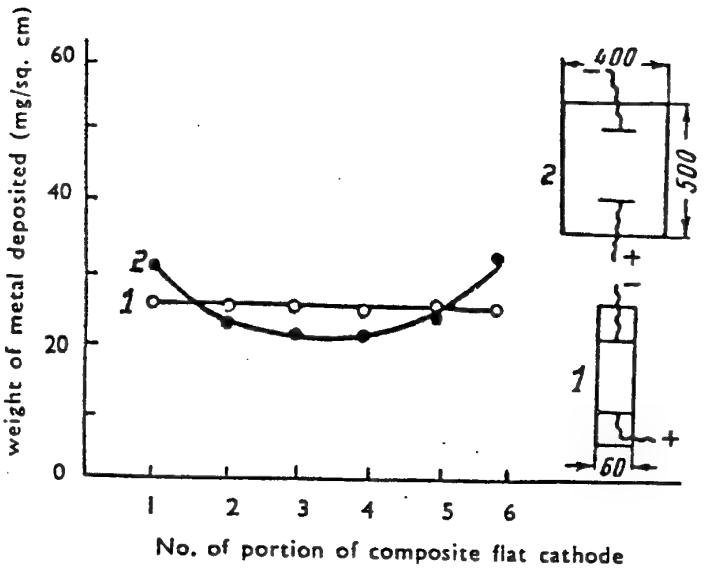

Fig. 18: [12] Distribution of metal deposit on a flat cathode in relation to bath shape

to the rest of the electrode. The current density variation on different parts of an electrode may be very high. Values of 5 or 10 to 1 are reported in [14]. Fig. 19 from reference [14] shows the current density distribution on a flat cathode in a chromium bath. The edge current density is about five times the value of the current density in the central part.

To make the current distribution more uniform one can employ (1) parallel or concentric electrodes, (2) non-conducting shields to reduce the current density at certain points, (3) conducting wires, or frames to detract the current from such points, (4) an appropriate ratio of anode to cathode area. Variation of the interelectrode distance can also be useful.

- Electrical and electrochemical factors: Factors which affect the current distribution are:

(1) The polarization of the electrode or, more precisely, the variation of the polarization with current density;

(2) the specific resistance of the electrolyte;

(3) the variation of current efficiency with current density.

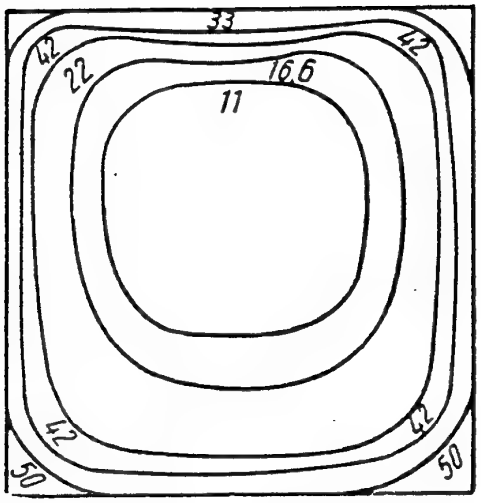

Fig. 19 [14]: The approximate current density distribution on a flat cathode in a chromium bath. The average current density is equal to 22A/dm^2

These factors depend mostly on solution properties such as its composition, temperature, viscosity, etc.

- The nature of the substrate and the condition of its surface, etc.

At this stage of the work our goal was to obtain a satisfactory uniform deposit without variation of the solid concentration and the deposition parameters. The only parameters varied related to the bath geometry: the interelectrode distance, the anode:cathode ratio and the use of screen and metal wire contours.

4.3.1 Non-conducting screens

Non-conducting screens are widely used in electroplating practice [11] for controlling the distribution of deposit thickness. By placing a non-conducting screen between the anode and part of the cathode being coated, the trajectories of the current of the cathode are extended and the current distribution is altered to produce a reduction in current density on this portion of the electrode.

A thin plastic disc was used of 30-50 mm diameter with an opening in the center, the diameter of the opening varying from 5 to 15 mm [Fig. 20]. The screen of such a shape was used to counteract edge effects.

No improvement in deposit thickness uniformity was found. This may be due to the very limited range of permissible interelectrode distances due to the reasons that will be described in section 4.3.3.

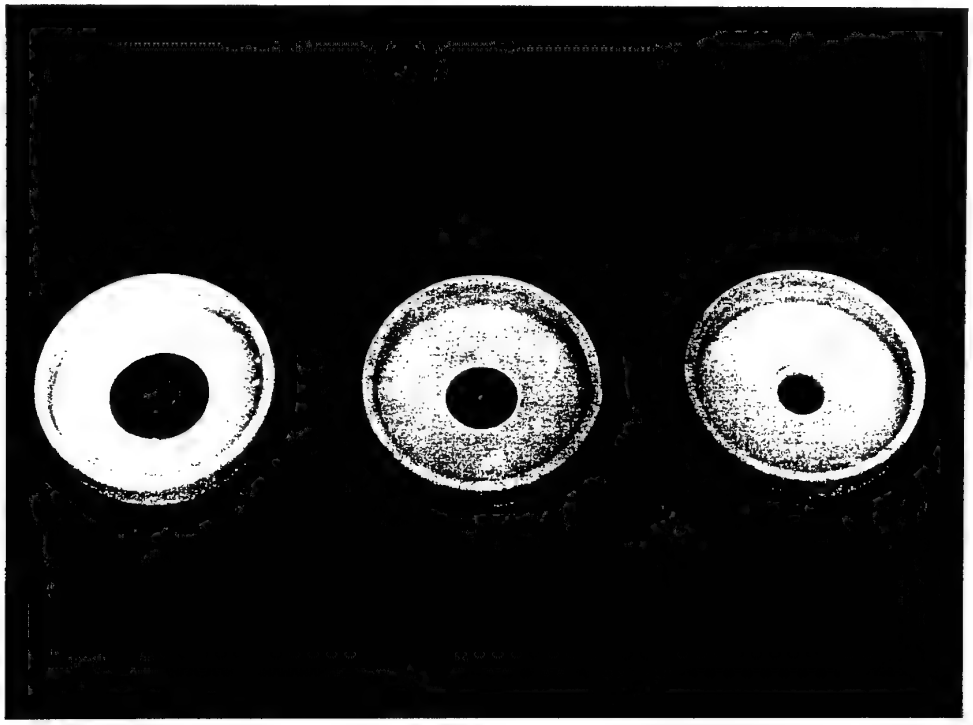

Fig. 20 Non-conducting screens

4.3.2 Additional cathodes - "thieves"

The concentration of electric field lines at the edges of the cathode in our case, may be avoided by providing an additional cathode that will divert part of the current and thereby eliminate or lower edge effects.

A stainless steel wire 1,5-3mm in diameter and strips of 1.5-3 mm width were used as additional cathodes [Fig. 21]. The additional cathode surrounded the cathode being coated, the distance between the two cathodes being 2-3 mm.

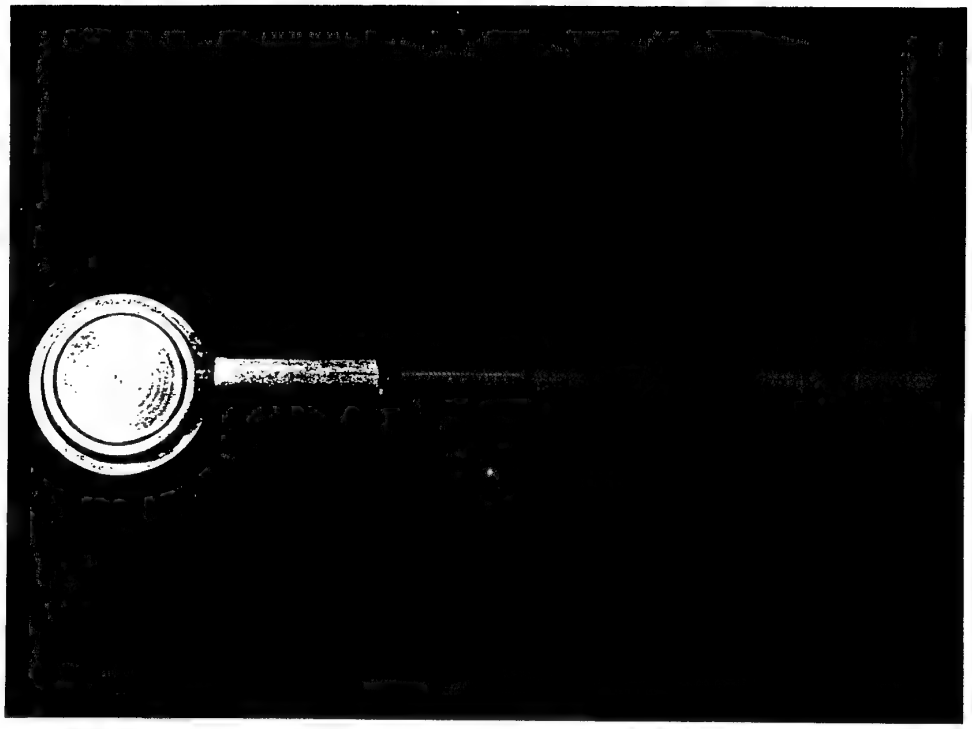

Fig. 21: An additional cathode (a stainless steel strip)

The additional cathodes considerably lowered edge effects. However, they proved to have a shortcoming. Due to the high current density a large amount of solids was deposited on the additional cathode. For example, when 3 grams were deposited on the main cathode, 10 grams of solids were deposited on the additional cathode.

The next attempt was to use the side surface of the cathode as an additional "thief". The cathodes used for the deposition were stainless steel discs of 2–4 mm height. Usually their side surfaces were masked and excluded from the deposition process. In this experiment the cathode side was not protected and used as an extension of the cathode of interest (Fig. 22). The edge effects decreased but the deposit on the side surface made it difficult to remove the multilayer from the substrate, often causing cracking along the contact line.

4.3.3 The interelectrode distance

The interelectrode distance has been varied from 6 to 30 mm. The anode:cathode ratio was kept at 1:12,5. No improvement in deposit distribution over the substrate surface was observed in this range of distances. It must be noted that the permissible range of 6–30mm is very limited. The limitation is related to a limited bath volume. The agitation

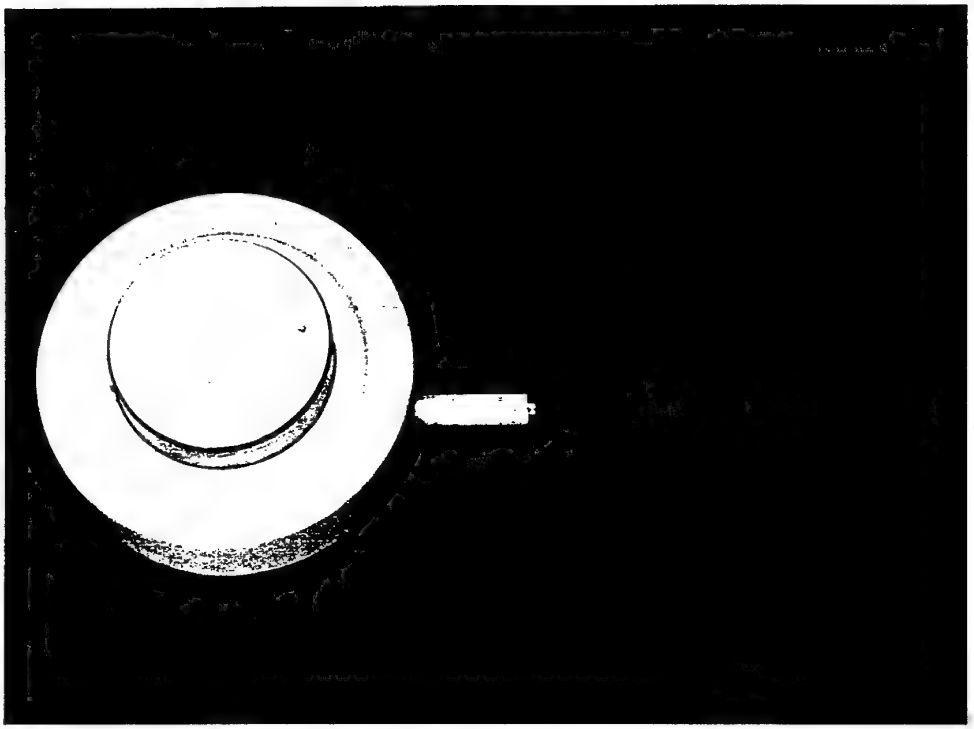

Fig. 22: A cathode with unprotected side surface

of suspensions made with a magnetic stirrer cannot maintain solids adequately dispersed in a large volume and therefore the bath volume is limited. The 17 mm distance between electrodes has been chosen for the reason of convenience.

4.3.4 The anode:cathode area ratio

The current density distribution over the electrode surface is influenced also by the ratio of anode to cathode areas. In order to diminish edge effects in a deposit on a cathode it was clear that the anode surface area had to be less than that of the cathode. The selection of the appropriate ratio was conducted experimentally. While keeping constant the surface of the cathode (35.4 mm diameter) and the interelectrode distance, the anode area was varied as follows:

anode diameter 5mm a:c = 1:50
anode diameter 7,5mm a:c = 1:22
anode diameter 10mm a:c = 1:12,5

The distribution of the deposit on the cathode surface for the three a:c ratios is given schematically in Fig. 23. At a large a:c ratio a higher thickness is obtained in the center of the specimen. At a low a:c ratio the thickness is high at the edges.

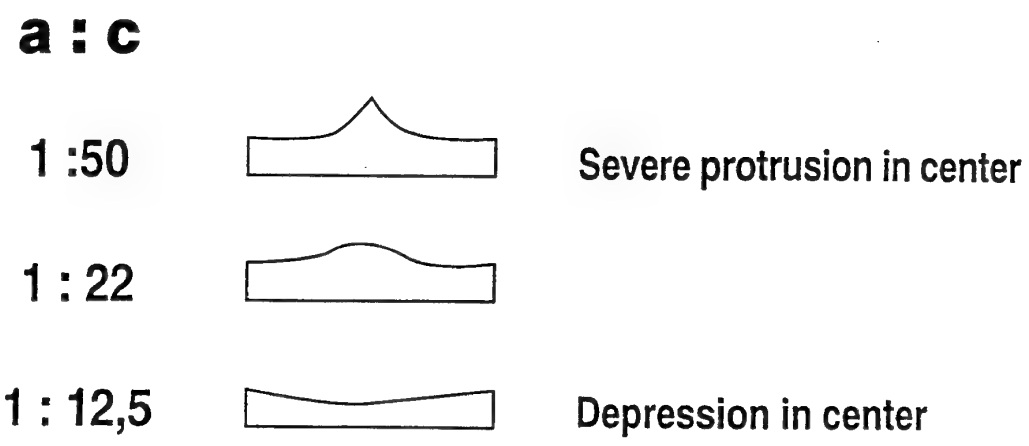

Fig. 23: Varying anode/cathode area ratio

Variation of the a:c value has proven to be an effective way in counteracting edge effects. The optimal ratio will be determined in future experiments.

4.4 The wavy surface of Al_2O_3 layers

An additional problem encountered in the process of the electrophoretic deposition of thick ZrO_2/Al_2O_3 multilayers was the wavy surface of Al_2O_3 layers as the deposit thickness grew. It is particularly remarkable that this effect existed for the Al_2O_3 layers only while the ZrO_2 layers corrected this effect.

Fig. 24 is an optical micrograph of a ZrO_2/Al_2O_3 composite with 90 layers and approximately 3 mm total thickness, the thickness of ZrO_2 layers ranging from 15 to 55μm and the thickness of Al_2O_3 layers from 15 to 40 μm. The micrograph demonstrates the formation of a wavy surface of a Al_2O_3 layer when the total thickness and Al_2O_3 layer thickness grew. The micrograph demonstrates also the correcting effect of the ZrO_2 layers.

Several attempts were made to eliminate this phenomenon:

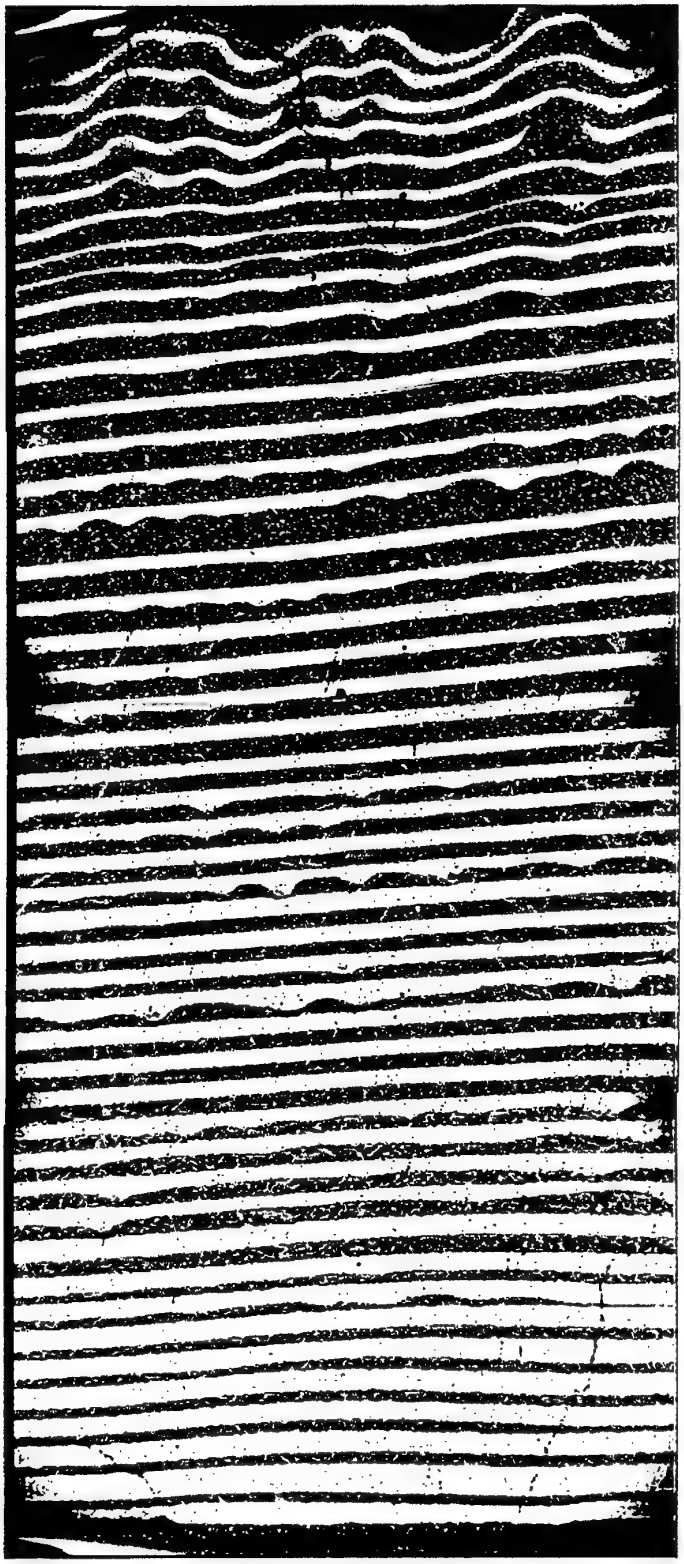

(× 50)

Fig. 24: Cross-section of Al_2O_3/ZrO_2 laminar composite

- Shaking of the growing composite after removing it from one bath and before transferring to another, see Figs. 25 and 26.
- Intermediate rinsing of the growing deposit in isopropanol (after one and before another bath), see Fig. 27.
- Intermediate rinsing in an appropriate suspension (in an Al_2O_3 suspension after removing the deposit from ZrO_2 and before transferring it to Al_2O_3 bath, and vice versa), see Fig. 28.
- Using new suspensions after the deposition of each 25 layers, see Fig. 29. This attempt was made because earlier experiments showed that the first twenty-thirty Al_2O_3 layers were satisfactory (if the layer thickness was not higher than 30 microns).

As it is evident in Figs. 25-29 all attempts to eliminate the effect have failed.

In order to improve the uniformity of the layers another approach was adopted. As pointed out the ZrO_2 layers do not exhibit a wavy surface. Moreover, they corrected the defects of the Al_2O_3 layers. Hence, we substituted mixed Al_2O_3 + ZrO_2 layers for Al_2O_3 layers in a ZrO_2/Al_2O_3 multilayer system. The alumina to zirconia ratio in a mixed layer was taken in accordance with [9, 11].

Al_2O_3 + ZrO_2 layers were deposited from suspensions of two different compositions:
- 96 weight % Al_2O_3 + 4 weight % ZrO_2
- 50 weight % Al_2O_3 + 50 weight5 % ZrO_2

The solid concentration of both suspensions was 100 gr/l.

Fig. 30 shows a ZrO_2/Al_2O_3+ZrO_2 laminate composite with mixed layers deposited from the 96% Al_2O_3 + 4% ZrO_2 suspensions. As it is seen the mixed layers have the same wavy surface as the Al_2O_3 layers.

Fig. 31 (b) presents a ZrO_2/Al_2O_3+ZrO_2 laminar structure with mixed layers deposited from 50% Al_2O_3 + 50% ZrO_2 suspension. It is seen that the wavy surface has disappeared for mixed layers of this composition. The multilayer is characterized with distinctly even layers of both kinds, mixed layers being as even as the ZrO_2 ones. For comparison the ZrO_2/Al_2O_3 multilayer is presented in Fig. 31 (a).

Thus the wavy surface problem in the ZrO_2/Al_2O_3 composite has been solved by substituting mixed Al_2O_3 + ZrO_2 layers (deposited from 50% Al_2O_3 + 50% ZrO_2 suspensions) for Al_2O_3 layers. We still have no clear answer or solution for a pure Al_2O_3

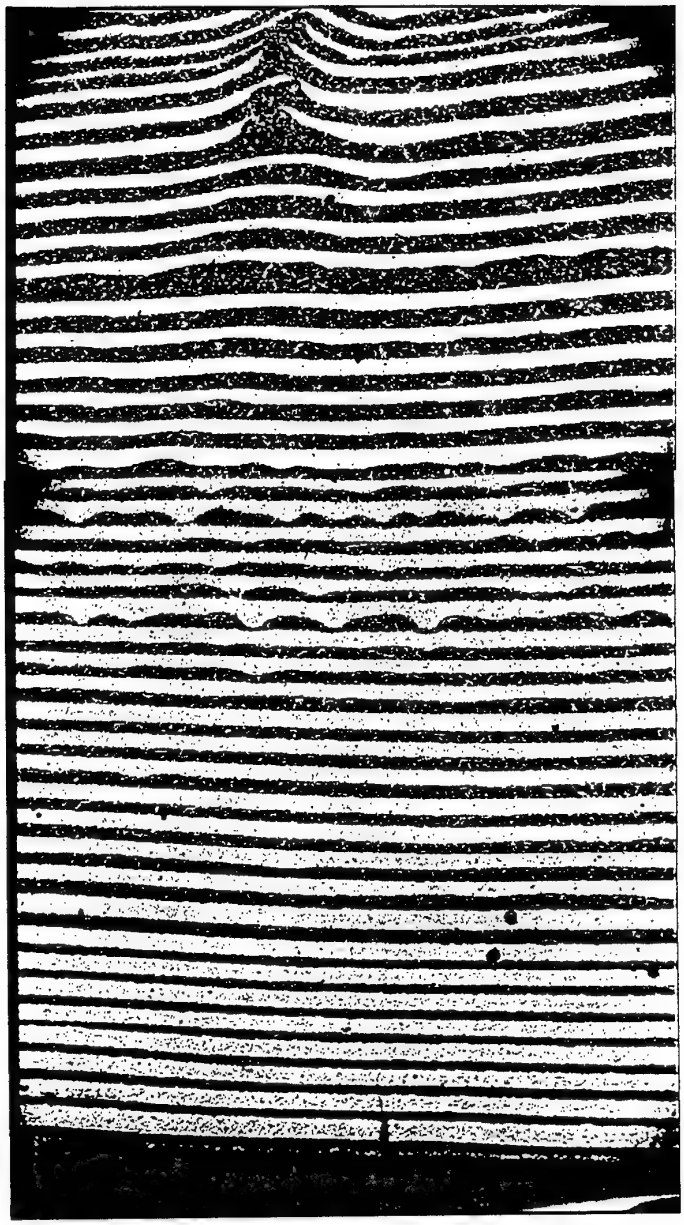

(× 50)

Fig. 25: Cross-section of a ZrO_2/Al_2O_3 laminar composite received without shaking of deposit while transferred from one bath to another.

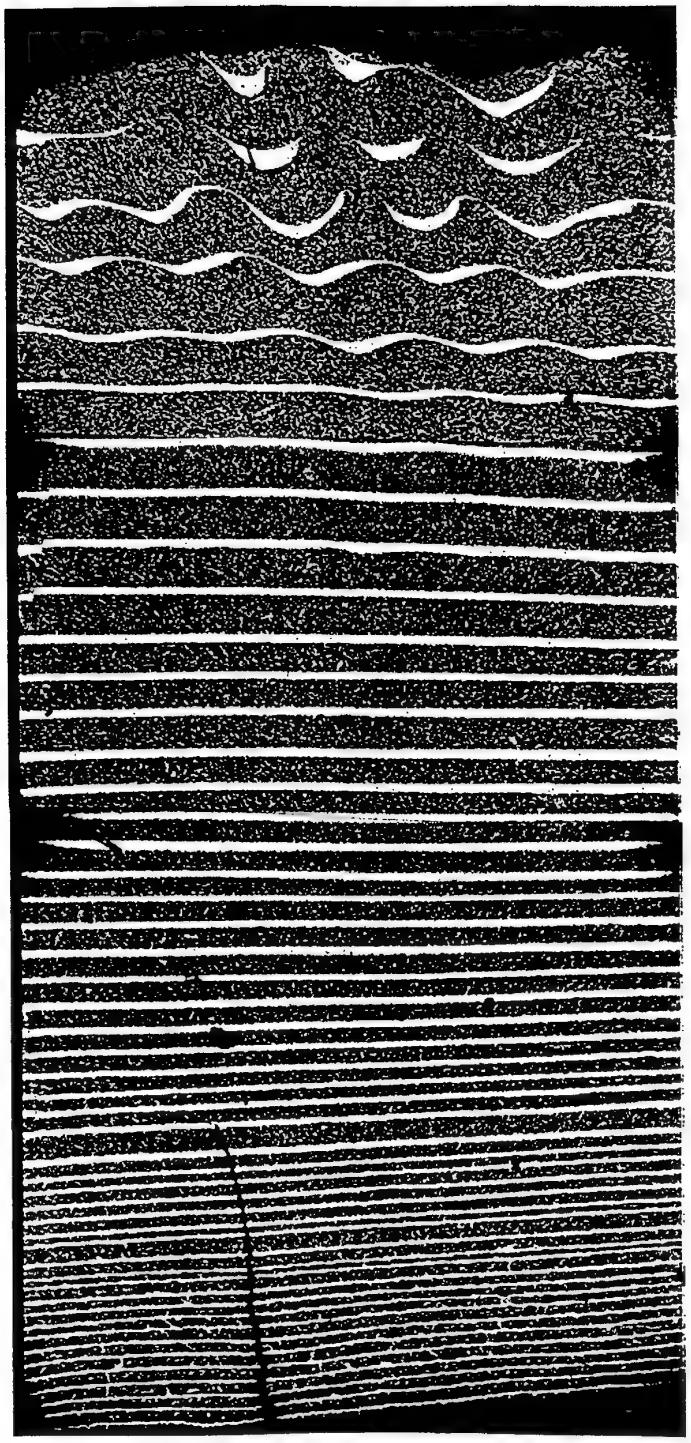

(× 50)

Fig. 26: Cross-section of a ZrO_2/Al_2O_3 laminar composite obtained with shaking of composite while transferred from one bath to another.

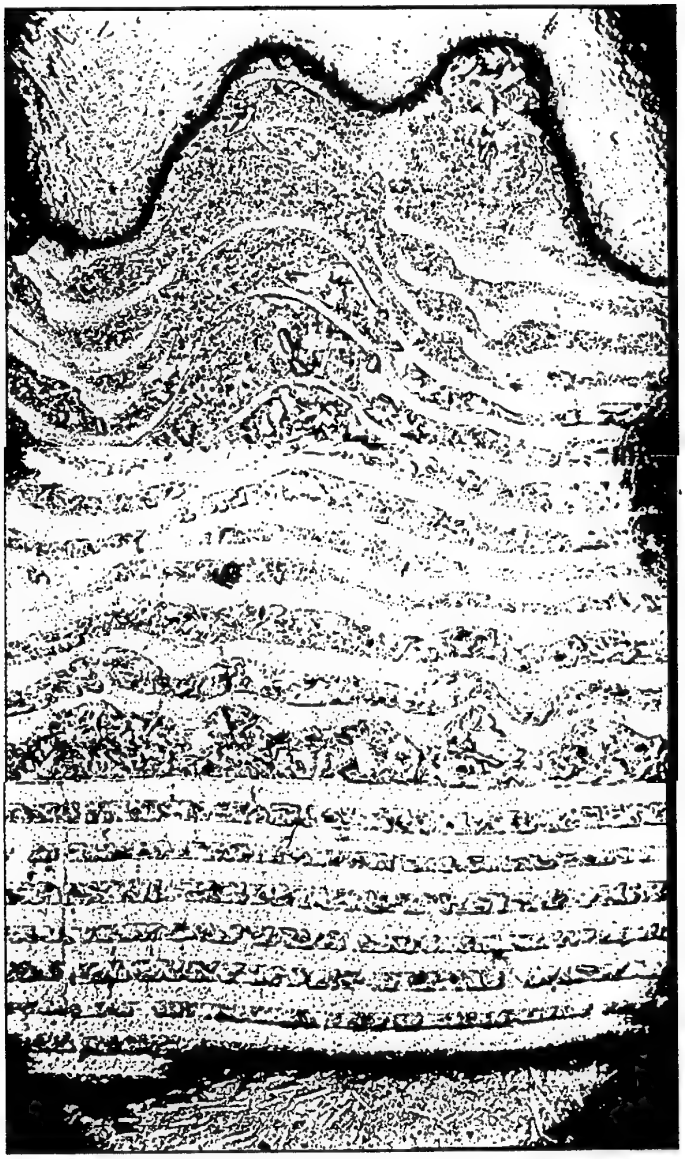

(× 50)

Fig. 27: Cross-section of a ZrO_2/Al_2O_3 laminar composite received with intermediate rinsing in isopropanol.

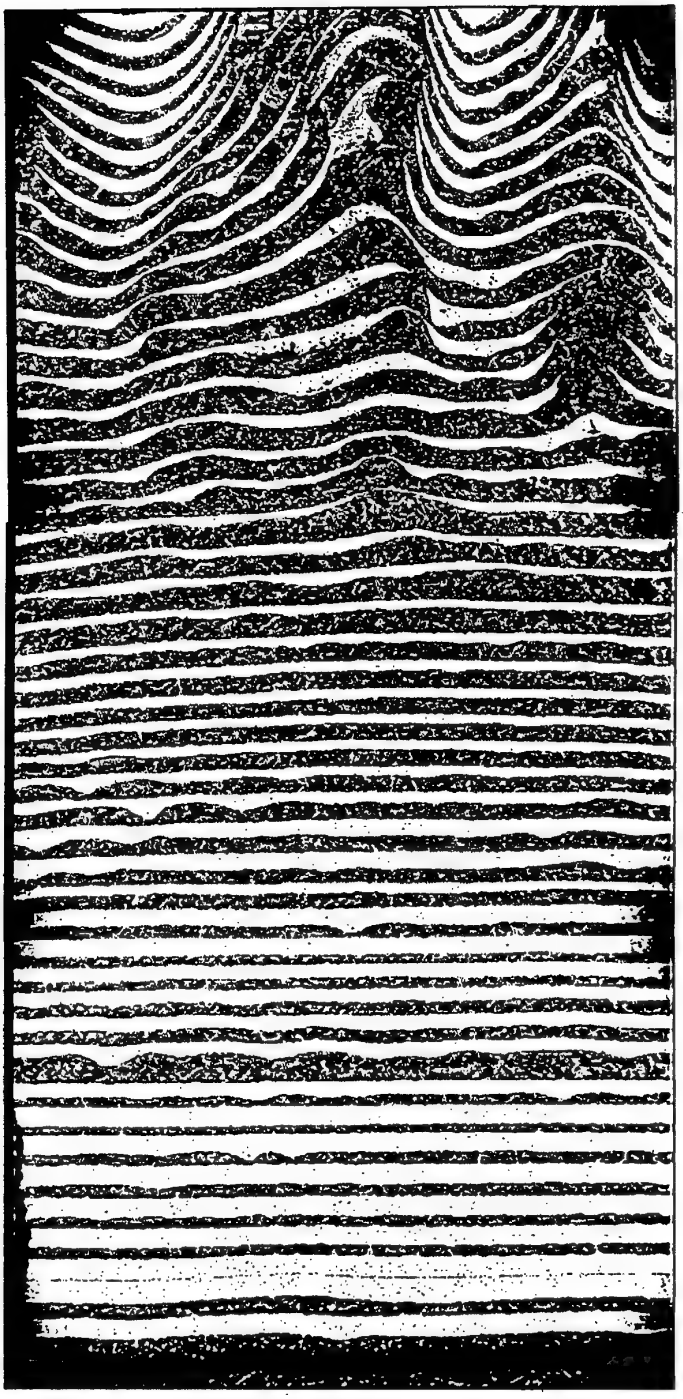

(× 50)

Fig. 28: Cross-section of a ZrO_2/Al_2O_3 laminar composite obtained with intermediate rinsing in an appropriate suspension.

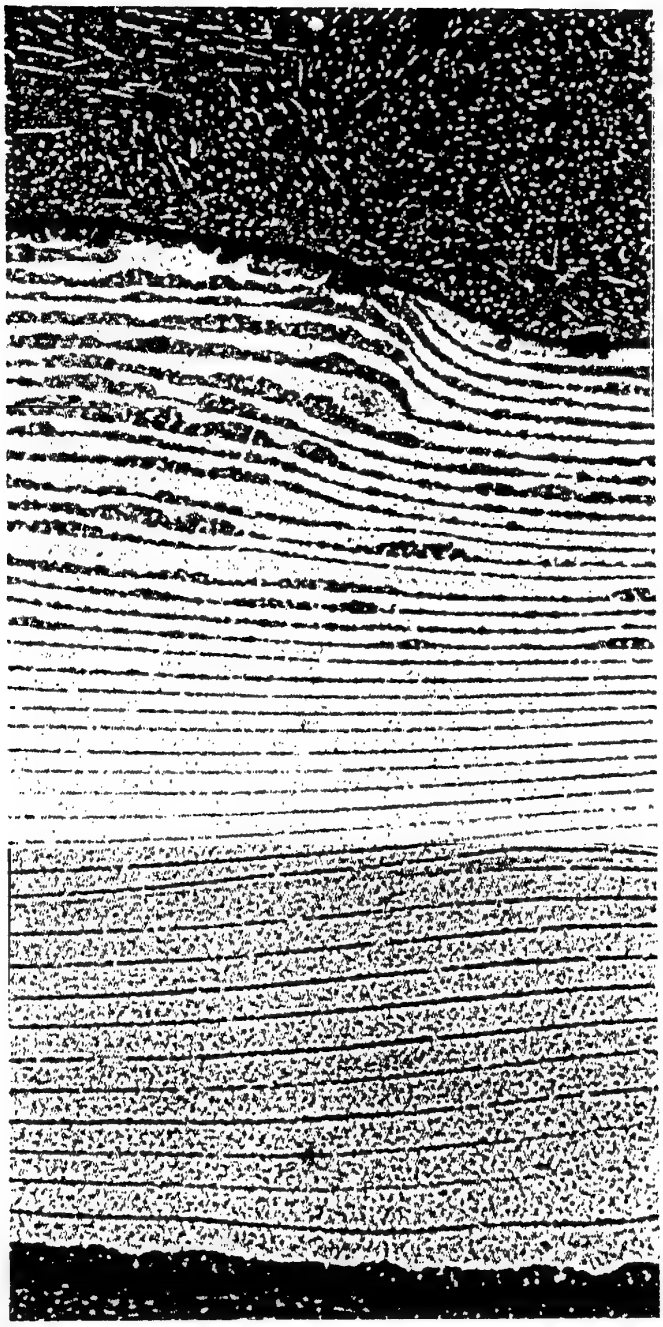

(× 50)

Fig. 29: Cross-section of a ZrO_2/Al_2O_3 laminar composite obtained by changing of suspensions after deposition of each group of 25 layers.

(× 50)

Fig. 30: Cross-section of a $ZrO_2/Al_2O_3 + ZrO_2$ laminar composite deposited from a ZrO_2 suspension and from a 96% w Al_2O_3 + 4% w ZrO_2 suspension

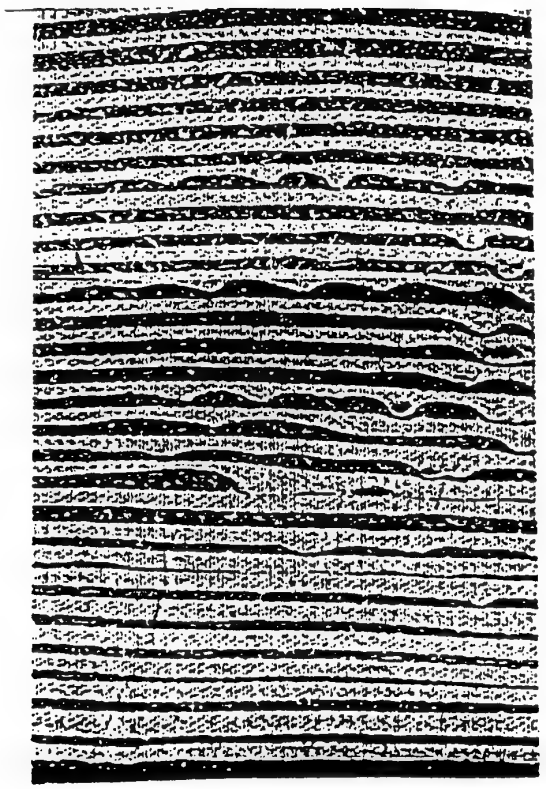

A

(× 50)

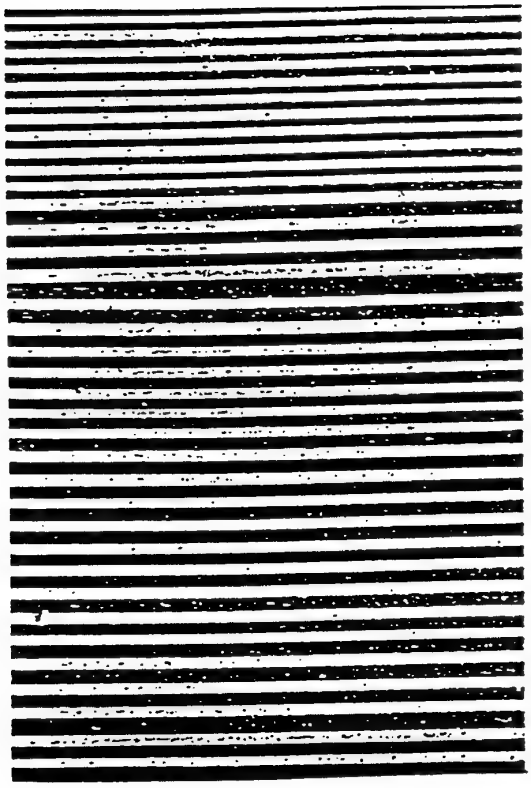

B

(× 50)

Fig. 31: Wavy surface of Al_2O_3 layer in Al_2O_3/ZrO_2 laminate

$Al_2O_3+ZrO_2/ZrO_2$ laminate

layer. Physical means for elimination of the problem did not work. However, the possibility exists for elimination of the wavy surface by increase of the ion concentration of the Al_2O_3 suspension.

4.5 Layer composition

The chemical composition of individual layers in a laminated structure is one of the parameters determining its properties [14]. Electrophoretic deposition of laminar composites poses problems that do not exist for centrifugal, slip or tape casting, namely:

- The chemical composition of the layers varies during deposition due to a carryover of suspension from one bath to the other causing a gradual contamination of both suspensions.
- The chemical composition of mixed layers (Al_2O_3+ZrO_2) does not correspond to the composition of the suspension since the deposition rates of its components (Al_2O_3 and ZrO_2) are different.

Therefore we studied the chemical composition of Al_2O_3+ZrO_2 mixed layers deposited from 50 weight % Al_2O_3 + 50 weight % ZrO_2 suspensions and also the variation in chemical composition of both mixed and "pure" ZrO_2 layers during deposition of ZrO_2/Al_2O_3+ZrO_2 laminar structures. The ZrO_2/Al_2O_3 composites were not studied because of the wavy surface of Al_2O_3 layers and because they were easily cracked during sintering due to different shrinkage of the ZrO_2 and Al_2O_3 layers [14].

The chemical composition of the layers was determined with the EDS unit of an electron microscope (JEOL 840 SM) on polished cross-sections of sintered specimens.

The results for three ZrO_2/Al_2O_3+ZrO_2 laminates described in Table 7 are presented in Table 8. Specimen No. 1 was deposited from "new" (not used) suspensions, specimens No. 2 and 3 were deposited from "used" suspensions, specimen No. 3 being deposited from a suspension used more than that from which specimen No. 2 was obtained.

The results may be summarized as follows:

- The composition of a mixed layer (69% Al_2O_3 + 31% CeO_2/ZrO_2, the first layer of specimen No. 1) differs considerably from the composition of the suspension (50% Al_2O_3+ 50% $CeZrO_2$) from which the layer was deposited. The result is not unexpected because the deposition rates of Al_2O_3 and ZrO_2 are different. The composition of mixed layers for specimens No. 2 and 3 is very close to that of specimen No. 1.

Table 7: The conditions of formation for the three laminar composites

Spec. No.	Initial concentration of suspensions (g/l)	Amount of solids (g)	Composition of Al_2O_3+ZrO_2 suspension	Solvent	Additive and its concentration	Field intensity	Deposition time for ZrO_2 layer	Deposition time for Al_2O_3+ZrO_2 layer	ZrO_2 layer thickness	Al_2O_3+ZrO_2 layer thickness	Amount of layers	Total thickness of specimen
1 67	100	90	50%w Al_2O_3+ 50%w ZrO_2	Isopropanol	1.5% (v/v) AcAc	200 v/cm was constant	120 sec was constant	90 sec was constant	75μ-15μ	90μ-17μ	151	5mm
2 51	100	39	"	"	"	200v/cm and after 119 layer 300v/cm	Gradual increase from 60 to 105 sec	Gradual increase from 10 to 52 sec	from 10μ to 35μ	from 6μ to 30μ	159	2.9mm
3 63	50	25	"	"	"	200v/cm and after 115 layer 300v/cm	Gradual increase from 64 to 124sec	Gradualy increase from 18 to 48sec	from 10μ to 33μ	from 3μ to 18μ	197	2.8mm

Table 8: Individual layer composition for ZrO_2/Al_2O_3+ZrO_2 laminar composites

		Beginning content in % W				End content in %w		
Specimen No.	Layer No.	Al_2O_3	ZrO_2	CeO_2	Layer No.	Al_2O_3	ZrO_2	CeO_2
Al_2O_3+ZrO_2 layer								
1	1	69	25	6	151	60	33	7
2	1	66	29	5	161	66	28	6
3	1	67	28	5	151	66	28	6
ZrO_2 layer								
1	2	0	82	18	150	8	75	17
2	2	3	80	17	160	14	71	15
3	2	11	73	16	152	11	73	16

During the deposition the content of CeO_2-ZrO_2 in a mixed layer increased by 9% as compared to the first layer (specimen No. 1) and the content of Al_2O_3 in a ZrO_2 layer increased by 8%. This result is also not unexpected, since we form a multilayer deposit by alternating the immersion of a substrate in two different suspensions and a carryover of suspension from one bath to another is unavoidable.

- Interestingly, the composition of a mixed layer in specimens No. 2 and 3 (deposited from "used" suspensions) practically does not change during the deposition.

The composition of a ZrO_2 layer in specimen No. 2 deposited from a less "used" suspension changes in the same way as it does in specimen No. 1. The composition of a ZrO_2 layer in specimen No. 3 obtained from a more "used suspension" (11% Al_2O_3 in the first ZrO_2 layer) practically does not change through the composite.

The above mentioned problems will be addressed in future work. The gradual contamination of ZrO_2 layers with Al_2O_3 and mixed layers with ZrO_2 due to a carryover of suspension from one bath to another will be minimized or eliminated when circulation of the suspension plus large reservoirs will be applied. The required composition of mixed layers can be achieved by adjusting properly the concentrations of both suspensions.

4.6 Initial Measurements of Mechanical Properties of Multilayered Laminates

The mechanical properties of thin Al_2O_3+ZrO_2/ZrO_2 multilayered laminates were characterized in a preliminary experimental program which included: evaluation of the modulus of rupture (MOR) in three and four point bend tests and micro-indentation of the layers within the laminate. Mechanical tests were carried out with an Instron 8562 electromechanical testing machine.

4.6.1 Three point bend (3PB) test

A flexure beam was prepared from an Al_2O_3+ZrO_2/ZrO_2 multilayered laminate. The laminate was prepared from a Ce-ZrO_2 and a 50% $CeZrO_2$-50% Al_2O_3 suspension. The beam dimensions were 20 mm in length, span of 13 mm. The areal section beneath the load point was measured to be 2.85 mm in height and 2.75 mm in width. The beam was not of a regular prismatic shape due to difficulties in specimen preparation. Visible processing flaws were observed in one of the surfaces, and were located so that they will experience compressive stresses during the test.

The beam was put in a 3PB fixture so that the layer planes were perpendicular to the neutral plane. It was loaded under displacement control with a cross-head velocity of 0.1 mm/min. The beam was fractured at a load of 1024.7 [N] in a brittle manner. Using simple beam theory, the MOR was calculated to be 895 MPa. Both three and four point bend test specimens had thin layers ($\sim 15\mu$) and therefore no transformation toughening nor crack deflection were observed.

4.6.2 Four point bend (4PB)test

In this test, the beam dimensions were 23 mm by length and 1.8 and 2.1 mm height and width, respectively. The span was of 20 mm and both external loads were located 3.2 mm from each support. The beam had a regular prismatic shape.

The beam was put in a 4PB fixture where, again, the layer planes were perpendicular to the neutral plane. It was loaded under displacement control with cross-head velocity of 0.1 mm/min. The beam was fractured at a load of 416 [N] in a brittle manner. Using simple beam theory, the MOR was calculated to be 587 MPa.

4.6.3 Microhardness tests evaluation

The microhardness tests were carried out on specimens of Al_2O_3/ZrO_2 with thicker layers. The average layer thickness was 55 μm for the ZrO_2 and 25 μm for the Al_2O_3 layers. When the ZrO_2 layer was indented by a Vickers microindentor under a load of 500 gr., only a well-defined pyramidal plastic indent was observed, without any visible cracking. This resulted from the well-known high fracture toughness of this layer (see Fig. 32).

When the Al_2O_3 layers were indented under similar load, plastic deformation in the form of a pyramidal indent was observed, together with two typical cracking patterns. The first type contained two radial cracks emanating from two of the indent corners developed parallel to the layers' surfaces (Fig. 33). No cracks were observed normal to the layer surface. In the second type, radial cracks were emanated from all four corners of the indentor traces, the normal to the surface cracks arrested at the interface of the adjacent layer (Fig. 34). It should be noted that the alumina layers were subjected to compressive stresses, while the zirconia was subjected to tensile stresses as a result of thermal expansion coefficient mismatch.

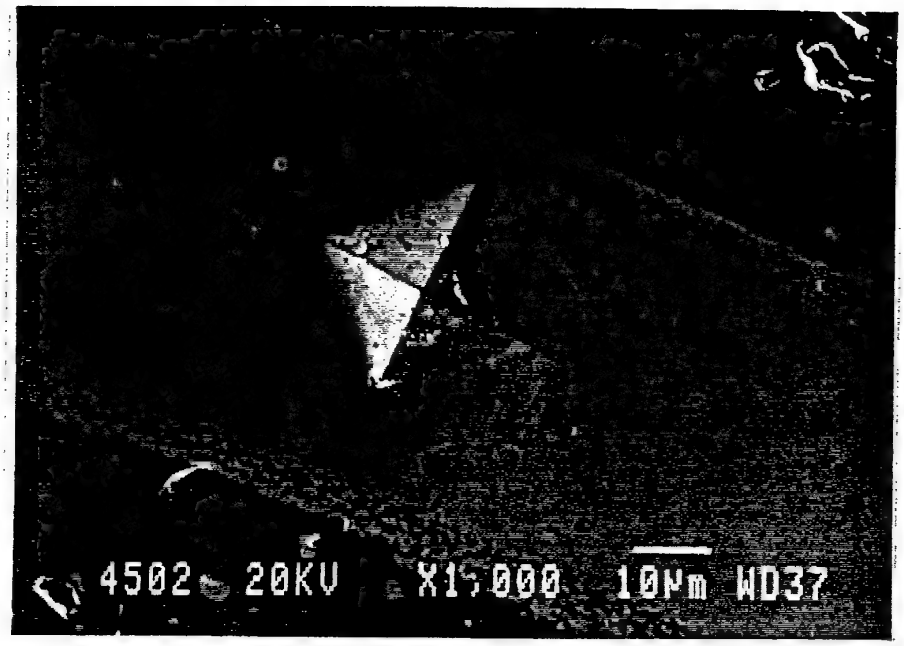

Fig. 32: Vickers microhardness test on ZrO_2 layer.

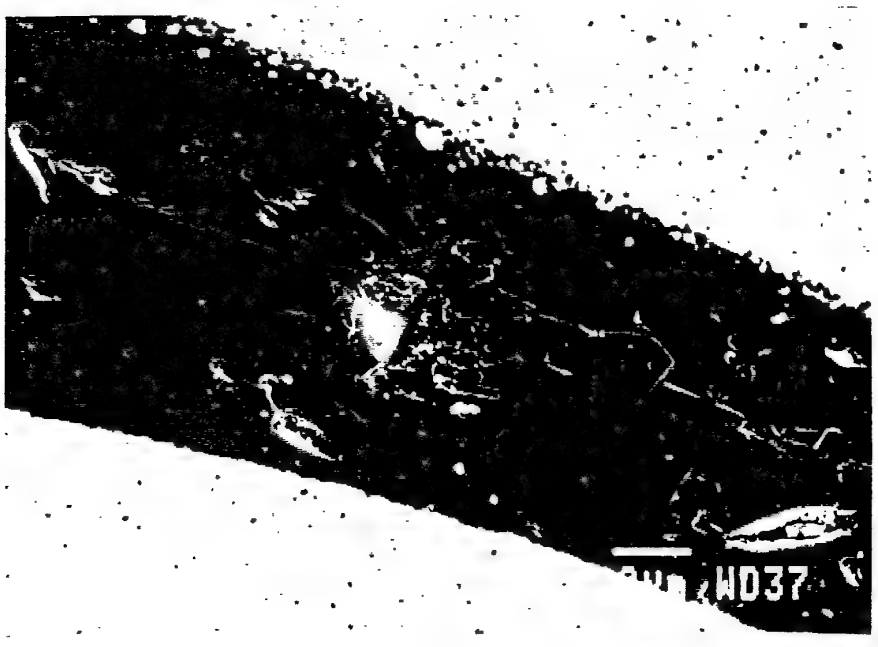

Fig. 33 : Indentation in Al_2O_3 layer

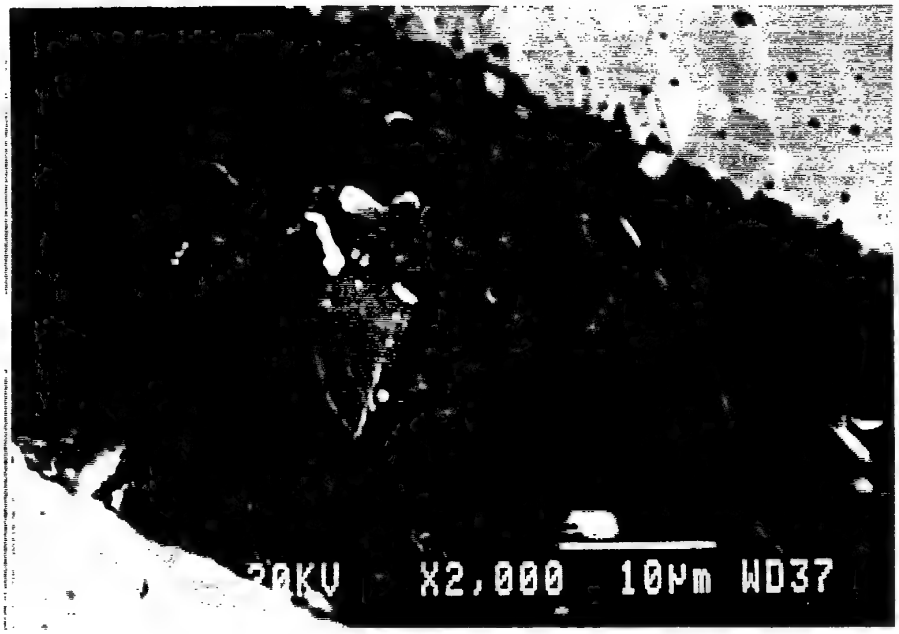

Fig. 34: Indentation in Al_2O_3 layer

CHAPTER 5. SUMMARY

The results obtained at this stage of the project can be summarized as follows:

- $Al_2O_3/Ce-ZrO_2$ and $Al_2O_3+Ce-ZrO_2/Ce-ZrO_2$ laminar composites of up to 300 layers and a total thickness of up to 5.5 mm were obtained by electrophoretic deposition from appropriate suspensions. The deposition was performed at a constant field intensity of 200 v/cm and particle concentration of 100 g/l.

- Individual layer thickness was varied in the range of $5-100\mu$.

- The composition of the deposited layers differs from that of the suspensions due to a lower deposition rate of the $Ce-ZrO_2$ as compared to that of the Al_2O_3.

- Improval in thickness uniformity of the composite was obtained by adjusting the anode/cathode ratio.

- Planarity of Al_2O_3 layers is achieved when $Ce-ZrO_2$ is added to the Al_2O_3 suspension. Planarity of $Ce-ZrO_2$ has been obtained at all experimental conditions.

- The electric resistance of the deposit increases with increase of deposit thickness. However, up to about 2 mm thickness this increase is negligible. This behaviour is explained by a preferential deposition of large particles resulting in an initial porous less resistant layer.

- As a result of suspension depletion and increase of deposit resistance the individual thickness of the layers decreases during deposition at constant field intensity and uncorrected suspension concentration.

- A $Ce-ZrO_2/Al_2O_3+Ce-ZrO_2$ laminar composite with small variation in layer thickness was obtained under conditions of increasing field strength and deposition time for each layer.

- Preliminary tests of microhardness of individual layers showed confinement of cracks to the Al_2O_3 layer.

CHAPTER 6. FUTURE WORK

At the present stage of the project the conditions for the formation of thick $Ce-ZrO_2/Al_2O_3+Ce-ZrO_2$ laminar composites were studied. However, optimization of the process requires further studies to be performed in the next stage. These are:

* Further improvement of "throwing power" (uniform thickness of whole cross-section)

* Control of concentration of suspension during deposition

* Control of layer thickness during deposition (varying parameters such as: deposition time, applied potential)

* Study of reproducibility of layer thickness

* Study of mechanical properties (strength and fracture toughness)

* Optimization of mechanical properties (e.g., layer thickness)

BIBLIOGRAPHY

1. J.O.M. Bockris, A.K.N. Reddy, "Modern Electrochemistry", Vol. 1, 1970. Plenum Press, New York.
2. R.J. Hunter, "Zeta Potential in Colloid Science", Academic Press, London, 1981.
3. O.M. Bockris, K.N. Reddy, "Modern Electrochemistry", Vol. 2, 1970. Plenum Press, New York.
4. P.W. Powers, J. Electrochem. Soc., *122* (4), 490, 1975.
5. Y. Hirata, A. Hishimoto, Y. Ishihara, Nippon Seramikkusu Kyokai Gakujutusu Ronbunshi, *99*(2), 108, 1991.
6. Z. Zhang, Y. Huang, Z. Jiang, J. Am. Ceram. Soc., *77*(7), 1946, 1994.
7. R., Nass, W. Storch, H. Schmidt, F. Harbach, R. Neff, H. Nienburg, Ceramic Processing, Sci. Proc. Int. Conf. 2nd, 1988, 625-32, Cologne, F.R.G.
8. J. Mizuguchi, K. Sumi, T. Muchi, J. Electrochem. Soc., *130* (9), 1819, 1983.
9. P.S. Nicholson, P. Sarkar, X. Haung, J. of Materials Science, *28*, 6274, 1993.
10. J. Mizuguchi, M. Suzuki, H. Yamato, M. Matsumuzo, J. Electrochem. Soc., *138* (10), 2942, 1991.
11. D.B. Marshall, J.J. Ratto, J. Am. Ceram. Soc., *74*(12), 2979, 1991.
12. A.T. Vagramyan, Z.A. Solovieva, "Technology of Electrodeposition", Teddington, 1961.
13. W. Blum, G.B. Hogäboom, "Principles of Electroplating and Electroforming", N.Y.-Toronto-London, 1949.
14. V.J. Lainer, "Sovremennaja galvanothechnika," 1967.

Multilayer Ceramic Composite Formation by Electrophoretic Deposition

L. Gal-Or, S. Liubovich, M. Folman

Israel Institute of Metals

Technion Research and Development Foundation

Interim Scientific Report

May 1, 1993 - April 30, 1994

Research Project 524-702

F4 9620-93-1-0233

Prepared for

EOARD - London, England

AFOSR - Bolling, Washington, D.C., 20332, U.S.A.

REPORT DOCUMENTATION PAGE

Form Approved
OMB No. 0704-0188

1. AGENCY USE ONLY (Leave blank)	2. REPORT DATE	3. REPORT TYPE AND DATES COVERED
	30 June 1994	Annual 1, May 1993-April 30 1994

4. TITLE AND SUBTITLE
Multilayer Ceramic Composite Formation by Electrophoretic Deposition

5. FUNDING NUMBERS
F49620-93-1-0233

6. AUTHOR(S)
L. Gal-Or, S. Liubovich, M. Folman

7. PERFORMING ORGANIZATION NAME(S) AND ADDRESS(ES)
Technion R&D Foundation
Technion - Israel Institute of Technology
Senate House, Technion City, Haifa 32000, Israel

8. PERFORMING ORGANIZATION REPORT NUMBER

9. SPONSORING/MONITORING AGENCY NAME(S) AND ADDRESS(ES)
EOARD 223/231 Old Marylebone Rd., London
NW1 5TH UK
AFOSR/NE Dr. A. Pechenik, Bolling AFB,
Washington DC 20332-6448

10. SPONSORING/MONITORING AGENCY REPORT NUMBER

11. SUPPLEMENTARY NOTES

12a. DISTRIBUTION/AVAILABILITY STATEMENT
Unlimited

12b. DISTRIBUTION CODE

13. ABSTRACT *(Maximum 200 words)*

Multilayer ceramic composites are of great interest due to prospects for enhancement of fracture toughness. A novel approach to multilayer formation based on electrophoretic deposition is adopted in this work. Alternating layers of ZrO_2 and Al_2O_3 are deposited by alternating immersion in two different suspensions. Deposition rates of Al_2O_3 and ZrO_2 as function of deposition parameters (electric field strength, particle concentration, deposition time) were studied. Green and fired densities of deposits were studied and improved by use of additives which stabilize the suspension and prevent agglomeration of particles.

14. SUBJECT TERMS
Electrophoresis, ceramics, multilayer, microcomposites

15. NUMBER OF PAGES

16. PRICE CODE

17. SECURITY CLASSIFICATION OF REPORT	18. SECURITY CLASSIFICATION OF THIS PAGE	19. SECURITY CLASSIFICATION OF ABSTRACT	20. LIMITATION OF ABSTRACT
Unclassified	Unclassified	Unclassified	Unlimited

List of Personnel

Dr. L. Gal-Or - Principal Investigator

Mrs. S. Liubovich - Research Associate

Dr. O. Korotkina - Research Associate

Mr. R. Goldner - Student

Prof. M. Folman - Consultant

Table of Contents

Table of Contents (cont.)

Chapter 1 – Introduction

Enhancement of fracture toughness of ceramic materials is of primary interest. Recently, the increase of fracture toughness in layered ceramic composites due to modification of size and shape of the transformation zones around cracks was demonstrated for Al_2O_3/ZrO_2 microcomposites.

Several approaches are currently adopted for the formation of multilayered structures. These include slip casting, tape casting and sequential centrifuging.

In the present work a novel approach to formation of a multilayered composite is studied. The approach is based on electrophoretic deposition of alternating layers of two kinds of ceramic materials by alternating immersion of a substrate in different suspensions while applying selected deposition parameters.

Electrophoretic deposition has several advantages over the existing methods of multilayer formation, these are:

- Rigid and easy control of layer thickness.
- Wide range of layer thickness variation (from a few microns to millimeters)
- The possibility to form intricate shapes of composites.
- Low cost equipment and possibility of automation.

The first year of this work concentrated on studies of the deposition rates of Al_2O_3 and ZrO_2 particles from suspensions based on isopropanol. The deposition parameters varied were: the electric field strength, particle concentration and

deposition time. In addition to the kinetics of deposition the effect of deposition parameters on the green and fired density of the deposits was studied. It is known that the stability and homogeneity of the suspension have a strong effect on the density of the deposit. Therefore the influence of additives which enhance these properties was studied. Initial green and sintered multilayer ZrO_2/Al_2O_3 structures were formed with individual layer thicknesses in the range of 10–100 microns.

Chapter 2 - Literature Survey

2.1 Electrophoretic deposition of ceramic particles

Electrophoretic deposition has several advantages over other existing methods of multilayer formation:

- rigid and easy control of layer thickness
- possibility to vary the layer thickness in a wide range (from a few microns to millimeters)
- possibility to form intricate shapes of composites
- possibility of automatization

Electrophoretic deposition includes two processes: (1) electrophoresis and (2) deposition:

- Electrophoresis is the migration of non-conductive but electrically charged particles in an electric field to one of the electrodes.
- The deposition is the process by which these electrically charged particles having arrived at an electrode are deposited on it.

2.1.1 Charging of particles

The electrical charges borne by particles in suspensions arise spontaneously when mixed with the solvent. The most important mechanisms of surface charge generation for ceramic particles are [1]:

- surface group dissociation
- ion (or polar molecules) adsorption from the liquid vehicle.
- crystal lattice defects

As a consequence of the electrical surface charge developed on colloidal particles, ions of opposite sign (counterions) present in the bulk of solution will concentrate (attracted by electrostatic forces) at the interface to balance the surface charge.

Thus a double layer is formed. The charged particle with its double layer is electrically neutral.

According to the model proposed by Stern the double layer consists of a rigid part (extending into the interface region for a distance δ which is approximately equal to the size of a hydrated counterion) with a linear, and a diffuse part with a non-linear potential gradient (Fig. 1). The distribution of counterions in the diffuse layer is determined by the interplay of electrostatic and thermal energy. As solid particles move through the fluid the counterions in the outer part of the diffuse layer slip away and do not migrate with the particles leaving some of the surface charge uncompensated. Thus the slipping plane (shear plane) arises.

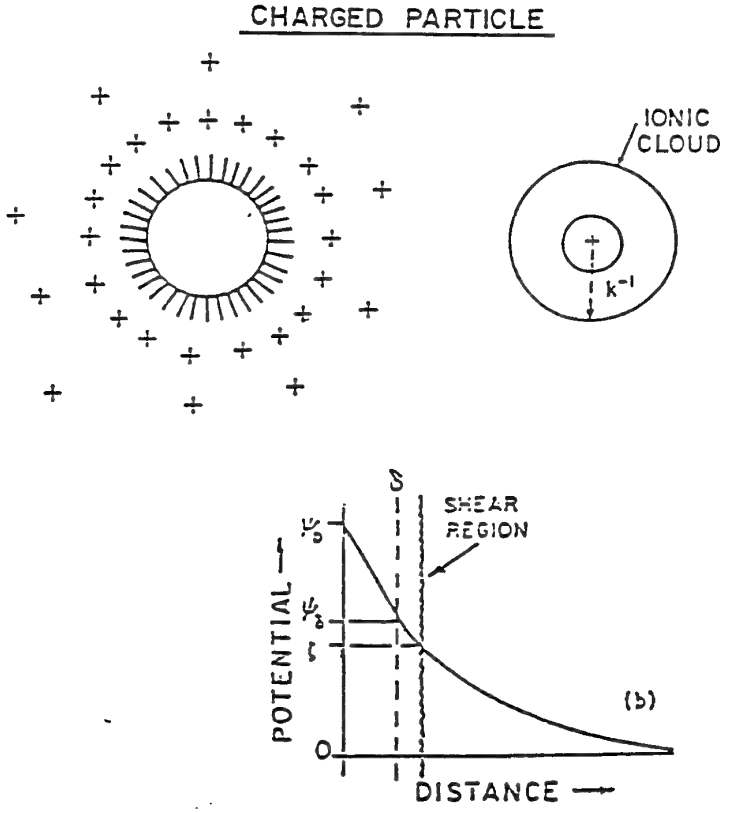

Fig. 1: The double layer and potential gradient surrounding a charged particle.

Fig. 1 shows the potential drop across the double layer ψ_0, consisting of a linear part $\psi_0-\psi_\delta$ in a Stern layer, and a non-linear part ψ_δ across the mobile diffuse layer. The part of a non-linear potential drop, namely, slipping (shear) plane potential, presenting the net charge of the particles, is termed zeta-potential and determined the electrophoretic behaviour of the particles. The zeta potential ς is often equated with the potential ψ_δ.

2.1.2 Electrophoresis

The equation for the mobility of a particle moving under an applied electric field in an unbounded fluid is derived by equating the driving electric force with the frictional resistance of a fluid and the relaxation force [2] (see Fig. 2). The relaxation force arises due to the tendency of the counterions in the diffuse double layer to move in the direction opposite to the movement of the particles, slowing down its velocity. The ionic cloud acquires an egg shape.

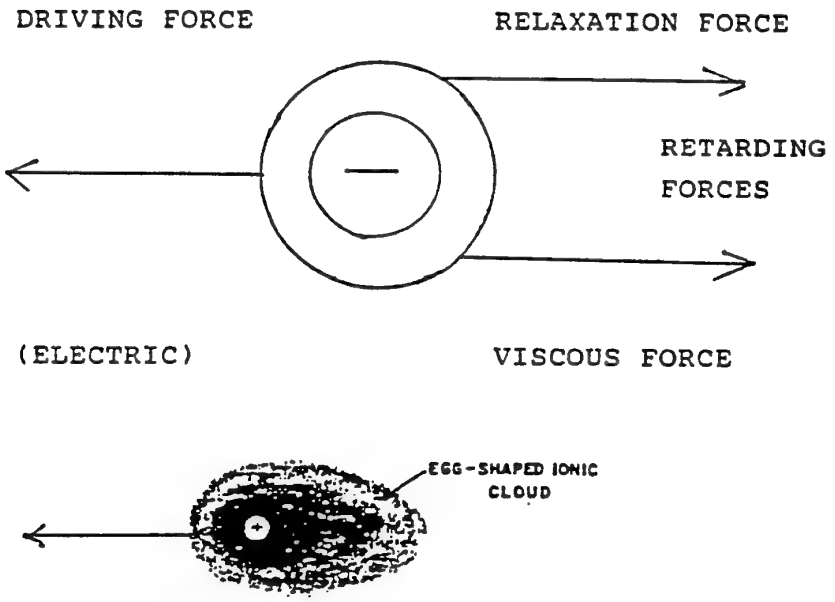

Fig. 2: Egg-shaped ionic cloud and forces acting on a moving particle.

The mobility $\mu \left(= \frac{V}{E}\right)$ is given by

$$\mu = \epsilon \zeta_p / 4\pi\eta \times [1+f(kr)]$$

where:

V – electrophoretic velocity

μ – mobility

E – field strength

ϵ – dielectric constant of fluid

ζ_p – zeta potential of particles

η – viscosity of fluid

k – 1/double layer thickness

r – radius of particle

f(kr) varies between 0 and 1 for small and large values of kr respectively.
f(kr) represents the relaxation phenomenon, if $k \ll r$ then the Smoluchowski equation is obtained and:

$$\mu = \frac{\epsilon}{4\pi\eta} \zeta_p$$

2.1.3 Deposition

There is no satisfactory theory which fully explains the mechanism by which a deposit forms and adheres when the particles reach the electrode. Three theories exist on this subject:

- One theory assumes that the particles that reach the electrode undergo an electrode reaction which neutralizes them . This theory cannot explain the fact reported in [3] that MgO deposits were obtained on a polymeric diaphragm located between two electrodes. But when the same arrangement was used for aluminium powder [3] no deposit was formed on the diaphragm showing that in this case the electrode reaction plays a part in deposition.

- The second theory states that the particles are brought to the electrode by a field which exerts sufficient force to overcome the repulsion between them allowing the particles to come close enough for the London–van der Waals forces of attraction to predominate. On the basis of Verwey & Overbeek theory [4] describing the behaviour of suspended particles in terms of the potential energy of interaction, the minimal field strength E necessary to overcome repulsion between particles and allow their deposition is given by:

$$E = \frac{2F}{3\epsilon a \zeta_p}$$

where:

F – the minimum force required to overcome repulsion between particles, determined as the maximum slope of the curve V_T in Fig. 12 to the right of the peak.

a – radius of a particle.

It must be noted that the zeta potential ζ_p determines both the electrophoretic mobility of the particle and the minimum electric field bringing about its electrophoretic deposition.

In [3] the calculated values of E were compared with experimentally observed ones. For some materials the agreement was found to be satisfactory, for other materials the deposition could not be explained in terms of the Verwey–Overbeek theory.

- The third theory presumes that secondary processes which take place at the electrode can produce ions which coagulate the particles by discharging them or produce hydroxides which polymerize and adsorb on the particles holding them together [5].

All three mechanisms are likely to play a part in the process of electrophoretic deposition. But it is not always possible to predict which of them will predominate and which (or all) will fail.

Parameters which affect electrophoretic deposition are the following:

- Particle charge
- Particle size distribution
- Particle concentration
- Dielectric constant of solvent
- Applied voltage
- Deposition time

According to [6] the potential distribution in a bath for electrophoretic deposition has to be as shown in Fig. 3 in order to supply voltages at the electrode interfaces necessary for deposition while retaining sufficient potential gradient in the bulk of the suspension needed for mass transfer.

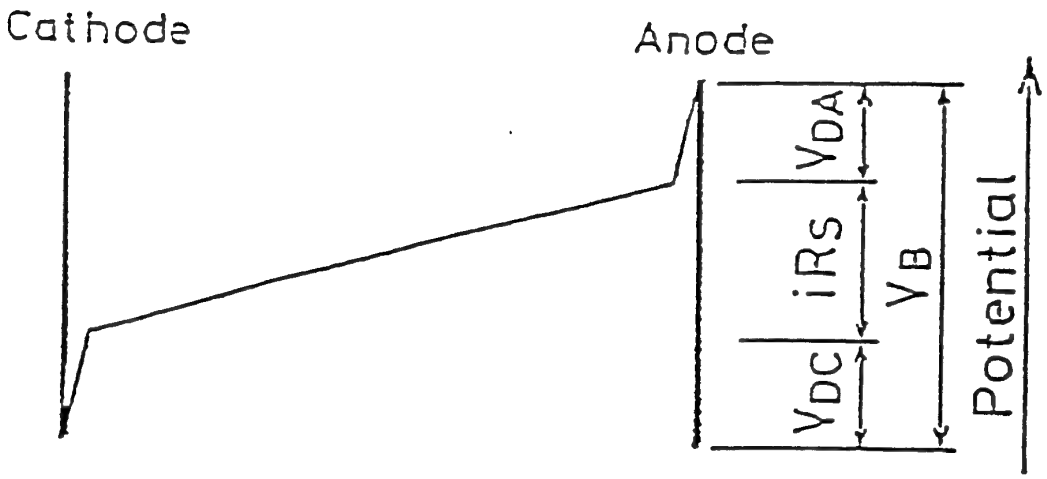

Fig. 3: The potential gradient ideal for electrophoretic deposition where the anodic and cathodic deposition voltages are denoted by V_{DA} and V_{DC} and bath voltage, the resistance of the solution and the flowing current by V_B, R_S and i, respectively.

This potential distribution can be obtained by adding an appropriate amount of electrolyte to the solution to control its resistance.

There is an optimum value for the dielectric constant ϵ . Solvents with too low ϵ do not possess the necessary dissociating power to obtain a charging effect on the particles. Yet a too high ϵ leads to a high conductivity and low deposition efficiency due to parasitic electrochemical reactions. Deposition from aqueous suspensions which is inevitably concurrent with electrolysis results in coarse deposit with voids due to gas evolution. It was found [7] that optimal deposition is obtained in solvents with $\epsilon \approx 14$ (see Fig. 4 for domain of ϵ where deposition can be obtained).

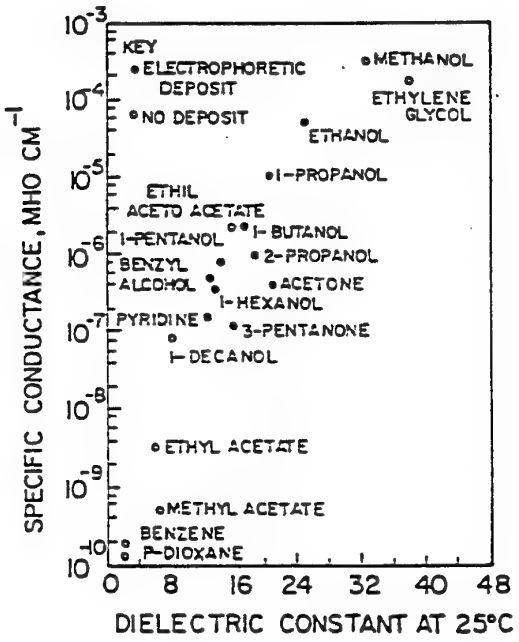

Fig. 4: Dielectric constants of various solvents. Dark dots designate solvents suitable for electrophoretic deposition.

The electrophoretic yield is given by [7]:

$$Y = A\int \mu ECSdt$$

where

A – yield constant

μ – mobility

E – field strength

C – concentration of particles

S – area of an electrode

t – time .

The polarity of the zeta potential (positive or negative) will determine whether anodic or cathodic deposition will take place.

2.2 Control of zeta potential

Zeta potential is a key factor in the electrophoretic deposition process. It determines the direction and velocity of particle migration and the field strength required to overcome mutual repulsion between particles and to bring about their deposition. It is also a key factor in the electrostatic stabilization of suspensions determining the intensity of electrostatic repulsive interactions between particles. In composite ceramic processing where more than one type of particles are involved the zeta potential signs and values of all types of particles must be carefully considered and controlled.

The zeta potential (section 2.1, Fig. 1) is determined by three categories of ionic species present in the solution:

1. The potential determining ions (p.d.i.). They exert a fundamental control on the surface charge of the particles. They generate the surface charge.

In the case of inorganic oxides p.d.i. are H^+ and OH^- ions. Oxide surfaces are considered to possess a large number of amphoteric hydroxide groups which can undergo reaction with either H^+ or OH^-:

$$MOH_2^+ \overset{H^+}{\leftarrow} M\text{–}OH \overset{OH^-}{\rightarrow} M(OH)_2^- \; (= MO^- + H_2O)$$

The surface charge density δ_0 is given by

$$\delta_0 = e(\nu_+ - \nu_-)$$

where:

e – electronic charge

ν_+, ν_- – numbers of positive and negative sites per unit area

At a particular bulk concentration of p.d.i.'s the surface charge will be zero. This is the point of zero charge (p.z.c.). This point can be determined by measuring the surface charge as a function of the p.d.i. concentration. Very often (in the absence of specifically adsorbed ionic species) this point coincides with the p.d.i. concentration at which the zeta potential is zero, this point being called the isoelectric point (i.e.p.).

At pH values lower than i.e.p. the zeta potential is positive and at pH higher than i.e.p. the zeta potential is negative. Fig. 5 (from [8]) demonstrates the zeta potential vs. pH for aqueous suspensions of Al_2O_3 and m–ZrO_2.

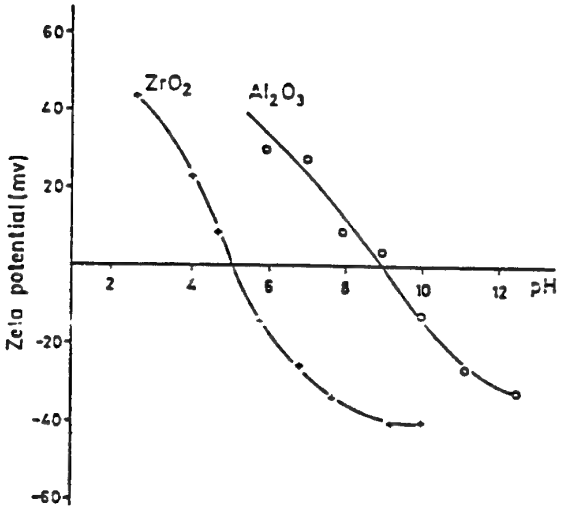

Fig. 5: Zeta potential vs. pH for Al_2O_3 and m–ZrO_2 suspensions.

Following are data on the p.z.c. (titration measurements) and i.e.p. (electrophoretic measurements) for some oxides. It must be noted that the chemical and physical conditions of the particle surface considerably affect the p.z.e./i.e.p. and zeta–potential. Their actual values for a particular material can be influenced by the source, preparation method, pretreatment and the presence of trace impurities.

Table 1:

Oxide	pH(i.e.p.)	pH (p.z.c.)	Ref.
αAl_2O_3	9,1 ± 0,2	9,1 ± 0,2	9
ZrO_2 monoclinic	5,0	—	10
ZrO_2 tetragonal (3,5 mol% Y_2O_3)	6,5	—	10
α SiO_2	2,0 ± 0,3	2,0 ± 0,3	9
TiO_2	5,8 ± 0,1	5,8 ± 0,1	9
α Fe_2O_3	8,5 ± 0,2	8,5 ± 0,2	9

For pure α alumina the p.z.c./i.e.p. point is of pH = 9,1. Doping with TiO_2 shifts pH value to less than 8. Doping with MgO shifts the value up to 10.

When i.e.p. and p.z.c. do not coincide in a given system (in the absence of specific interactions) the difference is most likely to be not fundamental. A charge determination (titration) is conducted on a dispersion at a high volume fraction of solids (i.e. a high surface area). So the effect of trace impurities introduced perhaps with the supporting electrolyte or with the solvent is minimized simply because the trace impurities are spread over a large area. Since a low percentage of solids dispersion is required in a microphoresis experiment the same amount of impurities is distributed over a much lower area. Their effect on the i.e.p. will be much greater than on the p.z.c.

2. The indifferent electrolyte ions. These do not interact specifically with the particle surface but control the extension of the double layer.

They are counterions of the double layer. Unlike potential determining ions simple counterions remain on the solution side of the interface and are not involved in any specific interaction with the surface. Their presence at the interface is solely due to electrostatic attraction.

Their influence on zeta potential is vast. The increase of indifferent ions concentration leads to compression of the double layer and the zeta potential decreases, approaching asymptotically to zero when the double layer shrinks to a monoionic Stern layer. They can't reverse the sign of the zeta potential and shift the i.e.p.

The effect of the indifferent electrolyte concentration on ζ_p (assuming the Gouy–Chapman model) is shown in Fig. 6 [11].

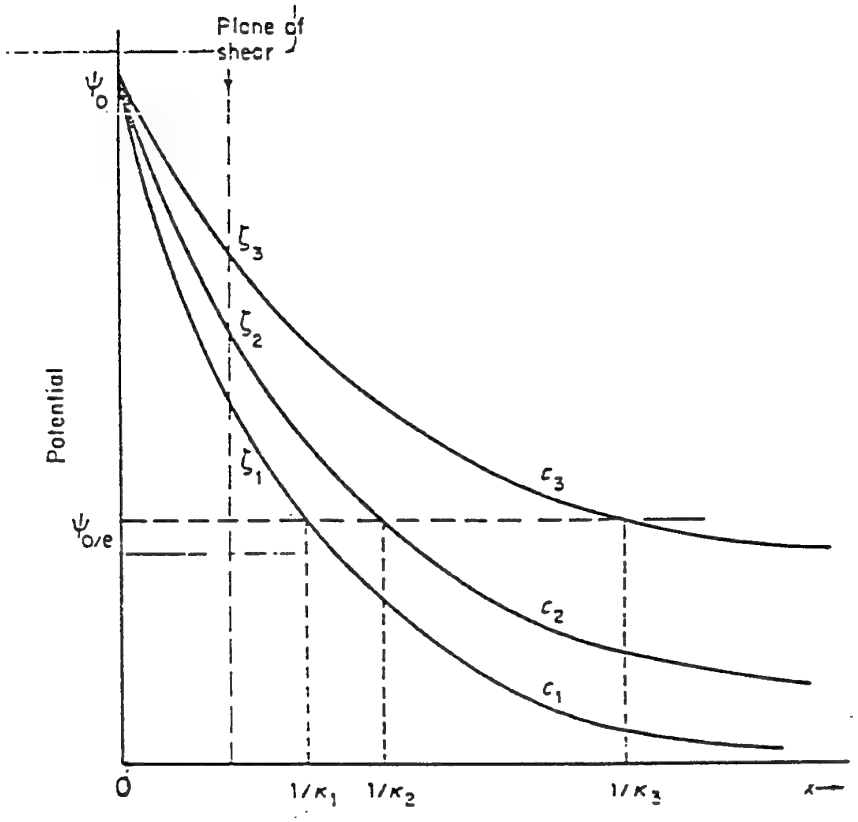

Fig. 6: Effect of indifferent electrolyte concentration c on ζ_p ($c_1 > c_2 > c_3$).

Fig. 7 [11] shows the variation of zeta potential of Al_2O_3 with pH at various concentrations of KNO_3. While ζ_p is affected by the electrolyte concentration (conc. of KNO_3), the i.e.p. is not, which confirms the fact that the KNO_3 is an indifferent electrolyte.

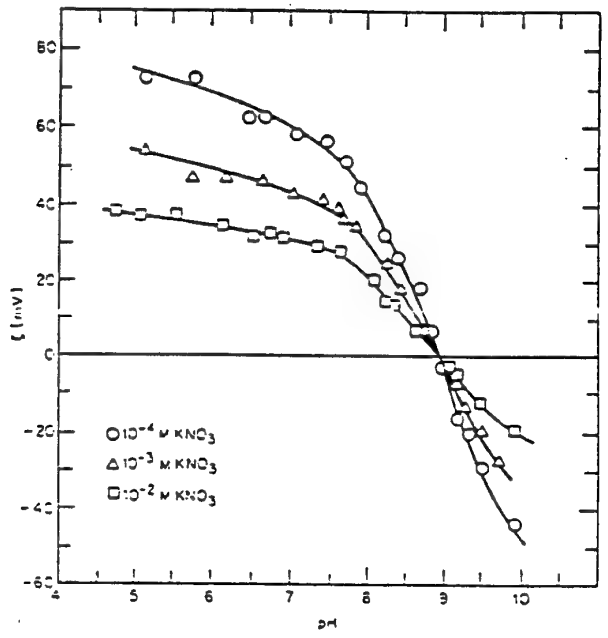

Fig. 7: Zeta potential as a function of pH for Al_2O_3 (0.15 gr/l) in an indifferent electrolyte solution.

3. Specifically adsorbed ions. They exhibit a strong affinity for the surface and adsorb in the inner region of the double layer (that is, in the Stern layer) through mechanisms that involve more than just electrostatic forces.

The specifically adsorbed ions can have the following effects on ζ_p:

- reversing the sign of ζ_p
- shifting the i.e.p.

This effect is drastically demonstrated in Fig. 8 [12] which shows the zeta potential as a function of electrolyte concentration ($BaCl_2$ and Na_2SO_4) when the ions Ba^{+2} and SO_4^{-2} are specifically adsorbed ions.

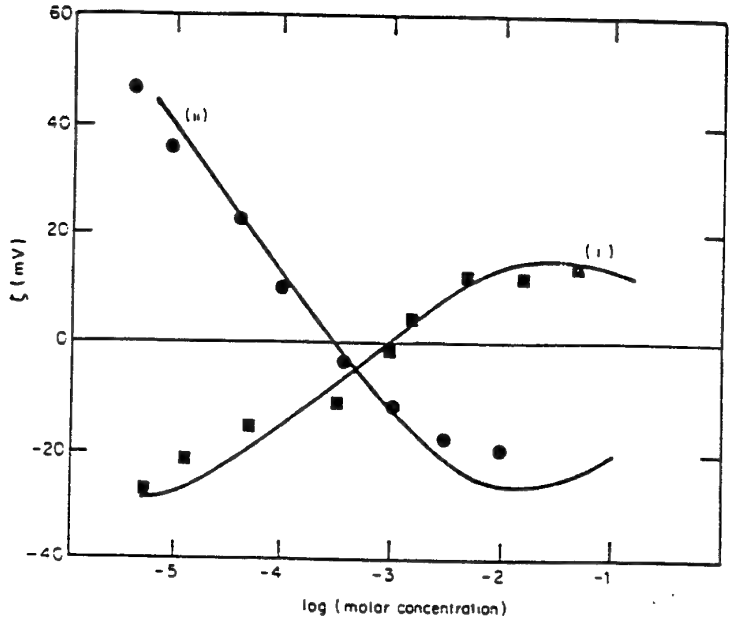

Fig. 8: ζ_p of Al_2O_3 as a function of electrolyte concentration.
(i) - pH 10 in $BaCl_2$ (ii) pH 6.5 in Na_2SO_4.

Fig. 9 [11] illustrates the mechanism by which the reversal of the zeta potential sign occurs (the Stern model).

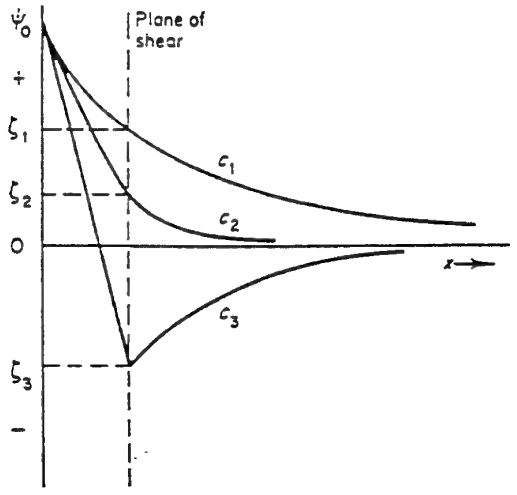

Fig. 9 [11]: The reversal of the zeta-potential sign by the specific adsorption of an anion (Stern model of the interface).

The effect of specific adsorption of polyelectrolytes, namely, ammonium polyacrylic acid (NH_4PAA, M.W. 3500) has been reported in [13], see figs. 10 and 11. Fig. 10 shows zeta potential vs. pH behaviour for aqueous suspensions of Al_2O_3 (A-16SG) and three ZrO_2 powders (SC30, TZ0, TZ2), SC30 and TZ0 being pure zirconia, TZ2 containing 3,53 wt% yttria. An indifferent electrolyte (10^{-3}M KCl) was added to maintain a constant ionic strength. The behaviour is typical for alumina and zirconia, their i.e.p.'s being in good accordance with literature data, table 1.

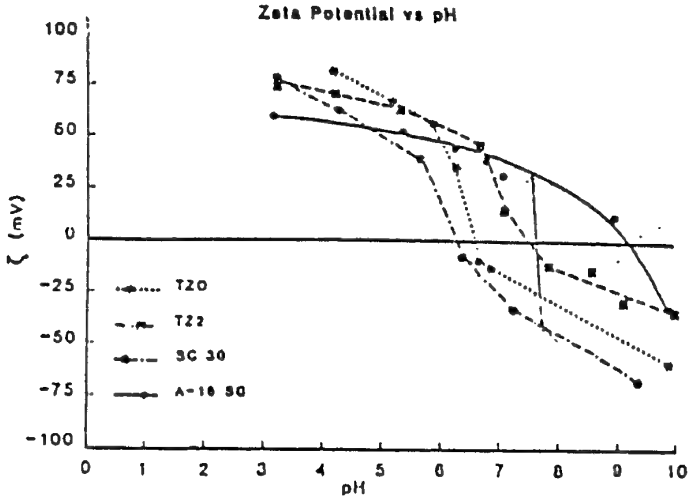

Fig. 10: Zeta potential of alumina (A-16 SG) and zirconia (SC30, TZ0 and TZ2) particles in 10^{-3}M KCl solution as a function of pH.

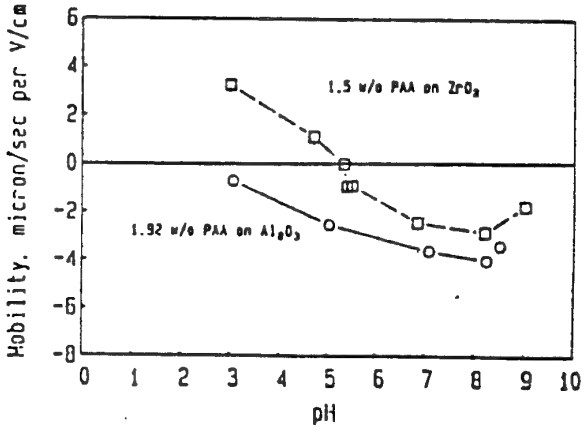

Fig. 11: Electrophoretic mobility of alumina (A-16SG) and zirconia (TZ2) particles in 10^{-3}M KCl solutions with the addition of NH_4PAA. The conc. of NH_4PAA is reported as a weight percent of polymer to solids.

Fig. 11 shows the electrophoretic mobility vs. pH behaviour for the same alumina and one zirconia (TZ2) in the presence of ammonium polyacrylic acid. I.e.p.'s have been shifted to lower pH, from 9.2 to 3.0 for alumina and from 7.4 to 5.4 for zirconia. NH_4PAA begins ionizing above pH 4. The highly negative charged polymer molecules specifically adsorb on the particle surface imparting a highly negative charge and reversing the zeta-potential sign and shifting the i.e.p.

T. Graule and L.J. Gauckler [14] have found that an aromatic sulfonic acid - Tiron (4,5-dihydroxy-1,3-benzenedisulfonic acid) added to an aqueous suspension of alumina shifts its isoelectric point from pH 9 to pH 3 and charges the alumina particles highly negative in the basic region. The high adsorption ability of Tiron with its two phenolic OH groups was explained by hydrogen bonding.

The above described analysis of the zeta potential of ceramic particles indicates that a variety of tools exists to affect it. Thus potential determining ions such as H^+ and OH^-, indifferent ions and specifically adsorbed species (simple metal ions and anions and more complex adsorbates usually called surfactants) can be used to manipulate the ζ_p value and sign.

There are many experimental techniques for measuring zeta potential. The most widely used are [11] microelectrophoresis, moving boundary methods, mass transport, all of them utilizing the electrophoresis phenomenon. Recently an ESA (Electrokinetic Sonic Amplitude) method using electroacoustic effects was proposed[14].

2.3 Stabilization of suspensions

The quality of a ceramic product manufactured by the processing of suspensions is controlled by the state of dispersion (particle size distribution and stability) which strongly affects the degree of packing in a green body, the sintering behaviour of the material and the reproducibility of the bath.

Lyophobic colloids (ceramic powder suspensions included) possess high positive surface energy because of their large specific surface area which results in the tendency to form aggregates. Lyophobic colloids are in principle unstable. So the importance of the stabilization of suspensions cannot be overestimated.

The stability of a suspension depends on the sign and magnitude of the total energy of interaction between particles V_T. The general equation for describing this interaction incorporates the sum of attractive and repulsive contributions:

$$V_T = V_A + V_R$$

where

V_A is the van der Waals attraction energy and V_R is electrostatic, steric or other repulsive interactions. The stability of suspension is achieved when the repulsive forces are high enough to dominate over the attractive London–van der Waals forces.

Van der Waals dispersion forces arise from fluctuations in the electron charge distribution around the atom or molecule. These fluctuations produce instantaneous dipoles so that one molecule in the neighbourhood of another always experiences an attraction. The van der Waals force between atoms is of quite short range, decreasing with the sixth power of the separation distance. But for particles of colloidal size this force as estimated by pairwise addition is of relatively long range decreasing with about the third power of the separation distance (see, for example [1]). Thus the van der Waals forces of attraction between colloidal particles always take place and are of quite long range.

The repulsive interaction can be provided by two different general mechanisms.

- One is electrostatic repulsion as a result of charging of colloidal particles.
- The other is steric hindrance. The particles can be coated with an adsorbed layer of a material (say a polymer) which itself prevents their close approach.

2.3.1 Electrostatic stabilization

As it was described above in Section 2.1 colloidal particles dispersed in a polar liquid bear an electric charge yet remain electrically neutral as a result of the development of an electrical double layer (Fig. 1). Between such two particles there is no electrostatic interaction unless their double layers overlap. Then repulsion arises due to interactions between counterions. The difficult task of calculating the double layer interaction has been carried out by Verwey and Overbeek [4] (DLVO theory).

The energy of repulsion between two spherical particles V_R is:

$$V_R = \frac{\epsilon a \zeta^2}{2} \ell n(1+e^{-\chi H_0}) \qquad \chi = \sqrt{\frac{4\pi e^2 \Sigma n_1 z_1^2}{\epsilon kT}} \qquad p = \frac{2\pi H_0}{\lambda}$$

The energy of attraction - V_A is : $V_A = \frac{Aa\alpha}{12H_0}$

if $0.5 < p < \infty$ $\qquad \alpha = \frac{-2,45}{5p} + \frac{2.17}{15p^2} + \cdots$

if $0 < p < 2$ $\qquad \alpha = \frac{1}{1+1.77p}$

The resultant energy V_T: $\quad V_T = V_R + V_A$, Fig. 12.

a - radius of a particle

H_0 - distance between surfaces

χ - 1/distance of the diffuse d.l.

n - No. of ions per unit volume

A - London-van der Waals const.

e - electronic charge

α - finite time of propagation of electromagnetic waves when particle separation is large.

λ - wavelength of intrinsic electronic oscillations of e.

The most important characteristic of the total energy curve (V_T) are:

- There is a potential barrier preventing contact between the particles
- There is a deep primary minimum at short separations in which agglomerated particles are bound
- There is a secondary minimum, not always present, that can provide some stabilization by means of a liquid film between the particles.

The most important parameters involved in electrostatic repulsion are the Zeta potential and the thickness of the double layer. With increasing of both these parameters V_R increases.

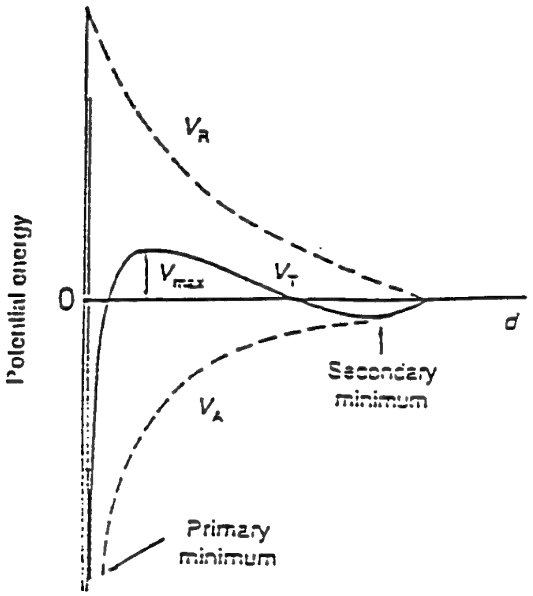

Fig. 12: Potential energy of interaction for electrostatic repulsion according to the DLVO theory.

Electrostatic stabilization requires two deflocculants: (1) surface charge controlling p.d.i.'s or specifically adsorbing species (surfactants) and (2) double layer thickness controlling counterions.

For aqueous suspensions of oxides the potential determining ions are usually H^+ and OH^+ and the pH is widely used to control the zeta potential and hence the suspension stability. The stability of a suspension can be achieved at pH values far enough from the i.e.p. (ζ_p=0) where the potential energy barrier opposing coagulation disappears and a suspension flocculates. Requena et al. [8] have found that the colloidal stability for both Al_2O_3 ($pH_{i.e.p.}$ 9) and m-ZrO_2 ($pH_{i.e.p.}$ 5) is achieved at pH $\leq$ 4 where the zeta potential values are high enough to obtain deflocculated systems.

The counterion effect on the double layer thickness, zeta potential and suspension stability is strongly dependent on its nature, namely, the charge and size. The higher the charge of a counterion the higher the energy of the electrostatic attraction between the ion and the surface and the lower the electrolyte

concentration that leads to double layer shrinkage to produce flocculation. Within the series of ions of the same charge the flocculation ability increases with increasing counterion size. The hydration sheath weakens the electrostatic interaction of the ion with the surface and the degree of ion hydration reduces when its size increases. The effect of counterions is measured by the concentration necessary to produce flocculation called the flocculation value. The order of flocculation values for monovalent and divalent ions is [15]:

$$[Li^+] > [Na^+] > [K^+] > [NH_4^+]$$

$$[Mg^{2+}] > [Ca^{2+}] > [Sr^{2+}] > [Ba^{2+}]$$

These series are known as the Hofmeister series. Fig. 13 is a good illustration [16].

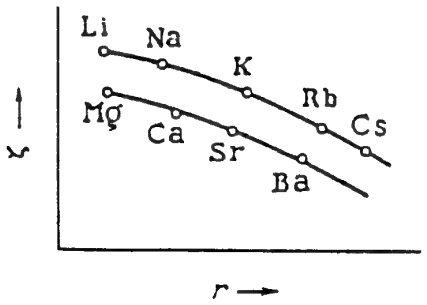

Fig. 13: The influence of the charge and size of counterions on the zeta potential of negatively charged clay particles.

The Na^+ is one of the best counterions. Widely used dispersants in ceramic processing are sodium silicates, sodium carbonates and sodium polyphosphates [17].

Surfactants [18] are used for electrostatic stabilization of both aqueous and nonaqueous suspensions. They are composed from a hydrocarbon chain soluble in the medium and a polar or ionic group such as OH^-, NH_4^+, -COOH, etc. which are surface active. The addition of surfactants to a suspension affects the

zeta potential and so the stability.

The surfactants can be classified in four different groups depending on the charge of the surface active part of the molecule: (1) nonionic, (2) anionic, (3) cationic and (4) zwitterionic, with both positive and negative charges.

A highly stabilizing effect of ammonium polyacrylic acid on aqueous suspensions of Al_2O_3 and ZrO_2 was reported in [13]. Negatively charged at pH $\geq$ 4 polymer molecules impart a high negative charge to powder. Citric acid and aromatic 4,5-dihydroxy-1,3-benzenedisulfonic acid (Tiron) were found to be good dispersants for Al_2O_3 aqueous suspensions (section 2.2). All three surfactants are of an anionic type.

Phosphate ester and ethoxylate which are anionic surfactants [15] appeared to be very effective dispersants for $BaTiO_3$ in 66% methyl ethyl ketone - 34% ethanol azeotrope [19]. Phosphate ester has been used successfully also for Al_2O_3 [20] and Al_2O_3/ZrO_2 [21] . The success of this dispersant is most likely related to ester ionization which provides a positive charge to the particle surface [15]. Triglycerides which have been used in tape casting of Al_2O_3 and ZrO_2 [22] are representatives of a zwitterionic group.

Some typical surfactants of current interest for nonaqueous ceramic slips are listed in [15]. It should be noted that electrostatic repulsion (and so electrostatic stabilization) is less effective in nonaqueous media than in water because of the lower ionic concentration and the lower dielectric constant of nonaqueous liquids.

2.3.2 Steric Stabilization

The steric repulsion forces between approaching colloidal particles are provided by macromolecules attached to the particle surface.

A polymer molecule is a molecule of relatively high molecular weight (tens of thousands and higher) with repeating units. If the repeating units are of more than one type such a polymer is called a copolymer. Copolymers can be classified into

three groups:

- random type	A A B B A B A B B A B
- block type	A A A A A A B B B B B
- graft type	A A A A A A A A A A A
	B B
	B B
	B B

Adsorbed polymers can provide steric stabilization only if two requirements are satisfied: (1) strong anchoring to the particle surface and (2) sufficient extension of the adsorbed long chain into solution to prevent the particles to approach more than 10-20nm from each other. Van der Waals attraction between colloidal particles is relatively long range in character, extending over a distance of a few nanometers. So repulsive interactions must be at least comparable, both in their range and magnitude, to that of the van der Waals attraction.

The best steric stabilizers are amphipathic block or graft copolymers if one homopolymer is soluble in the dispersion medium, while the other is insoluble. The insoluble homopolymer, termed the anchor polymer, serves to attach the soluble part to the colloidal particles. The soluble chains, which project away from the particle surface into the dispersion medium, are responsible for the observed colloid stability and thus are referred to as the stabilizing moieties.

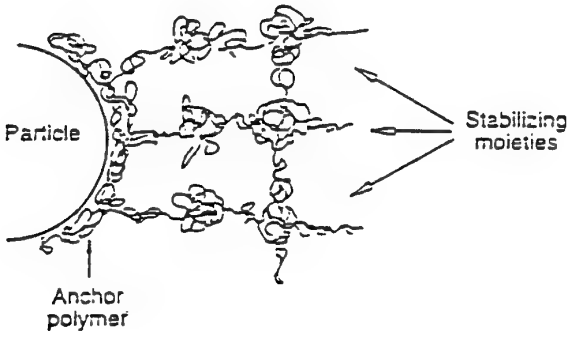

Fig. 14: Steric stabilization by an amphipathic copolymer.

The steric repulsion is due to a loss in configurational entropy that occurs when stabilizing moieties attached to approaching particles undergo interpenetration. In good solvents (better than θ-solvents) increasing the number of chain-chain contacts at the expense of chain-solvent interactions contributes (entalpy raise) to steric repulsion.

The potential energy curve for steric stabilization is plotted in Fig. 15 [15].

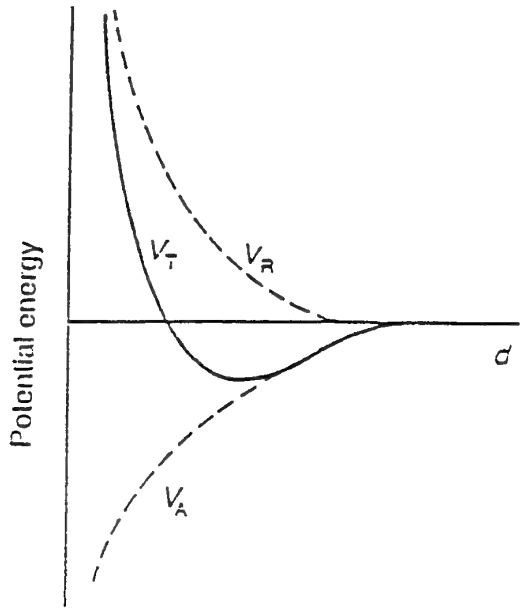

Fig. 15: Potential energy of interaction for steric stabilization.

The success of the steric stabilization depends on:

- The thickness of the adsorbed layer
- The firmness with which the polymer is anchored to the particle surface. A polymer can adsorb on the surface as a result of (a) Coulombic (charge-charge) interactions, (b) dipole interactions, (c) hydrogen bonding, (d) van der Waals interaction or (e) chemical bonding.
- The surface coverage. Complete surface coverage prevents (a) lateral movement of the stabilizing chains over the surface of the particle away from the interaction zone and (b) bridging two particles.

The steric stabilization is effective in both aqueous and nonaqueous media. In R. Moreno's review [15] several typical stabilizing moieties and anchor polymers for aqueous and nonaqueous media are reported. Menhaden fish oil containing polyunsaturated ester molecules, basically glyceryl esters of fatty acids such as oleate and linoleate, was found to be an effective polymer dispersant for alumina in toluene [22] and for $BaTiO_3$ in MEK-ethanol azeotrope [19]. This dispersant cannot be considered as a surfactant and steric stabilization is most likely to occur since no variation in zeta potential has been found when it was added to a slurry. According to [6] nitrocellulose is a very effective dispersant for acetone suspensions of several oxides such as MgO, Al_2O_3, TiO_2, ZnO, SiO_2, etc.

There are polymers that do not anchor to the surface, but react with it. These components are termed chemically bound dispersants. They usually have an organometallic compound that reacts with the powder surface forming a chemical bond. They are reported [23] to be very effective in nonaqueous media.

2.3.3 Depletion stabilization

There is one more mechanism of polymeric stabilization in which the macromolecules are free in the suspension, namely the depletion stabilization. The origin of repulsive forces is, as for the steric stabilization, the change in the free energy of polymer-solvent system that occurs when the free macromolecule is squeezed out of the interparticle region when particles approach one another [24].

We have not found in the literature the practice of utilizing this mechanism for the stabilization of suspensions. But it may be important to take in account its possible effect on the optimum polymer concentration for the steric stabilization as it is seen from the very simplified illustration shown in Fig. 16 [1]:

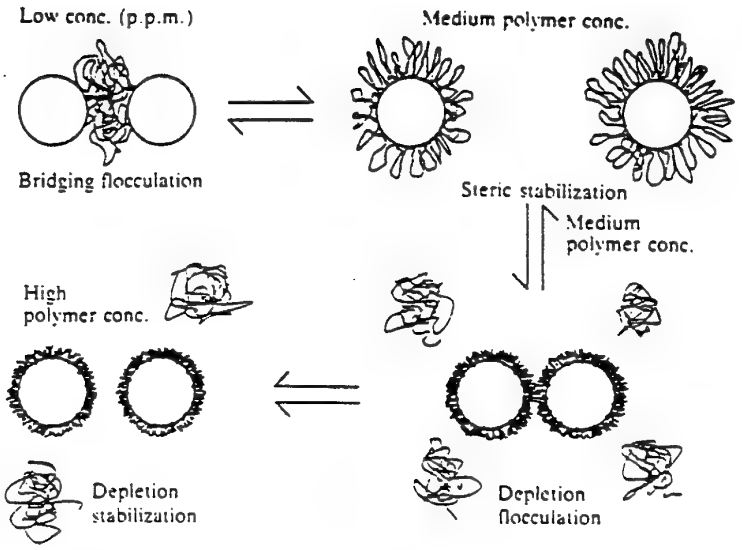

Fig. 16: Effect of polymer chains on colloidal dispersions.

A) Bridging flocculations can occur at very low polymer concentrations.
B) Steric stabilization requires moderate polymer concentrations. Polymer must be adsorbed and anchored.
C) Depletion flocculation may occur at low free polymer concentrations.
D) Depletion stabilization is favoured at high free polymer concentrations.

2.3.4 Semisteric stabilization

Some small molecules such as oleic acid or stearic acid can allow stabilization by adsorbing onto the particle but they do not have carbon chains long enough to provide the steric stabilization. These molecules do not create electrostatic or steric potential energy barriers but they act by reducing the London–van der Waals attraction between particles. This action has been termed semisteric stabilization [15, 25].

2.3.5 Electrosteric stabilization

The combination of both electrostatic (V_R) and steric (V_S) mechanisms referred to as the electrosteric stabilization is shown in Fig. 17 [15].

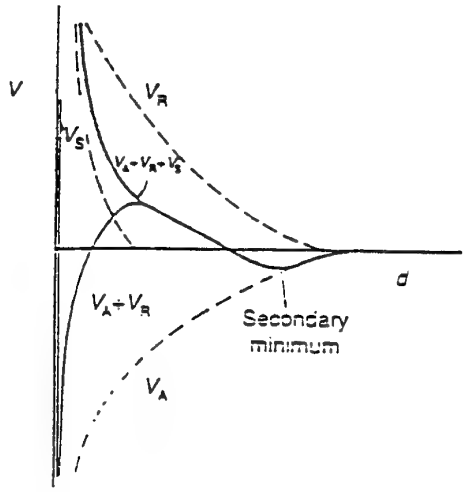

Fig. 17: Potential energy of interaction for electrosteric mechanism.

The energy potential curve for this combined mechanism does not have a primary minimum. The double layer provides a high potential energy barrier at the large distances and, at small separations, the steric stabilization prevents contacts between particles. The electrostatic component may originate from a net charge on the particle surface and/or charges associated with the anchored polymer.

The electrosteric combined mechanism was very successfully used in [6]. For several oxides such as Al_2O_3, MgO, TiO_2, ZnO, SiO_2 and other powder compounds in acetone nitrocellulose was used as a polymer (steric) dispersant and H_2SO_4 as an "electrostatic" dispersant, SO_4^{--} ion being charge determining.

2.4 Fracture toughness

To complete the literature survey chapter of the report devoted to multilayer composite formation a brief outline on ceramics fracture toughness is introduced.

The properties of a material are largely controlled by the nature of the atoms present and their bond structure. Ceramic materials are characterized by ionic and covalent bonds. Their crystal structure is influenced by (1) the size of the different atoms, (2) the balance of charge at the unit cell level as well as throughout the structure, (3) the degree of directionality of the bonds. In complex crystals of ceramics the mechanism of slip is very restrictive.

There are ceramics with high symmetrical "rock salt" cubic structure, such as, for example, MgO. Such a structure permits slip along {110} planes in the {110} direction, see Fig. 18 [26].

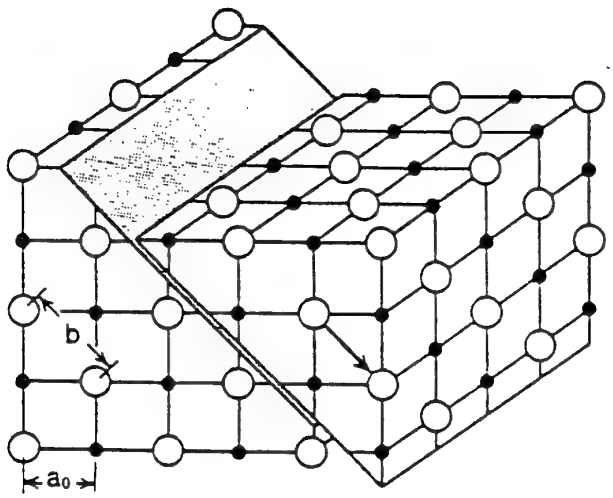

Fig. 18: Primary mode of slip for single crystals of the "rock salt" structure.

Fig. 19 [26] shows stress vs. strain curve for carefully prepared single crystals of MgO. It is well known that single crystal MgO ceramics are ductile in the same way as metals and due to the same reason, namely, the possibility of slips under applied stresses.

But rock salt structure is a very special case. Usually complex crystal structures of ceramics with high energy (electrostatic and steric) barriers to any movement do not permit slips at room temperature. Besides ceramics are polycrystalline. The

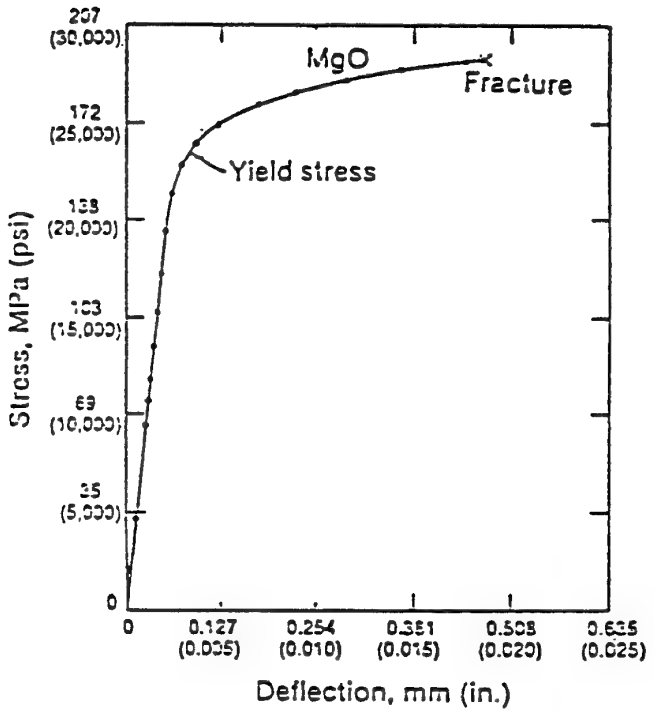

Fig. 19: Stress–strain curve for MgO single crystals tested in bending.

random orientation of individual crystals severely inhibits slips. Therefore ceramics fracture at room temperature in a brittle mode with no plastic deformation.

For nonductile materials the stress concentration at the tip of an elliptical crack is very high and their fracture toughness (resistance to crack propagation) is low. The fracture toughness is expressed as a critical stress intensity factor K_{1C} at which the crack will propagate and lead to fracture. The subscript "1" refers to the load direction perpendicular to the crack (the case that is most frequently encountered for ceramic materials). K_{1C} values for ceramic materials are appreciably lower than those for metals which exhibit crack–tip plasticity.

Ceramic materials contain structural and fabrication (sintering of powders) flaws and thermal stresses. Ceramic consists of an assembly of grains, grain boundary phases, pores, cracks, and surface scratches. The high degree of stress concentration of an applied load at very small microstructural or surface flaws leads to the extreme ease of crack initiation. Because of low fracture toughness the crack rapidly propagates through the ceramic and results in catastrophic (break–up into

two or more pieces) brittle fracture. The tensile strength of ceramics is much less (for example, 100 times for polycrystalline Al_2O_3) than the theoretical value determined by atomic bond strength.

Improving the ceramic strength therefore may be achieved by reducing the amount and size of flaws and by increasing its fracture toughness. The major efforts since the late 1960s were in the first direction. They include improvements in particle packing during the consolidation process and minimization of porosity through advanced sintering.

Since the mid-1970s additional efforts had been directed toward increasing the fracture toughness by building into the ceramic microstructure mechanisms that would allow the material to resist crack propagation. Among those are modulus transfer (incorporation of high elastic modulus fibers), prestressing (applying a residual compressive stress), crack deflection or impediment (dispersions of foreign particles, whiskers, controlled grain boundary phases), crack bridging (with long fibers), crack shielding (microcracking, transformation zones), and recently proposed multilayered structures [27,28] (interfacial mechanisms).

2.4.1 Transformation toughening [29-31]

The key ceramic material is zirconium dioxide ZrO_2. ZrO_2 goes through a martensitic phase transformation from the tetragonal-to-monoclinic crystal form while cooling through a temperature of approximately 1150°C, the transformation being accompanied by 3% volume increase. By control of composition, particle size and heat treatment cycle zirconia can be cooled so that the tetragonal phase is maintained as individual grains or precipitates to room temperature. This may be achieved only with additives such as CaO, MgO, Y_2O_3, CeO_2 and rare earth oxides.

The tetragonal phase is not in equilibrium at room temperature and would normally spontaneously transform to the stable monoclinic phase. However, such a transformation requires an increase in volume and the strength of adjacent grains prevents the transformation.

When a stress is applied to the zirconia and a crack starts to propagate, the

metastable tetragonal zirconia grains adjacent to the crack tip can now expand and transform to the stable monoclinic crystal form. The 3% volume increase of these grains places the crack in compression and stops it from propagating. The result is a considerably toughened ceramics, see Table 2 (taken from [26]).

Table 2 Fracture toughness values for ceramic-based materials

Material	K_{Ic} MPa·m$^{1/2}$(ksi·in.$^{1/2}$)
Glass	0.7 (0.6)
Single crystals	
NaCl	0.3 (0.27)
Si	0.6 (0.54)
MgO	1(0.91)
ZnS	1 (0.91)
SiC	1.5 (1.36)
Al_2O_3	2 (1.82)
WC	2 (1.82)
Polycrystalline ceramics	
Al_2O_3	3.5-4.0 (3.18-3.64)
SiC	3.0-3.5 (2.73-3.18)
Stabilized ZrO_2	2 (1.82)
RBSN	2.5 (2.7)
Sintered Si_3N_4	4-6 (3.64-5.46)
Transformation-toughened ceramics	
Mg-PSZ	9-12 (8.19-10.92)
Y-TZP	6-9 (5.46-8.19)
Ce-TZP	10-16 (9.1-14.56)
Al_2O_3-ZrO_2	6.5-13.0 (5.91-11.83)
Dispersed-particle ceramics	
Al_2O_3-TiC	4.2-4.5 (3.82-4.09)
Si_3N_4-TiC	4.5 (4.09)
Dispersed-whisker ceramics	
Al_2O_3-SiC whiskers	6-9 (5.46-8.19)
Fiber-reinforced ceramics	
SiC in borosilicate glass	15-25 (13.65 - 22.75)
SiC in LAS	15-25 (13.65 - 22.75)

Transformation toughening is not limited to ZrO_2. Very small grains of ZrO_2 added to another ceramic such as Al_2O_3 and retained as tetragonal during cooling cause considerable toughening, see Table 2.

2.4.2 Multilayered structures [27,28]

A multilayered structure is found to provide a mechanism for enhancing toughness of transformation-toughened zirconia. The autocatalytic transformation (i.e., the sequential triggering of tetragonal-monoclinic transformation in zirconia grains by transformation strains in adjacent grains) results in creation of transformation zones surrounding the cracks [27], and the degree of toughening is dependent on the distribution of transformation strains, i.e. on the shape of the zone [32,33]. The increase in fracture toughness is about 2 times smaller for an elongated frontal zone typical of Ce-TZP (the zone extends ahead of the crack a distance of 10-20 times the zone width) than for a semicircular frontal zone typical of Mg-PSZ [33]. The microstructure of Mg-PSZ is such that individual tetragonal precipitates are contained within grains which are larger by about 2 orders of magnitude. The grain boundaries are effective as barriers which arrest the propagating band. Ce-TZP does not possess large-scale barriers. Marshall et al. [27,28] introduced as barriers layers of Al_2O_3 or Al_2O_3/ZrO_2 in Ce-TZP ceramics.

The presence of the layers was found to modify dramatically the size and shape of transformation zones around the cracks. Two effects have been identified, namely, the truncation of the elongated frontal zone and the spreading of the transformation zones along the regions adjacent to the layers. These two effects combined cause an increase in the fracture toughness of the layered material by a factor of 3,5 (from 5 to 17,5 $MPa \cdot m^{1/2}$). The enhanced fracture toughness was observed for cracks growing both parallel and normal to the layers.

The important factor controlling the performance of a ceramic laminate is the layer thickness since it controls the length of the crack propagation before interception of an interface. Based on Mg-PSZ microstructure the optimum separation of the layers would be expected to be 10-100 times the grain size (which is $\sim 2\mu m$), with an individual layer thickness at the lower end of the range [27].

Multilayered ceramic composites are currently prepared by the "doctor-blade" process [21], sequential slip casting [8], sequential centrifugal casting [27] and electrophoretic deposition [34].

The minimum layer thicknesses were reported to be 150 μm for tape casted laminar composites [21], 100 μm for slip casted structures [8], 10 μm for composites obtained in centrifugal casting process [27] and 2 μm for electrophoretically deposited multilayer ceramic with an interface smoothness of submicrometer scale [34].

Chapter 3 - Materials and Methods

a) Ceramic Powders

- Al_2O_3 powder (Baikalox CR-1) acquired from Baikowski Ceramic Aluminas, USA, average particle size of 5 μm (used only for preliminary experiments).
- A submicrometer alumina powder Al_2O_3 (Baikalox SM-8) acquired from Baikowski Ceramic Aluminas, USA.

Table 3: Properties of alumina powders.

Powder	Baikalox CR-1	Baikalox SM-8
Purity, $\%Al_2O_3$	99.99	99,99
Specific surface area B.E.T.m^2/g	1	10±1
Major Phase	alfa	alfa
% Major phase	97%	95%
Crystal Density g/cm^3	3.98	3,98
Bulk density g/cm^3	0.7	0,93
Pressed density 2200 PSI g/cm^3	1.62	1,85
Ultimate particle size, microns	<15	0,15
Loss on ignition, %	—	—

Table 4: Al_2O_3 particles size distribution.

Size Distribution	Powder	
	Baikalox CR-1	Baikalox SM-8
<0,3μm	--	65
<0,4μm	8	78
<0,5μm	18	90
<0,6μm	25	95
<1.0μm	50	100
<2μm	88	--
<5μm	100	--

Table 5: Chemical analysis - Baikowski Aluminas (99,99% purity).

Element	Na	K	Si	Fe	Ca
Typical value of impurities ppm	8	35	35	6	3

- ZrO_2 acquired from Aldrich Chemical Company, USA, average size of 5 μm (used only for preliminary experiments).
- Submicrometer zirconia partially stabilized with CeO_2 acquired from TOSOH Zirconia Process Company, grade TZ-12CE with following characteristics:

1. Chemical composition

Table 6 Chemical Analysis
in wt%

CeO_2	Al_2O_3	SiO_2	Fe_2O_3	Na_2O	Ig. loss
16.69	—	<0.002	0.004	0.021	0.43

2. Crystallite Size 234 Å
3. Specific Surface Area 9.4 m^2/g

b. Solvent

Isopropanol, its relevant properties according to literature data (room temperature) are:

Density	0,785 g/cm^3
Boiling point	82.3°C
Surface tension	22 mN/M
Dielectric constant ϵ	18
Viscosity	2.4 cp
ϵ/η	7.5

c. Additives

- ⟨ORTHO⟩ Phosphoric acid, 85%, AR Grade
- Tetrametyl ammonium hydroxide (TMAH) $(CH_3)_4NOH$, 10% solution in methanol, AR Grade
- Triethanolamine, $C_6H_{15}NO_3$, AR Grade
- Diethylene glycol dibutyl ether $(CH_3CH_2CH_2CH_2OCH_2CH_2)_2O$, CP Grade
- Acetylacetone (2.4-Pentadion), $CH_3COCH_2COCH_3$, AR Grade
- Agar-Agar powder

- Gelatine powder "Gold normal".
- Fish oil from Menhaden

d. Substrates

Deposition experiments were carried out on two kinds of substrates:

- Low porous graphite acquired from the aeronautics faculty at the Technion. Graphite substrates were used only for preliminary experiments.
- Stainless steel AISI 316

e. Specimens

- Graphite plates of 16×9×7mm size.
- Stainless steel specimens were of two kinds: 15×15×1 mm plates and ϕ20×6mm discs.

f. Electrophoretic deposition

Deposition was carried out from Al_2O_3 and ZrO_2 suspensions in isopropanol with and without additives, at a constant voltage and at room temperature.
Stirring was applied during deposition.

Preparation of suspensions

Weighed amounts of powder were mixed with an appropriate amount of isopropanol with or without additives and subjected to 12 minutes ultrasonic treatment. A 600W vibra-cell ultrasonic disintegrator VC600, Sonic & Materials, USA was used.
Powders used were dried at 400°C for 30 minutes before being used.

Preparation of specimens

Specimens were cleaned ultrasonically in ethanol for 5 min and dried in oven with air circulation at 200°C. Graphite specimens were dried for 30 min, stainless steel specimens for 10 min.

Experimental set-up

The experimental set-up is shown in fig. 20. To minimize edge effects the surface area of the anode was one third of the cathode.

Deposition parameters

Particle concentration	60-500 gr/l
Field intensity	25-500v/cm
Deposition time	10-30 sec
Temperature	room
Distance between electrodes	10-15mm
Solvent	Isopropanol

Removal of composites from a substrate

Removal of a multilayer composite from a stainless steel substrate (cathode) with a blade was difficult. Short dipping of the deposit in glycerine immediately after its removal from the deposition cell made it more flexible and facilitated considerably the removal from the substrate without damage and cracking. This technique is nevertheless far from perfect, and sometimes bending of deposits occurred causing cracking during drying. This problem will be addressed at the next stage of the project.

Drying

Multilayered composites of 0,7-1,5 mm thickness removed from a substrate were immediately placed in a desiccator for 24 hours over a 10% solution of glycerine in isopropanol. After that they were dried in air at room temperature for 24 hours; then at 200 °C for two hours.

Green bodies for density measurements (about 3 mm thickness) together with the device were placed in a desiccator for 72 hours over a 10% solution of

1-Power supply
2-Ammeter
3-Voltmeter
4-Suspension
5-Teflon cover
6-Thermometer
7-Holder
8-Stainless steel anode
9-Cathode (specimen)
10-Stirrer
11-Plate

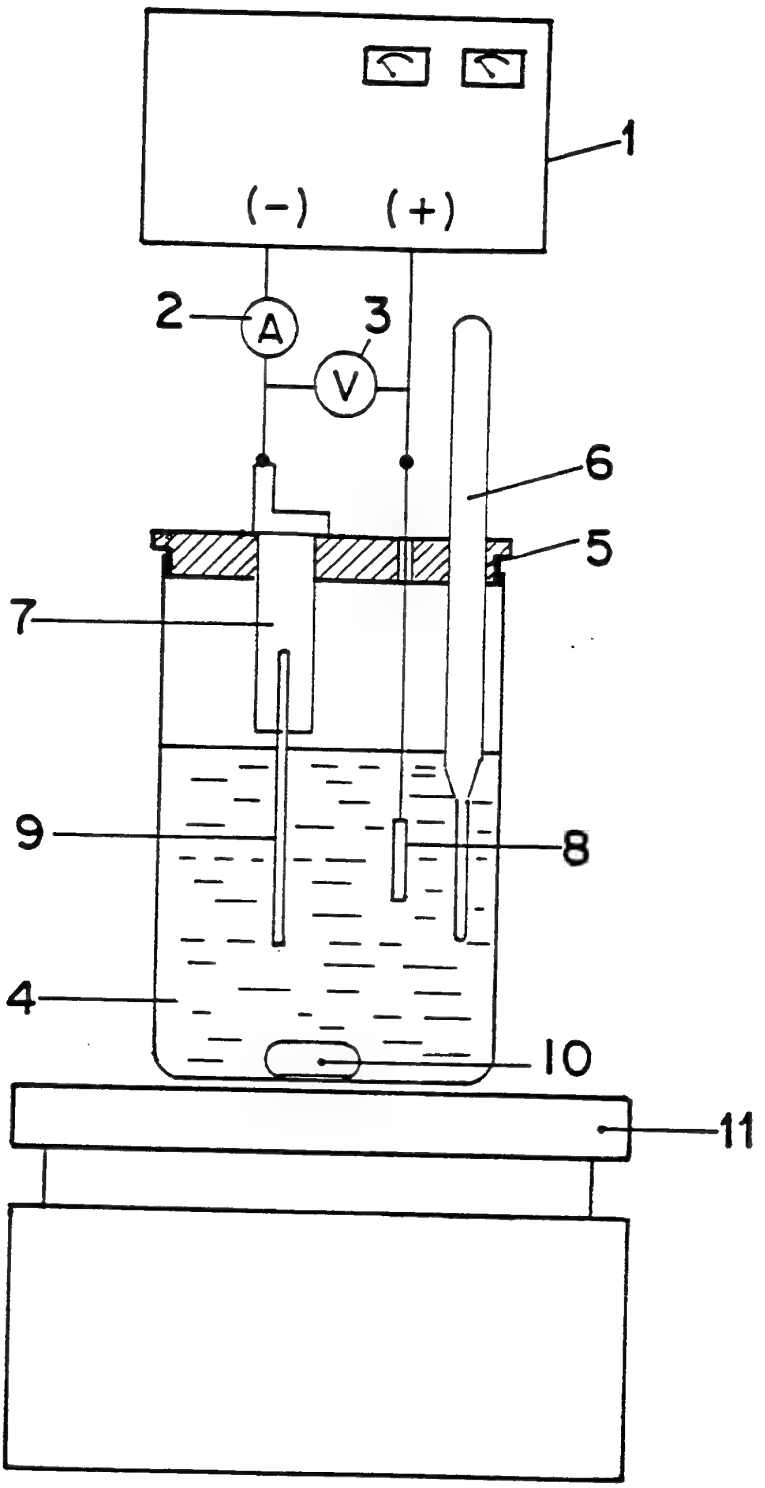

Fig. 20: Experimental set-up for electrophoresis.

glycerine in isopropanol immediately after removal from the deposition cell. Then they were dried in air at room temperature for 24 hours. After that they were removed from the device and dried in oven at 200°C for 6 hours.

Sintering

Specimens were sintered at 1550°C for 2 hours with a heating rate of 1°C/min and cooling rate of 2 °C/min.

g) Testing of deposits

The microstructure and composition of deposits were studied by an electron microscope (JEOL 840 SEM) on cross-sections and on fracture surfaces of green and sintered specimens. Cut or broken specimens were embedded in an Epofix (Struers) resin and cured for 24 hours at room temperature. The composite blocks with cut specimens were polished with SiC paper (400-2000 grits) and then with a diamond paste of 0.25 μm grain size. This procedure was satisfactory for sintered specimens. For green specimens strengthening by impregnating with an epoxy resin having a low curing shrinkage would be desirable before embedding in Epofix. This will be done at the next stage of our work.

h) Density measurements

Measurement of the bulk density of friable materials such as unfired ceramic deposits depends on the precise measurement of the volume of the sample. A number of displacement methods, involving techniques for sealing of pores, were found to be unsatisfactory. A method was developed [35] in which the linear dimensions of the sample were fixed during the forming process and it only remained to weigh the sample to determine the bulk density.

The deposition device (electrode) we used is shown in Fig. 21. The circular stainless steel disc is of 20 mm diameter. The teflon sleeve is adjusted so that the rim is 3 mm ($\pm$0,1) above the disc, and the electrophoretic deposit is allowed to fill the cylindrical cavity and project above the rim. The deposit is planed flat by sliding a

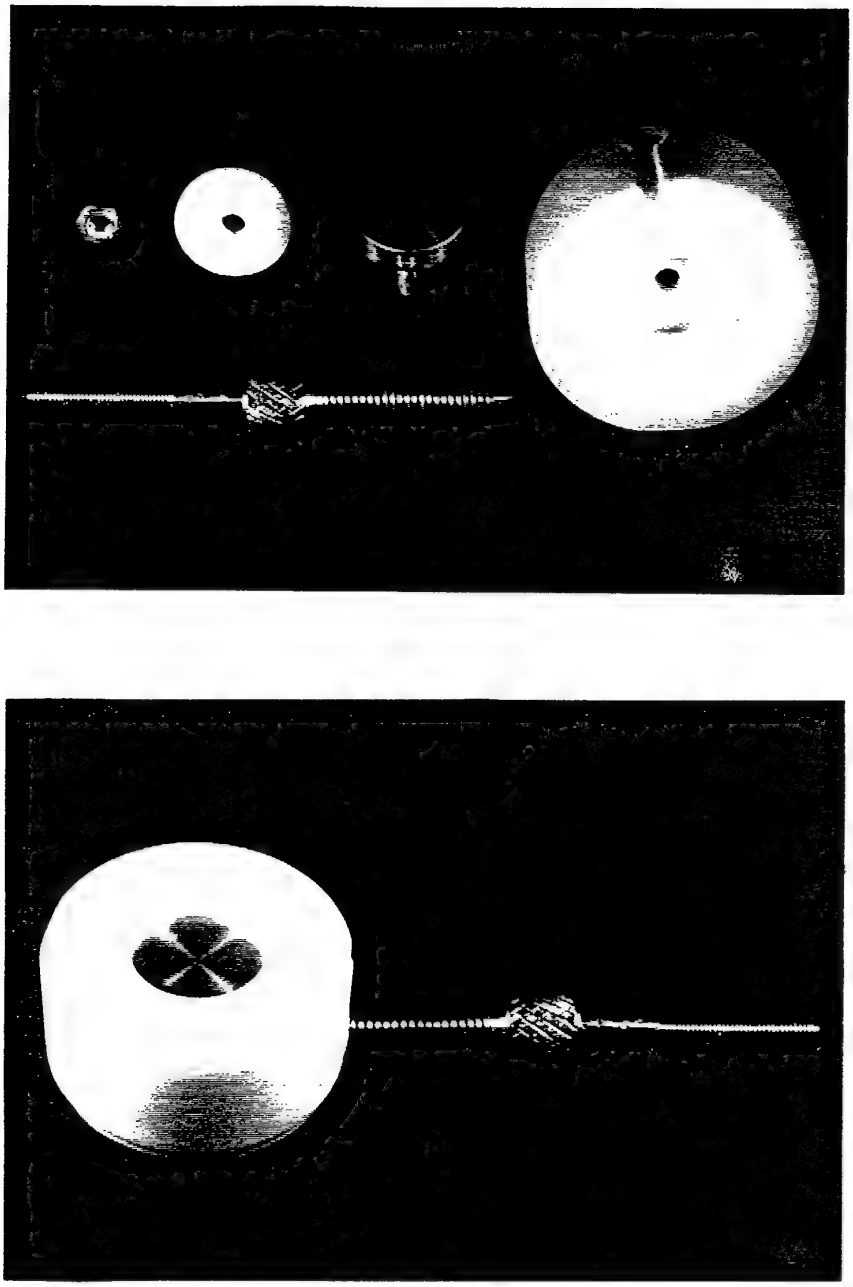

Fig. 21: The teflon device.

razor blade across the rim of the sleeve. Thus the deposit is being constrained into a disc-shape, the linear dimensions of which are precisely known. By pushing the steel disc with the deposit up, the tablet (body) can be removed for drying and weighing.

The experimental error of green density was approximately ±2.5% This error is due to inaccuracy in dimension determination, and incomplete removal of ceramic body from the substrate.

The fired density was determined by the ASTM C20-92 method using distilled water as the suspending fluid. The accuracy of measurements was within 5%. The high error was due to the small size of fired pieces, since often green bodies cracked while being dried.

i) Electrophoretic mobilities and zeta potential measurements

Electrophoretic mobilities of ceramic particles were measured using the moving-boundary method. The moving-boundary electrophoresis cell is shown in Fig. 22. It consists of a U-tube of a 9 mm cross-section with stainless steel electrodes in the top of each arm. Isopropanol through which the suspension was to pass was first added through the top of the U-tube. After that the stopcock at the bottom of the U-tube was carefully opened to permit a slow flow of a suspension into the tube. The apparatus was left for about 5 minutes to allow the suspension-isopropanol boundary to stabilize. About 2-5 minutes after switching the power on, when the boundary became satisfactorily sharp, the position of the boundary was marked. The time for motion of the descending boundary was observed for each 1 mm displacement. The duration of each test was 40-60 min. The descending boundary was chosen because it remained satisfactorily sharp during the test, while the ascending boundary became diffuse [36].

All runs in the electrophoresis cell were made under constant voltage of 475 v (19v/cm) at room temperature (19°-23°C) and a constant particle concentration of 10 g/l. Zeta potentials were calculated using Smoluchowski equation:

$$\zeta_p = \frac{4\pi\eta}{\epsilon}\mu$$

where: μ and ζ are the mobility and zeta potential of moving particles respectively.
ϵ and η are the dielectric constant and viscosity of the dispersion medium respectively.

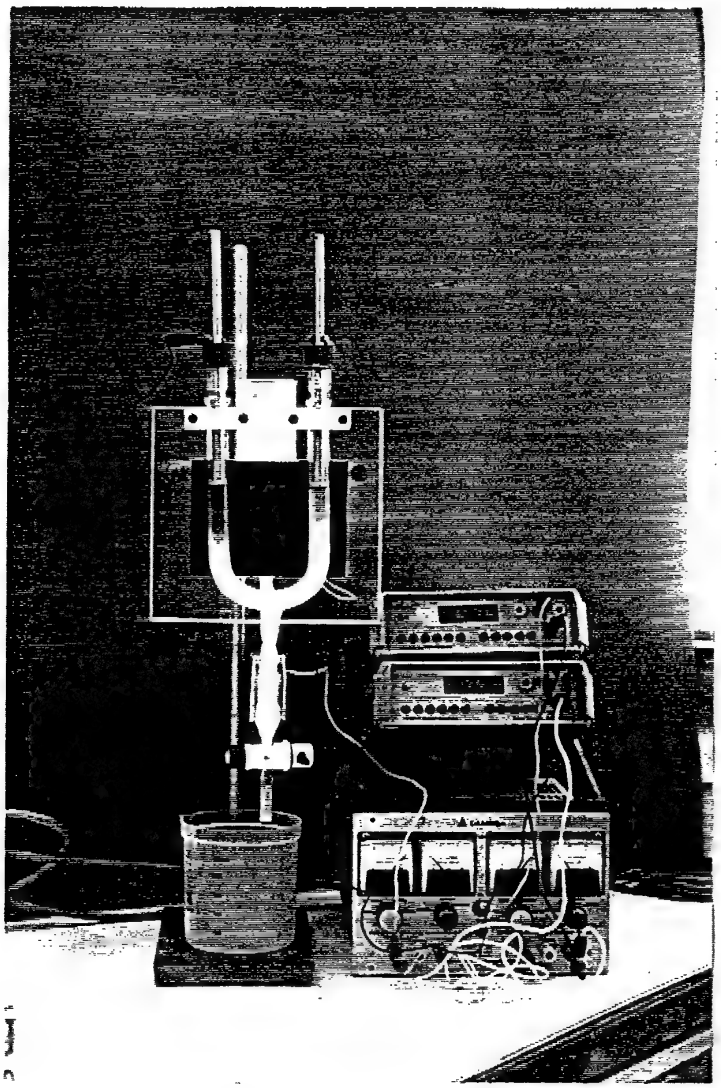

Fig. 22: Moving-boundary electrophoresis cell.

Chapter 4 – Results and Discussion

4.1 Preliminary experiments

Choice of solvent

The high value of its dielectric constant (ϵ=80) and environmental considerations would make water an ideal vehicle in the process of electrophoretic deposition. But the inevitably concurring electrolysis of water results in non-planar and pin holes possessing deposits with a low deposition efficiency. Therefore polar organic solvents such as methanol, ethanol, propanol, acetone are now widely used.

In our previous works isopropanol has proven to be very useful as a suspending medium for ceramic particles in the electrophoretic deposition process. Its dielectric constant is at an appropriate level [7] to enable charging of the particles and yet to prevent electrochemical decomposition of the fluid and gas evolution.

Therefore the possibility of electrophoretic deposition of Al_2O_3 and ZrO_2 particles from isopropanol suspensions has been verified. The results are presented further.

Choice of powders

The first starting materials were:

- Al_2O_2 powder (Baikalox CR-1) acquired from Baikowski Ceramic Aluminas, USA, average particle size of 5μm
- ZrO_2 acquired from Aldrich Chemical Company, Inc., USA, with an originally average size of 5μm.

The first qualitative experiments have shown that alumina precipitates on the cathode, deposits are continuous, while zirconia did not precipitate neither on the cathode nor on the anode up to 200 v/cm. The addition of 0.02% (v/v) TMAH (Tetrametyl ammonium hydroxide) resulted in charging of ZrO_2 particles negatively

and their deposition on the anode [37]. The pH value shifted from about 4.9 to about 8.5.

To make Al_2O_3 particles precipitate also on the anode, H_3PO_4 was added to the isopropanol suspension. Al_2O_3 particles precipitated on the anode, possibly due to the specific adsorption of phosphate ions, which impart a negative charge to the particle surface. The addition of 1.0% (v/v) phosphoric acid to isopropanol suspensions of Al_2O_3 increased the deposition rate and improved smoothness of deposits. The pH value shifted from about 8.6 to about 2.6.

It must be noted that although the meaning of pH is not clear for organic solvents, it served as a comparative measure of the acidity or alkalinity of the medium.

After the conditions for deposition of both powders on the same electrode (anode) were found preliminary kinetic experiments of deposition were performed. Fig. 23 shows thickness vs. field intensity dependence for Al_2O_3 (average size 5 μm) in isopropanol with 1% (v/v) H_3PO_4. Fig. 24 shows the same dependence for ZrO_2 in the presence of 0.02% (v/v) TMAH. The thickness increases with field intensity.

Figs. 25 and 26 show thickness vs. time dependence for Al_2O_3 and ZrO_2 respectively. The initial increase of Al_2O_3 layer thickness with time during the first 20 min is followed by a decrease in thickness that may be explained by slipping of the deposit, perhaps due to weak cohesion forces between the particle. For ZrO_2 the thickness vs. time dependence found is as usual for ceramics, where the deposition rate decreases with time due to the insulating layer formation.

The next step was the preparation of a multilayered structure. This was found to be possible and the laminated composite was formed on the anode. But SEM micrographs of its cross-section (after sintering) have revealed a large amount of pores and cracks across the structure.

The following stage was to utilize powders with much smaller particles. The driving force during the sintering process is the reduction of the surface energy. Therefore starting material with lower size particles could provide better results.

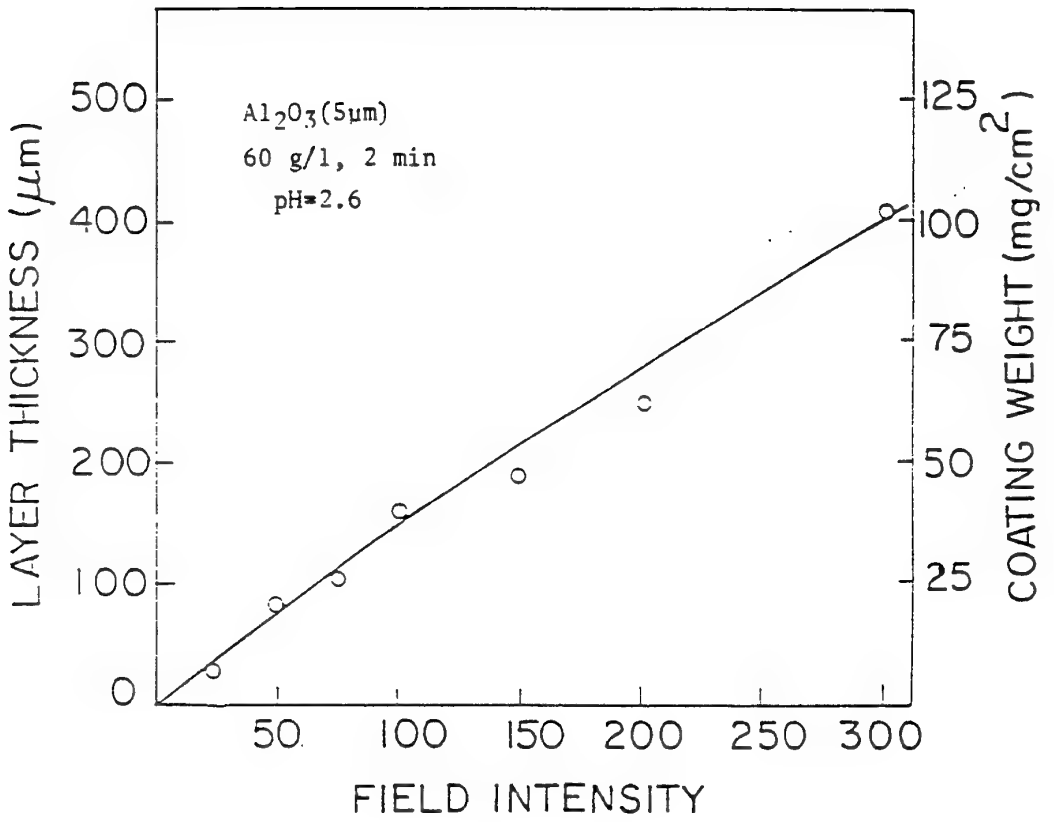

Fig. 23: Deposit thickness and weight of Al_2O_3 (CR-1, average 5μm) as a function of field intensity.

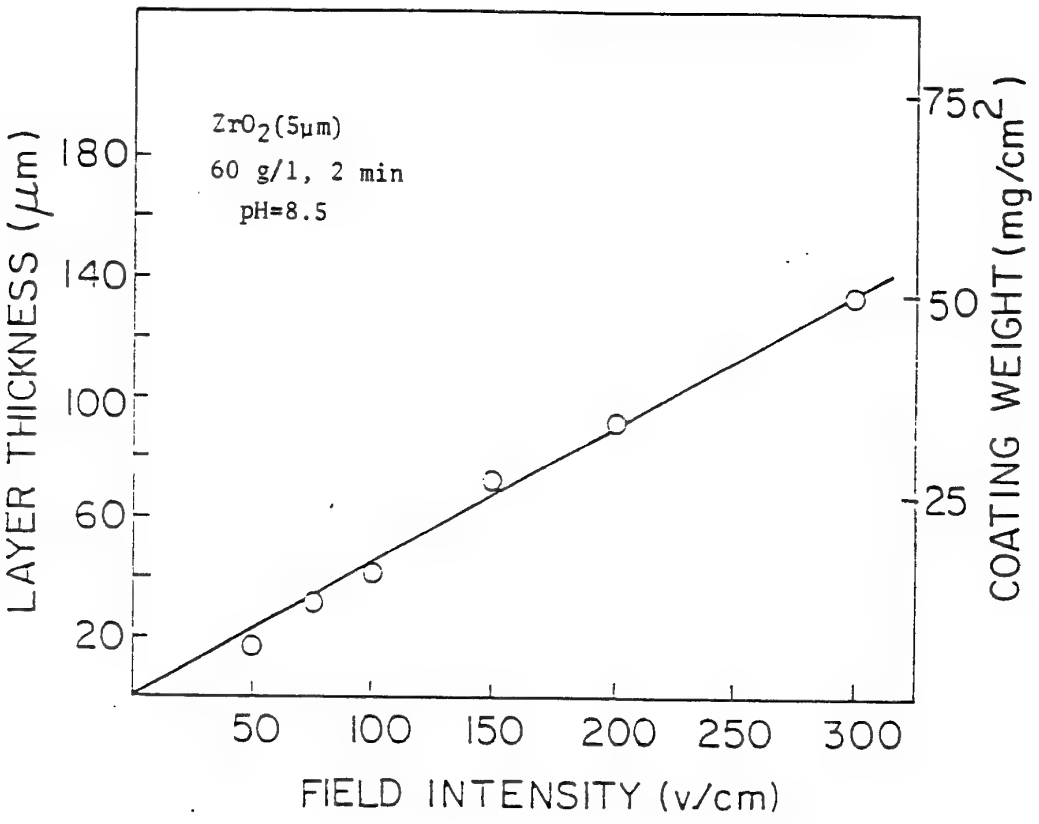

Fig. 24: Deposit thickness and weight of ZrO_2 (Aldrich, average 5μm) as a function of field intensity.

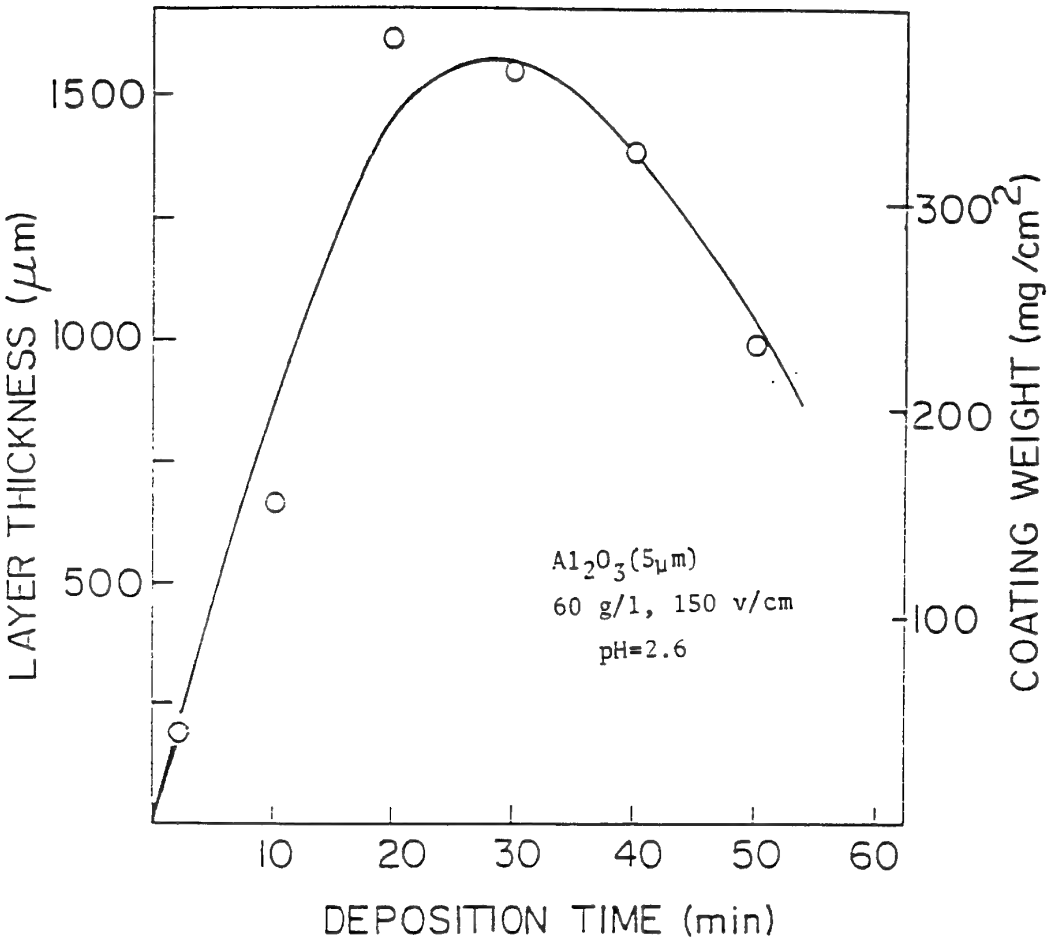

Fig. 25: Deposit thickness and weight of Al_2O_3 (CR-1, average 5mμ) as a function of deposition time .

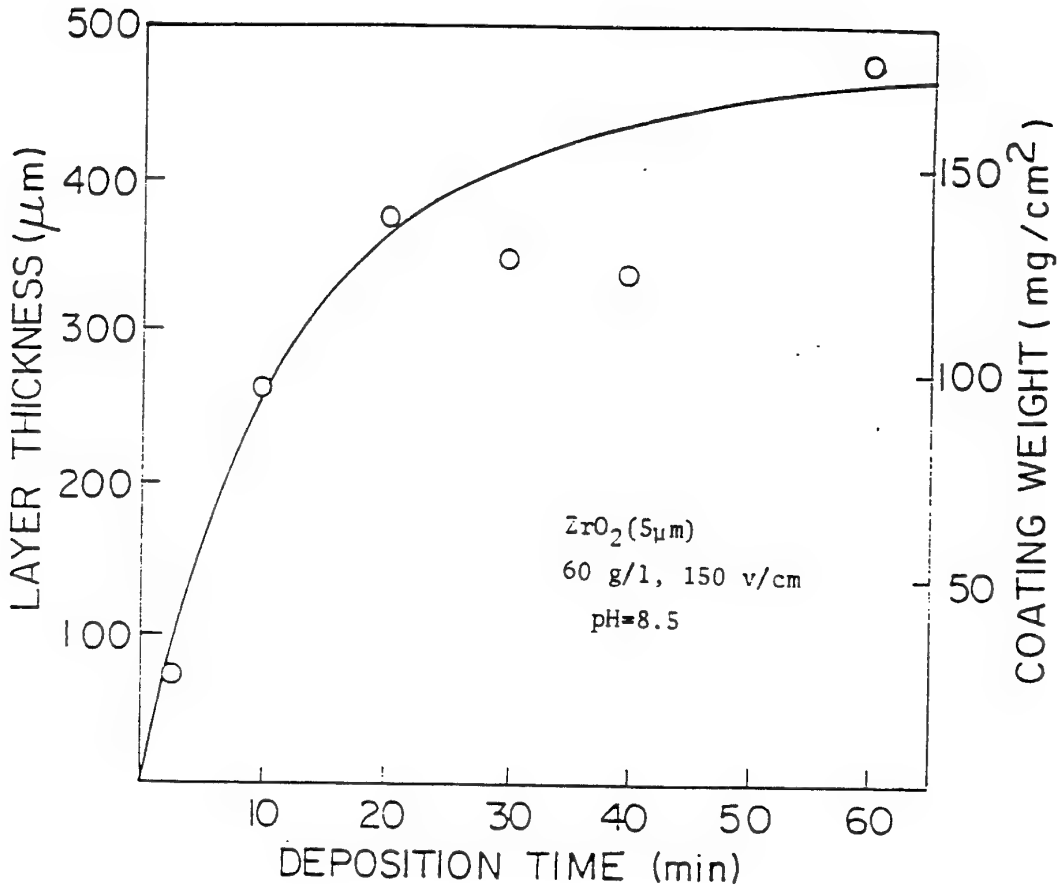

Fig. 26: Deposit thickness and weight of ZrO_2 (Aldrich, average 5mμ) as function of deposition time .

The following powders have been tested:

- a submicrometer alumina powder Al_2O_3 (Baikalox SM-8) acquired from Baikowski Ceramic Aluminas, USA.
- a submicrometer zirconia partially stabilized with CeO_2, grade TZ-12E acquired from TOSOH Zirconia Process Company.

It has been found that both Al_2O_3 and ZrO_2 particles precipitate on the cathode from isopropanol suspensions without any additives, their polarity (positive) in isopropanol coinciding.

Figs. 27 and 28 show thickness vs. field intensity dependencies for 60 g/l isopropanol suspensions of Al_2O_3 and ZrO_2 respectively. Figs. 29 and 30 demonstrate thickness vs. time dependencies for the same suspensions at 50 v/cm. The deposits were continuous and satisfactorily smooth.

Therefore we have chosen these low particle size powders as the ceramic materials and isopropanol as a suspending medium for further work.

4.2 Green density

A high green density of a deposit is the first step on the way to a high quality ceramic product.

4.2.1 Green body formation

For density determination green bodies of 20 mm in diameter and 3 mm in height were made. The fabrication of bodies was met with certain difficulties connected with the body removal from the device. Several devices (cathodes) tested are seen in Figs. 31-33. Two materials were tested, namely, perspex (polymethylmetacrylate) and teflon. Both of them were adequate for bodies produced from isopropanol suspensions; but only teflon was satisfactory for deposits from suspensions with AcAc additions (section 4.2.3). Perspex reacts with AcAc making the release of

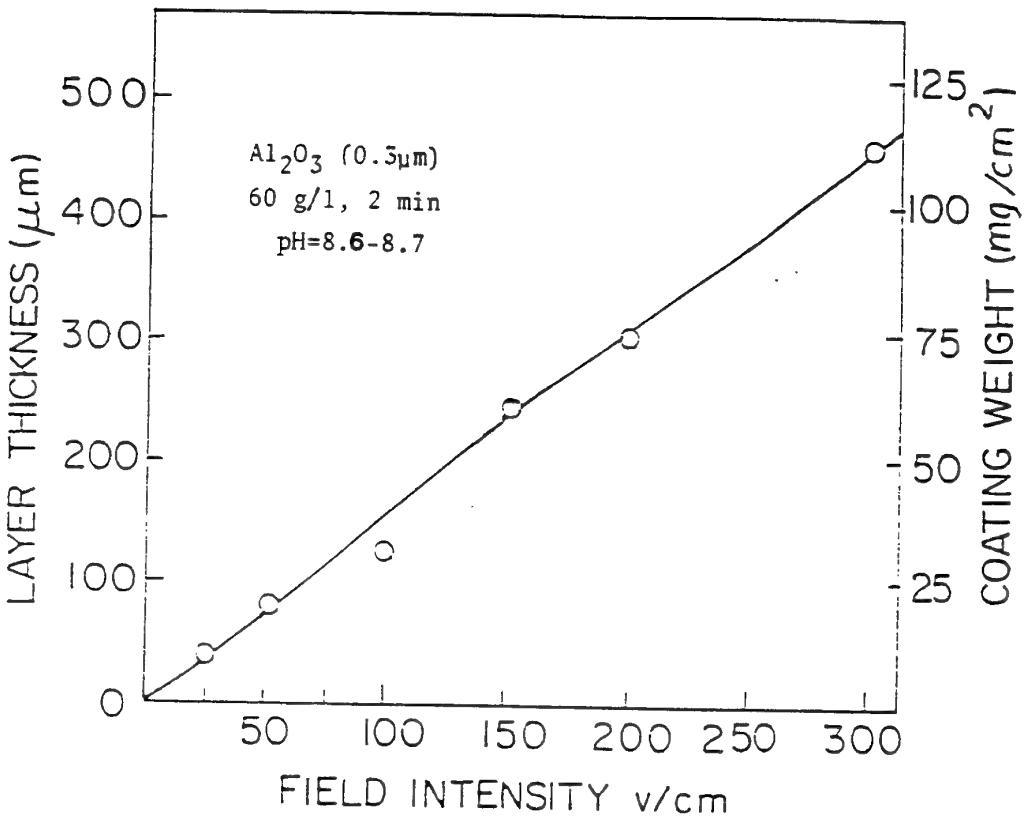

Fig. 27: Deposit thickness and weight of Al_2O_3 (SM-8, submicron) as a function of field intensity.

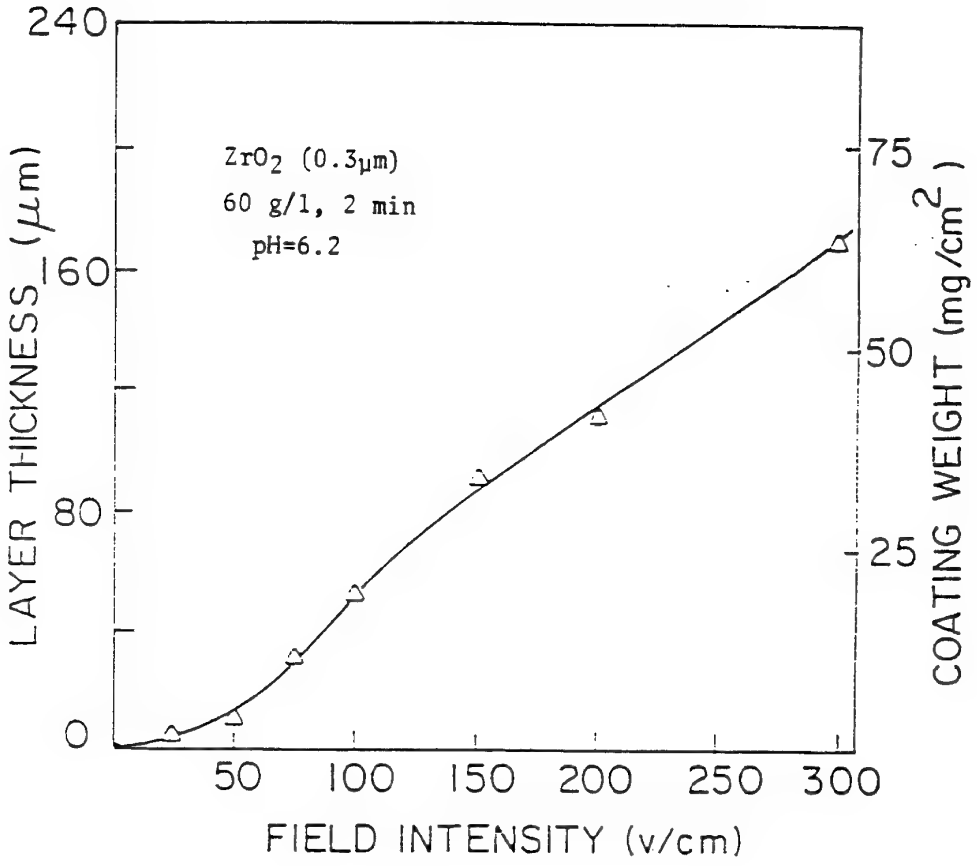

Fig. 28: Deposit thickness and weight of ZrO_2 (TZ-12CE, submicron) as a function of field intensity.

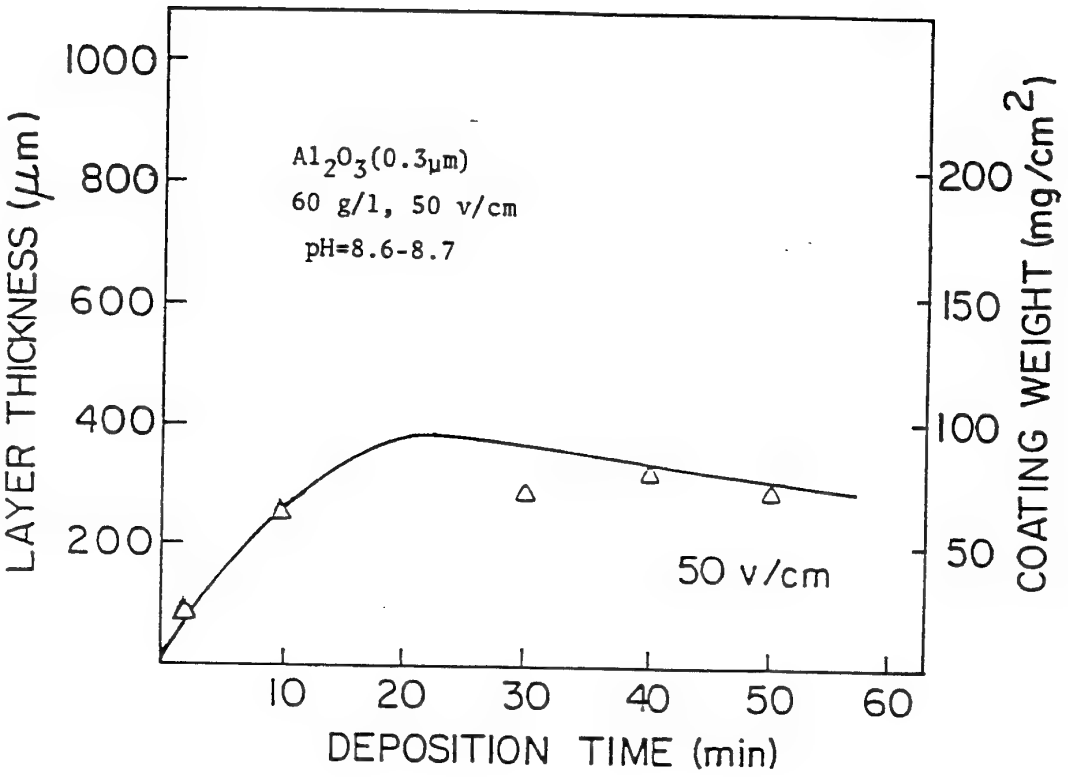

Fig. 29: Deposit thickness and weight of Al_2O_3 (SM-8, submicron) as a function of deposition time for different pH.

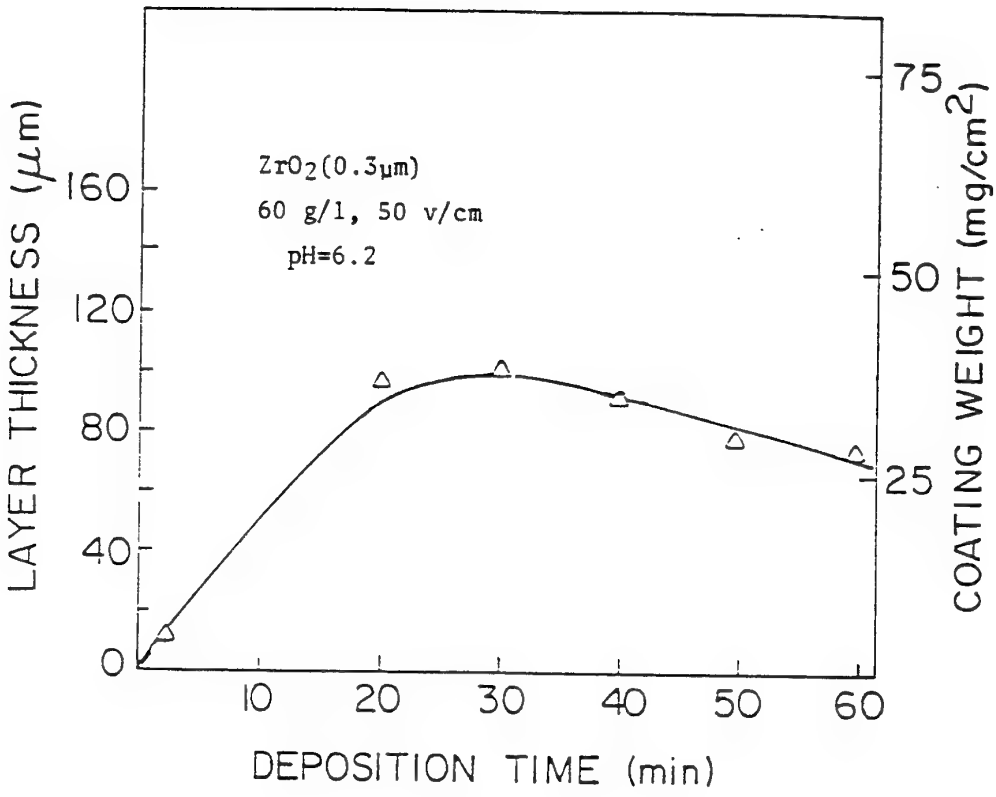

Fig. 30: Deposit thickness and weight of ZrO_2 (TZ-12CE, submicron) as a function of deposition time for different pH.

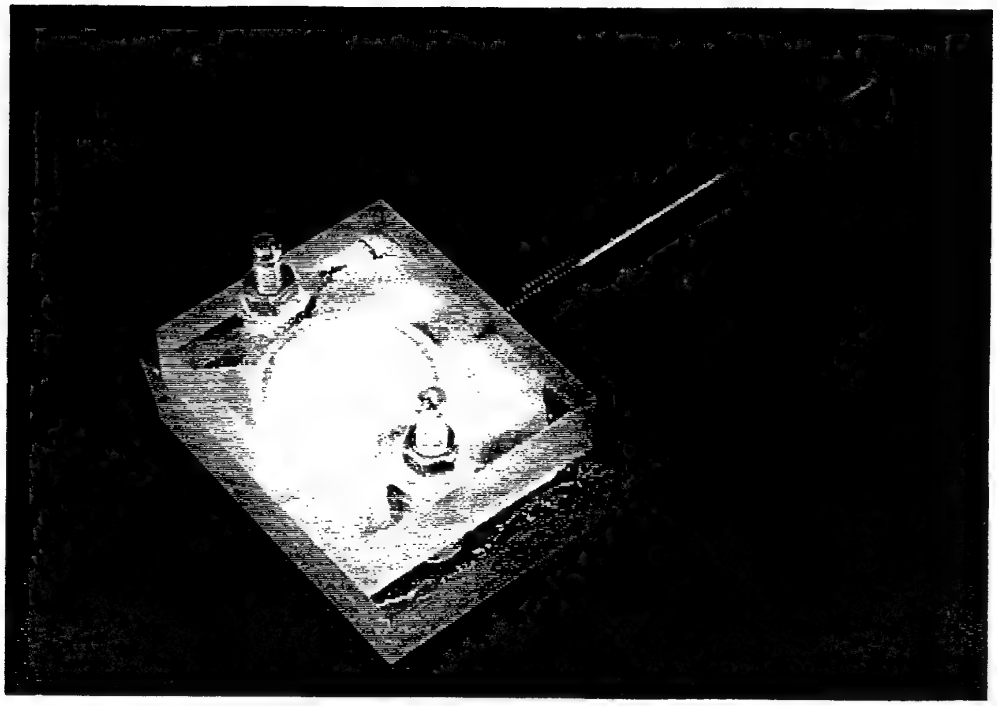

Fig. 31: Perspex device .

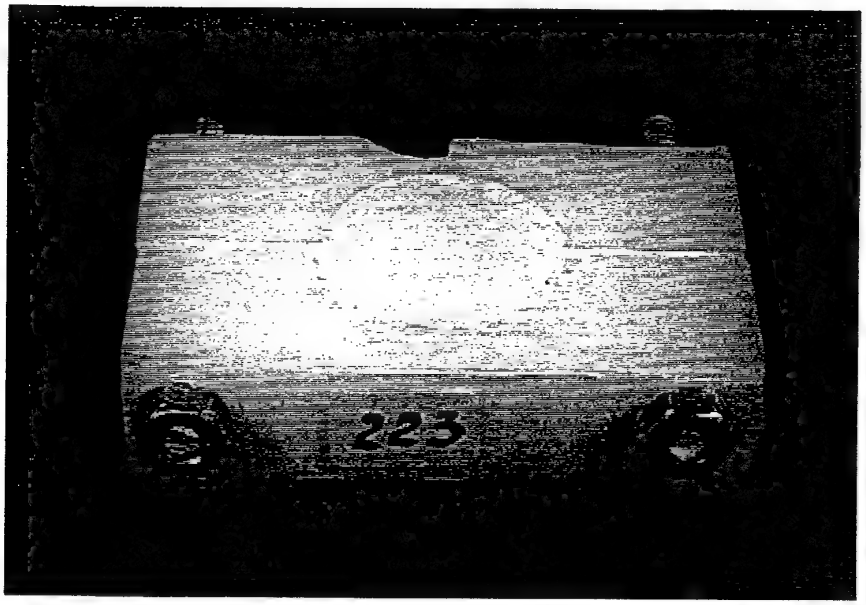

Fig. 32: Teflon device .

body without damage impossible. The optimal design of the device is shown in Fig. 33.

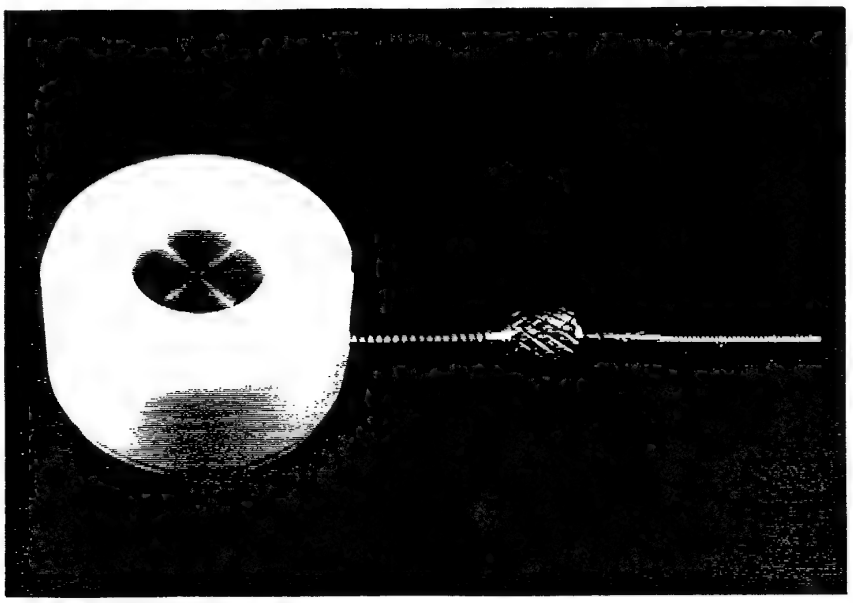

Fig. 33: Optimal teflon device.

4.2.2 The effect of deposition parameters

The green density of alumina and zirconia deposits from isopropanol suspensions was studied as a function of deposition parameters, namely, field intensity and concentration of the particles.

Fig. 34 shows the green density as a function of field intensity for Al_2O_3 at different concentrations of the suspensions. It is seen that the green density is not affected significantly by both parameters, its value being ~40% of the theoretical density. The density vs. field intensity dependence for ZrO_2 is shown in Fig. 35. The green density does not depend on field intensity, its value being ~ 30% of the theoretical density within experimental error.

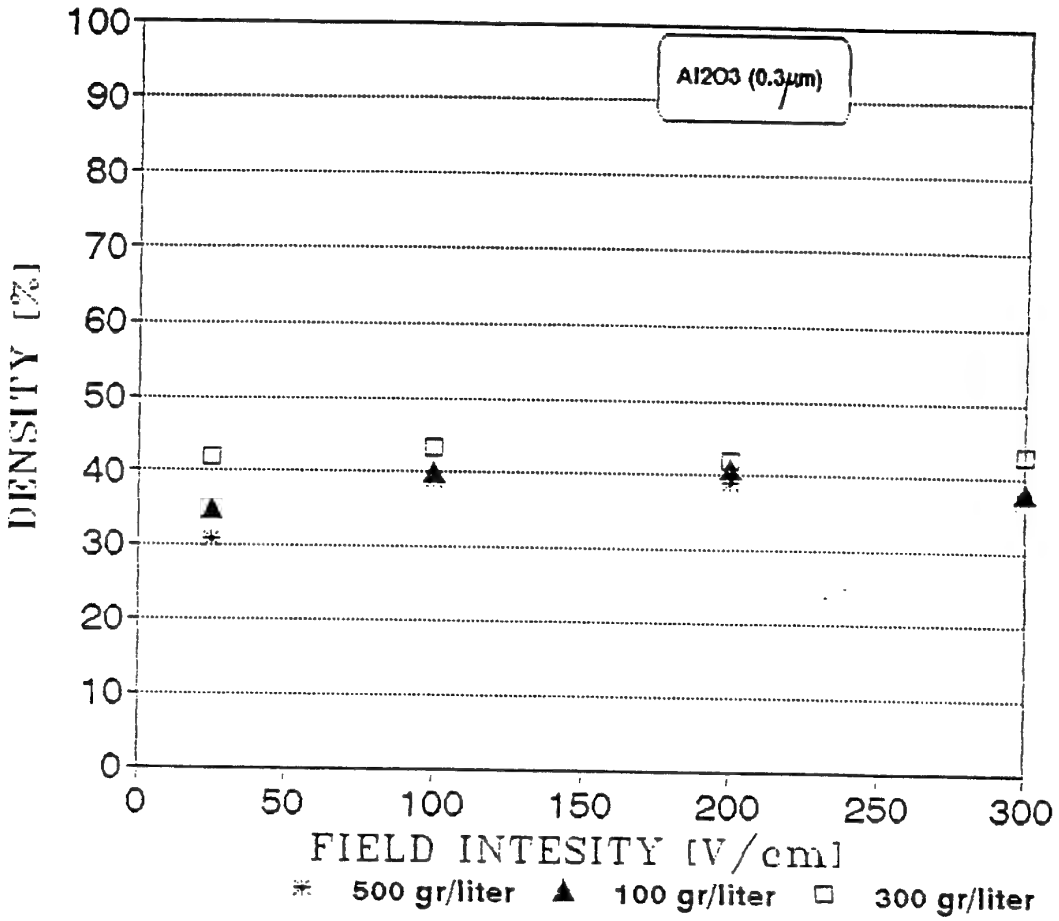

Fig. 34: Green density as a function of field intensity for Al_2O_3 (0.3μm).

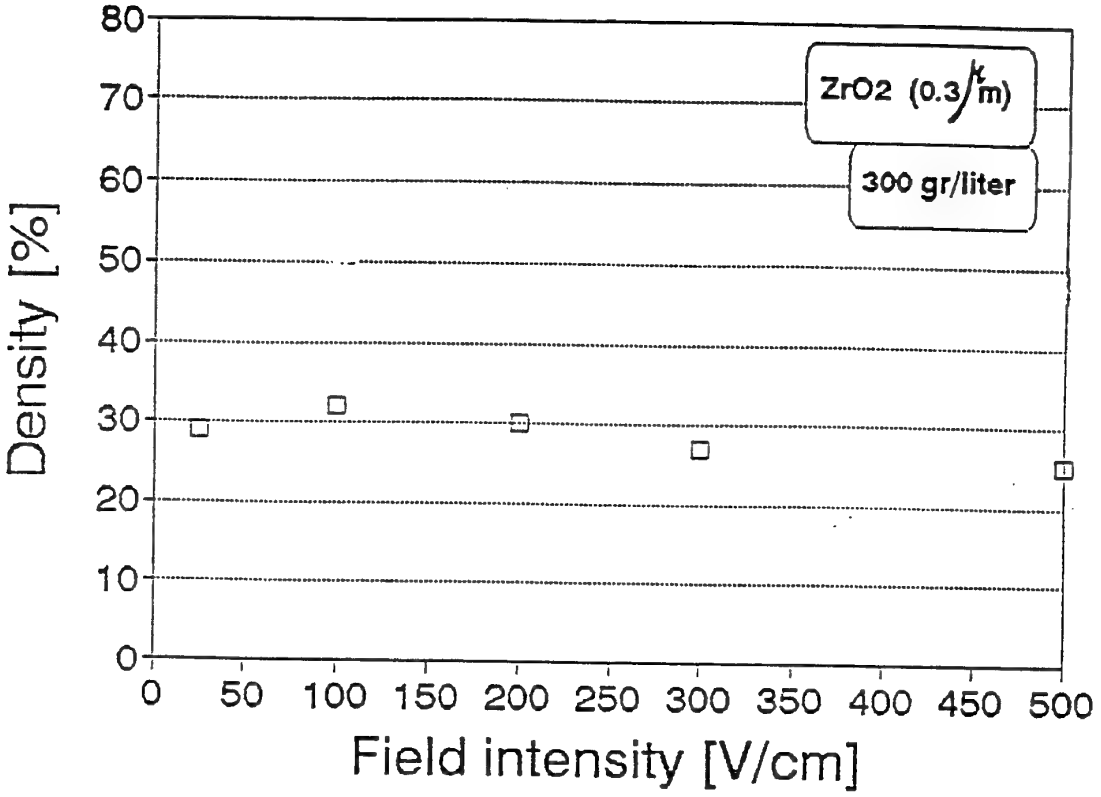

Fig. 35: Green density vs. field intensity for ZrO_2 (0.3μm).

Thus the green density of alumina and zirconia is not affected distinctly by the field intensity, which is in accordance with data in the literature [38]. The concentration of solids in the suspensions had also an insignificant effect on the alumina green density in the range of 100-500 g/l.

4.2.3 Effect of additives

It is well known that the stability and homogeneity of suspensions have a strong effect on the density of deposits. It is impossible to obtain satisfactory dense packing of particles if aggregation takes place.

It is not known with certainty whether flocculation takes place in isopropanol suspensions of Al_2O_3 and ZrO_2, although low green density values of the deposits are perhaps an indication of the phenomenon. Nevertheless under an applied electric field aggregation certainly exists. When an electric field is applied to suspensions of both Al_2O_3 and ZrO_2 the sedimentation to bottom of the container of the suspended material is accelerated considerably pointing at the formation of agglomerates. This phenomenon becomes more pronounced with increase in field intensity, and more rapid stirring is required to maintain the suspension in a homogeneous state.

A similar phenomenon was observed earlier in our laboratory. Coagulation of colloidal particles in an electric field was reported in [39]. The possible explanation of this phenomenon is as follows. When a charged particle moves in an electric field its diffuse double layer dragged by the field in the opposite direction shifts and acquires an egg-like shape (see fig. 2 in section 2.1). Close contacts at which attractive van der Waals forces prevail are possibly facilitated when particles collide with their "bare" parts (see fig. 2). And this leads to flocculation. Increase of the electric field makes both the diffuse double layer displacement and flocculation more pronounced.

Therefore several additives which act as dispersants were studied in an attempt to improve the green density and stability of suspensions.

Out of several additives tested (see section 3) only Acetylacetone (AcAc) had a pronounced effect on the stability of suspensions both for alumina and zirconia. Slower stirring was required to maintain homogeneity of suspensions under an applied electric field when AcAc was added. Complete sedimentation of the dispersed phase out of suspensions without AcAc occurred after approximately 12 hours for zirconia and 24 hours for alumina. In the presence of AcAc [1-1.5% (v/v)] only approximately one third of the disperse phase precipitated after one week for ZrO_2 and two weeks for Al_2O_3. The considerable difference in sedimentation velocities of Al_2O_3 and ZrO_2 particles (of approximately the same size (section 3)) may be partly explained by the difference in their specific densities (3.98 g/cm^3 for Al_2O_3 and 6.2 g/cm^3 for ZrO_2).

The green density of Al_2O_3 and ZrO_2 deposits was determined as a function of the amount of AcAc, see figs. 36-38.

Al_2O_3 deposits

A drastic increase in green density from 42% without AcAc up to ~ 62% at 0.05% AcAc occurs for all field intensities in the range of 25-300 v/cm (Fig. 36). For an AcAc content ranging from 0.05 to 3% (Figs. 36 and 37) the density does not change (within the experimental error). The green density of alumina deposits is strongly influenced by AcAc addition.

Above 3% of AcAc the influence of its concentration was not studied because the deposit surfaces lost their smoothness already at AcAc content of over 1.5%. A maximum green density value for alumina was obtained at 0.05-1.5% AcAc content. Field intensity and concentration of suspended particles had a negligible effect.

ZrO_2 deposits

The same drastic rise in green density from ~30% (without AcAc) up to ~50% at 0.05% AcAc takes place for zirconia (fig. 39). This value remains constant in an

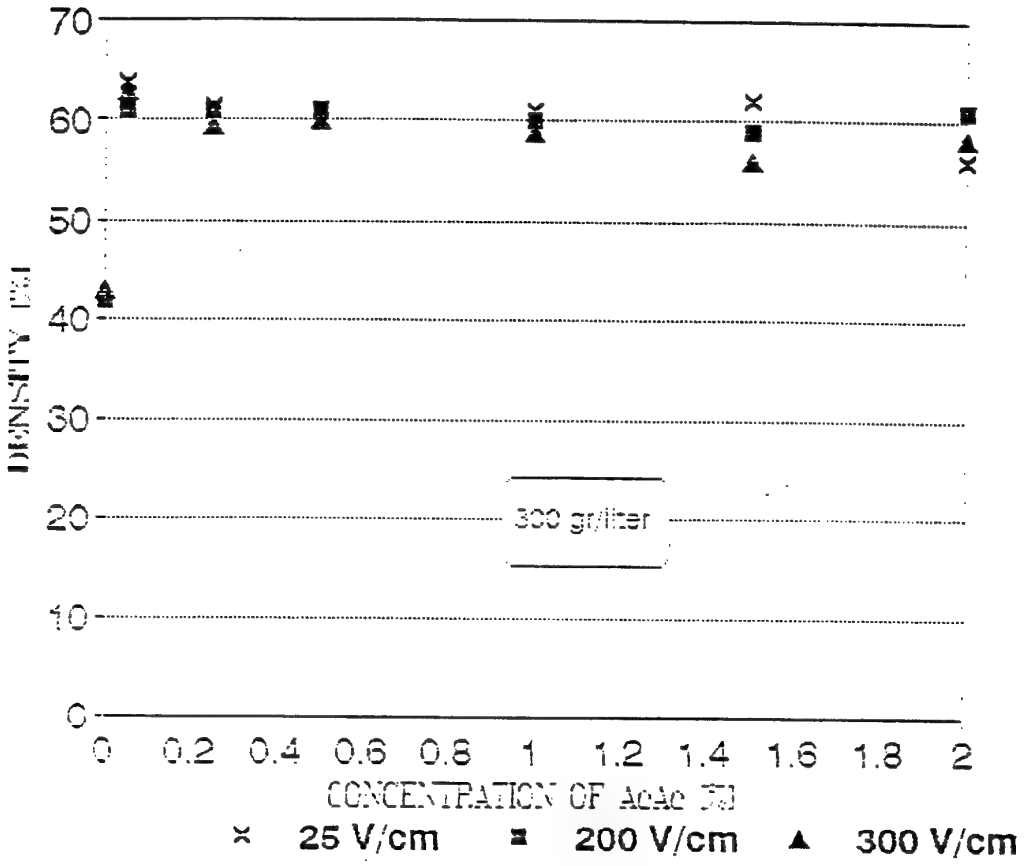

Fig. 36: Green density vs. concentration of AcAc for Al_2O_3 (0.3 μm).

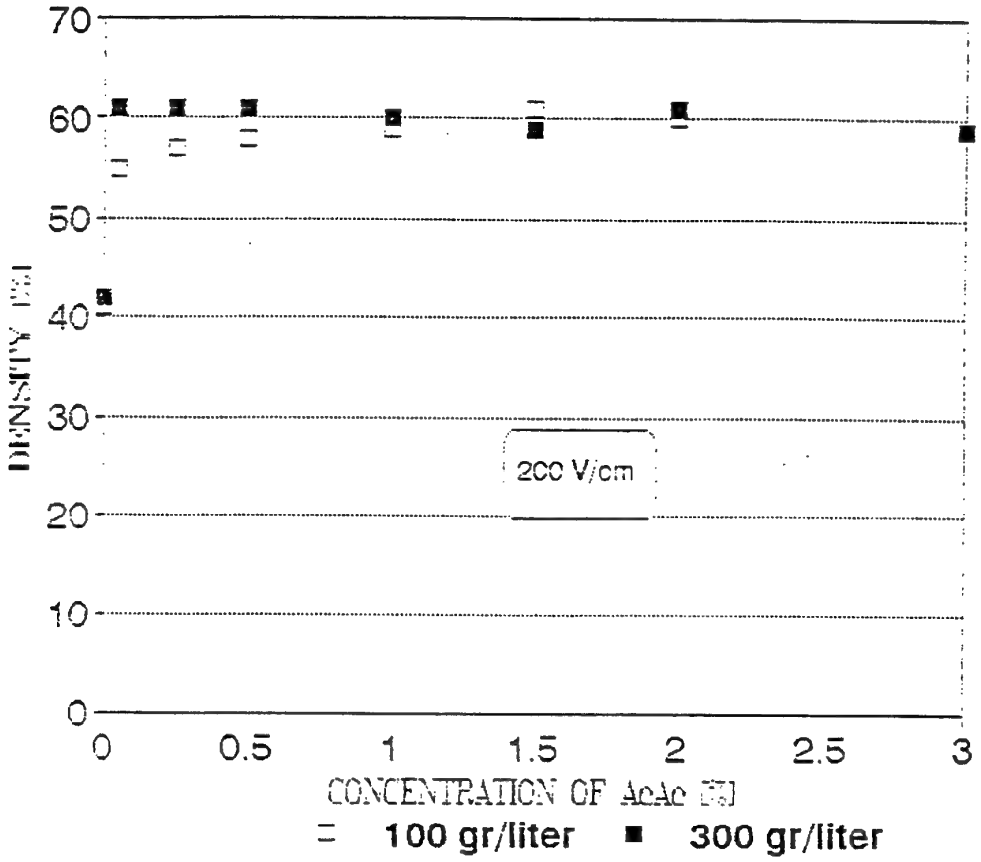

Fig. 37: Green density vs. concentration of AcAc for Al_2O_3 (0.3 μm).

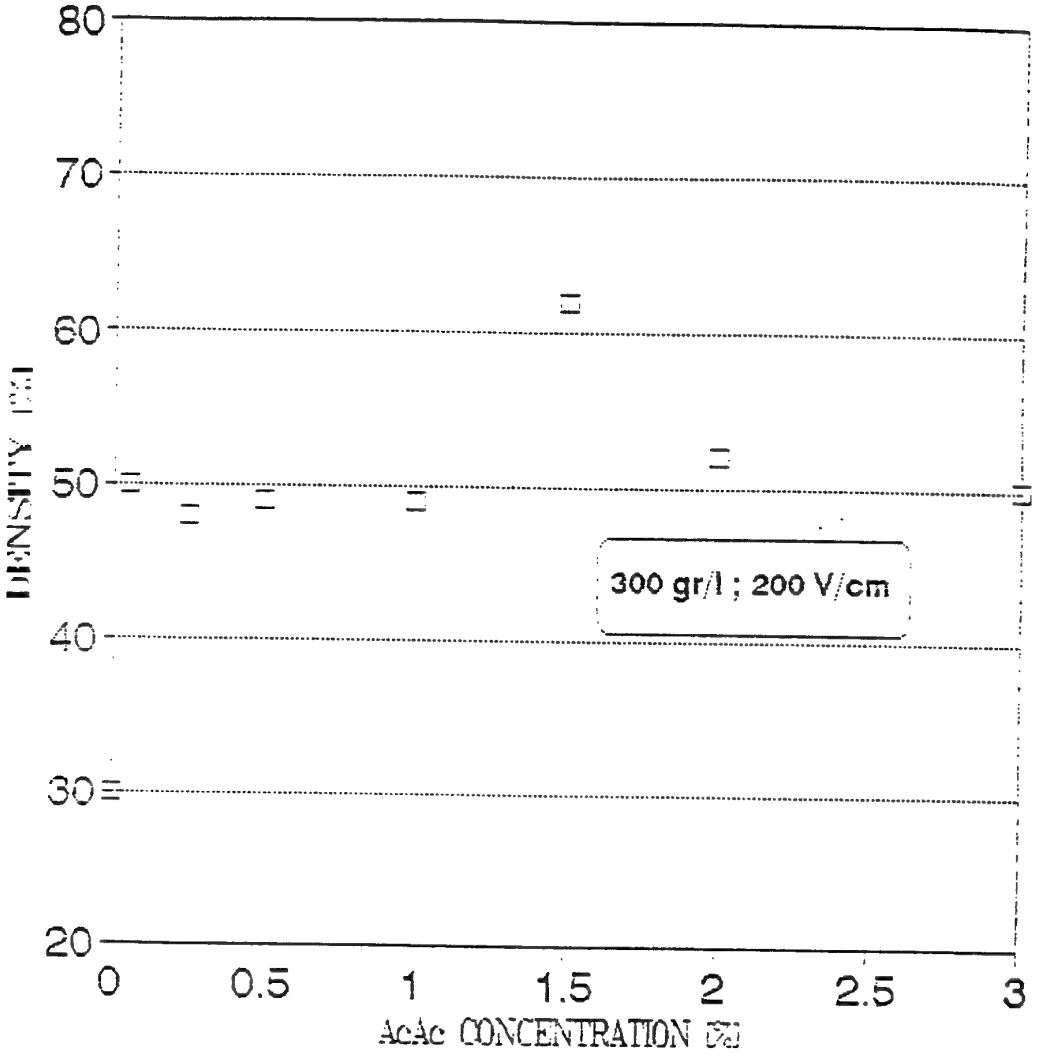

Fig. 38: Green density vs. concentration of AcAc additive for ZrO_2 (0.3μm) from propanol suspensions.

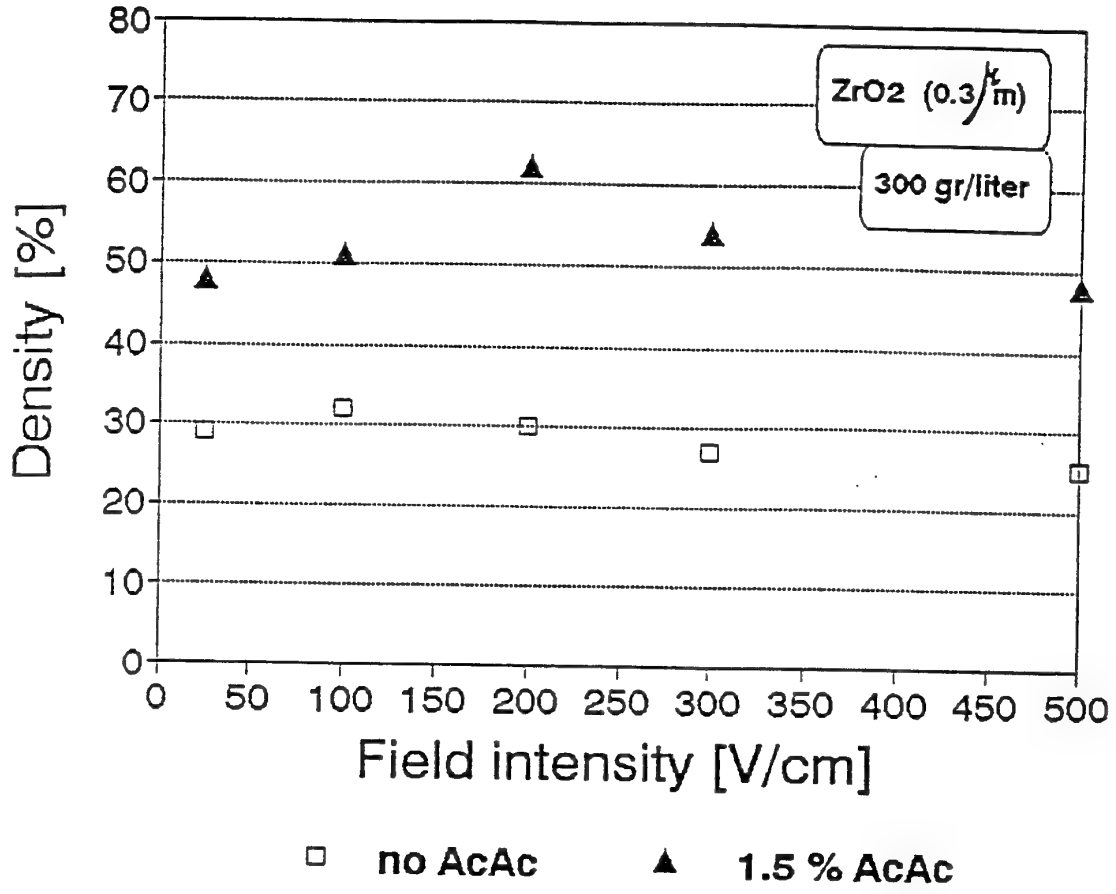

Fig. 39: Green density vs. field intensity for ZrO_2 (0.3 μm).

AcAc concentration range of 0.05-3%, except for a considerable increase to 62% at 1.5% AcAc content and 200 v/cm (See Fig. 38). The dependence of green density on field intensity at a 1,5% AcAc content is shown in Fig. 39. The maximum value of 62% corresponds to 200 v/cm. The maximum green density value for Zirconia was obtained at a 1.5% AcAc content at 200 v/cm. Deposits of zirconia obtained from suspensions with an AcAc content over 1.5% became uneven and contained pin holes.

4.3 Fired density

The fired densities of Al_2O_3 and ZrO_2 deposits obtained from isopropanol suspensions without AcAc as a function of field intensity are presented in figs. 40 and 41 respectively. All bodies were sintered at 1550°C for 2h with a heating rate of 1°C/min and cooling rate of 2°C/min. Fired density both for alumina and zirconia does not depend on field intensity in the range of 25-500 v/cm (within experimental error, as is for the green density) and is equal to 92-97% for alumina and 97-100% for zirconia.

The fired density of Al_2O_3 deposits obtained from suspensions with 0.5% AcAc at 200 v/cm and 300 g/l was found to be 99%. The fired density of ZrO_2 deposits obtained from suspensions with AcAc content in the range 0.05-1.5% at 200 v/cm and 300 g/l was about 100%.

4.4 Zeta potential

The data on the green densities presented above indicate that AcAc activates a mechanism of stabilization. The drastic slowing of sedimentation of both Al_2O_3 and ZrO_2 particles in the presence of AcAc (section 4.2) is a confirmation for that. In order to verify the stabilization mechanism measurements of zeta potentials were undertaken.

Figs. 42-45 show the distance (the boundary displacement from the initial position) vs. time dependencies from which mobilities and zeta potentials were calculated. These are presented in Table 7.

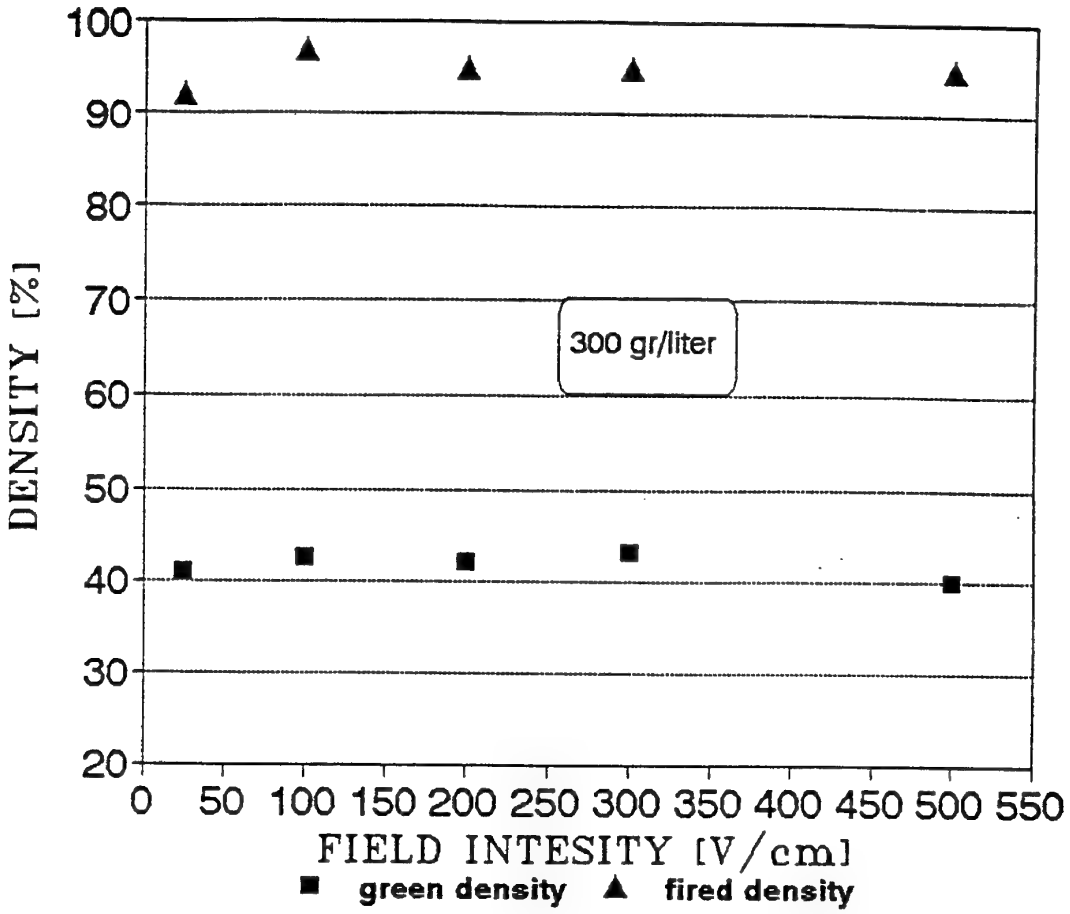

Fig. 40: Green and fired density as a function of field intensity for Al_2O_3 (0.3 μm).

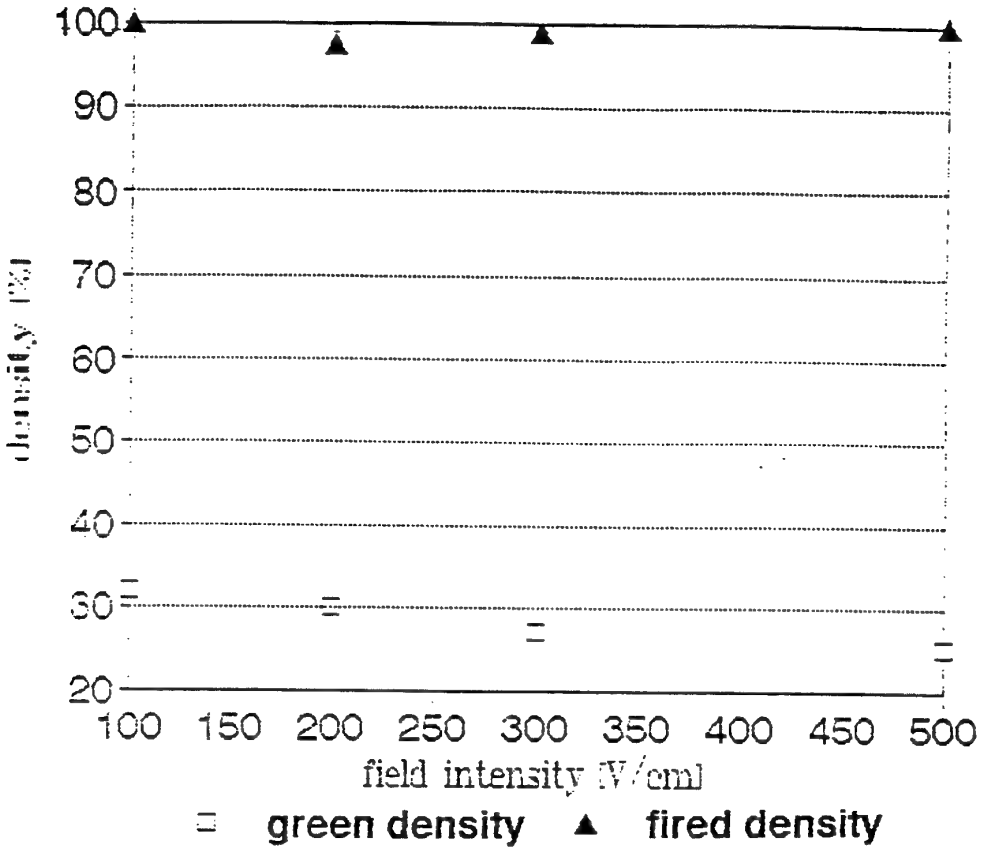

Fig. 41: Density (green, fired) vs. field intensity for ZrO_2 (0.3 μm). Concentration: 300 gr/liter.

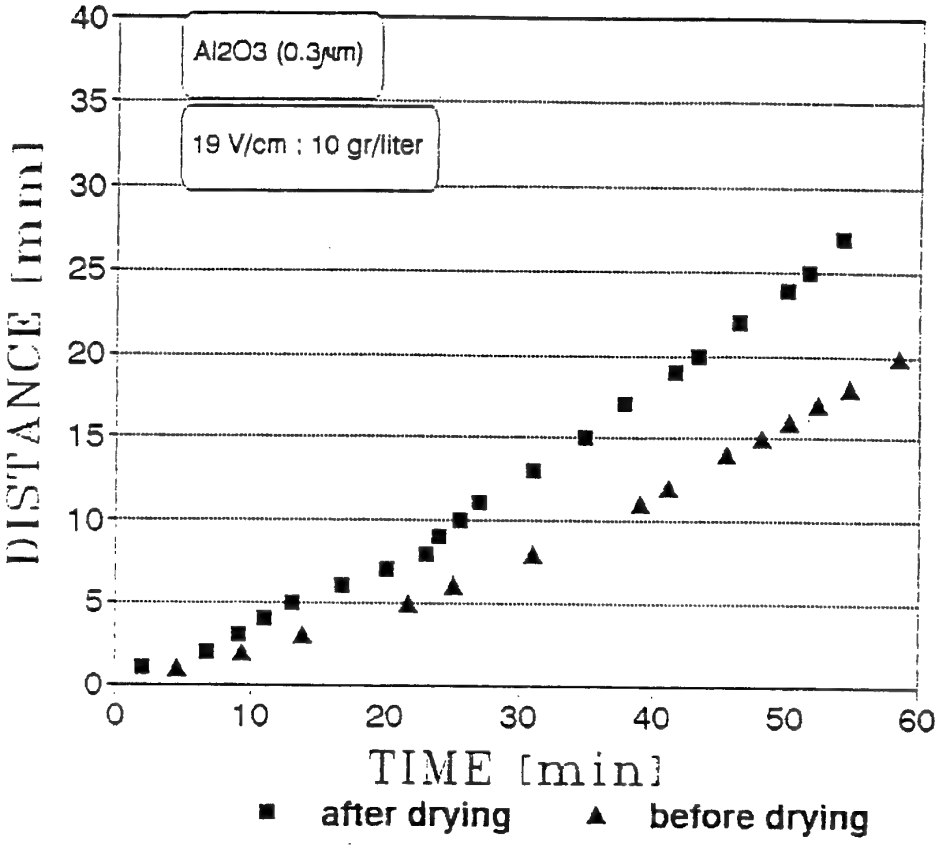

Fig. 42: Particle motion in propanol for Al_2O_3 (0.3 μm).

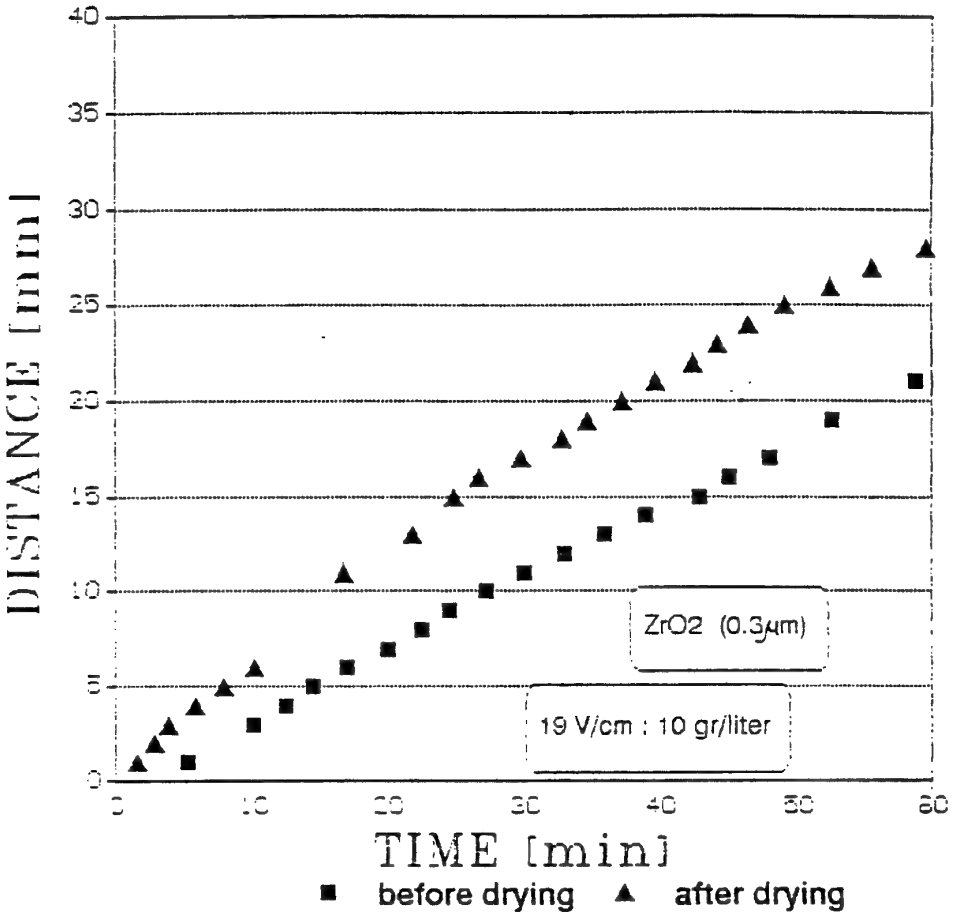

Fig. 43: Particle motion in propanol for ZrO_2 (0.3μm) without AcAc .

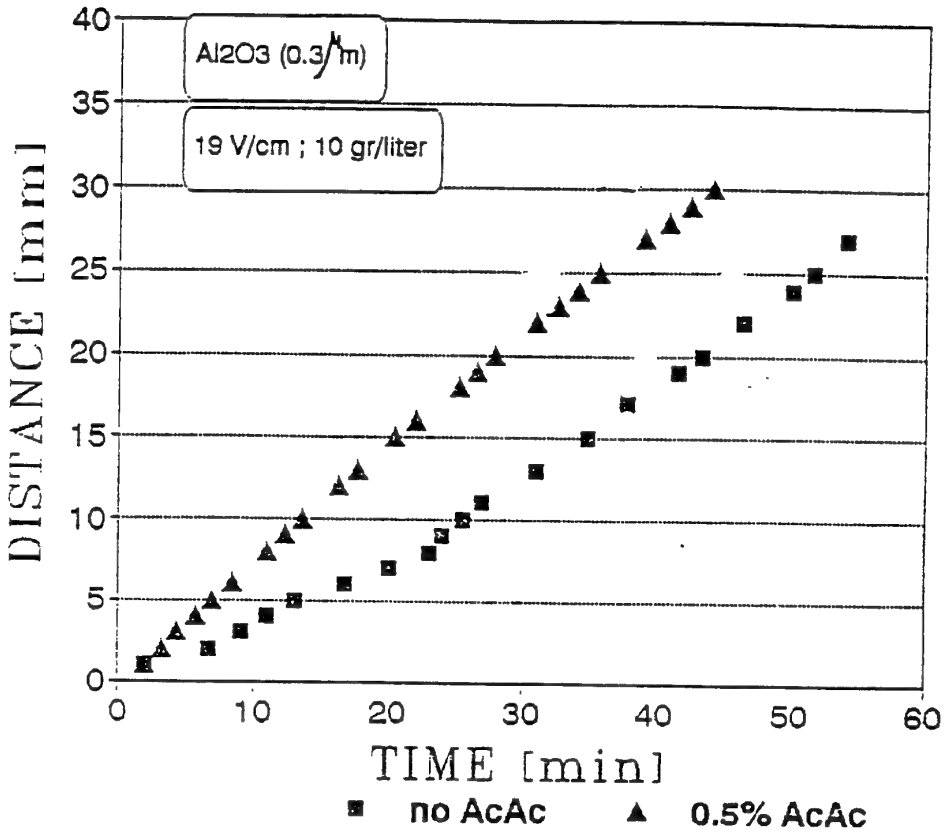

Fig. 44: Particle motion in propanol for Al_2O_3 (0.3μm) after drying.

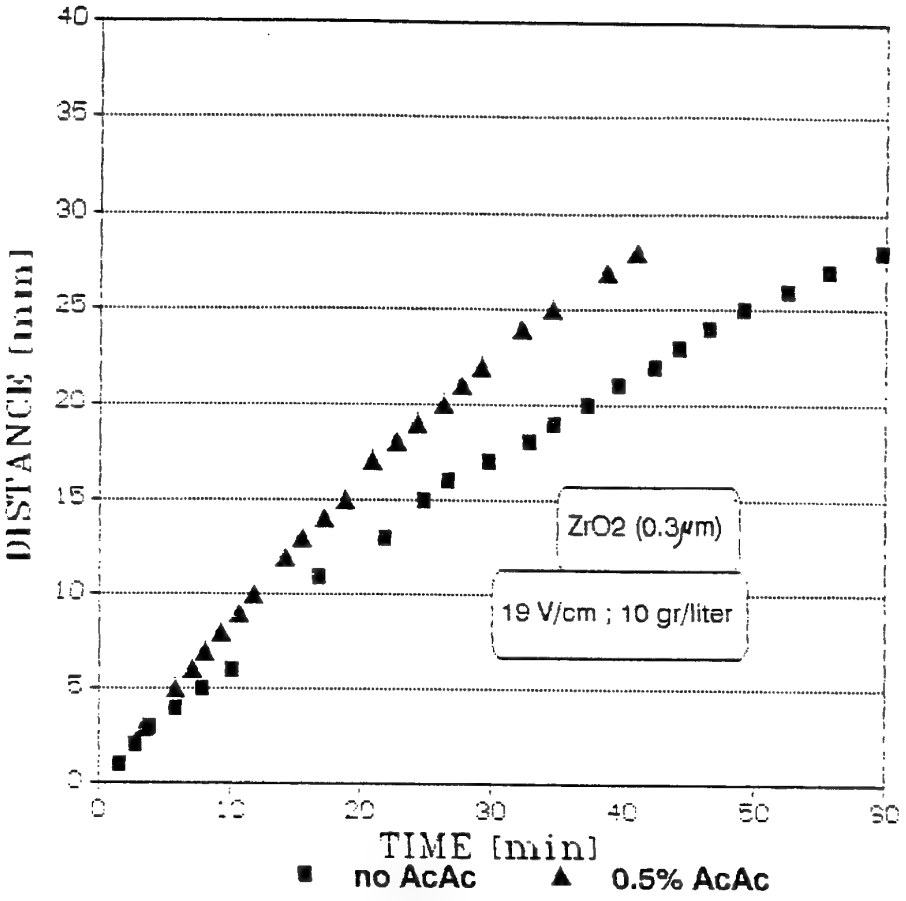

Fig. 45: Particle motion in propanol for ZrO_2 (0.3μm) after drying.

Effect of moisture on particle surface charge was studied for both alumina and zirconia (figs. 42 and 43). It is clearly seen that moisture has an appreciable effect on the zeta potential which is changing from 42 to 58 mV for Al_2O_3 and from 46 to 78 mv to ZrO_2 (see Table 3) after drying.

The motion of Al_2O_3 and ZrO_2 particles in isopropanol suspensions without and with 0.5% AcAc is shown in Figs. 44 and 45. The addition of 0.5% AcAc results in an increase of the zeta potential from 58 to 91 mv for Al_2O_3 and from 78 to 105 mv for zirconia (see Table 3). The effect of the AcAc can be explained by a keto-enolic reaction:

$$CH_3C{-}CH_2\,CCH_3 \longleftrightarrow CH_3\,C = CH{-}CO\,CH_3$$

Keto-enol Equilibrium

$$ROH \rightarrow RO^- + H^+$$

Table 7: Mobility and zeta potential of ceramic materials at various conditions for their suspensions

Conditions of Suspension	Suspension of Al_2O_3		Suspension of ZrO_2	
	Mobility $\mu \times 10^4$ cm sec^{-1} per volt cm^{-1}	Zeta Potential ζ (volts)	Mobility $\mu \times 10^4$ cm sec^{-1} per volt cm^{-1}	Zeta Potential ζ (volts)
Powder before drying without AcAc	0,2819	0,042	0,3081	0,046
Powder after drying, without AcAc	0,3862	0.058	0,5179	0,078
Powder after drying, with 0.5% AcAc	0,6429	0,091	0,6982	0,105

The dissociation of the enolic group results in H^+ formation. The subsequent adsorption of H^+ ions on the particles increases their positive charge and zeta potential. Thus AcAc provides an electrostatic mechanism of stabilization, enhancing the repulsive forces and stability of the suspensions.

4.5 Kinetics of deposition of Al_2O_3 and ZrO_2

The thickness of the individual layers is an important factor for laminar structures. Therefore the kinetics of deposition was studied.

a) Suspensions in isopropanol without additives.

Al_2O_3 and ZrO_2 were deposited from isopropanol suspensions on stainless steel cathodes under the following conditions:

particle concentration	100–300 g/l
field intensity	25–300 v/cm
deposition time	10–900 sec

The thickness of fired deposits was calculated from deposit weights using the theoretical density. The thickness vs. field intensity and the thickness vs. deposition time dependences for both Al_2O_3 and ZrO_2 are shown in figs. 46 and 47. The thickness of both the alumina and zirconia deposits increases with field intensity linearly up to 300 v/cm, Fig. 46. Fig. 47 displays the deposit thickness as a function of deposition time. The thickness increases linearly up to 150 sec for Al_2O_3 and 100 sec for ZrO_2, then the rate becomes slower. Such dependencies are characteristic for ceramic materials and are due to formation of an insulating layer. It is seen that, for any given time and voltage, the deposition rate of ZrO_2 is less than that of Al_2O_3.

Deposits of both the alumina and zirconia, in the range of 20–35 μm thicknesses, were continuous, smooth and did not crack during drying in air at room

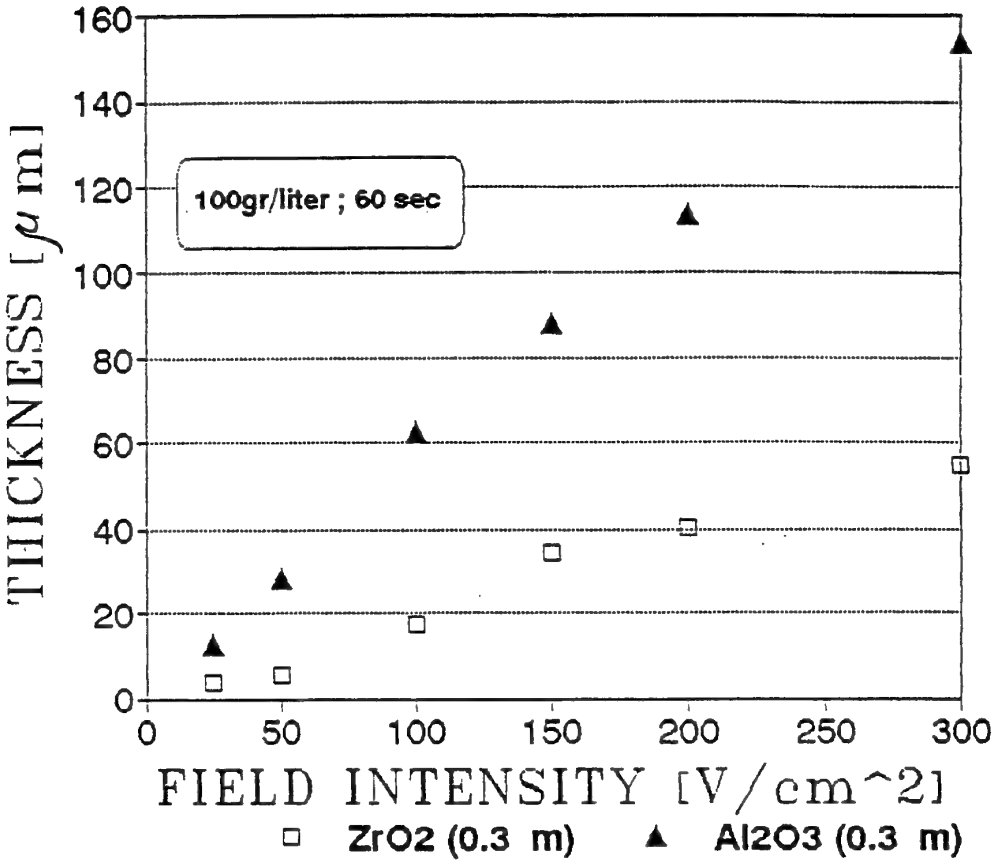

Fig. 46: Deposition rate vs. field intensity for Al_2O_3 (0.3μm) and ZrO_2 (0.3 μm) .

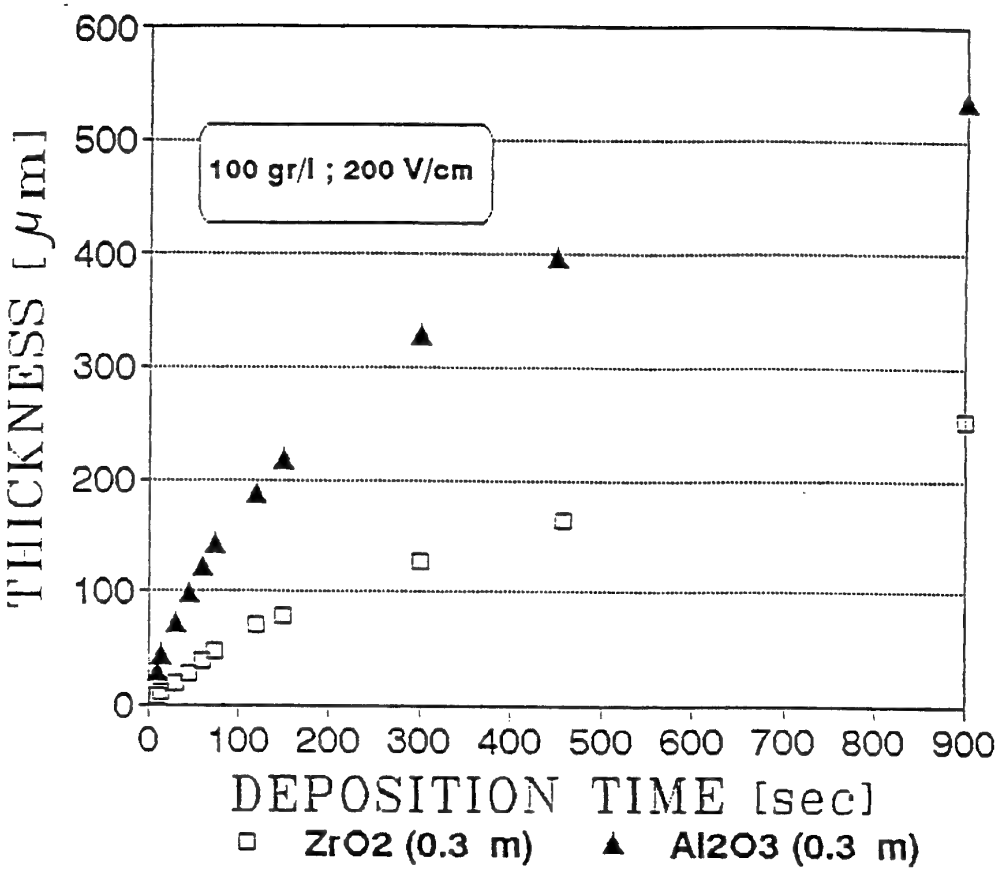

Fig. 47: Deposition rate for
Al_2O_3 (0.3 μm) and ZrO_2 (0.3 μm) .

temperature. With further increase of the thickness deposit surfaces became uneven, not smooth and cracked during drying. The cracking of ceramic green bodies during drying is a well-known problem in ceramic processing and will be studied in the future.

b) Suspensions in isopropanol with AcAc

The effect of AcAc on the deposition rate was studied at 1,5% AcAc content, at which its effect on green density was maximum (see section 4.2). The thickness vs. time dependencies for Al_2O_3 and ZrO_2 are shown in Figs. 48 and 49. The deposition rate increases considerably both for Al_2O_3 and ZrO_2 in the presence of AcAc and changes linearly in the studied time range. Figs. 50 and 51 demonstrate the deposition rate as a function of time for two concentrations of solids (100 and 300 g/l) for Al_2O_3 (Fig. 50) and for ZrO_2 (Fig. 51) in the presence of 1.5% AcAc. The deposition rate increases considerably with concentration. Fig. 52 shows deposit thickness vs. time curves for two constant field intensity values (25 and 200 v/cm) for ZrO_2 suspensions with 1.5% AcAc. A strong dependence of the deposition rate on the field intensity is clearly seen. The deposition rate of ZrO_2 is lower than that of Al_2O_3 in accordance with literature data [34]. This is illustrated in Fig. 53.

Deposits of thickness of up to $\sim$ 100μm for Al_2O_3 and up to 200 μm for ZrO_2 obtained from suspensions with 1.5% AcAc, were dense and satisfactorily smooth. Deposits obtained form suspensions with an AcAc content of over 1.5% were uneven and with pin holes for ZrO_2 and with an increased amount of "humps" for Al_2O_3.

While the mobility and zeta potential of ZrO_2 are higher than those of Al_2O_3 the deposition rate of ZrO_2 is lower than that of Al_2O_3. This behaviour is not clarified yet but may be related to other factors which determine the deposition rates.

4.6 Cross-sections of deposits

The microstructure and morphology of alumina and zirconia sintered deposits were studied by optical and electron microscopies. The study was performed on polished cross-sections and on fracture surfaces, fractures having originated in the green state.

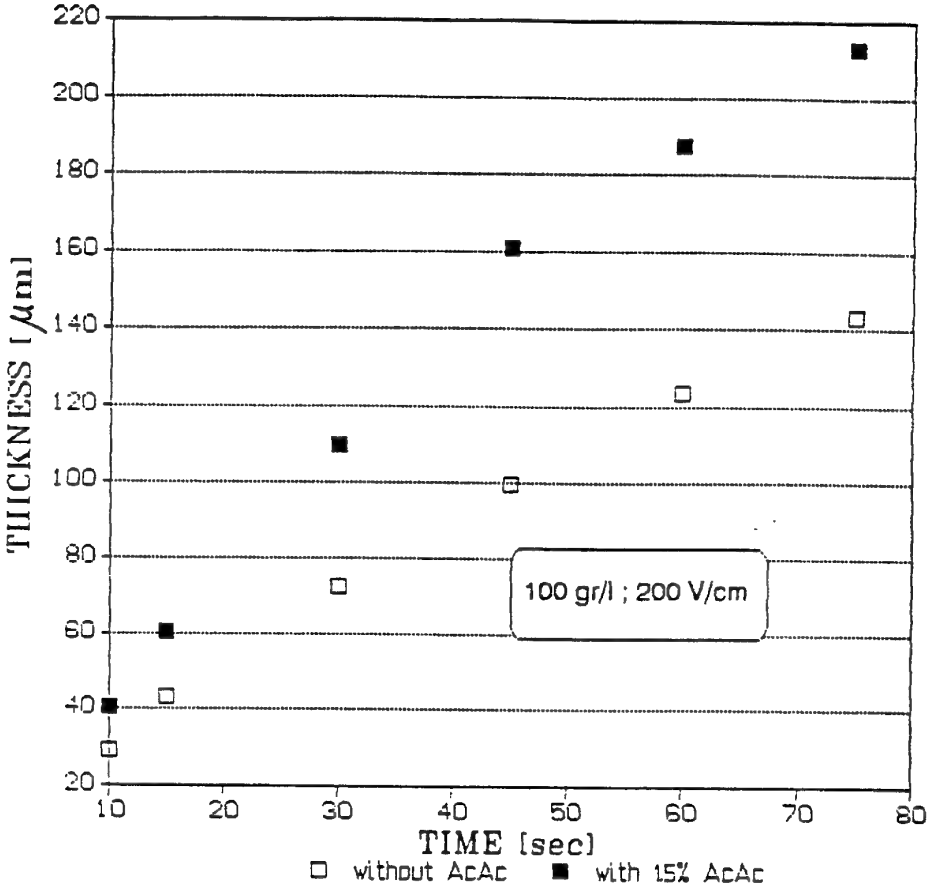

Fig. 48: Deposition rate for Al_2O_3(0.3μm).

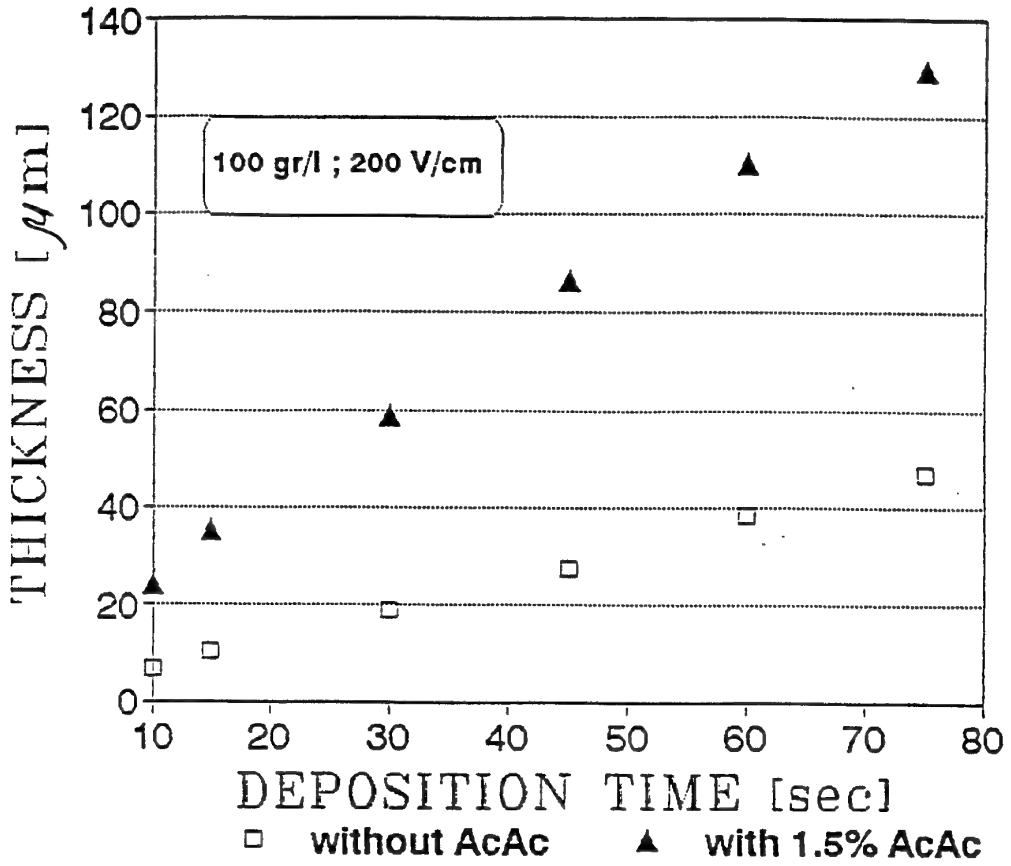

Fig. 49: Deposition rate for ZrO_2 (0.3μm).

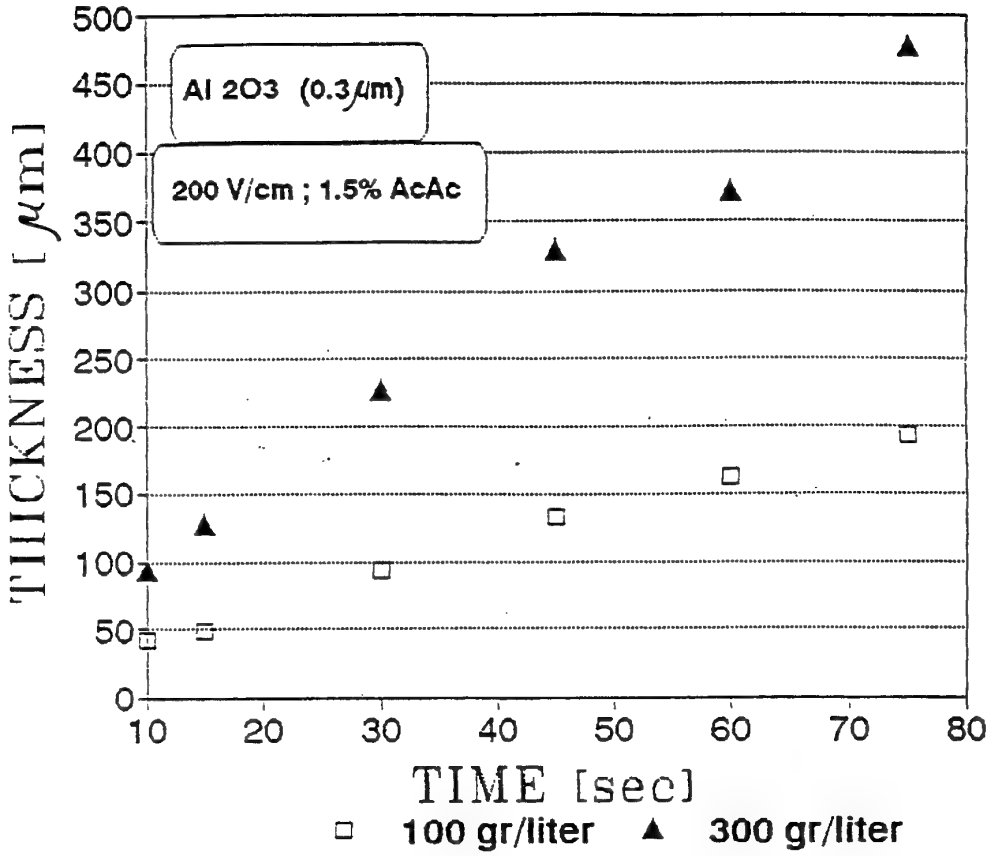

Fig. 50: Deposition rate for $Al_2O_3(0.3\mu m)$.

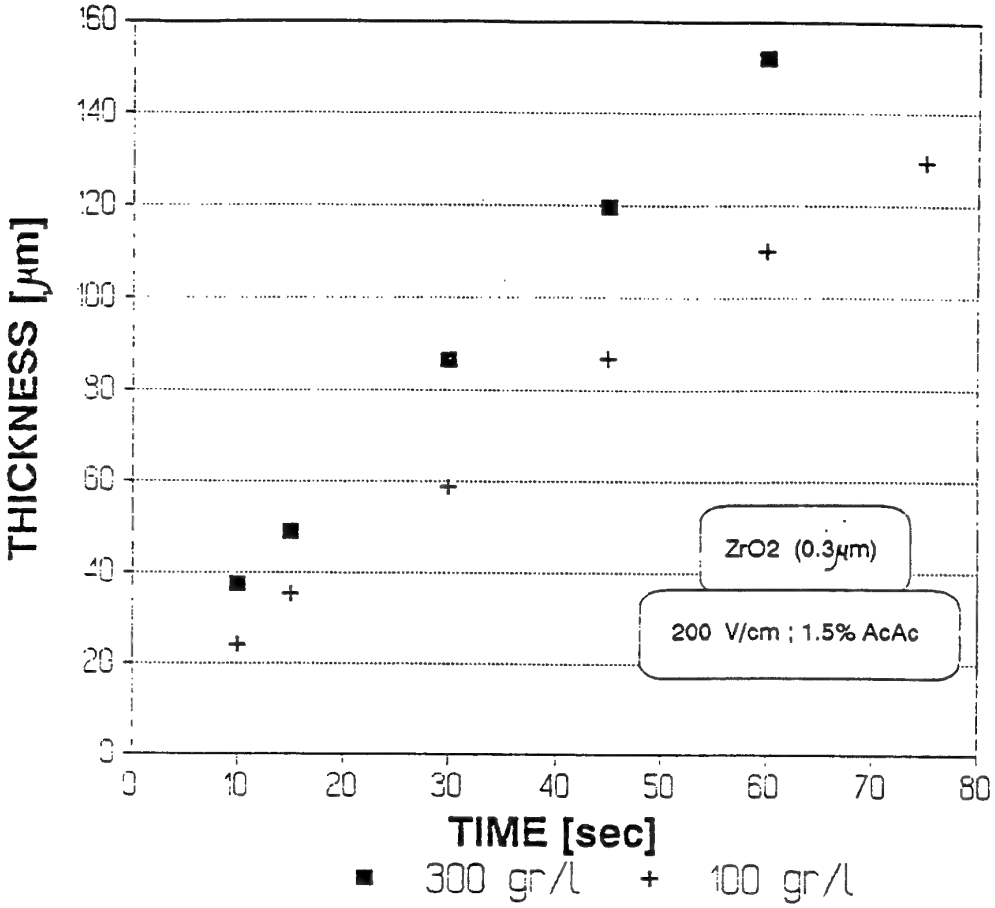

Fig. 51: Deposition rate for of ZrO_2 (0.3μm) .

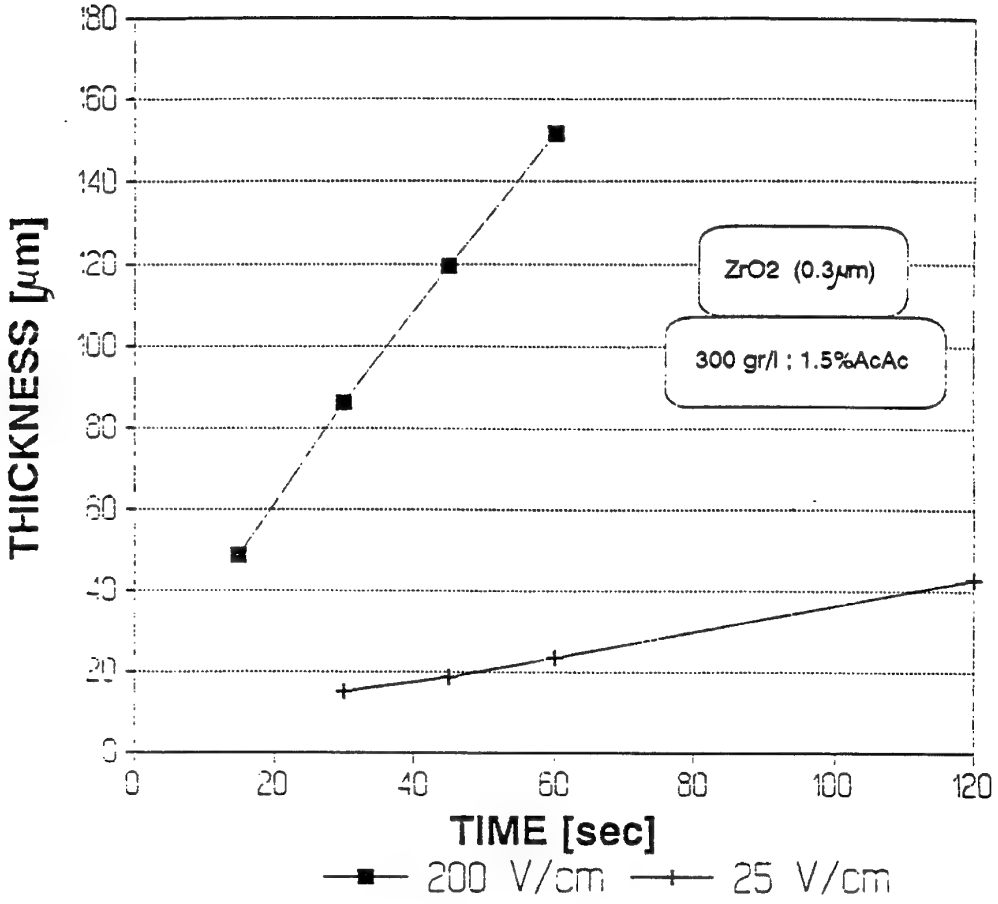

Fig. 52: Deposition rate for ZrO_2 (0.3 μm) .

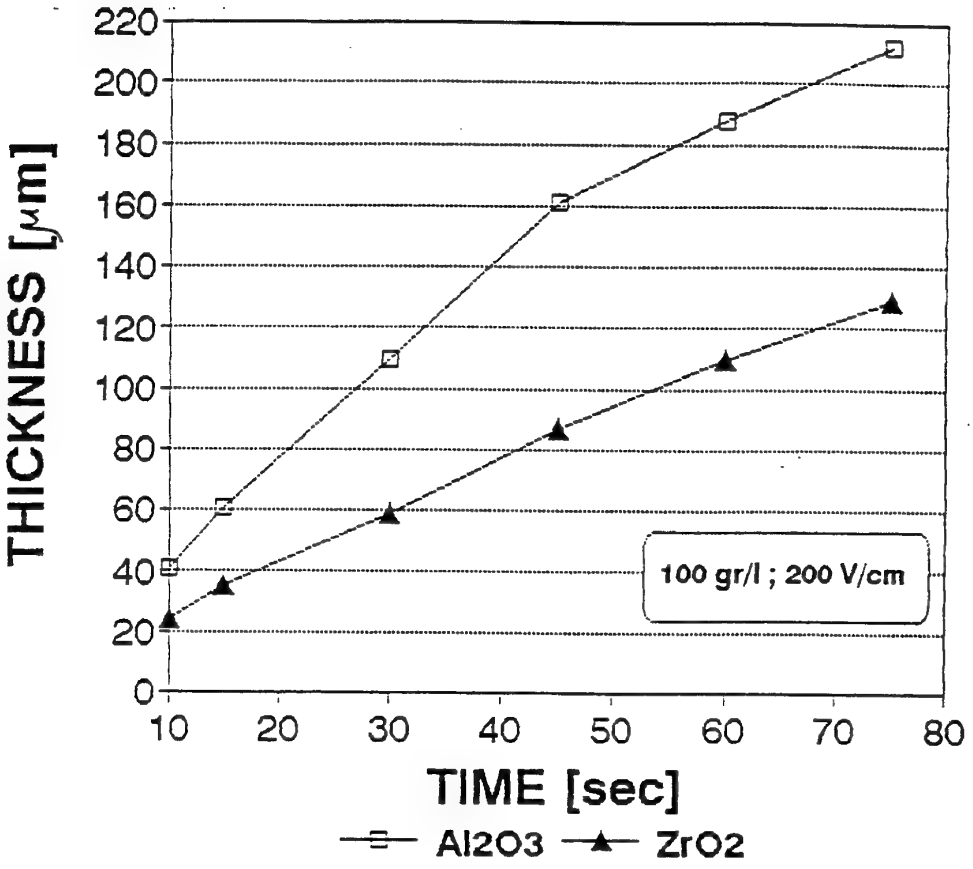

Fig. 53: Deposition rate for Al_2O_3 (0.3 μm) and ZrO_2 (0.3m) with 1.5% AcAc .

Fig. 54 shows the fracture surfaces of ZrO_2 bodies obtained at 200 v/cm from a 300 g/l suspension without (a) and with different amounts of AcAc (b-e) ranging from 0.05 to 3%. The grain size ranges from ~ 1μm to ~ 8μm. The influence of AcAc on the structure of the deposits is clearly seen. The addition of 0.05% AcAc results in a dense packed microstructure which is maintained up to 1.5% AcAc (b-d). At 3% AcAc (e) the packing becomes less dense. Then the deposits were uneven and contained pin holes (section 4.5).

Fig. 55 shows the same surface as in fig. 54b (0.05% AcAc) after polishing. During polishing some ZrO_2 grains were pulled out, leaving features on the micrograph. Although according to the fractograph in fig. 54b the primary grains are densely packed, in the micrograph (fig. 55) little pores are seen.

The micrograph of polished cross-sections of Al_2O_3 bodies obtained at 200 v/cm from 300 g/l suspensions without (Fig. 56a) and with 0.5% AcAc (Fig. 56b) are shown in Fig. 56. It is seen that the addition of AcAc results in decrease of size and amount of pores. The pores are mostly situated along the grain boundaries. It must be noted that Al_2O_3 grains have also been pulled out during polishing, leaving features on the micrographs.

Our technique of preparation of ceramic surface for microstructure studies has to be further improved. The systematic study of microstructure of deposits will be done at the next stage of the project.

4.7 Multilayers

Multilayered Al_2O_3/ZrO_2 structures have been prepared by immersing the substrate (stainless steel cathode) alternately in Al_2O_3 and ZrO_2 suspensions. Independent control of electrophoretic deposition conditions were held. The deposition parameters ought to be controlled very carefully for each layer thickness. The green compacts were dried and fired at conditions described in section 3.

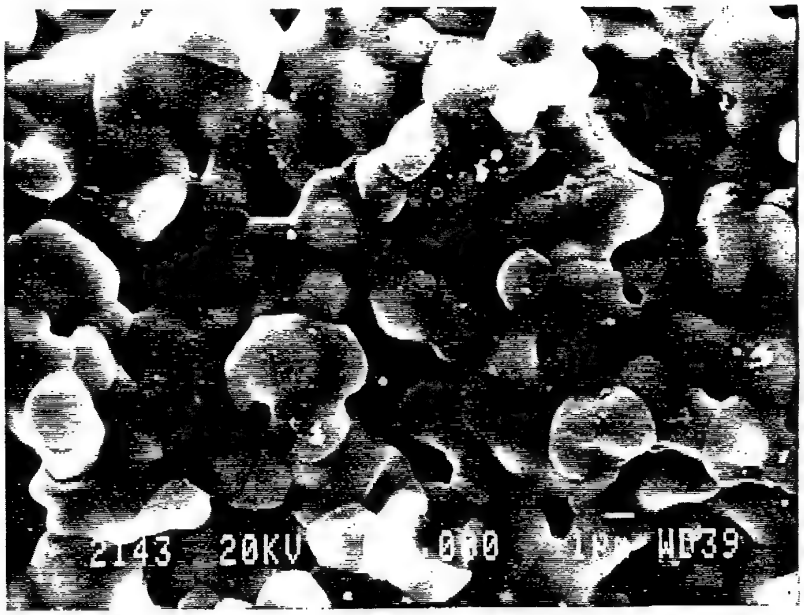

a

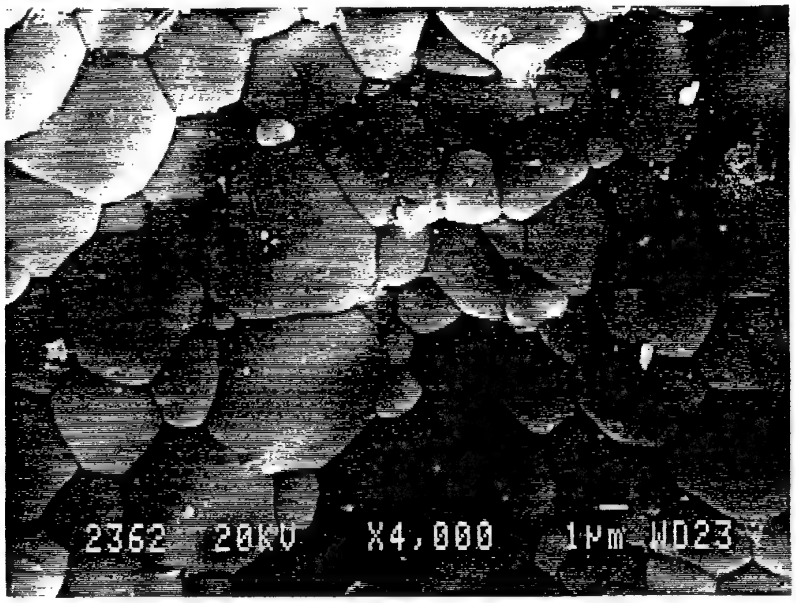

b

c

Fig. 54: Fracture surfaces of ZrO_2 sintered bodies:
a – Without AcAc, b – with 0.05% AcAc, c – with 0.25% AcAc /

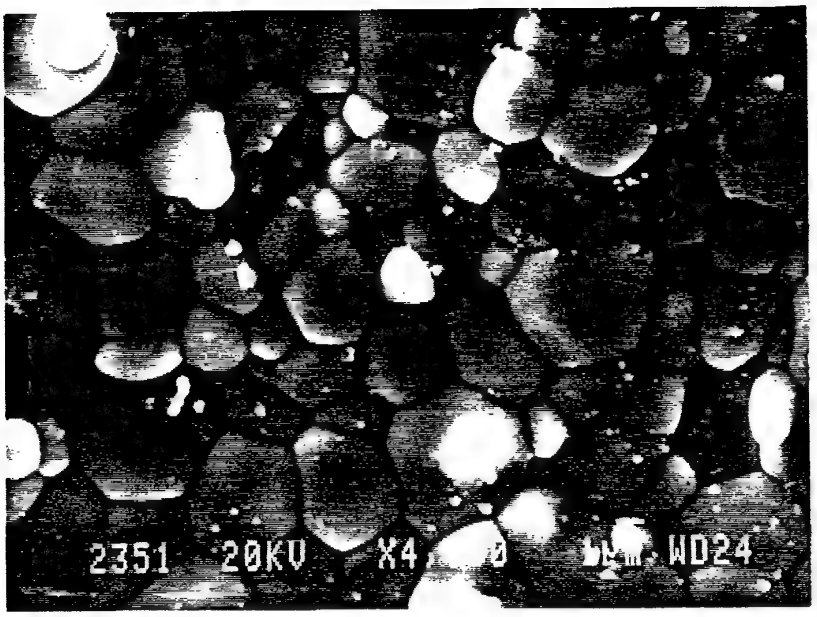

d

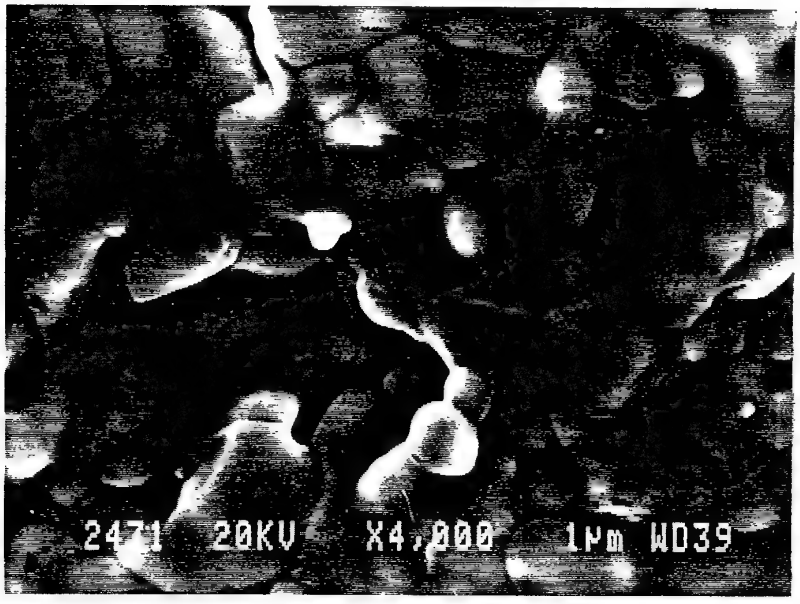

e

Continuation of Fig. 54: d – With 1.5% AcAc, e – with 3.0% AcAc.

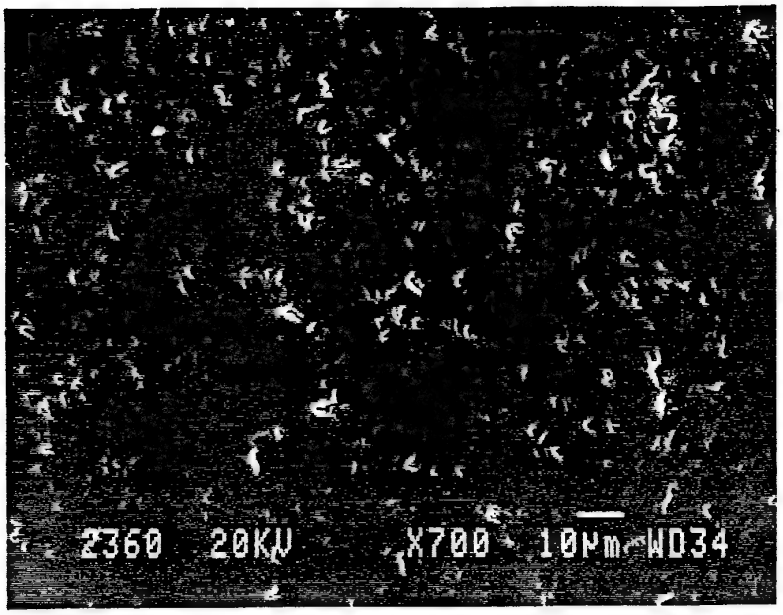

a

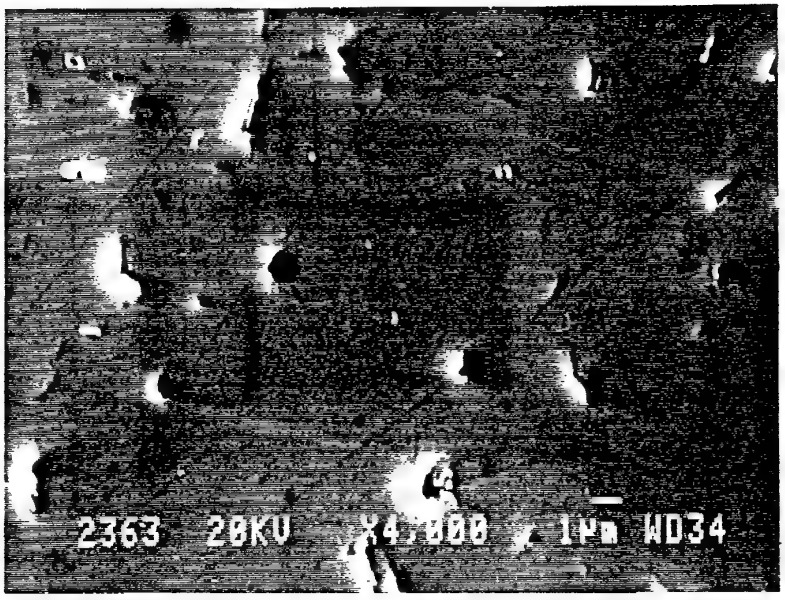

b

Fig. 55: Polished cross-section of a sintered zirconia body seen in Fig. 54b
a - low magnification, b - higher magnification.

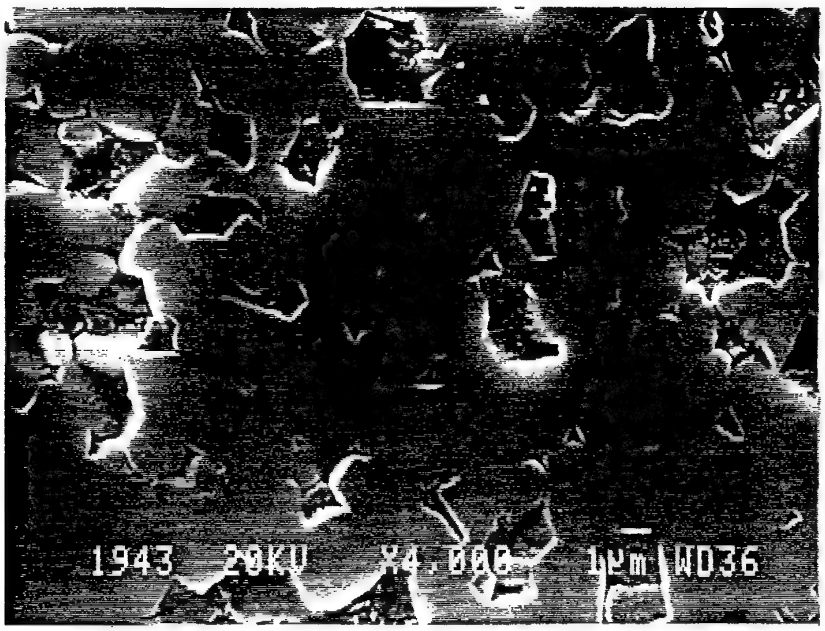

a

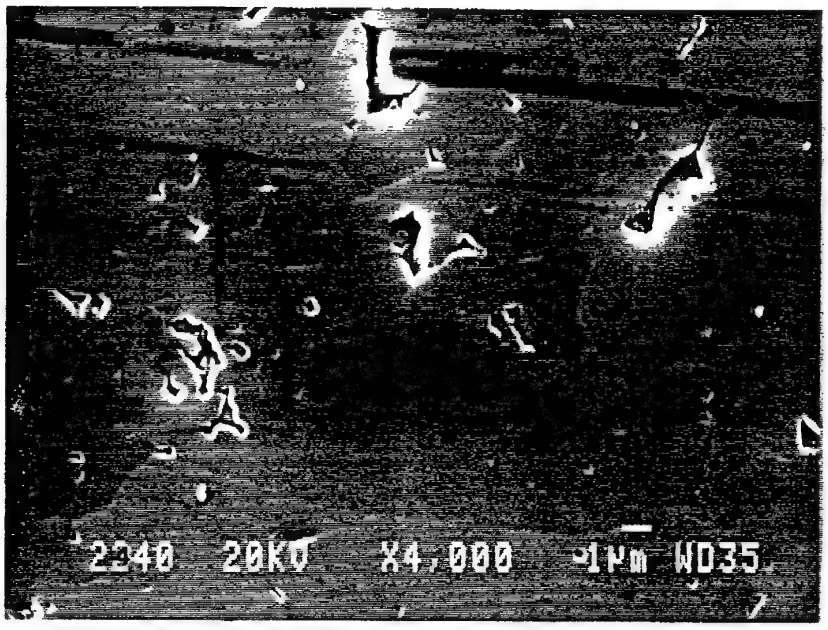

b

Fig. 56: Polished cross-sections of alumina bodies obtained from two suspensions of 300 g/l: a) - without AcAc, b - with 0.5% AcAc .

The following starting materials were used:

- a submicrometer alumina powder
- a submicrometer zirconia powder

Based on our previous experience (see section 4.5) the deposition of the sequential layers has been carried out under the following conditions:

- solids concentration	100 and 300 g/l
- AcAc content	1.5% (v/v)
- field intensity	200 v/cm
- time	10 sec

The solids concentration of $Al_2O_3$and ZrO_2 suspensions were the same in the laminar structure formation. The laminar structures with 13 layers were fabricated from 300 g/l suspensions. Laminar structures with 40 and 80 layers were prepared from 100 g/l suspensions:

It has been found that it is easier to remove alumina than zirconia from the stainless steel cathode. Therefore the first layer (adjacent to the cathode) in all composites was Al_2O_3, its thickness being slightly higher than the thickness of the others.

Figs. 57-59 show scanning electron micrographs of the 13 layer laminate structure with a total thickness (in sintered state) of about 0.7 mm. Figs 57 and 58 are the green compact, fig. 59 is the sintered compact. It is seen in Fig. 57 that the layers are well defined, the green thickness of the Al_2O_3layer is 60-75 μm, the thickness of the ZrO_2 layer is 30-40 μm.

Fig. 58 is high magnification of the zirconia layer showing its microstructure in the green state. Small pores are seen in a rather densely packed structure. The size of the particles is less than 1 μm. The average size of zirconia particles in the starting material is 0.3 μm. This confirms that AcAc functions as a dispersant preventing or diminishing agglomerate formation. The low magnification micrograph of the same 13 layers structure in the sintered state is seen in Fig. 59a; Figs. 59b and 59c are Al and Zr mappings on the same area.

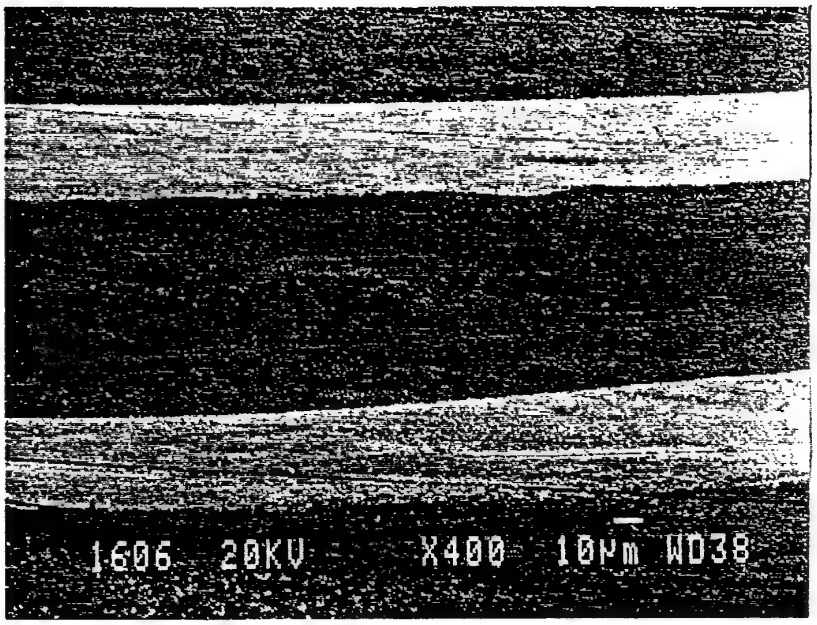

← ZrO_2

← Al_2O_3

a

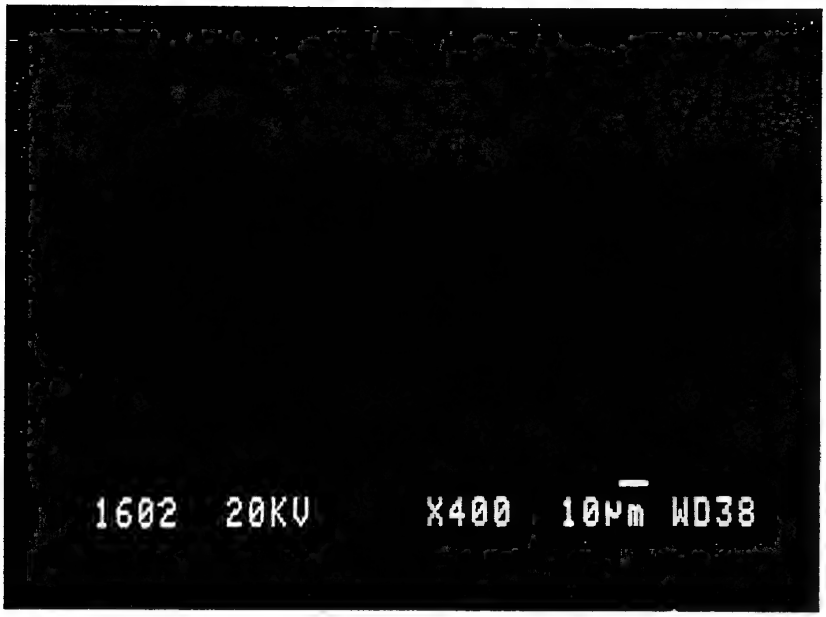

← Zr Mapping on area a

b

Fig. 57: Scanning electron micrographs of a green Al_2O_3/ZrO_2 microlaminate
300 g/l, 200 v/cm, 1.5% AcAc
a. Polished cross-section; b. Zr mapping of cross-section in a.

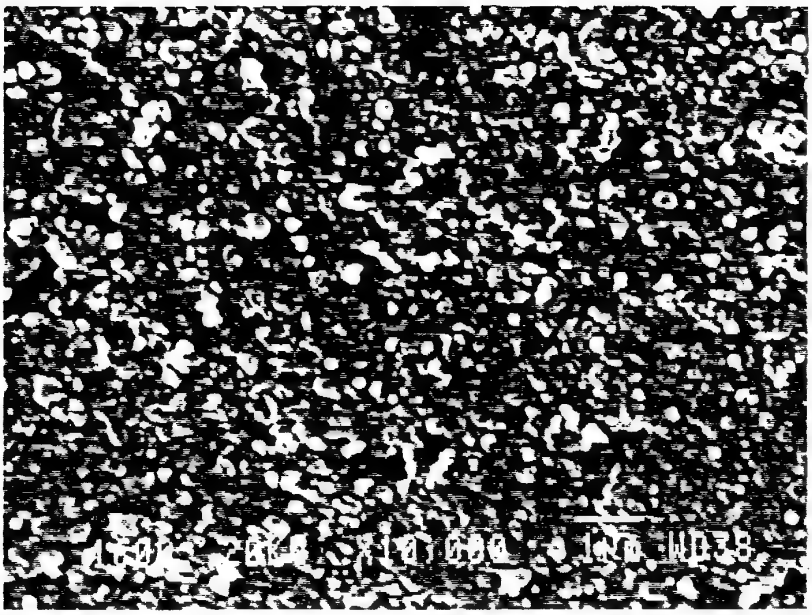

Fig. 58: Polished cross-section of green ZrO_2 layer, seen in Fig. 57a, under high magnification.

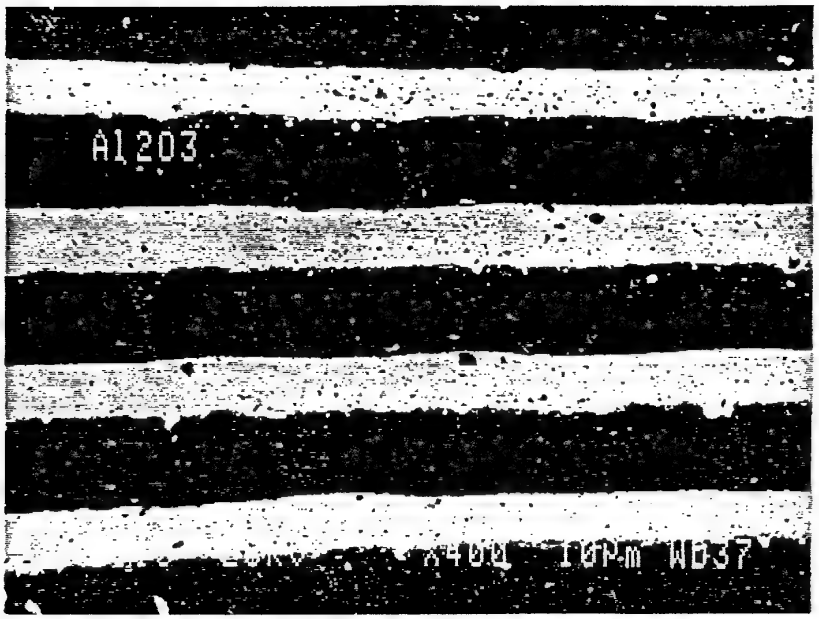

← Al_2O_3

← ZrO_2

a) polished cross-section

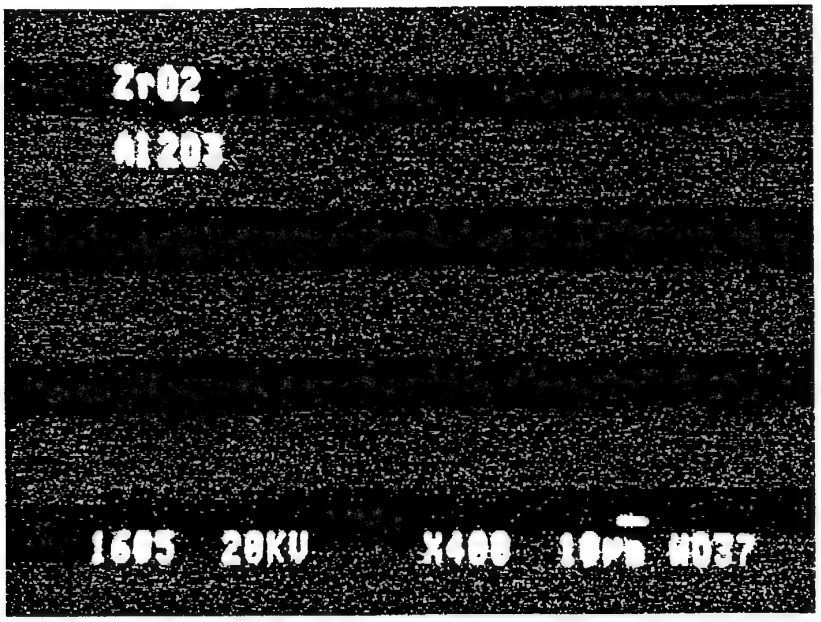

← Al Mapping on area a

b)

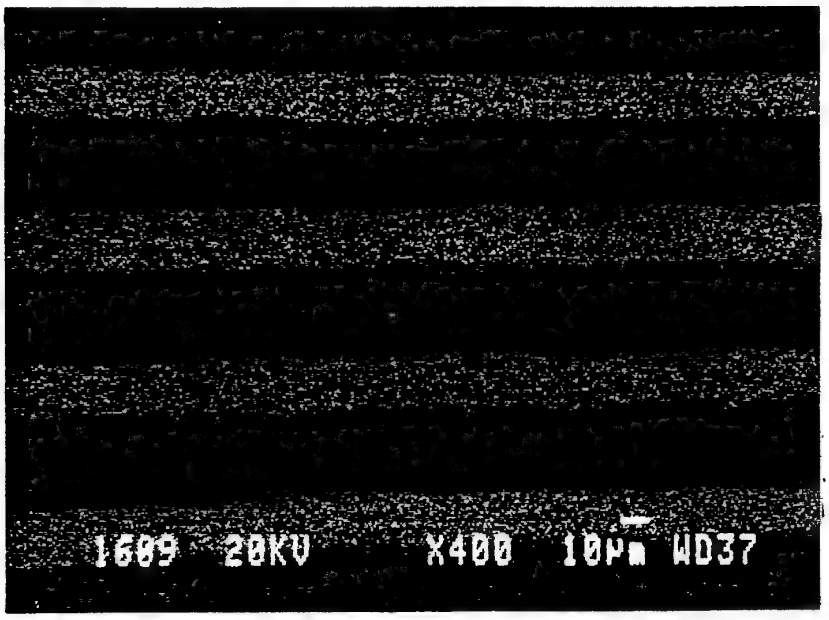

← Zr Mapping on area a

c)

Fig. 59: Scanning electron micrographs of an Al_2O_3/ZrO_2 sintered microlaminate.

The interface between Al_2O_3 and ZrO_2 remained well defined and dense. It is seen that the high temperature of sintering does not cause discernible interdiffusion, but element quantitative analysis by EDS is required for a final conclusion.

A laminate structure of 40 layers is shown in Figs. 60-62. Fig. 60 shows a polished cross-section for the green structure, and Fig. 61 (polished cross-section) and Fig. 62 (fracture surface) show the sintered multilayer.

The total thickness in the sintered state is about 0,7mm. The green layer thickness was 25-30 μm for Al_2O_3 and 15-23 μm for ZrO_2 and sintered layer thickness was 17-20 μm for Al_2O_3 and 10-15 μm for ZrO_2. The layer thickness has not changed considerably across the structure.

The layers of the 40 layer laminate structure are thinner than the layers of the 13 laminate structure because they have been deposited from less concentrated suspensions (100 g/l) at the same deposition time (10 sec) and at same field intensity. The layers are well defined. High magnification fractographs in Fig. 62 (b and c) display the microstructure. The grains of $Al_2O_3$are considerably larger than those of ZrO_2 (approximately by a factor 2). ZrO_2 particles seem to be packed more densely. But only the micrographs of well polished and etched cross-sections scanned under high magnification will allow to draw more precise conclusions about the microstructure.

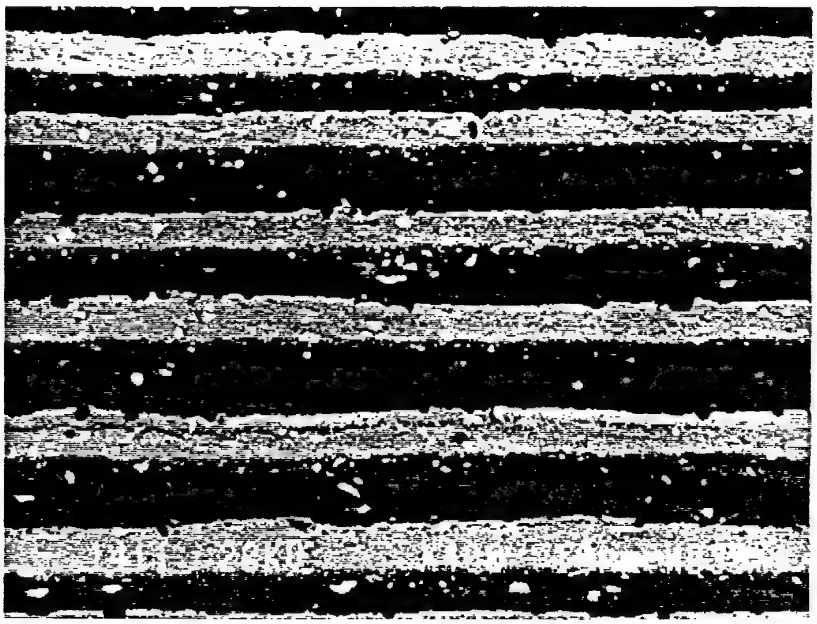

← Al_2O_3

← ZrO_2

a) polished cross-section

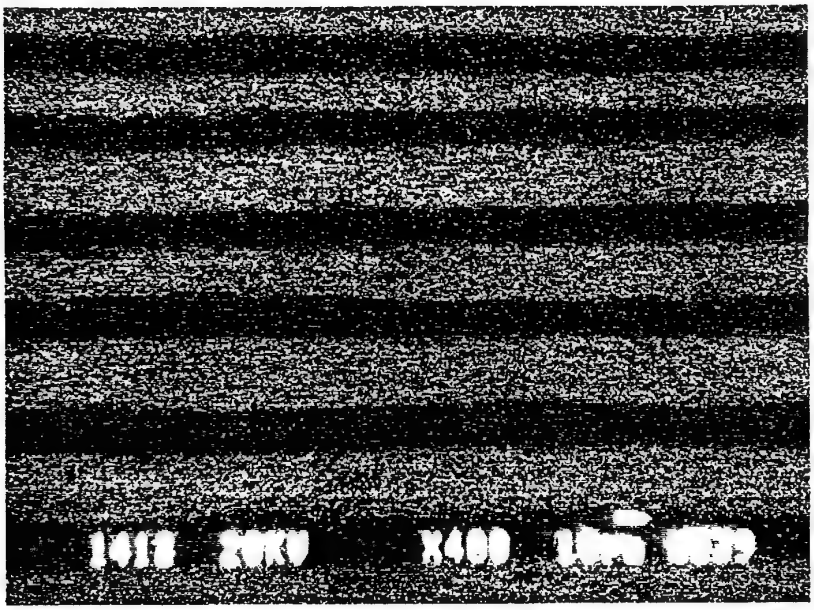

← Al

Mapping on area a

b)

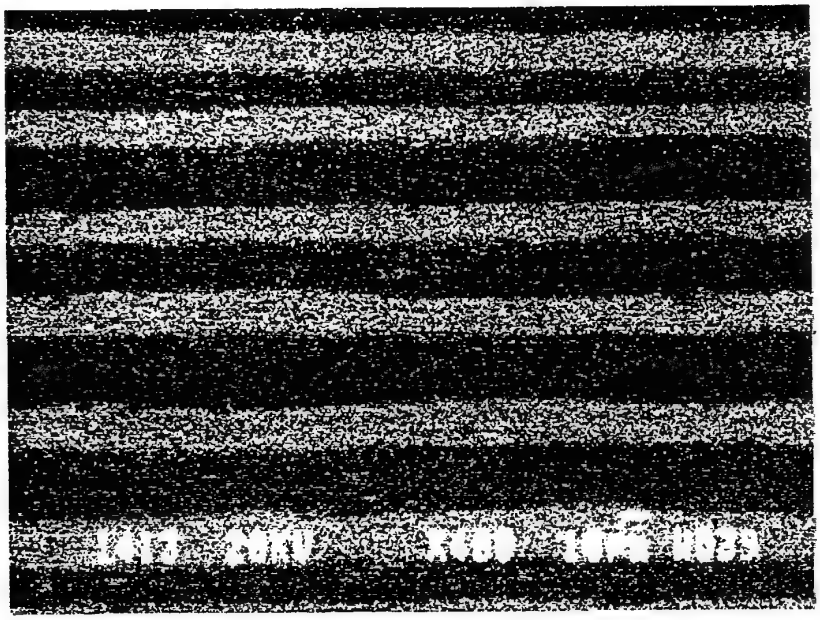

← Zr

Mapping on area a

c)

Fig. 60: Scanning electron micrographs of an Al_2O_3/ZrO_2 green microlaminate.

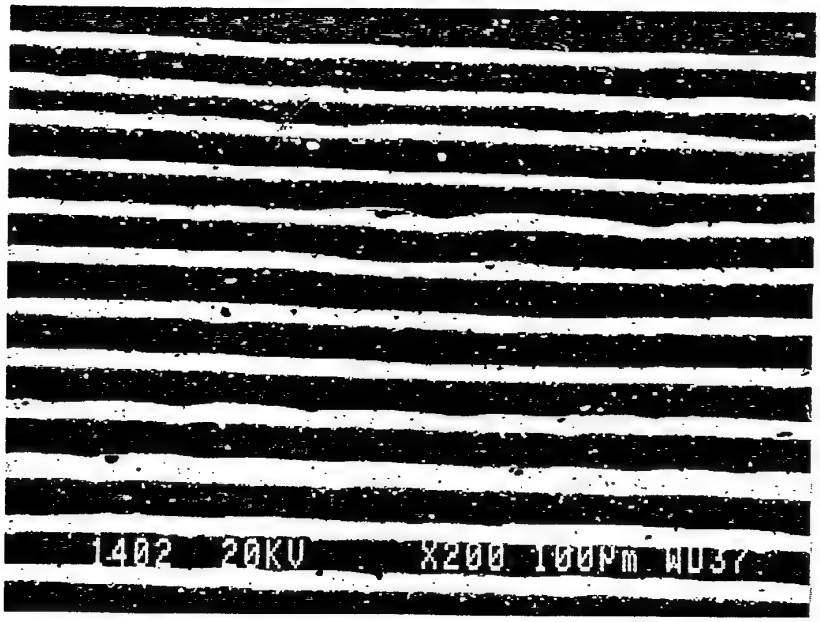

← Al_2O_3

← ZrO_2

a) polished cross-section

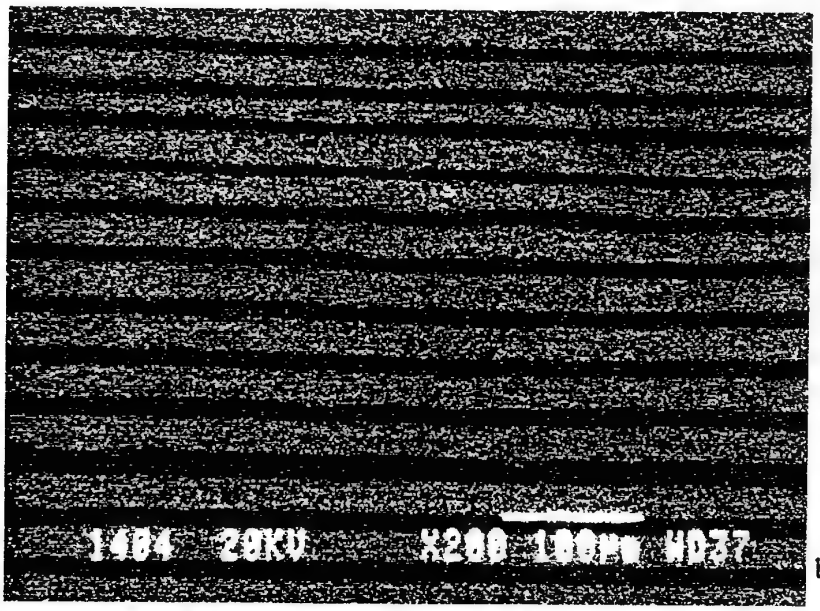

← Al Mapping on area a

b)

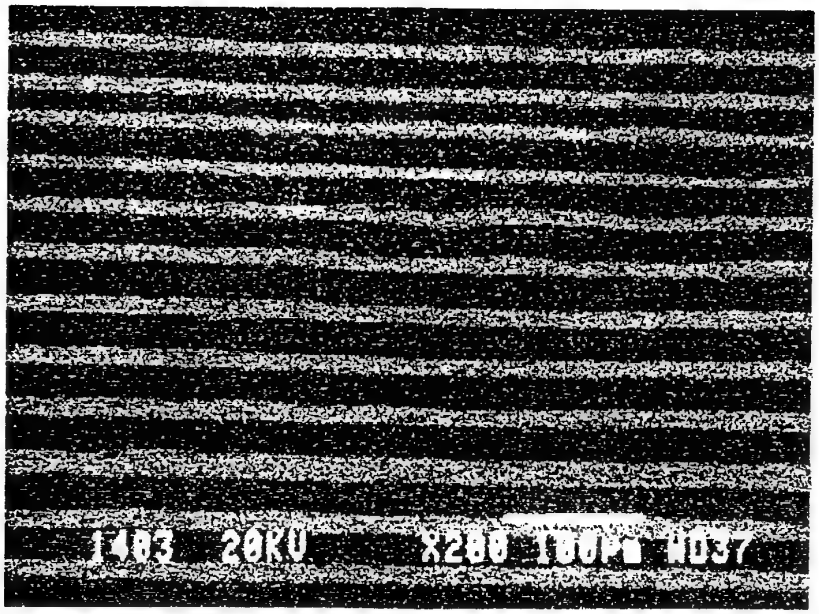

← Zr Mapping on area a

c)

Fig. 61: Scanning electron micrographs of a sintered Al_2O_3/ZrO_2 microlaminate.

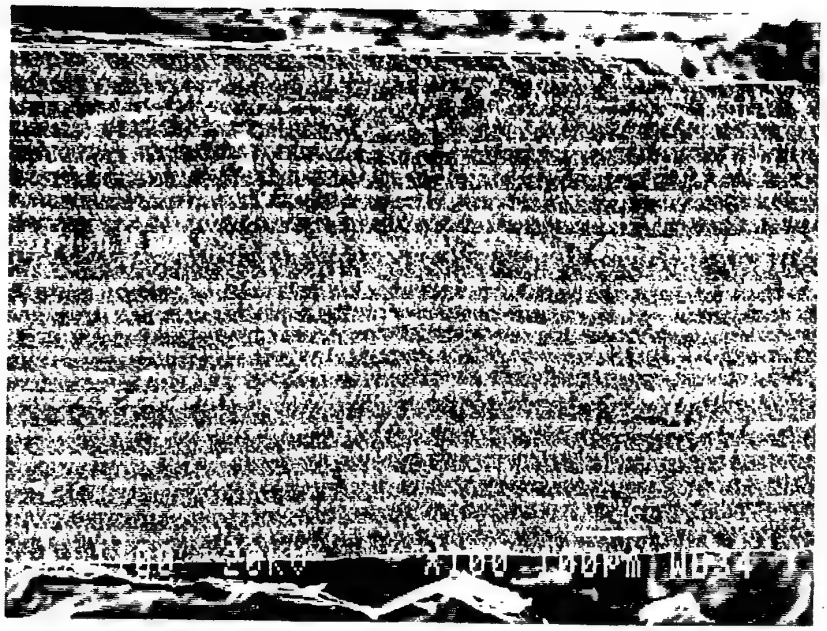

$\longleftarrow$ Al_2O_3

$\longleftarrow$ ZrO_2

a)

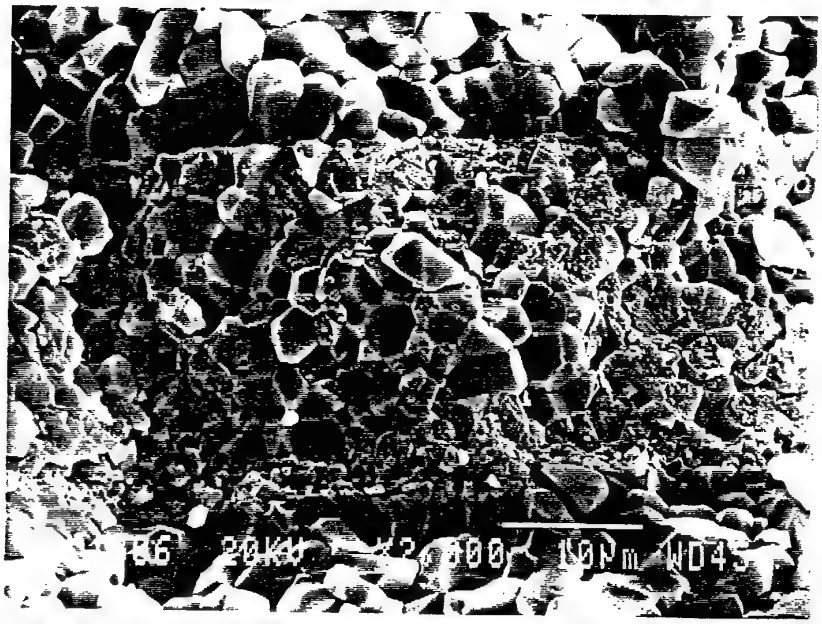

$\longleftarrow$ Al_2O_3

$\longleftarrow$ ZrO_2

$\longleftarrow$ Al_2O_3

b)

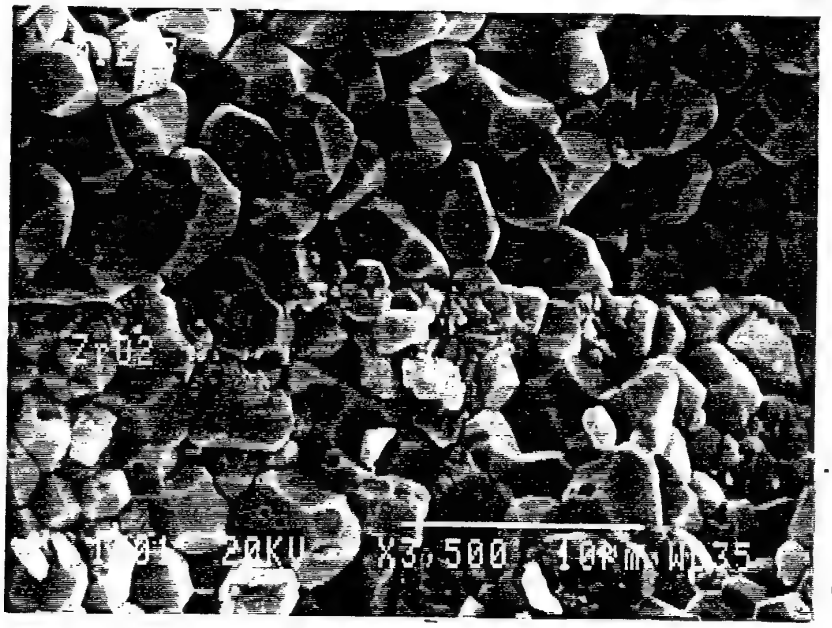

$\longleftarrow$ Al_2O_3

$\longleftarrow$ ZrO_2

c)

Fig. 62: Fractures sintered multilayer structure.

Chapter 5. Summary

The results obtained at this stage of the project can be summarized as follows:

- The kinetics of deposition of Al_2O_3 and ZrO_2 particles from isopropanol suspensions on both anode and cathode was studied. It was found that submicron Al_2O_3 (Baikalox SM-8) and ZrO_2 (TOSOH, TZ-12CE) particles suspended in isopropanol acquired spontaneously a positive charge and were deposited on the cathode.

- The addition of AcAc to isopropanol suspensions of both Al_2O_3 and ZrO_2 improves the suspension stability and increases the deposition rate.

- AcAc increases the zeta potential of both Al_2O_3 and ZrO_2 particles in isopropanol.

- AcAc increases appreciably the green density of the deposits. Alumina and zirconia deposits with a green density of 62% (of the theoretical value) were obtained from respective isopropanol suspensions with 0.05-1.5% (v/v) AcAc at 200 v/cm and 100-300 g/l concentration of solids. Addition of AcAc increased the green density from 42 to 62% for Al_2O_3 and from 33 to 62% for ZrO_2.

- The effect of AcAc is explained by the following mechanism:
  A keto-enolic equilibrium exists for the AcAc molecular structure. The enolic group has a relatively high dissociation constant resulting in the formation of H^+ ions. These are adsorbed on the ceramic particles increasing their positive charge, leading to the increase in zeta potential which in turn increases the deposition rate and the stability of the suspension due to enhanced electrostatic repulsion between particles. The increased green density of the deposits is due to hindrance of agglomeration of particles.

- Al_2O_3/ZrO_2 laminar composites of up to 80 layers and total thickness of 1,5 mm

were prepared by alternating deposition of the two powders from respective isopropanol suspensions at a constant field intensity of 200 v/cm, 100 and 300 g/l concentration of solids in the presence of 1.5% (v/v) AcAc.

- The composites were characterized by well defined and dense interfaces between layers and a rather dense packing of grains, the Al_2O_3 grains being about twice the size of ZrO_2 grains.

- The separation of the multilayer structure from the steel substrate (electrode) is facilitated by dipping in glycerine immediately after removal from the deposition bath. Nevertheless, the problem of damage of the structure due to occasional bending exists and will be studied further.

- The drying procedure used has not fully prevented cracking of deposits. Drying will be optimised in the next stage.

Chapter 6. Future Work

In the present stage of the project the experimental foundation for the formation of Al_2O_3/ZrO_2 multilayer composites by electrophoretic deposition has been laid. However, further studies are needed both for optimization of the process as well as for a better understanding of the accompanying phenomena. Future work should include the following investigations:

- Further studies on suspension stability.
- Study of reproducibility of layer thickness and morphology.
- Control of layer thickness in the progress of deposition (use of stepped-up voltage or deposition duration).
- Determination of overall thickness limits.
- Study of drying conditions to prevent cracking.
- Optimization of sintering conditions of multilayer structures.
- Study of mechanical properties (fracture toughness and strength) of multilayer composites.
- Feasibility of FGM (functionally graded materials) formation.

Bibliography

1. R.J. Hunter, "Foundations of Colloid Science", Vol. 1, 1987, Clarendon Press, Oxford.

2. O.M. Bockris, K.N. Reddy, "Modern Electrochemistry," Vol. 1, 1970.

3. D.R. Brown, E.W. Salt, J. Appl. Chem., 15, 40, 1965.

4. E.J.W. Verwey, J. Th. Overbeek, "Theory of the Stability of Lyophobic Colloids," 1948, Elsevier, Amsterdam-New York.

5. P. Benson et al., Electrochimica Acta, 9, 275, 1964.

6. J. Mizuguchi, K. Sumi, T. Muchi, J. Electrochem. Soc., 130 (9), 1819, 1983.

7. P.W. Powers, J. Electrochem. Soc., 122(4), 490, 1975.

8. J. Requena, R. Moreno, J.S. Moya, J. Am. Ceram. Soc., 72, 1511, 1989.

9. G.A. Parks, Chem. Revs. 65, 177, 1965.

10. M. Hashiba, H. Okomoto, Y. Nurishi, K. Hiramatsu, J. of Material Science, 23, 2893, 1988.

11. R.J. Hunter, "Zeta Potential in Colloid Science", Academic Press, London, 1981.

12. H.J. Modi, D.W. Feuerstenau, J. Phys. Chem. 61, 640, 1957.

13. E.M. Deliso, W.R. Cannon, A.S. Rao, Advances in Ceramics, 24, 335, 1988.

14. T. Graule, L.J. Gauckler, Cer. Acta 5 (3), 5, 1993.

15. R. Moreno, Am. Cerm. Soc. Bull. 71 (10), 1521, 1992.

16. S.S. Vojutsky, Colloid Chemistry (in Russian), Moskwa, 1964.

17. J. Faisson, R.A. Haber, Ceram. Eng. Sci. Proc., 12, 106, 1991.

18. Ceramics and Glasses, Engineering Materials Handbook, V. 4.

19. K. Mikeska, W.R. Cannon, Advances in Ceramics, vol. 9, p. 164, American Ceramic Society, Columbus, 1983.

20. T. Chartier, E. Striecher, P. Boch, Am. Ceramic Soc. Bull., 66 (11), 653, 1987.

21. P. Boch, T. Chartier, M. Huttepain, J. Am. Ceram. Soc., 69, 191, 1986.

22. D. Calvert, E.S. Tormey, R.S. Rober, Am. Ceram. Soc. Bull., 65(4), 669, 1986.

23. M. Green et al., Advances in Ceramics, vol. 21, p. 449, Am. Ceramic Soc., Westerville, 1987.

24. R.I. Feigin, D.H. Napper, J. Colloid Interface Sci., 75, 525, 1980.

25. R.E. Johnson, W.H. Morrison, Advances in Ceramics, vol. 21, pp. 323-48. Am. Ceram. Soc., Westerville, 1989.

26. D.W. Richerson, "Modern Ceramic Engineering", New York - Basel - Hong Kong, 1992.

27. D.B. Marshall, J.J. Ratto, J. Am. Cearm. Soc., 74 (12), 2979-87, 1991.

28. D.B. Marshall, Ceram. Bull., 71 (6), 969-973, 1992.

29. R.S. Garvie, R.H. Hannink, R.T. Paskoe, Nature (London), 258, 703-705, 1975.

30. A.G. Evans, R.M. Cannon, Acta Metall., 34 (5), 761-800, 1986.

31. R.H.J. Hannink, M.V. Swain, J. Am. Ceram. Soc., 72, 90, 1989.

32. D.B. Marshall, J. Am. Ceram. Soc., 73 (9), 2659-66, 1990.

33. D.B. Marshall, J. Am. Ceram. Soc., 73 (10), 3119-21, 1990.

34. P.S. Nicholson, P. Sarkar, X. Haung, Journal of Materials Science, 28, 6274-78, 1993.

35. J.M. Andrews, A.H. Collins, D.S. Cornish and J. Dracass, British Scientific Instrument Research Association, Chislehurst, Kent.

36. W.F. Caley, S.N. Flengas, Canadian Metallurgical Quarterly, 15 (4) 375-382, 1976.

37. Dana Goski, Jan. C.T. Kwak, Ceramic. Eng. Sci. Proc., 12, 2075-83,1991.

38. R. Nass, W. Storch, H. Schmidt, Ceramic Process, Sci. Proc. Int Conf. 2nd, 1988, 625-32, Cologne, F.R.G.

39. W.M. Winslow, J. of Applied Physics, 20, 1137, 1949.